# SCALABLE ONLINE ESTIMATION WITH PERFORMANCE GUARANTEES: APPLICATION TO TRAFFIC NETWORK MONITORING

BY

YE SUN

DISSERTATION

Submitted in partial fulfillment of the requirements
for the degree of Doctor of Philosophy in Civil Engineering
in the Graduate College of the
University of Illinois at Urbana-Champaign, 2018

Urbana, Illinois

Doctoral Committee:

Professor Daniel B. Work, Chair
Professor Geir E. Dullerud
Professor Yanfeng Ouyang
Professor Richard B. Sowers

# ABSTRACT

This work is motivated by the need for scalable online estimation with provable performance in *cyber-physical systems*, especially in traffic monitoring applications. While model-based traffic estimation has achieved great success via experimental deployments, there are substantial open questions on the theoretical understanding of the performance of these estimators. This gap is largely due to the nonlinearity of the underlying traffic flow and the nonobservability of the estimation problems. The main contribution of this dissertation is to explicitly address performance guarantees of filtering algorithms on traffic networks, with specific focus on systems that are unobservable, or even switch among observable and unobservable scenarios.

We first consider one-dimensional road sections to establish the main proof techniques before considering more general road networks. To tackle the non-linearity issue in traffic models, the *Lighthill-Whitham-Richards partial differential equation* (LWR PDE) is transformed to a discrete-time switched linear form, i.e., the *switching mode model* (SMM). We provide a rigorous analysis on the performance of the *Kalman filter* (KF) on the SMM. Although the error dynamics of the KF is very likely to diverge under general unobservable systems, we show that in the context of traffic estimation, a uniform upper bound for the mean error exists when the system is unobservable. This is done by exploring the interactions between the physical properties of traffic flows, the stability conditions in the discretization scheme, and the information update in the filter. We also derive error bounds for the KF when the system switches among the observable and unobservable modes of the SMM.

The above analysis is then extended to traffic networks with junctions. To support the analysis, we develop a switched linear model describing traffic dynamics on a freeway section

with a junction inside. The model, namely the *switching mode model with junctions* (SMM-J), combines the discretized LWR PDE with a junction solver. Based on the SMM-J, the error bounds of the KF are extended to freeway networks.

This dissertation also studies two essential problems related to the scalability issue in the estimation of general cyber-physical systems: (*i*) state space scalability, where the enormous state dimension causes computational burden on estimators, and (*ii*) data scalability, where massive data transmission incurs considerable energy, bandwith, or monetary costs. First, we design a *distributed local Kalman consensus filter* (DLKCF) for large-scale estimation, where the entire state is partitioned into local sections, and the computation task is distributed to local agents. In addition, a consensus term is designed to promote agreement on the estimates of neighboring agents. We also derive the error bounds of the DLKCF used for traffic estimation. Next, we study sensor scheduling schemes designed to select the most informative data to transmit to the estimator, thus reducing data transmission while preserving estimation accuracy. In this context, we propose a filtering algorithm that extracts the implicit information in the scheduling policy and update both the state estimate and the error covariance when data transmission is not triggered, which achieves better estimation accuracy compared to existing algorithms that only update the error covariance in the absence of data transmission.

*To my parents,*

*Fengchun Sun and Yunping Ye*

# ACKNOWLEDGEMENTS

This work would not have been possible without the people who have helped and influenced me significantly in the past five years.

I would like to express my gratitude to my advisor, Professor Dan Work, for all the support along the way. I am greatly indebted to the days when we worked together to go through line-by-line the early versions of the proof on estimator performance in traffic monitoring, fought together to address all of the hard reviews in my first journal submission, and attended various conferences and workshops together in all parts of the world. He gave me the courage to pursue what I thought was impossible and the spirit to seek for perfectionism, which have been constant motivations for me during my PhD, and beyond.

I would also like to thank Dr. Sebastien Blandin, my supervisor at *IBM Research*, who guided my exploration in many fascinating areas of data analytic and estimation, e.g., sensor scheduling, differential privacy, inference in graphical models, etc. I am extremely fortunate to work with him on the mathematically challenging problems, to experience the purest beauty of research, in the amazing city of Singapore.

I am greatly honored to have Professor Geir Dullerud, Professor Yanfeng Ouyang, and Professor Richard Sowers in my doctoral committee. Professor Dullerud has been a great mentor since six years ago when I interned at his lab as a visiting undergraduate student. The book he wrote on robust control theory, which he gave me as a gift when I finished the internship, inspired my curiosity and enthusiasm in control / estimation theory. His course in convex control, which I completed after I came back to Illinois as a PhD student, has become a core supporting resource for my research. Professor Ouyang introduced me to the areas of logistic system and car-following model, which significantly broadened my horizon in the field of transportation. As my academic elder brother from Tsinghua, his diligence,

sharpness and sense of humor have always been the targets for me to learn from. Professor Sowers's vision and inspiring work on video as sensors and internet of things encouraged me to explore the frontiers of cyber-physical systems, and transfer technology to deliver business value and real-world impact, which helped me shape my career goal to a great extent.

It has been a privilege for me to work with Professor Benjamin Seibold at Temple University and Professor Benedetto Piccoli at Rutgers University. During my PhD research, I have benefited a lot from Professor Seibold's insights on second-order macroscopic traffic models and Professor Piccoli's expertise in traffic flow modeling on networks.

In the first two years of my PhD study, I had the opportunity to take numerous valuable classes taught by professors at the *Coordinated Science Lab*, e.g., Professor Seth Hutchinson's class on linear systems, Professor Prashant Mehta's class on nonlinear systems, Professor Daniel Liberzon's class on switched systems, and Professor Ali Belabbas's class on stochastic control. These classes have become solid foundations and critical building blocks of my PhD research. I am greatly indebted to the fantastic academic environment and interdisciplinary research community here at Illinois.

I would also like to thank my fellow students in the Work lab. I appreciate all the time we spent together brainstorming ideas, writing reports, preparing for field experiments, practicing conference and exam talks, and working on demos. It has been a true pleasure to work with each of you.

Several organizations also contributed to sustain this research work via various awards and fellowship, notably the *National Science Foundation*, the *Women's Transportation Society*, and the *Institute for Pure and Applied Math* (IPAM). Special thanks to the three-month long program, "New Directions in Mathematical Approaches for Traffic Flow Management," hosted by IPAM, which granted me opportunities to watch plenty of prestigious talks given by leaders in academia and industry, and discuss research ideas with a number of successful professors in the research community of smart and connected transportation.

In addition, I would like to thank all my friends at Illinois for the days we fought together for our PhD degrees, for the restaurants and bars we explored together, for our field trips

and all the amazing memories. I am also very grateful to my friends since high school, for all the ups and downs in life we experienced together, for always being here for me when I need to talk on the phone, and for all the moments we spent together in Beijing, the West Coast, Champaign, Chicago, and New York.

Finally, I would like to thank my parents, Fengchun Sun and Yunping Ye, for their constant love and support. They have been my role models, best friends, and solid shelters since the first day of my life. They are the cause of all of this.

# TABLE OF CONTENTS

# CHAPTER 1

# INTRODUCTION

## 1.1 Motivation

The ubiquitous sensing prevalent in many *cyber-physical systems* (CPS) has been enabled by the unprecedented growth of *wireless sensor network* (WSN) technologies, with broad applications including environmental monitoring [1, 2, 3], crowd tracking [4, 5, 6], and intelligent transportation systems [7, 8, 9]. However, several issues remain to be addressed in many real-time estimation problems, especially for large-scale traffic network estimation. These issues primarily include:

**Theoretical performance guarantees.** Nearly all model-based traffic estimation algorithms proposed to monitor real-time traffic conditions are only verified through experiments [7, 8, 10, 11, 12, 13], while a theoretical analysis on the estimator performance is lacking. This is mainly due to the complexity of the physics of traffic flows (e.g., which lead to non-linear and non-differentiable models) [14] and the non-observability [15, 16, 17] of the system given common measurement model. When a system is not observable, the available sensor measurements (in conjunction with the model describing system dynamics) are insufficient to correctly reconstruct the full state to be estimated. The non-observability issue is mainly driven by the following two factors:

- **Shocks:** When shocks exist, traffic models are irreversible if the sensors cannot measure every state variable in the freeway section of interest. This is due to the fact that the presence of a shock results in information loss which makes it impossible to reconstruct the initial condition based on the sensor measurements. Indeed, various initial conditions can result in the same sensor measurements in this regime. Hence, the non-observability issue is inevitable in the presence of shocks.

- **Junctions:** In the presence of road junctions (i.e., merges or diverges), the issue of non-observability is shown to be even more critical [17]. For instance, a freeway section with a junction inside can be unobservable even if boundary measurements are available and the freeway section is congested everywhere (while a one-dimensional freeway section without junctions will always be observable under the same scenario). As a consequence, for freeway sections with junctions, unobservable cases happen way more frequently than observable ones.

In classical estimation and filtering theory, an unobservable system is very likely to result in estimation errors that diverge [18, 19]. Nevertheless, as shown in this dissertation, theoretical error bounds for traffic estimators can be obtained through exploring the interactions between the physical properties of the traffic models (e.g., mass conservation and flow-density relationship) and measurement feedback of estimators. The problem is not only mathematically interesting, but also provides rigorous technical support for the widely successful field implementations.

**Scalability.** Scalability is another critical issue for the real-time estimation of many large scale and spatially distributed cyber-physical systems, such as transportation networks. Here, the computational burden can be imposed by both the enormous size of the state space and the massive volume of sensor data to be processed.

- **State space scalability:** In many real-time estimation problems, the entire state vector is too large (e.g., usually of order at least $10^5$ [7] for transportation systems) for a central estimator to scale in real time. Hence, an alternative is to partition the large state space into local states, with each local state estimated by a cheap commodity computer (referred hereafter as an agent). In this case, each agent performs computation on the dimension of the local state. Meanwhile, information sharing among agents to compensate for the lack of a central estimator is critical to maintain estimation consistency. Hence, it is also important to ensure that the inter-agent coordination is scalable in terms of communication, i.e., each agent only communicates with its one-hop neighbors.

- **Data scalability:** The increasing amount of high fidelity data allows for more reliable real-time estimation. However, when the data volume is sufficiently large, additional

data transmission may only contribute marginally to the estimation accuracy [20]. Moreover, in many settings such as the *remote estimation* [21] problem, the cost of data transmission between sensors and the estimator (e.g., energy and channel bandwidth costs) becomes a design concern, especially when the data needs to be purchased (e.g., traffic companies pay for the data used for traffic monitoring). This motivates techniques that adaptively select the most informative data to be transmitted to the estimator, thus reducing data acquisition cost while preserving a satisfactory estimation accuracy.

This dissertation aims at addressing the above issues on theoretical performance analysis (in the context of traffic estimation applications) and scalability. The first part of the dissertation is dedicated to theoretically deriving the error bounds for the *Kalman filter* (KF) estimating unobservable one-dimensional freeway sections (with out junctions), even when the traffic states switch among observable and unobservable system dynamics. Next, the results on one-dimensional freeway sections are extended to traffic networks with junctions. The third part introduces a (spatially) *distributed local Kalman consensus filter* (DLKCF) for large-scale multi-agent estimation, with the consensus term designed to promote estimation consistency among neighboring agents. The last part of the dissertation studies filtering algorithms embedded with *sensor scheduling* techniques, and designs a *Kalman filter with synthetic measurements* (KF-SM) to reduce data transmission while preserving estimation accuracy. In line with the effort to obtain theoretical performance guarantees for the studied estimators, the stability of the DLKCF and the KF-SM is also proved in the dissertation.

## 1.2 Related work

### 1.2.1 Theoretical performance analysis of traffic estimators

The classical conservation law describing the evolution of traffic density on a one-dimensional freeway section (i.e., a freeway section without junctions) is the *Lighthill-Whitham-Richards partial differential equation* (LWR PDE) [22, 23]. The *cell transmission model* (CTM) [24, 25, 26] is a discretization of the LWR PDE using the *Godunov scheme* [27]. The LWR

PDE and the CTM are non-linear and non-differentiable [14], making it hard to analyze theoretical performance of traffic estimators in these models. In [15, 28], the CTM is transformed to a switched linear system known as the *switching mode model* (SMM) that switches among different linear *modes*. Among theses modes of the SMM, some are observable, and others are not due to the existence of shocks.

To extend the traffic model on road links to networks, a model is needed to describe how the traffic exiting the road links on the upstream side of a junction is received by the road links on the downstream side of the junction. A well known issue is that the conservation of vehicles across the junction is insufficient to uniquely define the flows at the junction. To address this issue, a number of junction models [25, 29, 30, 31, 32, 33, 34, 35, 36, 37] have been proposed via additional rules governing the distribution or priority of the flows on different road links.

In parallel to the ongoing development of traffic models, a number of sequential traffic estimation algorithms have been proposed to integrate model predictions with real-time sensor measurements. For example, the *mixture Kalman filter* is applied to the SMM in [28] to estimate traffic densities for ramp metering. The *parallelized particle filters* and the *parallelized Gaussian sum particle filter* are designed in [8] for computational scalability. In [38], an *efficient multiple model particle filter* is proposed for joint traffic estimation and incident detection on freeways. Other treatments of traffic estimation include [10, 11, 12, 13, 39, 40, 41]. A comprehensive survey of sequential estimation techniques for traffic models can be found in [42].

Although many traffic estimation algorithms proposed in the existing literature are verified experimentally, very few theoretical results exist that analyze the performance of traffic estimators (e.g., bounds on the estimation error), especially under unobservable scenarios. The main results to date are as follows. In [43], the KF is applied on a Gaussian approximation of a stochastic traffic model, and the stochastic observability of the system is proved. To ensure observability of the system, a warm-up period is required where the initial conditions are restricted to be freeflow traffic conditions. In [44], the local observability around an equilibrium traffic state is studied using a Lagrangian formulation of the traffic model. The authors of [45] prove the performance of a noise-free Luenberger observer for traffic estimation based on the SMM, which is the first work to provide theoretical performance

analysis for any traffic estimator under both observable and unobservable scenarios. The Luenberger observer in [45] discards measurement feedback in unobservable modes, ensuring the spatial integral of the estimation error is conserved. Similarly in [46], the estimator runs an open-loop predictor under unobservable cases to ensure that the estimation error does not diverge. Although conserving the spatial integral of the estimation error, it is illustrated in [47] that dropping measurement feedback can lead to physically unreasonable estimates. Rather than providing a single-value estimate of the state variable, another line of research explores the bounds of the state estimates under *set-valued estimation* [48], which is conducted under the assumptions that model parameters as well as model and measurement noise are all bounded inside some known intervals. In the context of set-valued estimation, intervals of state estimates can be derived which are guaranteed to include the true states [49]. However, unrealistic set-valued estimates may occur if the assumptions on the model parameters and model/measurement noise are imperfect. Note that the theoretical performance analysis of traffic estimators at transportation networks with junctions is even more rarely observed. Among the works summarized above, only the set-valued estimation [49] deals with traffic dynamics at junctions, and all the results in [43, 44, 45, 46, 47] are restricted to one-dimensional road stretches without considering junction dynamics.

### 1.2.2 Collaborative information processing in estimation problems

Research on collaborative information processing is driven by the broad applications of estimation on multi-agent systems. A complete communication network with all-to-all links is required in the *decentralized Kalman filter* [50], or relaxed in the *channel filter* [51] for the fixed tree communication topology. Recently, the application of consensus strategies in distributed estimation is widely studied to promote agreement on estimates among agents [52, 53, 54], and/or to reconstruct sensor data not directly accessible through purely sharing measurements with neighbors [55, 56, 57], thus approximating the central estimator. To ensure the stability of the estimators, each local system is assumed to be observable (or detectable) in [52, 53, 54], or the full system observability is only achieved given all the sensor data in the network [55, 56, 57]. A common feature of [50, 51, 52, 53, 54, 55, 56, 57] is that all agents estimate the same full state of dimension $n$, which may not scale in large-scale networks for Kalman filter based algorithms whose computational complexity is

$O(n^3)$.

There are also notable works on scalable distributed estimation algorithms where each agent estimates (or performs computation on) a small subset of the full state. Specifically in [58, 59], the state vector is partitioned into overlapping local states of dimension $n_l \ll n$, and the computation task is distributed across local agents. In [58], the cross-correlation of neighboring agents is incorporated in the estimation error covariance at the expense of requiring a $O(n_l^4)$ complexity at each local agent. However, the stability of the proposed estimator is not analyzed. In [59], a consensus term is designed to help each local agent reconstruct the estimates of other local states, and is its theoretical performance is analyzed when all local filters are detectable and have achieved a steady state. Other relevant treatments include moving-horizon estimation [60] and *distributed Kriged Kalman filtering* [61]. However, they either require extensive communication, or rely on the statistics of random fields which do not incorporate the intrinsic properties of physical systems (e.g., the conservation law).

### 1.2.3 Online sensor scheduling techniques

*Sensor scheduling* techniques are designed to reduce data transmission while preserving a satisfactory estimation accuracy, which determine when the sensor data is most informative for state estimation and transmit it accordingly (e.g., see [21] and references therein).

In a centralized sensor scheduling scheme [62, 63, 64, 65, 66], the optimal sensor selection strategies are developed from the estimator perspective, assuming that the estimator can obtain data at any time from any sensor it queries. Comparatively, in a decentralized sensor scheduling scheme, data transmission decisions are made locally at the sensors. For example, in *delta sampling* (e.g., [67]), a new measurement is transmitted when it moves away from the previously transmitted data by a distance delta. *Relevant sampling* is proposed in [68] which triggers an event to send relevant measurements to the estimator (i.e., measurements that contribute to reducing the estimator uncertainty and estimation error). In the stochastic communication protocol studied in [69], each sensor transmits data at least once over a predefined number of time steps. Data transmission decisions can also be computed by minimizing a cost function consisting of the expected estimation error and the data transmission cost (e.g., [70, 71]), or by integrating physical constraints on the

sensors [72, 73, 74]. In [70, 71, 72, 75, 76, 77], the event that triggers transmission of sensor data is the fact that the (normalized) gap between the true and predicted measurements (computed based on the latest state estimates) exceeds a threshold, which is very close to the sensor scheduling criteria applied in this dissertation.

## 1.3 Contributions and organization of the dissertation

### 1.3.1 Contributions

This dissertation contains several new contributions to the problem of large-scale online estimation with performance guarantees, especially in the context of traffic monitoring applications.

**Theoretical performance analysis of traffic estimation algorithms [16, 17].** This dissertation addresses the main algorithmic challenge in traffic estimation problems: obtaining theoretical error bounds on the performance of the estimators, even as the state switches between observable and unobservable system dynamics (also referred to as observable and unobservable modes in this work). This dissertation contains the first result on the theoretical performance of any traffic filter under unobservable scenarios as well as under switches among observable and unobservable modes, and contains the first theoretical result that analyzes the performance of traffic filters under unobservable junction dynamics. In this dissertation, it is proved that the estimation error of the Kalman filter used for traffic monitoring has the following properties, where the model to describe traffic dynamics is the SMM (and its extension to incorporate junction dynamics):

- *Bounds on the infinity norm of the Kalman gain.* Under unobservable scenarios, the Kalman gain has bounded infinity norm whose mathematical formula can be derived explicitly, which is essential to ensure bounded mean estimation error for the Kalman filter when the system is unobservable.

- *Maximum increase of the mean error during unobservable time interval.* When a freeway section remains unobservable, the mean estimate is ultimately bounded inside a physically meaningful interval. Given the upper bound of the infinity norm of

the Kalman gain, a uniform upper bound on the 2-norm of the mean estimation error is derived, which characterizes the maximum increase of the mean error under unobservable scenarios.

- *Minimum residence time in the observable modes.* The convergence rate of the mean estimation error when the freeway section stays in observable modes is derived based on the properties of the KF update scheme and the state transition matrices of the SMM. Given the above convergence rate and the maximum increase of the mean error under unobservable modes, the minimum residence time required in observable modes to offset the error increase occurred in unobservable modes is derived.

- *Upper bounds of the mean error under switches among observable and unobservable modes.* Based on the above results, the 2-norm of the mean estimation error is shown to be upper bounded for freeway sections that switch among observable and unobservable modes, provided a minimum residence time in the observable mode(s) is satisfied.

- *Extension to networks.* We extend the results for one-dimensional freeway sections to transportation networks with junctions. To facilitate the analysis, we combine the SMM with a junction solver to develop a switched linear model which is able to handle junction dynamics. It turns out that when junctions exist, unobservable scenarios are very frequently encountered, motivating attentions to the unobservable scenarios in the presence of junctions. Nevertheless, we show that the theoretical performance analysis of traffic estimators on junctions can be derived following a similar line of analysis as the one-dimensional road sections, and extend the error bounds derived above to traffic networks based on the newly developed model.

Specifically, in unobservable scenarios, the physical properties of the traffic model (e.g., mass conservation and a flow-density relationship) and the stability requirements of the discretization scheme embedded in the traffic models are combined with the measurement feedback in the correction step of the filter to analyze the theoretical performance of the filter.

**Distributed consensus-based filtering algorithm for large-scale estimation problems [16].** To tackle the issue of enormous state space dimensionality, a (spatially) *dis-*

*tributed local Kalman consensus filter* (DLKCF) is designed and analyzed in this dissertation. The large-scale network is partitioned into overlapping sections, and the local state in each section is estimated by an agent associated with the section. Additionally, inter-agent communication is introduced for better estimation consistency. Each agent shares sensor data and estimates with its neighbors, and a consensus term is introduced to promote agreement among neighboring agents on the estimates of their shared states:

- *Design of the consensus term:* The consensus term is designed such that the DLKCF is scalable both in the sense of computation (i.e., with computation conducted in the local dimension) and communication (i.e., each agent only communicates with its one-hop neighbors, and the global communication topology is not needed). This is an improvement compared to the author's previous work [47], where each agent needs information from all the other agents as well as the global communication topology to compute the consensus term.

- *Unbiasedness of the consensus term:* It is shown that the DLKCF has *globally asymptotically stable* (GAS) error dynamics when all the local sections are uniform complete observable, which ensures that the consensus term preserves the unbiasedness of the estimates.

- *Error bounds of the DLKCF in traffic estimation.* The theoretical error bounds of the DLKCF under traffic estimation applications are derived, which extends the results on the error bounds of the KF discussed above.

**Online estimation with event-triggered sensor scheduling schemes for data transmission reduction [78, 79].** To reduce the costly data transmission present in many CPS estimation problems, a *Kalman filter with synthetic measurements* (KF-SM) is designed and analyzed in this dissertation, with the sensor scheduling scheme chosen to be a deterministic threshold-based sensor scheduler, i.e., a sensor measurement is sent to the estimator only when the disparity between the sensor measurement and the predicted measurement (computed through the latest state estimate) exceeds a deterministic threshold. The new contributions in the KF-SM are summarized as follows:

- *Updating both the state estimate and error covariance in the absence of data transmission.* When no data is sent, the scheduling policy in the sensor schedulers provides

additional implicit information to the estimator, which can be utilized to improve estimation accuracy. While state-of-the-art algorithms [80, 81, 82, 83] leverage this implicit information to update only the estimation error covariance, the KF-SM further extracts implicit information from the sensor schedulers to update both the state estimate and the estimation error covariance.

- *Refining the state estimate using synthetic measurements.* When data transmission is declined by the sensor scheduler, the KF-SM draws synthetic measurements based on the estimated distribution of the true measurements (computed based on the sensor scheduling policy), and use the synthetic measurements to update the state estimate in place of the true measurements. This work designs a synthetic measurement generation algorithm and the corresponding update schemes of the KF-SM which ensures both the optimality and stability of the filter. By correcting the estimate with synthetic measurements, the KF-SM can further reduce the estimation error.

- *Input-to-state stability of the error dynamics.* The estimation error dynamics of the KF-SM is shown to be input-to-state stable when treating the synthetic measurement error (with respect to the true measurement) as an input to the error dynamics. This indicates that the estimation error of the KF-SM is small if the synthetic measurement is close to the true measurement, which is ensured by the deterministic threshold in the sensor scheduler.

### 1.3.2 Organization

This dissertation is organized as follows. In Chapter 2, we provide a brief introduction of the cell transmission model as well as its switched linear representation, i.e., the switching mode model, and discuss the observability of the SMM under different modes.

In Chapter 3, we study the theoretical performance of the KF estimating traffic conditions on a one-dimensional freeway section, with the SMM applied to describe traffic dynamics on the freeway section. Here, we consider one-dimensional road sections to establish the main proof techniques on a simple road structure that does not include junctions, which will be treated in Chapter 4. We first show that when a section stays unobservable, the Kalman gain has bounded infinity norm, and the mean estimate of each state variable is ultimately

bounded inside a physically meaningful interval. Next, the explicit upper bound of the mean estimation error is derived when the section switches inside the unobservable mode of the SMM. Then, we leverage the convergence rate of the mean error under observable modes to show that the mean error is upper bounded when the section switches among observable and unobservable modes, provided a minimum residence time in the observable mode(s) is satisfied.

In Chapter 4, we show that the results in Chapter 3 can be extended to traffic networks with junctions. We first propose a switched linear system to model the evolution of traffic densities on freeway networks with junctions, namely the *switching mode model with junctions* (SMM-J). Compared to the one-dimensional freeway sections, the issue of non-observability is more frequently encountered when junctions exists. Next, we show that similar to one-dimensional sections, exploring the interactions between the physical properties of the SMM-J and the update schemes of the KF enables us to derive the error bounds of the KF under unobservable systems. We conclude Chapter 4 by some remarks on the generalization of the results to systems that switch among observable and unobservable modes.

Chapter 5 is dedicated to address the issue of state space scalability, and introduces the DLKCF for large-scale multi-agent estimation problems. The large state space is partitioned into overlapping local states, with each local state estimated by its own agents. We first show that the mean error dynamics of the DLKCF is GAS when all the local states are uniformly completely observable. Next, we extend the results in Chapter 3 to the DLKCF, and show the theoretical error bounds of the DLKCF estimating traffic conditions when the system switches among observable and unobservable modes. Numerical results show the effect of the consensus term on reducing disagreement among estimates given by neighboring agents (with 50% reduction), and that the DLKCF outperforms a purely local KF on estimation accuracy.

Chapter 6 focuses on the issue of data scalability, where we introduce the KF-SM designed to reduce sensor-to-estimator data transmission while preserving estimation accuracy. When data transmission is not triggered by the sensor scheduler, using synthetic measurements to correct the state estimate introduces a positive semidefinite extra term on the error covariance. However, we show that this extra term is small and is dominated by the

reduction of the error covariance derived based on the implicit information embedded in the sensor scheduling scheme. Moreover, under the Gaussian assumption of the estimation error distribution, the KF-SM is shown to be a *minimum mean square error* (MMSE) estimator which incorporates the randomness of the synthetic measurements. Next, *the input-to-state stability* (ISS) of the KF-SM is proved. To justify the effectiveness of the synthetic measurements on reducing the estimation error, we compare numerically the performance of the KF-SM with state-of-the-art algorithms embedded with various sensor scheduling schemes.

We present concluding remarks and some open problems in Chapter 7.

**Notation** We list some notation which will be used for the remainder of this dissertation. Let $I_n$ and $\mathbf{0}_{n,m}$ be the $n \times n$ identity matrix and the $n \times m$ zero matrix, respectively. The subscripts of $I_n$ and $\mathbf{0}_{n,m}$ are sometimes omitted, when dimensionality is clear from the context. Denote as $\mathbb{E}[\cdot]$ the expectation operator, and the bold font is used to denote the expected value of random vector $x$, i.e., $\boldsymbol{x} = \mathbb{E}[x]$. The symbol $^\top$ is used to denote the transpose operator.

# CHAPTER 2

# OBSERVABILITY ANALYSIS ON TRAFFIC MODELS

## 2.1 Introduction

In this chapter, we review the fundamental elements of observability in linear time-varying system, and analyze their implications on traffic estimation problems. In particular, the *cell transmission model* (CTM) [24, 25, 26] is transformed to a switched linear system, namely the *switching mode model* (SMM) [15, 28],facilitating the analysis of observability in the context of traffic monitoring. The new contributions of this chapter are summarized below.

- **Properties of the state transition matrices of the SMM.** Based on the explicit formula of the SMM, we summarize several properties of the state transition matrices of the SMM. These properties reflect the intrinsic physical properties embedded in the traffic flows and discretization schemes, and assume critical roles in proving the error bounds of the Kalman filters in the forthcoming chapters.

- **Uniform complete observability of the SMM under arbitrary switches among the observable modes.** Given that the existing literature only contains the observability results of the SMM on each single mode, we derive the observability of the SMM under switches among different modes. We show that the SMM is uniformly completely observable when it switches arbitrarily among the observable modes (an arbitrary switching sequence containing an unobservable mode is unobservable).

This chapter is organized as follows. In Section 2.2, we review the definition of observability on linear time-varying systems. An overview of the CTM and the SMM is provided in Section 2.3, where the properties of the state transition matrices of the SMM are presented in Section 2.3.2.2. Finally, the uniform complete observability of the SMM under switches among the observable modes is derived in Section 2.4.

## 2.2 Definition of observability

Consider a general linear time-varying system

$$\rho_{k+1} = A_k \rho_k + u_k + \omega_k, \quad \rho_k \in \mathbb{R}^n, \tag{2.1}$$

$$z_k = H_k \rho_k + v_k, \quad z_k \in \mathbb{R}^m, \tag{2.2}$$

where $\rho_k$ and $z_k$ are the state vector and sensor measurement vector at time $k \in \mathbb{N}$, respectively. The matrices $A_k$ and $H_k$ are the state transition matrix and the observation matrix at time $k$. The term $u_k$ in (2.1) is a deterministic system input. The noise terms $\omega_k \sim \mathbf{N}(\mathbf{0}, Q_k)$ and $v_k \sim \mathbf{N}(\mathbf{0}, R_k)$ are the white Gaussian model and measurement noise, where $Q_k$ and $R_k$ denote the model and measurement error covariance matrices at time $k$.

The observability of a system characterizes whether the sensor measurements of the system are sufficient for the estimators to correctly estimate the state vector. We provide below the formal definition of observability for time-varying linear systems.

**Definition 1.** *The discrete system* (2.1)-(2.2) *is uniformly completely observable (UCO) if there exists a positive integer* $T$ *and positive constants* $\alpha$, $\beta$ *such that*

$$\alpha I < \mathcal{I}_{k,k-T} < \beta I, \quad \textit{for all } k \geq T, \tag{2.3}$$

*where* $\mathcal{I}_{\bar{k},\underline{k}}$ *is defined as the information matrix for time interval* $k \in [\underline{k}, \bar{k}]$[1]*:*

$$\mathcal{I}_{\bar{k},\underline{k}} = \sum_{k=\underline{k}}^{\bar{k}} \Xi_{k,\bar{k}}^{\top} H_k^{\top} R_k^{-1} H_k \Xi_{k,\bar{k}}, \tag{2.4}$$

*where*

$$\Xi_{k,\bar{k}} = \prod_{\kappa=k}^{\bar{k}-1} A_\kappa^{-1}, \quad \textit{and} \quad \Xi_{\bar{k},k} = \Xi_{k,\bar{k}}^{-1} = \prod_{\kappa=\bar{k}-1}^{k} A_\kappa. \tag{2.5}$$

[1]Recall that the time instant $k \in \mathbb{N}$, hence $k \in [\underline{k}, \bar{k}]$ denotes $k \in \{\underline{k}, \underline{k}+1, \cdots, \bar{k}\}$, and $k \in (\underline{k}, \bar{k}]$ denotes $k \in \{\underline{k}+1, \underline{k}+2, \cdots, \bar{k}\}$

## 2.3 Macroscopic scalar traffic models

Macroscopic traffic modeling considers traffic flowing dynamics as a continuum of vehicles, rather than modeling behaviors of individual vehicles on a stretch of freeway. Macroscopic traffic models are originally motivated by constitutive hydrodynamics models, where the fluid dynamics resembles properties of traffic flow. Scalar traffic models classically consider the traffic state at a point $x$ at time $t$ to be fully represented by the vehicle density $\rho(t, x)$, as opposed to non-scalar models which also include additional state variables such as driver properties [84], etc., to take into account additional physical principles. To simplify the analysis, the discretized link models (e.g., the CTM and SMM) describe the vehicle densities on a discretization grid of the spacial-temporal domain.

### 2.3.1 Cell transmission model

The classical conservation law describing the evolution of traffic density $\rho(t, x)$ on a road at location $x$ and time $t$ is the LWR PDE [22, 23]:

$$\partial_t \rho + \partial_x \mathrm{F}(\rho) = 0. \tag{2.6}$$

The function $\mathrm{F}(\rho) = \rho \mathrm{v}(\rho)$ is called the flux function, where $\mathrm{v}(\rho)$ is an empirical velocity function used to close the model.

The CTM [24, 25, 26] is a discretization of (2.6) using a Godunov scheme [27]. Consider a uniformly sized discretization grid defined by a space step $\Delta x > 0$ and a time step $\Delta t > 0$. Let $l$ index the cell defined by $x \in [l\Delta x, (l+1)\Delta x)$, and denote as $\rho_k^l$ the spatial average of $\rho(k\Delta t, x)$ for $l\Delta x \leq x < (l+1)\Delta x$, where $k \in \mathbb{N}$ and $l \in \mathbb{N}^+$. Moreover, denote as $\mathrm{f}(\rho_k^{l-1}, \rho_k^l)$ the flux between cell $l-1$ and $l$. In the CTM, the discretized model (2.6) becomes

$$\rho_{k+1}^l = \rho_k^l + \frac{\Delta t}{\Delta x}\left(\mathrm{f}(\rho_k^{l-1}, \rho_k^l) - \mathrm{f}(\rho_k^l, \rho_k^{l+1})\right), \tag{2.7}$$

where $\mathrm{f}(\rho_k^{l-1}, \rho_k^l)$ is computed by

$$\mathrm{f}(\rho_k^{l-1}, \rho_k^l) = \min\left\{\mathrm{s}\left(\rho_k^{l-1}\right), \mathrm{r}\left(\rho_k^l\right)\right\}. \tag{2.8}$$

In (2.8), $\mathrm{s}(\rho_k^{l-1})$ is the *sending capacity* (i.e., maximum sending flow) of cell $l-1$ at time $k$, which is a function of $\rho_k^{l-1}$, and $\mathrm{r}(\rho_k^l)$ is the *receiving capacity* (i.e., maximum receiving flow) of cell $l$ at time $k$, which is a function of $\rho_k^l$. Note that the solution of the CTM converges in $L^1$ to the weak solution of the LWR PDE as $\Delta x \to 0$ [85] if the following *Courant-Friedrichs-Lewy* (CFL) condition is satisfied:

$$\Delta t \max_{\rho} \left|\mathrm{F}'(\rho)\right| \leq \Delta x, \tag{2.9}$$

where $\mathrm{F}'(\rho)$ is the derivative of $\mathrm{F}(\rho)$ with repect to $\rho$.

**Remark 1.** *Note that the terminologies sending capacity and receiving capacity are equivalent to the notions of demand and supply. Both sending/receiving and demand/supply terminologies are widely used in the traffic community, with the former introduced in [24, 25], and the latter introduced in [26]. Here, we use the sending/receiving terminology to ensure consistency with the publications related to this dissertation.*

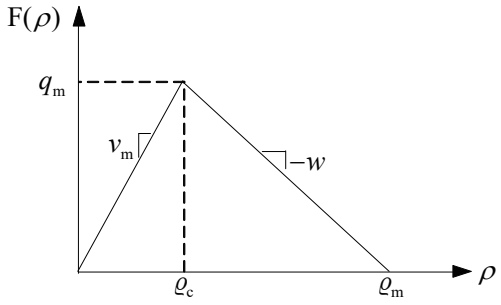


Figure 2.1: The triangular fundamental diagram in (2.10).

The flux function [25] used in this dissertation is the triangular flux function (shown in Figure 2.1) given by

$$\mathrm{F}(\rho) = \begin{cases} \rho v_{\mathrm{m}} & \text{if } \rho \in [0, \varrho_{\mathrm{c}}] \\ w(\varrho_{\mathrm{m}} - \rho) & \text{if } \rho \in [\varrho_{\mathrm{c}}, \varrho_{\mathrm{m}}], \end{cases} \tag{2.10}$$

where $v_{\mathrm{m}}$ denotes the *freeflow speed*, $w = \frac{\varrho_{\mathrm{c}} v_{\mathrm{m}}}{\varrho_{\mathrm{m}} - \varrho_{\mathrm{c}}}$, and $\varrho_{\mathrm{m}}$ denotes the *maximum density*. The parameter $\varrho_{\mathrm{c}}$ is the *critical density* at which the maximum flux is realized. For the triangular fundamental diagram, the flux function has different slopes in *freeflow* ($0 < \rho \leq \varrho_{\mathrm{c}}$) and *congestion* ($\varrho_{\mathrm{c}} < \rho \leq \varrho_{\mathrm{m}}$). In freeflow, the slope is $v_{\mathrm{m}}$, and in congestion, it is $w$. Under

the triangular flux function, the sending and receiving capacities are determined by:

$$\mathrm{s}(\rho) = \begin{cases} \rho v_{\mathrm{m}} & \text{if } \rho \in [0, \varrho_{\mathrm{c}}] \\ q_{\mathrm{m}} & \text{if } \rho \in [\varrho_{\mathrm{c}}, \varrho_{\mathrm{m}}] \end{cases} \qquad \mathrm{r}(\rho) = \begin{cases} q_{\mathrm{m}} & \text{if } \rho \in [0, \varrho_{\mathrm{c}}] \\ w(\varrho_{\mathrm{m}} - \rho) & \text{if } \rho \in [\varrho_{\mathrm{c}}, \varrho_{\mathrm{m}}], \end{cases} \tag{2.11}$$

where $q_{\mathrm{m}}$ is the maximum flow given by $q_{\mathrm{m}} = v_{\mathrm{m}} \varrho_{\mathrm{c}}$.

### 2.3.2 Switching mode model

In the SMM [15], (2.7) is written as a switched linear system whose system dynamics switches among different modes depending on the state of the boundary cells.

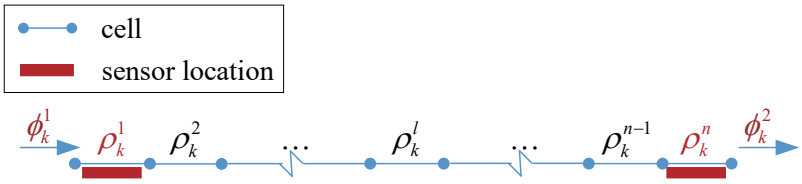


Figure 2.2: One-dimensional freeway section wit $n$ cells. Sensors are located at the boundary of the freeway section, and the densities of the first and last cells (i.e., $\rho_k^1$ and $\rho_k^n$) are directly measured. The boundary flows $\phi_k^1$ and $\phi_k^2$ are considered to be system inputs.

As shown in Figure 2.2, consider a freeway section with $n$ cells, and the state variable at time step $k \in \mathbb{N}$ is denoted as $\rho_k = \left(\rho_k^1, \cdots, \rho_k^n\right)^\top$. The SMM is derived from (2.6)-(2.8) and the triangular fundamental diagram (2.10) under the following assumption:

(Asm.1): There is at most one transition between freeflow and congestion in each section, which is motivated by the fact that freeway sections are generally partitioned to be sufficiently short with no more than one queue building up or dissipating.

Given (Asm.1), the SMM may switch between the following modes:

1. *freeflow–freeflow* (FF), in which all cells in the section are in freeflow;
2. *congestion–congestion* (CC), in which all cells in the section are in congestion;
3. *congestion–freeflow* (CF), in which the cells in the upstream part of the section (i.e., the cells in the upstream side of the transition between freeflow and congestion based

on the direction of travel) are congested, and the cells in the downstream part are in freeflow;

4. *freeflow–congestion* (FC), in which the upstream part of the section is in freeflow, the downstream part is in congestion.

In each mode stated above, the traffic state $\rho_k$ evolves with linear dynamics, forming a switched system:

$$\begin{aligned}\rho_{k+1} &= A^{s(k)}_{\sigma(k)}\rho_k + B^{\rho,s(k)}_{\sigma(k)}\mathbf{1}\varrho_{\mathrm{m}} + B^{q,s(k)}_{\sigma(k)}\mathbf{1}q_{\mathrm{m}} + B^{\phi}_{\sigma(k)}\phi_k \\ &= A_k\rho_k + B^{\rho}_k\mathbf{1}\varrho_{\mathrm{m}} + B^{q}_k\mathbf{1}q_{\mathrm{m}} + B^{\phi}_k\phi_k \end{aligned} \tag{2.12}$$

where $\mathbf{1}$ is the vector of all ones, the vector $\phi_k = (\phi^1_k, \phi^2_k)^\top$ with $\phi^1_k$ (resp. $\phi^2_k$) denoting the upstream (resp. downstream) boundary flow. The matrices and $A^{s(k)}_{\sigma(k)}$, $B^{\rho,s(k)}_{\sigma(k)}$, $B^{q,s(k)}_{\sigma(k)} \in \mathbb{R}^{n\times n}$ and $B^{\phi}_{\sigma(k)} \in \mathbb{R}^{n\times 2}$ are to be defined precisely later. The index $\sigma(k) \in \mathcal{S}$ where $\mathcal{S} = \{\text{FF, CC, CF, FC}\}$ is the set of the four modes, and $s(k) \in \{1, \cdots, n-1\}$ is the index introduced to precisely locate the transition between freeflow and congestion when it exists. We say $s(k) = l$ when the transition occurs between cell $l$ and $l+1$. For notation simplicity, we use $A_k$, $B^{\rho}_k$, $B^{q}_k$ and $B^{\phi}_k$ later to represent matrices $A^{s(k)}_{\sigma(k)}$, $B^{\rho,s(k)}_{\sigma(k)}$, $B^{q,s(k)}_{\sigma(k)}$ and $B^{\phi}_{\sigma(k)}$, where the time index $k$ combines the effect of $\sigma(k)$ and $s(k)$.

**Remark 2.** *As a common treatment [15, 28, 41, 45, 46], the boundary flows, denoted by $\phi^1_k$ and $\phi^2_k$, are considered to be system inputs (please refer to [86] for the concept of using ghost cells to compute boundary flows using boundary state measurements). Another treatment of the SMM does not assume that the boundary flows are available, and assign a constant dynamics for the boundary cells subject to some uncertainty (under the precondition that boundary measurements will be available and will be integrated through the update equations within the filter in the estimation process). Note that all results and proofs regarding the performance analysis of the KF in traffic estimation problems hold for either formulation, and the reader is referred to [16] for the analysis under the alternative formulation.*

#### 2.3.2.1 Explicit formula of the SMM

Before showing the precise formula of the SMM under different modes, we first introduce some notation which will be used as elements of the matrices in the SMM. For all $p \in$

$\{1, 2, \cdots, n-1\}$, define $\Theta_p \in \mathbb{R}^{p\times p}$ and $\Delta_p \in \mathbb{R}^{p\times p}$ by their $(i,j)^{\text{th}}$ entries as

$$\Theta_p(i,j) = \begin{cases} 1 - \frac{v_{\text{m}}\Delta t}{\Delta x} & \text{if } i = j \\ \frac{v_{\text{m}}\Delta t}{\Delta x} & \text{if } i = j+1 \\ 0 & \text{otherwise,} \end{cases}$$

$$\Delta_p(i,j) = \begin{cases} 1 - \frac{w\Delta t}{\Delta x} & \text{if } i = j \\ \frac{w\Delta t}{\Delta x} & \text{if } i = j-1 \\ 0 & \text{otherwise.} \end{cases}$$

For $p_1 \in \mathbb{N}^+$, $p_2 \in \mathbb{N}^+$, $p_3 \in \mathbb{N}^+$ and $p_4 \in \mathbb{N}^+$, define $E_{p_1,p_2}^{p_3,p_4} \in \mathbb{R}^{p_1\times p_2}$ as the $p_1 \times p_2$ matrix with all entries zero except its $(p_3,p_4)^{\text{th}}$ entry, which is one. Explicitly,

$$E_{p_1,p_2}^{p_3,p_4}(i,j) = \begin{cases} 1 & \text{if } i = p_3 \text{ and } j = p_4 \\ 0 & \text{otherwise.} \end{cases}$$

Moreover, define $\tilde{\Theta}_p \in \mathbb{R}^{p\times p}$ and $\tilde{\Delta}_p \in \mathbb{R}^{p\times p}$ as:

$$\tilde{\Theta}_p = \begin{cases} \begin{pmatrix} \Theta_{p-1} & \mathbf{0}_{p-1,1} \\ \frac{v_{\text{m}}\Delta t}{\Delta x} E_{1,p-1}^{1,p-1} & 1 \end{pmatrix} & \text{if } p \geq 2 \\ 1 & \text{if } p = 1, \end{cases}$$

and

$$\tilde{\Delta}_p = \begin{cases} \begin{pmatrix} 1 & \frac{w\Delta t}{\Delta x} E_{1,p-1}^{1,1} \\ \mathbf{0}_{p-1,1} & \Delta_{p-1} \end{pmatrix} & \text{if } p \geq 2 \\ 1 & \text{if } p = 1. \end{cases}$$

In the FF mode, the mode index $\sigma = \text{FF}$, and the transition does not exist. The explicit forms of $A_\sigma^s$, $B_\sigma^{\rho,s}$, $B_\sigma^{q,s}$, and $B_\sigma^\phi$ are:

$$A_{\text{FF}} = \tilde{\Theta}_n, \;\; B_{\text{FF}}^\rho = B_{\text{FF}}^q = \mathbf{0}_{n,n}, \;\; B_{\text{FF}}^\phi = \frac{\Delta t}{\Delta x}\left(E_{n,2}^{1,1} - E_{n,2}^{n,2}\right).$$

In the CC mode, the transition also does not exist, and

$$A_{\mathrm{CC}} = \tilde{\Delta}_n,\ \ B^{\rho}_{\mathrm{CC}} = \frac{w\Delta t}{\Delta x}\left(-E^{1,2}_{n,n} + E^{n,n}_{n,n}\right),\ \ B^{q}_{\mathrm{CC}} = \mathbf{0}_{n,n},\ \ B^{\phi}_{\mathrm{CC}} = \frac{\Delta t}{\Delta x}\left(E^{1,1}_{n,2} - E^{n,2}_{n,2}\right).$$

In the CF mode, the matrices in the SMM read:

$$A^{s}_{\mathrm{CF}} = \begin{pmatrix} \tilde{\Delta}_s & \mathbf{0}_{s,n-s} \\ \mathbf{0}_{n-s,s} & \tilde{\Theta}_{n-s} \end{pmatrix}, \qquad B^{\rho,s}_{\mathrm{CF}} = \frac{w\Delta t}{\Delta x}\left(-E^{1,2}_{n,n} + E^{s,s}_{n,n}\right),$$
$$B^{q,s}_{\mathrm{CF}} = -\frac{\Delta t}{\Delta x}\left(E^{s,s+1}_{n,n} + E^{s+1,s+1}_{n,n}\right), \qquad B^{\phi,s}_{\mathrm{CF}} = \frac{\Delta t}{\Delta x}\left(E^{1,1}_{n,2} - E^{n,2}_{n,2}\right),$$

Note that $s$ may take any value in $\{1, \cdots, n-1\}$, depending on the location of the center of the expansion fan connecting the congested and freeflow states.

The matrices in the SMM for the FC mode are defined as follows. When the shock (i.e., transition from freeflow to congestion) has positive velocity (or is stationary) and $s \in \{1, \cdots, n-2\}$, or the shock has negative velocity and $s \in \{2, \cdots, n-1\}$, the matrices $A^{s}_{\sigma}$, $B^{\rho,s}_{\sigma}$, $B^{q,s}_{\sigma}$, and $B^{\phi,s}_{\sigma}$ read:

$$A^{s}_{\sigma} = \begin{pmatrix} \Theta_{\tilde{s}} & \mathbf{0}_{\tilde{s},1} & \mathbf{0}_{\tilde{s},\bar{s}} \\ \frac{v_{\mathrm{m}}\Delta t}{\Delta x}E^{1,\tilde{s}}_{1,\tilde{s}} & 1 & \frac{w\Delta t}{\Delta x}E^{1,1}_{1,\bar{s}} \\ \mathbf{0}_{\bar{s},\tilde{s}} & \mathbf{0}_{\bar{s},1} & \Delta_{\bar{s}} \end{pmatrix}, \qquad B^{\rho,s}_{\sigma} = \frac{w\Delta t}{\Delta x}\left(-E^{\bar{s}+1,\bar{s}+2}_{n,n} + E^{n,n}_{n,n}\right),$$
$$B^{q,s}_{\sigma} = \mathbf{0}, \qquad B^{\phi,s}_{\sigma} = \frac{\Delta t}{\Delta x}\left(E^{1,1}_{n,2} - E^{n,2}_{n,2}\right),$$

where

$$\tilde{s} = \begin{cases} s & \text{if the shock has positive velocity (or is stationary),} \\ s-1 & \text{if the shock has negative velocity,} \end{cases}$$

and $\bar{s} = n - 1 - \tilde{s}$. When the shock has positive velocity (or is stationary) and $s = n-1$, the system dynamics of the SMM coincide with that when $\sigma = \mathrm{FF}$. When the shock has negative velocity and $s = 1$, the system dynamics of the SMM is the same as when $\sigma = \mathrm{CC}$.

#### 2.3.2.2 Properties of the state transition matricides of the SMM

Some properties of the state transition matrices $A_k$ of the SMM are summarized below. These properties assume important roles in the theoretical performance analysis of the KF when it is used for traffic estimation based on the SMM.

(P.1): For $A_k$ in all modes of the SMM, each entry satisfies

$$0 \leq A_k(r,c) \leq 1, \quad \text{for all } k \in \mathbb{N} \text{ and } r,c \in \{1,2,\cdots,n\}.$$

This property is true due to the CFL condition (2.9) in the discretization scheme (2.7).

(P.2): The sum of the entries in $A_k$ at the same column satisfies

$$\sum_{r=1}^{n} A_k(r,c) \leq 1, \quad \text{for all } k \in \mathbb{N} \text{ and } c \in \{1,2,\cdots,n\}.$$

This property is due to the CFL condition as in (P.1) and the conservation law embedded in the traffic model.

## 2.4 Observability of the switching mode model

Incorporating model noise in the SMM (2.12) yields:

$$\rho_{k+1} = A_k \rho_k + u_k + \omega_k, \quad \rho_k \in \mathbb{R}^n, \tag{2.13}$$

where $\omega_k \sim \mathbf{N}(0, Q_k)$ is the white Gaussian model noise, and the deterministic system input is defined as:

$$u_k = B_k^{\rho} \mathbf{1} \varrho_{\mathrm{m}} + B_k^{q} \mathbf{1} q_{\mathrm{m}} + B_k^{\phi} \phi_k. \tag{2.14}$$

The boundary sensor measurements are modeled as follows:

$$z_k = H_k \rho_k + v_k, \quad z_k \in \mathbb{R}^m, \tag{2.15}$$

where $H_k$ is the observation matrix at time $k$, and $v_k \sim \mathbf{N}(0, R_k)$. Hence, as shown in (2.13)-(2.15), the system dynamics of the SMM is rewritten in the form of (2.1)-(2.2). From an estimation point of view, the following assumptions are made regarding sensor location and model/measurement accuracy:

(Asm.2): As shown in Figure 2.2, for each freeway section, sensors are located at the first and last cells, such that the densities $\rho_k^1$ and $\rho_k^n$ are directly measured. This is motivated by the fact that freeway sections can be partitioned at locations where the sensors are physically located.

(Asm.3): The boundary density measurements are sufficiently accurate to distinguish between the modes of the SMM, but they cannot determine the precise location or direction of a shock.

(Asm.4): The noise models satisfy $q_1 I < Q_k < q_2 I$ and $r_1 I < R_k < r_2 I$ for all $k$, where $q_1$, $q_2$, $r_1$ and $r_2$ are positive constants.

Given (Asm.2), the observation matrix is expressed as follows for all $k$:

$$H_k = H_b = \begin{pmatrix} 1 & 0 & \cdots & 0 & 0 \\ 0 & 0 & \cdots & 0 & 1 \end{pmatrix} \in \mathbb{R}^{2\times n}. \tag{2.16}$$

The observability of system (2.13)-(2.15) under different modes are listed in Table 2.1, which can be derived directly from the definition of observability stated in Definition 1, i.e., checking the boundedness of the information matrix. According to Table 2.1, there are three observable modes and one unobservable mode in the SMM. We classify the state transition matrices according to the observability of the SMM. Define the matrix set with state transition matrices associated with the observable and unobservable modes as $\mathcal{A}_{\mathrm{O}} = \{A_{\mathrm{FF}}, A_{\mathrm{CC}}, A_{\mathrm{CF}}^s \,|s \in \{1, 2, \cdots, n-1\}\}$ and $\mathcal{A}_{\mathrm{U}} = \{A_{\mathrm{FC}}^s \,|s \in \{1, 2, \cdots, n-1\}\}$, respectively. The set of all state transition matrices is thus defined as $\mathcal{A} = \mathcal{A}_{\mathrm{O}} \cup \mathcal{A}_{\mathrm{U}}$.

**Remark 3.** *In this dissertation, we define the modes of the SMM based only on the freeflow / congestion status of the two boundary cells, which means that we combine the FC1 and FC2 modes in [16] into one mode (i.e., no matter the shock has positive or negative speed or is stationary, we treat them as the same mode as long as the upstream part of the section is in freeflow, and the downstream part is in congestion). This choice is made to ensure*

Table 2.1: Observability of the SMM[15]

| Mode | Upstream | Downstream | Observability[1] |
|---|---|---|---|
| FF | Freeflow | Freeflow | Uniformly completely observable |
| CC | Congested | Congested | Uniformly completely observable |
| CF | Congested | Freeflow | Uniformly completely observable |
| FC | Freeflow | Congested | unobservable |

[1] The FC mode is not observable unless density measurements of all the cells are available, which does not occur in practical discretizations of road networks.

*consistency with the criteria of mode definition in the switching mode model with junctions (SMM-J) discussed in Chapter 4. Note that the state transition matrices of the SMM can switch while remaining in the FC mode, since the location and the velocity of the shock can change.*

The results in Table 2.1 state the observability of the SMM when it stays inside a single mode. In fact, the observability result of the SMM can be even stronger. In the next lemma, we show that the SMM is UCO when the system switches arbitrarily among the observable modes. As a related note, under switching sequences containing the unobservable mode of the SMM, the system cannot be UCO under arbitrary switches.

**Lemma 1** (Uniform complete observability of the SMM under switches among observable modes)**.** *Given boundary measurements shown in* (2.15)-(2.16)*, the switching mode model is uniformly completely observable under arbitrary switches among the observable modes (i.e., FF, CC, and CF). Explicitly, define*

$$T_1 = \max\{1, n-2\}, \tag{2.17}$$

*and*

$$\begin{aligned}
\alpha_{\mathcal{I}} &= r_2^{-1} \min_{M_\kappa \in \mathcal{A}_{\mathrm{O}}} \left\{ \lambda_{\min} \left( \left( H_b^\top H_b + \sum_{\iota=1}^{T_1} \left( \prod_{\kappa=\iota}^{T_1} M_\kappa^{-1} \right)^\top H_b^\top H_b \left( \prod_{\kappa=\iota}^{T_1} M_\kappa^{-1} \right) \right) \right) \right\}, \\
\beta_{\mathcal{I}} &= r_1^{-1} \max_{M_\kappa \in \mathcal{A}_{\mathrm{O}}} \left\{ \lambda_{\max} \left( \left( I + \sum_{\iota=1}^{T_1} \left( \prod_{\kappa=\iota}^{T_1} M_\kappa^{-1} \right)^\top \left( \prod_{\kappa=\iota}^{T_1} M_\kappa^{-1} \right) \right) \right) \right\},
\end{aligned} \tag{2.18}$$

*where $\lambda_{\min}(\cdot)$ and $\lambda_{\max}(\cdot)$ are the minimum and maximum eigenvalues of a matrix, respec-*

*tively. The information matrix satisfies*

$$\alpha_{\mathcal{I}} I < \mathcal{I}_{k,k-T_1} < \beta_{\mathcal{I}} I, \quad \textit{for all } k \geq T_1,$$

*which meets the requirements of uniform complete observability in Definition 1.*

*Proof.* The proof is reported in Appendix C.1. □

Now we have introduced the SMM and derived basic properties related to its state transition matrices and observability. In the next chapter, we provide a formal analysis of the performance of the Kalman filter estimating traffic conditions based on the SMM.

# CHAPTER 3

# ERROR BOUNDS OF THE KALMAN FILTER ON ONE-DIMENSIONAL ROAD SECTIONS

## 3.1 Introduction

In this chapter, we derive the analytical error bounds of the *Kalman filter* (KF) [87] estimating traffic conditions based on the SMM. We consider both observable and unobservable scenarios, even when the system switches among the observable and unobservable modes. Here, we consider one-dimensional road sections to establish the main proof techniques on a simple road structure that does not include junctions. Based on the analysis in this chapter, the error bounds on road networks with junctions will be treated in Chapter 4. The new contributions of this chapter are listed as follows.

- **Convergence rate of the mean error under switches among the observable modes of the SMM.** Given the uniform complete observability of the SMM under switches among the observable modes, we first derive the analytical forms of the upper and lower bounds of the estimation error covariance of the KF. Next, based on the derived bounds, we obtain the convergence rate of the mean estimation error of the KF when the system is observable.

- **Uniform upper bound of the mean error under the unobservable mode of the SMM.** We first leverage the properties of the state transition matrices of the SMM to derive a uniform upper bound of the infinity norm of the Kalman gain under unobservable time intervals. Next, given the derived bounds for the Kalman gain, we combine the intrinsic properties of the traffic model and the update schemes of the KF to derive an uniform upper bound for the 2-norm of the mean estimation error, which characterizes the maximum increase of the mean error when the system is unobservable.

- **Error bounds of the KF under switches among the observable and unobservable modes.** We combine the above results to derive the minimum residence time in the observable mode(s) to offset the increase of the mean error in the unobservable mode, and the error bounds of the KF under switches among the observable and unobservable modes.

This chapter is organized as follows. In Section 3.2, we review the KF and its general performance under general observable and unobservable systems. The convergence rate of the mean error under observable modes is studied in Section 3.3. Section 3.4 shows the uniform upper bound of the infinity norm of the Kalman gain (Section 3.4.1) and the ultimate boundedness of the mean error (Section 3.4.2) when the system is unobservable. Finally in Section 3.5, the upper bound of the mean error in unobservable time intervals (Section 3.5.1) and the minimum residence time in observable time intervals (Section 3.5.2) are combined together to derive the error bounds of the KF under switches among the observable and unobservable modes (Section 3.5.3).

## 3.2 Kalman filter

Given a dynamic system with a collection of state measurements up to the current time, the *filtering problem* aims at computing real-time estimate of the current state. This consists of iteratively predicting the state using the system model, and updating the state estimate once new measurements become available. The KF is one of the most well-known sequential estimation algorithm which relies on the *Bayes' rule* to compute the conditional distribution of the state given the available measurements and the system model describing the evolution of the state.

Consider a general linear time-varying system (2.1)-(2.2), given the sensor data up to time $k$ (i.e., $z_0, \cdots, z_k$), the *prior estimate* and *posterior estimate* of the state can be expressed as $\rho_{k|k-1} = \mathbb{E}[\rho_k|z_0, \cdots, z_{k-1}]$ and $\rho_{k|k} = \mathbb{E}[\rho_k|z_0, \cdots, z_k]$, respectively. Let $\eta_{k|k-1} = \rho_{k|k-1} - \rho_k$ and $\eta_{k|k} = \rho_{k|k} - \rho_k$ denote the prior and posterior estimation errors. The estimation error covariance matrices associated with $\rho_{k|k-1}$ and $\rho_{k|k}$ are given by $\Gamma_{k|k-1} = \mathbb{E}[\eta_{k|k-1}\eta_{k|k-1}^\top|z_0, \cdots, z_{k-1}]$ and $\Gamma_{k|k} = \mathbb{E}[\eta_{k|k}\eta_{k|k}^\top|z_0, \cdots, z_k]$. The KF sequentially

computes $\rho_{k|k}$ from $\rho_{k-1|k-1}$ as follows:

$$\text{Time update:} \begin{cases} \rho_{k|k-1} = A_{k-1}\rho_{k-1|k-1} + u_{k-1} \\ \Gamma_{k|k-1} = A_{k-1}\Gamma_{k-1|k-1}A_{k-1}^{\top} + Q_{k-1}, \end{cases} \tag{3.1}$$

$$\text{Information update:} \begin{cases} \rho_{k|k} = \rho_{k|k-1} + K_k(z_k - H_k\rho_{k|k-1}) \\ \Gamma_{k|k} = \Gamma_{k|k-1} - K_kH_k\Gamma_{k|k-1} \\ K_k = \Gamma_{k|k-1}H_k^{\top}(R_k + H_k\Gamma_{k|k-1}H_k^{\top})^{-1}, \end{cases} \tag{3.2}$$

where the matrix $K_k$ is denoted as the *Kalman gain* at time $k$. In the KF, the forecast step updates the state estimate and the estimation error covariance based on the system model given in (2.1), and the analysis step refines the estimates based on the latest obtained sensor measurements. Note that for all $k$, the state estimates $\rho_{k|k-1}$ and $\rho_{k|k}$ are random vectors. The mean posterior estimate and the mean posterior estimation error[1] are denoted as $\boldsymbol{\rho}_{k|k}$ and $\boldsymbol{\eta}_{k|k}$, respectively.

### 3.2.1 Performance of the Kalman filter under observable and unobservable systems

When the KF (3.1)-(3.2) estimates a system which is uniformly completely observable, its estimation error covariance is guaranteed to be bounded (both from below and above), and its mean estimation error converges exponentially to zero, as stated in the next lemma.

**Lemma 2** (Chapter 7.6 in [19])**.** *If the dynamical system* (2.1)-(2.2) *is uniformly completely observable, and there exist positive constants* $q_1$*,* $q_2$*,* $r_1$ *and* $r_2$ *such that* $q_1I_n < Q_k < q_2I_n$ *and* $r_1I_m < R_k < r_2I_m$ *for all* $k$*. Moreover, assume the following conditions hold:*

*(Asm.5): the initial error covariance is positive definite, i.e.,* $\Gamma_{0|0} > \mathbf{0}$*;*

*(Asm.6): the state transition matrix* $A_k$ *is nonsingular for all* $k$*,*

*then there exist positive constants* $c_1 > 0$ *and* $c_2 > 0$ *such that the error covariance of the KF* (3.1)-(3.2) *satisfies*

$$c_1I < \Gamma_{k|k} < c_2I, \quad \textit{for all } k \geq 0.$$

[1]For the remainder of this dissertation, the term state estimates/estimation errors/error covariance refers to the posterior estimates, unless specified otherwise.

*Moreover, there exists positive constants* $a > 0$ *and* $0 < q < 1$ *such that the 2-norm*[2] *of the mean estimation error satisfies*

$$\left\|\boldsymbol{\eta}_{k|k}\right\| \leq aq^k \left\|\boldsymbol{\eta}_{0|0}\right\|, \quad \textit{for all } k \geq 0.$$

When system (2.1)-(2.2) is not observable, the mean estimation error $\boldsymbol{\eta}_{k|k}$ and the error covariance $\Gamma_{k|k}$ of the KF will diverge, unless the unobservable part of the state is bounded or converges to zero automatically [18, 19]. We present in Appendix A an example illustrating the evolution of the mean estimation error given by the KF when tracking an unobservable system.

## 3.3 Convergence rate of the mean error under observable scenarios

In this section, we derive the upper and lower bounds of the error covariance, as well as the convergence rate of the mean estimation error stated in Lemma 2, explicitly for the KF estimating observable traffic conditions under system (2.13)-(2.16), i.e., the system switches among the observable modes of the SMM ($A_k \in \mathcal{A}_{\mathrm{O}}$ for all $k \in \mathbb{N}$). Note that (Asm.1)-(Asm.6) are necessary for the results derived for the remainder of this chapter. As stated in Section 2.3.2 and Section 2.4, (Asm.1)-(Asm.3) are motivated by practical applications, (Asm.4)-(Asm.5) can be ensured when setting up the parameters in the KF, and it can be verified that (Asm.6) always holds for the state transitions matrices of the SMM.

### 3.3.1 Upper and lower bounds of the error covariance matrix

The explicit forms of the upper and lower bounds of the error covariance are given in Lemma 5. The derivation of the bounds is divided into the following three parts.

1. In Lemma 3, the upper and lower bounds of $\Gamma_{k|k}$ for a freeway section are derived for $k \geq \max\{1, n-2\}$, which are independent of the initial conditions.

2. In Lemma 4, the upper and lower bounds of $\Gamma_{k|k}$ for the freeway section are derived for $0 \leq k < \max\{1, n-2\}$, which are functions of the initial error covariance $\Gamma_{0|0}$.

[2]For the remainder of this dissertation, we denote as $\|\cdot\|$ the 2-norm of a matrix or a vector.

3. The results in Lemma 3 and Lemma 4 are combined together in Lemma 5 to express the upper and lower bounds of $\Gamma_{k|k}$ for the freeway section, and the derived bounds are uniform across all time steps $k \geq 0$.

The next lemma shows that the upper and lower bounds of $\Gamma_{k|k}$ for a freeway section are independent of the initial condition $\Gamma_{0|0}$ when $k \geq \max\{1, n-2\}$.

**Lemma 3.** *Consider a freeway section of dimension $n \geq 2$ under system (2.13)-(2.16), and the system switches arbitrarily among observable modes of the SMM. If $\Gamma_{0|0} > \mathbf{0}$, the error covariance of the KF (3.1)-(3.2) satisfies*

$$\mathbf{0} < \tilde{c}_1 I < \Gamma_{k|k} < \tilde{c}_2 I, \quad \textit{for all } k \geq T_1,$$

*where*

$$\tilde{c}_1 = \frac{\min\{\alpha_{\mathcal{I}}, \alpha_{\mathcal{C}}\}}{1 + \min\{\alpha_{\mathcal{I}}, \alpha_{\mathcal{C}}\} \max\{\beta_{\mathcal{I}}, \beta_{\mathcal{C}}\}} > 0, \quad \tilde{c}_2 = \tilde{c}_1^{-1} > 0, \tag{3.3}$$

*with $T_1$, $\alpha_{\mathcal{I}}$, $\beta_{\mathcal{I}}$ defined in (2.17)-(2.18) and* [3]

$$\begin{aligned} \alpha_{\mathcal{C}} &= q_1 \min_{M_\kappa \in \mathcal{A}_{\mathrm{O}}} \left\{ \lambda_{\min} \left( I + \sum_{\iota=1}^{T_1-1} \left( \prod_{\kappa=\iota}^{T_1-1} M_\kappa \right) \left( \prod_{\kappa=\iota}^{T_1-1} M_\kappa \right)^\top \right) \right\}, \\ \beta_{\mathcal{C}} &= q_2 \max_{M_\kappa \in \mathcal{A}_{\mathrm{O}}} \left\{ \lambda_{\max} \left( I + \sum_{\iota=1}^{T_1-1} \left( \prod_{\kappa=\iota}^{T_1-1} M_\kappa \right) \left( \prod_{\kappa=\iota}^{T_1-1} M_\kappa \right)^\top \right) \right\}. \end{aligned} \tag{3.4}$$

*Proof.* The proof is reported in Appendix C.2. □

The next lemma derives the upper and lower bounds of $\Gamma_{k|k}$ for a freeway section when $0 \leq k < \max\{1, n-2\}$, which are functions of the initial condition $\Gamma_{0|0}$.

**Lemma 4.** *Consider a freeway section of dimension $n \geq 2$ under system (2.13)-(2.16), and the system switches arbitrarily among observable modes of the SMM. If $\Gamma_{0|0} > \mathbf{0}$, the error covariance of the KF (3.1)-(3.2) satisfies*

$$\mathbf{0} < \tilde{\mathrm{c}}_1 \left(\Gamma_{0|0}\right) I \leq \Gamma_{k|k} \leq \tilde{\mathrm{c}}_2 \left(\Gamma_{0|0}\right) I, \quad \textit{for all } 0 \leq k < \max\{1, n-2\},$$

[3] When $T_1 = 1$, the definitions of $\alpha_{\mathcal{C}}$ and $\beta_{\mathcal{C}}$ are given by $\alpha_{\mathcal{C}} = q_1$ and $\beta_{\mathcal{C}} = q_2$, respectively.

*where* $\tilde{\mathrm{c}}_1(\cdot)$ *and* $\tilde{\mathrm{c}}_2(\cdot)$ *are functions of* $M \in \mathbb{R}^{n\times n}$*, and are defined as follows:*

$$\tilde{\mathrm{c}}_1(M) = \min\left\{\lambda_{\min}(M), \left(q_1^{-1} + r_1^{-1}\right)^{-1}\right\}. \tag{3.5}$$

*and*

$$\tilde{\mathrm{c}}_2(M) = \begin{cases} 2(2n-5)\|M\| + \left(2(n-3)^2 - 1\right) q_2 & \text{if } n \geq 4 \\ \|M\| & \text{if } 2 \leq n < 4. \end{cases} \tag{3.6}$$

*Proof.* The proof is reported in Appendix C.3. □

Combining Lemma 3 and 4, the upper and lower bounds for the error covariance is obtained for all $k \geq 0$, as stated next in Lemma 5.

**Lemma 5** (Uniform lower and upper bounds of the error covariance under observable modes of the SMM)**.** *Consider a freeway section of dimension* $n \geq 2$ *under system* (2.13)-(2.16)*, and the system switches arbitrarily among observable modes of the SMM. If* $\Gamma_{0|0} > \mathbf{0}$*, the error covariance of the KF* (3.1)-(3.2) *satisfies*

$$\mathbf{0} < \mathrm{c}_1\left(\Gamma_{0|0}\right) I \leq \Gamma_{k|k} \leq \mathrm{c}_2\left(\Gamma_{0|0}\right) I, \quad \text{for } k \geq 0, \tag{3.7}$$

*independent of the switching sequence, where* $\mathrm{c}_1(\cdot)$ *and* $\mathrm{c}_2(\cdot)$ *are functions of* $M \in \mathbb{R}^{n\times n}$ *defined as follows:*

$$\mathrm{c}_1(M) = \min\left\{\tilde{\mathrm{c}}_1(M), \tilde{c}_1\right\}$$
$$\mathrm{c}_2(M) = \max\left\{\tilde{\mathrm{c}}_2(M), \tilde{c}_2\right\},$$

*with* $\tilde{\mathrm{c}}_1(\cdot)$*,* $\tilde{\mathrm{c}}_2(\cdot)$ *defined in* (3.5)-(3.6) *(cf. Lemma 4), and* $\tilde{c}_1$*,* $\tilde{c}_2$ *defined in* (3.3) *(cf. Lemma 3).*

### 3.3.2 Convergence rate of the mean estimation error

This subsection computes the convergence rate of the mean error (i.e., deriving the values of $a$ and $q$ in Lemma 2) for the KF when the system switches arbitrarily among the observable modes of the SMM. According to the update schemes (3.1)-(3.2) of the KF, the evolution

of the mean estimation error is given by:

$$\boldsymbol{\eta}_{k|k} = \prod_{\kappa=k-1}^{0} F_{\kappa+1} A_{\kappa} \boldsymbol{\eta}_{0|0}, \tag{3.8}$$

where

$$F_k = I - K_k H_k. \tag{3.9}$$

According to (3.8), we need to analyze the magnitude of $\left\| \prod_{\kappa=k-1}^{0} F_{\kappa+1} A_{\kappa} \right\|$ in order to study the convergence rate of the mean error, which is detailed in the next lemma.

**Lemma 6** (Convergence rate of the mean error under observable modes of the SMM)**.** *Consider a freeway section of dimension $n \geq 2$ under system* (2.13)-(2.16)*, and the system switches arbitrarily among the observable modes of the SMM while $k \in [\underline{k}_{\mathrm{O}}, +\infty)$. If the error covariance satisfies $\mathbf{0} < c_1 I \leq \Gamma_{k|k} \leq c_2 I$ for all $k \in [\underline{k}_{\mathrm{O}}, +\infty)$, where $c_1, c_2 \in \mathbb{R}^+$, then*

$$\left\| \boldsymbol{\eta}_{k|k} \right\| \leq \left\| \prod_{\kappa=k-1}^{\underline{k}_{\mathrm{U}}} F_{\kappa+1} A_{\kappa} \right\| \left\| \boldsymbol{\eta}_{0|0} \right\| \leq \hat{a} \hat{q}^k \left\| \boldsymbol{\eta}_{0|0} \right\|, \quad \textit{for all } k \in [\underline{k}_{\mathrm{O}}, +\infty), \tag{3.10}$$

*where $\hat{a} = \left(c_1^{-1} c_2\right)^{\frac{1}{2}} \geq 1$, $0 < \hat{q} = \left(1 - \mathrm{d}\left(c_1, c_2\right) c_1\right)^{\frac{1}{2}} < 1$, and $\mathrm{d}\left(\cdot, \cdot\right)$ is a function of $c_1, c_2$ defined by*

$$\mathrm{d}\left(c_1, c_2\right) = \left( c_2 + q_1^{-1} c_2^2 \max_{M \in \mathcal{A}_{\mathrm{O}}} \sigma_{\max}^2 \left(M\right) \right)^{-1}.$$

*Proof.* The proof is reported in Appendix C.4. □

## 3.4 Ultimate boundedness of the mean error under unobservable scenarios

Challenges for estimating an unobservable system stem from the fact that the estimation error covariance could grow unbounded, thus the mean estimation error also potentially diverges (as shown in Appendix A). In this section, we show that when combining the physical properties of the traffic model (i.e., vehicle conservation, flow–density relationship, and conditions on the discretization scheme) with the update scheme of the KF, the bounds of the mean estimation error can be derived.

In particular, we show that all the cells in an unobservable section are ultimately bounded inside $(-\epsilon, \varrho_{\mathrm{m}} + \epsilon)$ for all $\epsilon > 0$, provided that the density measurements of the boundary cells are available. This ensures that the mean estimates of the KF for the unobservable mode are always physically meaningful to within $\epsilon$. Comparatively, it is shown in [47] that an open-loop observer may result in non-physical state estimates in unobservable scenarios. The ultimate boundedness of the mean state estimate also ensures that the mean estimation error is ultimately bounded.

### 3.4.1 Boundedness of the Kalman gain

Let $(\underline{k}_{\mathrm{U}}, \bar{k}_{\mathrm{U}}]$ be the time interval inside which the road section stays in the unobservable mode of the SMM. In this subsection, we present a lemma (i.e., Lemma 7) stating the boundedness of the Kalman gain for $k \in (\underline{k}_{\mathrm{U}}, \bar{k}_{\mathrm{U}}]$. According to the KF update scheme in (3.2), the boundedness of the Kalman gain is a necessary condition for the boundedness of the state estimate. Note that Lemma 7 is also applicable for the KF estimating traffic condition under the *switching mode model with junctions* (SMM-J), hence the bound of the Kalman gain is presented in a general form. The reader is referred to [88, Lemma 2] for a bound of the infinity norm of the Kalman gain derived exclusively for the SMM.

The boundedness of the Kalman gain is derived based on the boundedness of the cross-covariance of the observable and unobservable subsystems in the *Kalman observability canonical form*, where the state is transformed such that the observable and unobservable parts of the state are separated:

$$\check{\rho}_k = U\rho_k = \begin{pmatrix} \check{\rho}_k^{(1)} \\ \check{\rho}_k^{(2)} \end{pmatrix},$$

where $\check{\rho}_k$ is the transformed state at time $k$, $U$ is an orthogonal matrix, $\check{\rho}_k^{(1)} \in \mathbb{R}^{d_1}$ and $\check{\rho}_k^{(2)} \in \mathbb{R}^{d_2}$ are the state in the observable and unobservable subsystems, respectively, with $d_1 + d_2 = n$. In addition, the state transition matrix $A_k$ is also transformed as follows:

$$\check{A}_k = UA_kU^\top = \begin{pmatrix} \check{A}_k^{(1)} & \mathbf{0}_{d_1,d_2} \\ \check{A}_k^{(21)} & \check{A}_k^{(2)} \end{pmatrix}.$$

A detailed discussion regarding the observable and unobservable subsystems in the unobservable modes is provided in Appendix B.

**Lemma 7** (Boundedness of the Kalman gain under the unobservable modes of SMM and SMM-J)**.** *Consider an road section shown in Figure 2.2 (resp. Figure 4.3). The system switches inside*[4] *an unobservable mode of the SMM (resp. SMM-J) while* $k \in (\underline{k}_{\mathrm{U}}, \bar{k}_{\mathrm{U}}]$*, where* $0 \leq \underline{k}_{\mathrm{U}} < \bar{k}_{\mathrm{U}} \leq +\infty$*. Define*

$$a_1 = \max_{k\in(\underline{k}_{\mathrm{U}},\bar{k}_{\mathrm{U}}]} \left\{\|A_k\|_\infty\right\}, \;\; a_2 = \max_{k\in(\underline{k}_{\mathrm{U}},\bar{k}_{\mathrm{U}}]} \left\{\left\|A_k^\top\right\|_\infty\right\}, \tag{3.11}$$

*and*

$$\check{a}_1 = \max_{k\in(\underline{k}_{\mathrm{U}},\bar{k}_{\mathrm{U}}]} \left\|A_k^{(1)}\right\|_\infty, \qquad \check{a}_2 = \max_{k\in(\underline{k}_{\mathrm{U}},\bar{k}_{\mathrm{U}}]} \left\|\left(A_k^{(1)}\right)^\top\right\|_\infty, \tag{3.12}$$

$$\check{a}_3 = \max_{k\in(\underline{k}_{\mathrm{U}},\bar{k}_{\mathrm{U}}]} \sigma_{\max}\left(\check{A}_k^{(1)}\right), \qquad \check{a}_4 = \max_{k\in(\underline{k}_{\mathrm{U}},\bar{k}_{\mathrm{U}}]} \left\|\check{A}_k^{(21)}\right\|_\infty. \tag{3.13}$$

*Moreover, define as* $\check{c}_1$ *and* $\check{c}_2$ *the lower and upper bound of the error covariance of the observable subsystem, i.e.,*

$$\check{c}_1 I < \check{\Gamma}_{k|k}^{(1)} < \check{c}_2 I, \quad \textit{for all } k \in (\underline{k}_{\mathrm{U}}, \bar{k}_{\mathrm{U}}], \tag{3.14}$$

*and let*

$$\check{c}_3 = \left(\check{c}_2 + q_1^{-1}\check{c}_2^2\check{a}_3\right)^{-1}, \;\; \bar{t} = n^2\sqrt{d_1}\left(\check{c}_2\check{c}_1^{-1}\right)^{\frac{1}{2}}, \;\; \bar{q} = (1-\check{c}_3\check{c}_1)^{\frac{1}{2}}$$
$$\bar{p} = d_1\check{c}_2\check{a}_4\left(\check{a}_1\check{a}_2\check{c}_2 + q_2\right)q_1^{-1} + q_2, \;\; \bar{\gamma} = n\sqrt{n}\left\|\Gamma_{\underline{k}_{\mathrm{U}}|\underline{k}_{\mathrm{U}}}\right\|(a_1a_2)^2 + n\sqrt{n}a_1a_2q_2 + \sqrt{n}q_2,$$

*where* $d_1$ *is the dimension of the observable subsystem. Given density measurements of the three boundary cells, the infinity norm*[5] *of the Kalman gain computed by the KF* (3.1)-(3.2) *satisfies*

$$\|K_k\|_\infty \leq \mathrm{k}\left(\Gamma_{\underline{k}_{\mathrm{U}}|\underline{k}_{\mathrm{U}}}\right), \quad \textit{for all } k \in (\underline{k}_{\mathrm{U}}, \bar{k}_{\mathrm{U}}], \tag{3.15}$$

[4]Recall from Remark 3 that the state transition matrix of the SMM can switch within a mode (if a transition between freeflow and congestion exists), which is also true for the SMM-J.

[5]Recall that for matrix $M \in \mathbb{R}^{p\times q}$, its infinity norm is defined as $\|M\|_\infty = \max_{r\in[p]}\sum_{c=1}^{q}|M(r,c)|$.

*where* $\mathrm{k}(\cdot)$ *is a function of the error covariance at time* $\underline{k}_{\mathrm{U}}$ *defined as*

$$\mathrm{k}\left(\Gamma_{\underline{k}_{\mathrm{U}}|\underline{k}_{\mathrm{U}}}\right) = \frac{d_1\sqrt{m}}{r_1}\max\left\{\frac{\sqrt{n}}{d_1}\left(\left\|\Gamma_{\underline{k}_{\mathrm{U}}|\underline{k}_{\mathrm{U}}}\right\| a_1a_2+q_2\right), \frac{1}{\sqrt{d_1}}\left(\check{a}_1\check{a}_2\check{c}_2+q_2\right), \right.$$
$$\left. \bar{\gamma}, \bar{t}\bar{q}\bar{\gamma}+\bar{p}, \frac{\bar{t}\bar{p}\bar{q}}{1-\bar{q}}+\bar{p}\right\}.$$

*Proof.* The proof is reported in Appendix C.5. □

In the proof of Lemma 7, the Kalman gain is partitioned into blocks corresponding to the observable and unobservable subsystems (as shown in (C.12)). The part corresponding to the observable subsystem is a function of the estimation error covariance of the observable subsystem (see (C.13)), thus its boundedness is relatively straightforward to justify. On the other hand, the block of the Kalman gain that corresponds to the unobservable subsystem is a function of the cross-covariance of the observable and the unobservable subsystems (see (C.14)). By exploring the interaction between the evolution equation of the cross-covariance (shown in (B.4)) and the physical properties of the traffic model (reflected in (P.1)-(P.2) for the SMM and (P.3)-(P.5) for the SMM-J), we also derive the boundedness of the unobservable block of the Kalman gain. In summary, the combination of the update scheme of the KF and the intrinsic properties of the traffic model is critical in showing the boundedness of the Kalman gain under unobservable scenarios.

### 3.4.2 Ultimate boundedness of the mean error in the unobservable mode

Given the necessary condition stated in Lemma 7, the ultimate boundedness of the mean error is shown in the next proposition.

**Proposition 1** (Ultimate bounded mean error under the unobservable mode of SMM)**.** *Consider a road section shown in Figure 2.2 that switches inside the unobservable mode of the SMM while* $k \in (\underline{k}_{\mathrm{U}}, \infty)$*. For all* $\epsilon > 0$*, a finite time* $\bar{\mathrm{t}}(\epsilon)$ *exists such that* $\boldsymbol{\rho}^l_{k|k} \in (-\epsilon, \varrho_{\mathrm{m}}+\epsilon)$ *for all* $k > \underline{k}_{\mathrm{U}} + \bar{\mathrm{t}}(\epsilon)$ *and for all* $l \in \{1, 2, \cdots, n\}$*, independent of the initial estimate. Moreover, the mean estimation error satisfies* $\|\boldsymbol{\eta}_{k|k}\| < \sqrt{n}(\varrho_{\mathrm{m}}+\epsilon)$ *for all* $k > \underline{k}_{\mathrm{U}} + \bar{\mathrm{t}}(\epsilon)$*, independent of the initial estimate.*

*Proof.* The proof is by induction. For all $\epsilon > 0$, since the upstream cell is in the observable

subsystem, we have $\boldsymbol{\rho}^1_{k|k} \to \rho^1_k$, where $\rho^1_k \geq 0$. Hence a finite time $\bar{\mathrm{t}}^1(\epsilon)$ exists such that $\boldsymbol{\rho}^1_{k|k} > -\frac{\epsilon}{n}$ for all $k > \underline{k}_{\mathrm{U}} + \bar{\mathrm{t}}^1(\epsilon)$.

Suppose $\boldsymbol{\rho}^{l-1}_{k|k} > -\frac{(l-1)\epsilon}{n}$. For all $l \in \{2, \cdots, n\}$, if $\boldsymbol{\rho}^l_{k|k} < -\frac{(l-1)\epsilon}{n}$, we obtain from (2.8) that

$$\mathrm{f}\left(\boldsymbol{\rho}^{l-1}_{k|k}, \boldsymbol{\rho}^l_{k|k}\right) > -v_{\mathrm{m}}\frac{(l-1)\epsilon}{n}, \tag{3.16}$$

$$\mathrm{f}\left(\boldsymbol{\rho}^l_{k|k}, \boldsymbol{\rho}^{l+1}_{k|k}\right) \leq v_{\mathrm{m}}\boldsymbol{\rho}^l_{k|k}. \tag{3.17}$$

Combining (3.16) and (3.17) with (2.7), and adding an information update term from the analysis step yields

$$\boldsymbol{\rho}^l_{k+1|k+1} > \boldsymbol{\rho}^l_{k|k} + \frac{v_{\mathrm{m}}\Delta t}{\Delta x}\left|\boldsymbol{\rho}^l_{k|k} + \frac{(l-1)\epsilon}{n}\right| - \mathrm{k}\left(\Gamma_{\underline{k}_{\mathrm{U}}|\underline{k}_{\mathrm{U}}}\right)\left\|\check{\boldsymbol{\eta}}^{(1)}_{k|k}\right\|_\infty, \tag{3.18}$$

where $\mathrm{k}\left(\Gamma_{\underline{k}_{\mathrm{U}}|\underline{k}_{\mathrm{U}}}\right)$ is obtained from Lemma 7, and we denote $\check{\boldsymbol{\eta}}^{(1)}_{k|k} = \left(\boldsymbol{\eta}^1_{k|k}, \boldsymbol{\eta}^n_{k|k}\right)^\top$ as the posterior estimation error of the upstream and downstream cells, which form an observable subsystem (as discussed in Appendix B). It is concluded from (3.18) that there exists scalar $\bar{v}_1 > \frac{\Delta x \mathrm{k}\left(\Gamma_{\underline{k}_{\mathrm{U}}|\underline{k}_{\mathrm{U}}}\right)}{v_{\mathrm{m}}\Delta t}$ such that

$$\boldsymbol{\rho}^l_{k+1|k+1} - \boldsymbol{\rho}^l_{k|k} > \bar{v}_0\left|\boldsymbol{\rho}^l_{k|k} + \frac{(l-1)\epsilon}{n}\right|, \quad \text{for all } \left|\boldsymbol{\rho}^l_{k|k} + \frac{(l-1)\epsilon}{n}\right| \geq \bar{v}_1\left\|\check{\boldsymbol{\eta}}^{(1)}_{k|k}\right\|_\infty,$$

where $\bar{v}_0 = \frac{v_{\mathrm{m}}\Delta t}{\Delta x} - \frac{\mathrm{k}\left(\Gamma_{\underline{k}_{\mathrm{U}}|\underline{k}_{\mathrm{U}}}\right)}{\bar{v}_1} > 0$. Also note that $\left\|\check{\boldsymbol{\eta}}^{(1)}_{k|k}\right\|_\infty \to 0$ as $k \to \infty$, which indicates that the one-step change of the estimates is ultimately positive, and large enough so that a finite time $\bar{\mathrm{t}}^l(\epsilon)$ exists such that $\boldsymbol{\rho}^l_{k|k} > -\frac{l\epsilon}{n}$ for all $k > \underline{k}_{\mathrm{U}} + \bar{\mathrm{t}}^l(\epsilon)$ [89].

By induction we conclude that if $\boldsymbol{\rho}^{n-1}_{k|k} > -\frac{(n-1)\epsilon}{n}$, a finite time $\bar{\mathrm{t}}^n(\epsilon)$ exists such that $\boldsymbol{\rho}^n_{k|k} > -\epsilon$ for all $k > \underline{k}_{\mathrm{U}} + \bar{\mathrm{t}}^n(\epsilon)$. Letting $\bar{\mathrm{t}}(\epsilon) = \max_l\{\bar{\mathrm{t}}^l(\epsilon)\} = \bar{\mathrm{t}}^n(\epsilon)$, we obtain $\boldsymbol{\rho}^l_{k|k} > -\epsilon$ for all $k > \underline{k}_{\mathrm{U}} + \bar{\mathrm{t}}(\epsilon)$ and $l \in \{1, 2, \cdots, n\}$. This proves the ultimate lower bound of the estimates. The proof for an ultimate upper bound is similar, with a variation that the induction is conducted from cell $n$ to cell 1. □

Proposition 1 indicates that when the estimation error of the boundary cells converges to zero, it will drive the state estimate of the interior cells inside $[0, \varrho_{\mathrm{m}}]$ due to the conservation law and the flow-density relationship embedded in the traffic model. Hence, it is important

to ensure that the errors of the boundary cells are asymptotic stable, which is achieved by the KF through feeding measurements into the state estimates in the information update step. In contrast, an open-loop observer may lead to physically unreasonable estimates due to the lack of measurement feedback, as shown in [47].

## 3.5 Boundedness of the mean error under switches among observable and unobservable modes

This section derives the upper bound for the 2-norm of the mean estimation error when a freeway section switches among observable and unobservable modes. We first analyze the upper bound of the mean error when the section switches inside the unobservable mode, which quantifies the increase of the mean error while the section is unobservable. Next, we leverage the convergence rate of the mean error in observable modes (studied in Lemma 6) to derive the minimum number of time steps (i.e., the residence time) required in observable modes to offset the increase of the mean error during the unobservable scenario. Finally, we combine the analysis above to derive the boundedness of the mean error under switched among observable and unobservable modes.

### 3.5.1 Upper bound of the mean error in the unobservable mode

Let $(\underline{k}_{\mathrm{U}}, \bar{k}_{\mathrm{U}}]$ be the time interval inside which a section switches inside the unobservable mode, i.e., the mode index $\sigma(k) \in \{\mathrm{FC}\}$ for $k \in (\underline{k}_{\mathrm{U}}, \bar{k}_{\mathrm{U}}]$, and $\sigma(k) \in \{\mathrm{FF}, \mathrm{CC}, \mathrm{CF}\}$ for $k = \underline{k}_{\mathrm{U}}$ and $k = \bar{k}_{\mathrm{U}} + 1$. Based on Lemma 7, the next proposition derives an upper bound for $\|\boldsymbol{\eta}_{k|k}\|$ which is uniform across all $k \in (\underline{k}_{\mathrm{U}}, \bar{k}_{\mathrm{U}}]$. The derived bound is a function of $\epsilon$ and $\Gamma_{\underline{k}_{\mathrm{U}}|\underline{k}_{\mathrm{U}}}$ (where $\epsilon$ is the upper bound for $\|\boldsymbol{\eta}_{\underline{k}_{\mathrm{U}}|\underline{k}_{\mathrm{U}}}\|$). Moreover, the derived bound does not depend on the length of the time interval $(\underline{k}_{\mathrm{U}}, \bar{k}_{\mathrm{U}}]$.

**Proposition 2** (Uniform upper bound of the mean error under the unobservable mode of SMM)**.** *Consider a road section shown in Figure 2.2 that switches inside the unobservable*

*mode of the SMM while* $k \in (\underline{k}_{\mathrm{U}}, \bar{k}_{\mathrm{U}}]$*, where* $0 \leq \underline{k}_{\mathrm{U}} < \bar{k}_{\mathrm{U}} \leq +\infty$*. Let*

$$\begin{aligned} c_0 &= \max\left\{1, r_2 q_1^{-1}\sqrt{\check{c}_2\check{c}_1^{-1}}\right\}, \\ \mathrm{c}\left(\Gamma_{\underline{k}_{\mathrm{U}}|\underline{k}_{\mathrm{U}}}\right) &= c_0 \Delta x \mathrm{k}\left(\Gamma_{\underline{k}_{\mathrm{U}}|\underline{k}_{\mathrm{U}}}\right)\left(\Delta t \min\left\{v_{\mathrm{m}}, w\right\}\right)^{-1}, \end{aligned} \tag{3.19}$$

*where* $\check{c}_1$*,* $\check{c}_2$ *are defined in* (3.14)*, and* $\mathrm{k}(\cdot)$ *is given in* (3.15)*. For all* $\epsilon > 0$*, if* $\left\|\boldsymbol{\eta}_{\underline{k}_{\mathrm{U}}|\underline{k}_{\mathrm{U}}}\right\| < \epsilon$*, then* $\|\boldsymbol{\eta}_{k|k}\| < \mathrm{h}(\epsilon, \Gamma_{\underline{k}_{\mathrm{U}}|\underline{k}_{\mathrm{U}}})$ *for all* $k \in (\underline{k}_{\mathrm{U}}, \bar{k}_{\mathrm{U}}]$*, where*

$$\mathrm{h}(\epsilon, \Gamma_{\underline{k}_{\mathrm{U}}|\underline{k}_{\mathrm{U}}}) = \sqrt{n}\left(\varrho_{\mathrm{m}} + \epsilon\left(c_0 + (n-2)\mathrm{c}\left(\Gamma_{\underline{k}_{\mathrm{U}}|\underline{k}_{\mathrm{U}}}\right)\right)\right).$$

*Proof.* The proof is by induction.

**Step 1**: Denote as $\check{\boldsymbol{\eta}}^{(1)}_{k|k} = (\boldsymbol{\eta}^1_{k|k}, \boldsymbol{\eta}^n_{k|k})^\top$ the mean error of the observable subsystem (i.e., the boundary cells). The error covariance of the observable subsystem $\check{\Gamma}^{(1)}_{k|k}$ satisfies

$$\check{\Gamma}^{(1)}_{k|k} < r_2 I, \quad \text{and} \quad \check{\Gamma}^{(1)}_{k|k-1} > q_1 I, \quad \text{for } k \in (\underline{k}_{\mathrm{U}}, \bar{k}_{\mathrm{U}}].$$

Let $\check{A}^{(1)}_k$ be the state transition matrix associated with the observable subsystem, it follows that

$$\begin{aligned} &\left\|\check{\boldsymbol{\eta}}^{(1)}_{\underline{k}_{\mathrm{U}}+1|\underline{k}_{\mathrm{U}}+1}\right\| \leq \left\|\left(I - \check{K}^{(1)}_{\underline{k}_{\mathrm{U}}+1}\check{H}^{(1)}\right)\check{A}^{(1)}_k\right\|\left\|\check{\boldsymbol{\eta}}^{(1)}_{\underline{k}_{\mathrm{U}}|\underline{k}_{\mathrm{U}}}\right\| \\ =& \left\|\check{\Gamma}^{(1)}_{\underline{k}_{\mathrm{U}}+1|\underline{k}_{\mathrm{U}}+1}\left(\check{\Gamma}^{(1)}_{\underline{k}_{\mathrm{U}}+1|\underline{k}_{\mathrm{U}}}\right)^{-1}\check{A}^{(1)}_k\right\|\left\|\check{\boldsymbol{\eta}}^{(1)}_{\underline{k}_{\mathrm{U}}|\underline{k}_{\mathrm{U}}}\right\| < r_2 q_1^{-1}\left\|\check{\boldsymbol{\eta}}^{(1)}_{\underline{k}_{\mathrm{U}}|\underline{k}_{\mathrm{U}}}\right\|. \end{aligned}$$

Define the Lyapunov function of the observable subsystem as

$$\check{V}_k = \left(\check{\boldsymbol{\eta}}^{(1)}_{k|k}\right)^\top\left(\check{\Gamma}^{(1)}_{k|k}\right)^{-1}\check{\boldsymbol{\eta}}^{(1)}_{k|k},$$

then $\check{c}_2^{-1}\left\|\check{\boldsymbol{\eta}}^{(1)}_{k|k}\right\|^2 < \check{V}_k < \check{c}_1^{-1}\left\|\check{\boldsymbol{\eta}}^{(1)}_{k|k}\right\|^2$ and $\check{V}_{k+1} < \check{V}_k$ for all $k \in (\underline{k}_{\mathrm{U}}, \bar{k}_{\mathrm{U}})$ due to [53, Lemma 3]. Consequently,

$$\left\|\check{\boldsymbol{\eta}}^{(1)}_{k|k}\right\| < \left(\check{c}_2\check{V}_k\right)^{\frac{1}{2}} < \left(\check{c}_2\check{V}_{\underline{k}_{\mathrm{U}}+1}\right)^{\frac{1}{2}} < \sqrt{\check{c}_2\check{c}_1^{-1}}\left\|\check{\boldsymbol{\eta}}^{(1)}_{\underline{k}_{\mathrm{U}}+1|\underline{k}_{\mathrm{U}}+1}\right\|,$$

for all $k \in (\underline{k}_{\mathrm{U}}+1, \bar{k}_{\mathrm{U}}]$. It follows that for all $k \in (\underline{k}_{\mathrm{U}}, \bar{k}_{\mathrm{U}}]$,

$$\left\|\check{\boldsymbol{\eta}}^{(1)}_{k|k}\right\| < \sqrt{\check{c}_2\check{c}_1^{-1}} r_2 q_1^{-1} \left\|\check{\boldsymbol{\eta}}^{(1)}_{\underline{k}_{\mathrm{U}}|\underline{k}_{\mathrm{U}}}\right\| < \sqrt{\check{c}_2\check{c}_1^{-1}} r_2 q_1^{-1}\epsilon \le c_0\epsilon.$$

**Step 2**: We use induction to show that $\boldsymbol{\rho}^l_{k|k} > -c_0\epsilon - (l-1)\mathrm{c}\left(\Gamma_{\underline{k}_{\mathrm{U}}|\underline{k}_{\mathrm{U}}}\right)\epsilon \ge -\epsilon(c_0 + (n-2)\mathrm{c}(\Gamma_{\underline{k}_{\mathrm{U}}|\underline{k}_{\mathrm{U}}}))$ for all $k \in (\underline{k}_{\mathrm{U}}, \bar{k}_{\mathrm{U}}]$ and $l \in \{2, \cdots, n-1\}$. Since $|\boldsymbol{\eta}^1_{k|k}| < c_0\epsilon$ for all $k \in (\underline{k}_{\mathrm{U}}, \bar{k}_{\mathrm{U}}]$, it holds that $\boldsymbol{\rho}^1_{k|k} > -c_0\epsilon = -c_0\epsilon - (1-1)\mathrm{c}\left(\Gamma_{\underline{k}_{\mathrm{U}}|\underline{k}_{\mathrm{U}}}\right)\epsilon$. Hence when $l=1$, $\boldsymbol{\rho}^1_{k|k} > -c_0\epsilon - (l-1)\mathrm{c}\left(\Gamma_{\underline{k}_{\mathrm{U}}|\underline{k}_{\mathrm{U}}}\right)\epsilon$ holds for all $k \in (\underline{k}_{\mathrm{U}}, \bar{k}_{\mathrm{U}}]$.

For $l \in \{1, 2, \cdots, n-2\}$, suppose $\boldsymbol{\rho}^l_{k|k} > -c_0\epsilon - (l-1)\mathrm{c}\left(\Gamma_{\underline{k}_{\mathrm{U}}|\underline{k}_{\mathrm{U}}}\right)\epsilon$ for all $k \in (\underline{k}_{\mathrm{U}}, \bar{k}_{\mathrm{U}}]$. If $\boldsymbol{\rho}^{l+1}_{k|k} < -c_0\epsilon - l\mathrm{c}\left(\Gamma_{\underline{k}_{\mathrm{U}}|\underline{k}_{\mathrm{U}}}\right)\epsilon$, we obtain from (2.8) that

$$\begin{aligned}
&\mathrm{f}\left(\boldsymbol{\rho}^l_{k|k}, \boldsymbol{\rho}^{l+1}_{k|k}\right) > v_{\mathrm{m}}\left(-c_0\epsilon - (l-1)\mathrm{c}\left(\Gamma_{\underline{k}_{\mathrm{U}}|\underline{k}_{\mathrm{U}}}\right)\epsilon\right),\\
&\mathrm{f}\left(\boldsymbol{\rho}^{l+1}_{k|k}, \boldsymbol{\rho}^{l+2}_{k|k}\right) \le v_{\mathrm{m}}\boldsymbol{\rho}^{l+1}_{k|k}.
\end{aligned}$$

It follows that the estimate of cell $l+1$ satisfies

$$\begin{aligned}
\boldsymbol{\rho}^{l+1}_{k+1|k+1} &= \boldsymbol{\rho}^{1+1}_{k|k} + \tfrac{\Delta t}{\Delta x}\left(\mathrm{f}\left(\boldsymbol{\rho}^l_{k|k}, \boldsymbol{\rho}^{l+1}_{k|k}\right) - \mathrm{f}\left(\boldsymbol{\rho}^{l+1}_{k|k}, \boldsymbol{\rho}^{l+2}_{k|k}\right)\right)\\
&\qquad -K_{k+1}(l+1,1)\boldsymbol{\eta}^1_{k+1|k} - K_{k+1}(l+1,2)\boldsymbol{\eta}^n_{k+1|k}\\
&> \boldsymbol{\rho}^{l+1}_{k|k} + \tfrac{v_{\mathrm{m}}\Delta t}{\Delta x}\left|\boldsymbol{\rho}^{l+1}_{k|k} + c_0\epsilon + (l-1)\mathrm{c}\left(\Gamma_{\underline{k}_{\mathrm{U}}|\underline{k}_{\mathrm{U}}}\right)\epsilon\right| - \mathrm{k}\left(\Gamma_{\underline{k}_{\mathrm{U}}|\underline{k}_{\mathrm{U}}}\right)c_0\epsilon\\
&= \boldsymbol{\rho}^{l+1}_{k|k} + \tfrac{v_{\mathrm{m}}\Delta t}{\Delta x}\left|\boldsymbol{\rho}^{l+1}_{k|k} + c_0\epsilon + l\mathrm{c}\left(\Gamma_{\underline{k}_{\mathrm{U}}|\underline{k}_{\mathrm{U}}}\right)\epsilon\right| + \tfrac{v_{\mathrm{m}}\Delta t}{\Delta x}\mathrm{c}\left(\Gamma_{\underline{k}_{\mathrm{U}}|\underline{k}_{\mathrm{U}}}\right)\epsilon - \mathrm{k}\left(\Gamma_{\underline{k}_{\mathrm{U}}|\underline{k}_{\mathrm{U}}}\right)c_0\epsilon\\
&\ge \boldsymbol{\rho}^{l+1}_{k|k} + \tfrac{v_{\mathrm{m}}\Delta t}{\Delta x}\left|\boldsymbol{\rho}^{l+1}_{k|k} + c_0\epsilon + l\mathrm{c}\left(\Gamma_{\underline{k}_{\mathrm{U}}|\underline{k}_{\mathrm{U}}}\right)\epsilon\right|,
\end{aligned} \tag{3.20}$$

where the first inequality is due to $\|K_k\|_\infty \le \mathrm{k}(\Gamma_{\underline{k}_{\mathrm{U}}|\underline{k}_{\mathrm{U}}})$ given in Lemma 6 and the fact that $\|\check{\boldsymbol{\eta}}^{(1)}_{k+1|k}\| = \|\check{A}^{(1)}_k\check{\boldsymbol{\eta}}^{(1)}_{k|k}\| < \|\check{\boldsymbol{\eta}}^{(1)}_{k|k}\| < c_0\epsilon$ for all $k \in (\underline{k}_{\mathrm{U}}, \bar{k}_{\mathrm{U}}]$, and the last inequality is obtained by $\frac{v_{\mathrm{m}}\Delta t}{\Delta x}\mathrm{c}(\Gamma_{\underline{k}_{\mathrm{U}}|\underline{k}_{\mathrm{U}}})\epsilon - \mathrm{k}(\Gamma_{\underline{k}_{\mathrm{U}}|\underline{k}_{\mathrm{U}}})c_0\epsilon = \frac{v_{\mathrm{m}}}{\min\{v_{\mathrm{m}},w\}}\mathrm{k}(\Gamma_{\underline{k}_{\mathrm{U}}|\underline{k}_{\mathrm{U}}})c_0\epsilon - \mathrm{k}(\Gamma_{\underline{k}_{\mathrm{U}}|\underline{k}_{\mathrm{U}}})c_0\epsilon \ge 0$. Also since $\boldsymbol{\rho}^{l+1}_{\underline{k}_{\mathrm{U}}|\underline{k}_{\mathrm{U}}} > -\epsilon \ge -c_0\epsilon > -c_0\epsilon - l\mathrm{c}(\Gamma_{\underline{k}_{\mathrm{U}}|\underline{k}_{\mathrm{U}}})\epsilon$, it is concluded that $\boldsymbol{\rho}^{l+1}_{k|k} > -c_0\epsilon - l\mathrm{c}(\Gamma_{\underline{k}_{\mathrm{U}}|\underline{k}_{\mathrm{U}}})\epsilon$ for all $k \in (\underline{k}_{\mathrm{U}}, \bar{k}_{\mathrm{U}}]$. Continuing the induction along the cells, we obtain $\boldsymbol{\rho}^{n-1}_{k|k} > -c_0\epsilon - (n-2)\mathrm{c}(\Gamma_{\underline{k}_{\mathrm{U}}|\underline{k}_{\mathrm{U}}})\epsilon$ for all $k \in (\underline{k}_{\mathrm{U}}, \bar{k}_{\mathrm{U}}]$.

We can use a similar induction to show $\boldsymbol{\rho}^l_{k|k} < \varrho_{\mathrm{m}} + c_0\epsilon + (n-l)\mathrm{c}(\Gamma_{\underline{k}_{\mathrm{U}}|\underline{k}_{\mathrm{U}}})\epsilon \le \varrho_{\mathrm{m}} + \epsilon(c_0 + (n-2)\mathrm{c}(\Gamma_{\underline{k}_{\mathrm{U}}|\underline{k}_{\mathrm{U}}}))$ for all $k \in (\underline{k}_{\mathrm{U}}, \bar{k}_{\mathrm{U}}]$ and $l \in \{2, \cdots, n-1\}$.

Since $|\boldsymbol{\eta}^n_{k|k}| < c_0\epsilon$ for all $k \in (\underline{k}_{\mathrm{U}}, \bar{k}_{\mathrm{U}}]$, we have $\boldsymbol{\rho}^n_{k|k} < \varrho_{\mathrm{m}} + c_0\epsilon = \varrho_{\mathrm{m}} + c_0\epsilon + (n-$

$n)\mathrm{c}\left(\Gamma_{\underline{k}_{\mathrm{U}}|\underline{k}_{\mathrm{U}}}\right)\epsilon$. Hence when $l = n$, $\boldsymbol{\rho}^{l}_{k|k} < \varrho_{\mathrm{m}} + c_0\epsilon + (n-l)\mathrm{c}\left(\Gamma_{\underline{k}_{\mathrm{U}}|\underline{k}_{\mathrm{U}}}\right)\epsilon$ holds for all $k \in (\underline{k}_{\mathrm{U}}, \bar{k}_{\mathrm{U}}]$.

For $l \in \{n-1, n-2, \cdots, 2\}$, suppose $\boldsymbol{\rho}^{l}_{k|k} < \varrho_{\mathrm{m}} + c_0\epsilon + (n-l)\mathrm{c}\left(\Gamma_{\underline{k}_{\mathrm{U}}|\underline{k}_{\mathrm{U}}}\right)\epsilon$ for all $k \in (\underline{k}_{\mathrm{U}}, \bar{k}_{\mathrm{U}}]$. If $\boldsymbol{\rho}^{l-1}_{k|k} > \varrho_{\mathrm{m}} + c_0\epsilon + (n-l+1)\mathrm{c}\left(\Gamma_{\underline{k}_{\mathrm{U}}|\underline{k}_{\mathrm{U}}}\right)\epsilon$, following the similar argument as in (3.20) yields

$$\begin{aligned}
\boldsymbol{\rho}^{l-1}_{k+1|k+1} &< \boldsymbol{\rho}^{l-1}_{k|k} - \frac{w\Delta t}{\Delta x}\left|\boldsymbol{\rho}^{l-1}_{k|k} - \varrho_{\mathrm{m}} - c_0\epsilon - (n-l)\mathrm{c}\left(\Gamma_{\underline{k}_{\mathrm{U}}|\underline{k}_{\mathrm{U}}}\right)\epsilon\right| + \mathrm{k}\left(\Gamma_{\underline{k}_{\mathrm{U}}|\underline{k}_{\mathrm{U}}}\right)c_0\epsilon \\
&= \boldsymbol{\rho}^{l-1}_{k|k} - \frac{w\Delta t}{\Delta x}\left|\boldsymbol{\rho}^{l-1}_{k|k} - \varrho_{\mathrm{m}} - c_0\epsilon - (n-l+1)\mathrm{c}\left(\Gamma_{\underline{k}_{\mathrm{U}}|\underline{k}_{\mathrm{U}}}\right)\epsilon\right| \\
&\qquad - \frac{w\Delta t}{\Delta x}\mathrm{c}\left(\Gamma_{\underline{k}_{\mathrm{U}}|\underline{k}_{\mathrm{U}}}\right)\epsilon + \mathrm{k}\left(\Gamma_{\underline{k}_{\mathrm{U}}|\underline{k}_{\mathrm{U}}}\right)c_0\epsilon \\
&\leq \boldsymbol{\rho}^{l-1}_{k|k} - \frac{w\Delta t}{\Delta x}\left|\boldsymbol{\rho}^{l-1}_{k|k} - \varrho_{\mathrm{m}} - c_0\epsilon - (n-l+1)\mathrm{c}\left(\Gamma_{\underline{k}_{\mathrm{U}}|\underline{k}_{\mathrm{U}}}\right)\epsilon\right|.
\end{aligned}$$

Also since $\boldsymbol{\rho}^{l-1}_{\underline{k}_{\mathrm{U}}|\underline{k}_{\mathrm{U}}} < \varrho_{\mathrm{m}} + \epsilon \leq \varrho_{\mathrm{m}} + c_0\epsilon < \varrho_{\mathrm{m}} + c_0\epsilon + (n-l+1)\mathrm{c}\left(\Gamma_{\underline{k}_{\mathrm{U}}|\underline{k}_{\mathrm{U}}}\right)\epsilon$, it is concluded that $\boldsymbol{\rho}^{l-1}_{k|k} < \varrho_{\mathrm{m}} + c_0\epsilon + (n-l+1)\mathrm{c}\left(\Gamma_{\underline{k}_{\mathrm{U}}|\underline{k}_{\mathrm{U}}}\right)\epsilon$ for all $k \in (\underline{k}_{\mathrm{U}}, \bar{k}_{\mathrm{U}}]$. Continuing the induction, we obtain $\boldsymbol{\rho}^{2}_{k|k} < \varrho_{\mathrm{m}} + c_0\epsilon + (n-2)\mathrm{c}\left(\Gamma_{\underline{k}_{\mathrm{U}}|\underline{k}_{\mathrm{U}}}\right)\epsilon$ for all $k \in (\underline{k}_{\mathrm{U}}, \bar{k}_{\mathrm{U}}]$.

**Step 3**: Combining Steps 1 and 2, we obtain $\boldsymbol{\rho}^{l}_{k|k} \in (-\epsilon(c_0 + (n-2)\mathrm{c}(\Gamma_{\underline{k}_{\mathrm{U}}|\underline{k}_{\mathrm{U}}})), \varrho_{\mathrm{m}} + \epsilon(c_0 + (n-2)\mathrm{c}(\Gamma_{\underline{k}_{\mathrm{U}}|\underline{k}_{\mathrm{U}}})))$ for all $l \in \{1, \cdots, n\}$ and $k \in (\underline{k}_{\mathrm{U}}, \bar{k}_{\mathrm{U}}]$. Consequently, $\|\boldsymbol{\eta}_{k|k}\| < \sqrt{n}(\varrho_{\mathrm{m}} + \epsilon(c_0 + (n-2)\mathrm{c}(\Gamma_{\underline{k}_{\mathrm{U}}|\underline{k}_{\mathrm{U}}}))) = \mathrm{h}(\epsilon, \Gamma_{\underline{k}_{\mathrm{U}}|\underline{k}_{\mathrm{U}}})$ for all $k \in (\underline{k}_{\mathrm{U}}, \bar{k}_{\mathrm{U}}]$. □

### 3.5.2 Residence time in observable modes

When a freeway section switches from an unobservable mode at time $\underline{k}_{\mathrm{O}}$ to an observable mode at $\underline{k}_{\mathrm{O}} + 1$, the next proposition derives the residence time the section must remain in the set of observable modes in order to reduce the mean estimation error below a given threshold. The residence time is a function of the mean error and error covariance of the section at time $\underline{k}_{\mathrm{O}}$, and also depends on the magnitude of the mean error to be satisfied.

**Proposition 3** (Residence time and error bounds of KF in the observable modes of SMM)**.** *Consider a road section shown in Figure 2.2 that switches arbitrarily among the observable modes of the SMM while $k \in (\underline{k}_{\mathrm{O}}, \bar{k}_{\mathrm{O}}]$, where $0 \leq \underline{k}_{\mathrm{O}} < \bar{k}_{\mathrm{O}} \leq +\infty$. Define*

$$\begin{aligned}
\mathrm{a}\left(\Gamma_{\underline{k}_{\mathrm{O}}|\underline{k}_{\mathrm{O}}}\right) &= \left(\left(\mathrm{c}_1\left(\Gamma_{\underline{k}_{\mathrm{O}}|\underline{k}_{\mathrm{O}}}\right)\right)^{-1}\mathrm{c}_2\left(\Gamma_{\underline{k}_{\mathrm{O}}|\underline{k}_{\mathrm{O}}}\right)\right)^{\frac{1}{2}}, \\
\mathrm{q}\left(\Gamma_{\underline{k}_{\mathrm{O}}|\underline{k}_{\mathrm{O}}}\right) &= \left(1 - \mathrm{c}_3\left(\Gamma_{\underline{k}_{\mathrm{O}}|\underline{k}_{\mathrm{O}}}\right)\mathrm{c}_1\left(\Gamma_{\underline{k}_{\mathrm{O}}|\underline{k}_{\mathrm{O}}}\right)\right)^{\frac{1}{2}},
\end{aligned} \tag{3.21}$$

*where $\mathrm{c}_1(\cdot)$, $\mathrm{c}_2(\cdot)$ are the bounds on the error covariance from* (3.7)*, and $\mathrm{c}_3\left(\Gamma_{\underline{k}_{\mathrm{O}}|\underline{k}_{\mathrm{O}}}\right)$ is*

*given by* $\mathrm{c}_3\left(\Gamma_{\underline{k}_\mathrm{O}|\underline{k}_\mathrm{O}}\right) = \mathrm{d}\left(\mathrm{c}_1\left(\Gamma_{\underline{k}_\mathrm{O}|\underline{k}_\mathrm{O}}\right), \mathrm{c}_2\left(\Gamma_{\underline{k}_\mathrm{O}|\underline{k}_\mathrm{O}}\right)\right)$ *with* $\mathrm{d}(\cdot,\cdot)$ *defined in Lemma 6.*

*For all* $\epsilon > 0$*, there exists* $\mathrm{t}\left(\epsilon, \left\|\boldsymbol{\eta}_{\underline{k}_\mathrm{O}|\underline{k}_\mathrm{O}}\right\|, \Gamma_{\underline{k}_\mathrm{O}|\underline{k}_\mathrm{O}}\right)$ *such that if*

$$\bar{k}_\mathrm{O} - \underline{k}_\mathrm{O} > \mathrm{t}\left(\epsilon, \left\|\boldsymbol{\eta}_{\underline{k}_\mathrm{O}|\underline{k}_\mathrm{O}}\right\|, \Gamma_{\underline{k}_\mathrm{O}|\underline{k}_\mathrm{O}}\right),$$

*the mean error at time* $\bar{k}_\mathrm{O}$ *satisfies* $\left\|\boldsymbol{\eta}_{\bar{k}_\mathrm{O}|\bar{k}_\mathrm{O}}\right\| < \epsilon$*. Explicitly,*

$$\mathrm{t}\left(\epsilon, \left\|\boldsymbol{\eta}_{\underline{k}_\mathrm{O}|\underline{k}_\mathrm{O}}\right\|, \Gamma_{\underline{k}_\mathrm{O}|\underline{k}_\mathrm{O}}\right) = \begin{cases} 0, & \text{if } \mathrm{a}\left(\Gamma_{\underline{k}_\mathrm{O}|\underline{k}_\mathrm{O}}\right)\mathrm{q}\left(\Gamma_{\underline{k}_\mathrm{O}|\underline{k}_\mathrm{O}}\right)\left\|\boldsymbol{\eta}_{\underline{k}_\mathrm{O}|\underline{k}_\mathrm{O}}\right\| \le \epsilon, \\ \log_{\mathrm{q}\left(\Gamma_{\underline{k}_\mathrm{O}|\underline{k}_\mathrm{O}}\right)}\left(\epsilon\left(\mathrm{a}\left(\Gamma_{\underline{k}_\mathrm{O}|\underline{k}_\mathrm{O}}\right)\left\|\boldsymbol{\eta}_{\underline{k}_\mathrm{O}|\underline{k}_\mathrm{O}}\right\|\right)^{-1}\right), & o.w. \end{cases} \tag{3.22}$$

*Furthermore, for all* $k \in (\underline{k}_\mathrm{O}, \bar{k}_\mathrm{O}]$*,*

$$\left\|\boldsymbol{\eta}_{k|k}\right\| \le \mathrm{a}\left(\Gamma_{\underline{k}_\mathrm{O}|\underline{k}_\mathrm{O}}\right)\mathrm{q}\left(\Gamma_{\underline{k}_\mathrm{O}|\underline{k}_\mathrm{O}}\right)\left\|\boldsymbol{\eta}_{\underline{k}_\mathrm{O}|\underline{k}_\mathrm{O}}\right\|.$$

*Proof.* According to Lemma 5, when $\underline{k}_\mathrm{O} < k \le \bar{k}_\mathrm{O}$ the error covariance satisfies $\mathrm{c}_1(\Gamma_{\underline{k}_\mathrm{O}|\underline{k}_\mathrm{O}})I \le \Gamma_{k|k} \le \mathrm{c}_2(\Gamma_{\underline{k}_\mathrm{O}|\underline{k}_\mathrm{O}})I$. Given Lemma 6, it follows that for $\underline{k}_\mathrm{O} < k \le \bar{k}_\mathrm{O}$,

$$\left\|\prod_{\kappa=k-1}^{\underline{k}_\mathrm{O}} F_{\kappa+1}A_\kappa\right\| \le \mathrm{a}\left(\Gamma_{\underline{k}_\mathrm{O}|\underline{k}_\mathrm{O}}\right)\mathrm{q}\left(\Gamma_{\underline{k}_\mathrm{O}|\underline{k}_\mathrm{O}}\right)^{k-\underline{k}_\mathrm{O}},$$

where $\mathrm{a}\left(\Gamma_{\underline{k}_\mathrm{O}|\underline{k}_\mathrm{O}}\right) \ge 1$ provides an upper bound for the increase of the mean estimation error when the section first switches to an observable mode at time $\underline{k}_\mathrm{O}+1$, and $0 < \mathrm{q}\left(\Gamma_{\underline{k}_\mathrm{O}|\underline{k}_\mathrm{O}}\right) < 1$ describes the convergence rate of the mean estimation error in observable modes. Hence when $\underline{k}_\mathrm{O} < k \le \bar{k}_\mathrm{O}$, the 2-norm of $\boldsymbol{\eta}_{k|k}$ satisfies

$$\left\|\boldsymbol{\eta}_{k|k}\right\| \le \left\|\prod_{\kappa=k-1}^{\underline{k}_\mathrm{O}} F_{\kappa+1}A_\kappa\right\|\left\|\boldsymbol{\eta}_{\underline{k}_\mathrm{O}|\underline{k}_\mathrm{O}}\right\| \le \left\|\boldsymbol{\eta}_{\underline{k}_\mathrm{O}|\underline{k}_\mathrm{O}}\right\|\mathrm{a}\left(\Gamma_{\underline{k}_\mathrm{O}|\underline{k}_\mathrm{O}}\right)\mathrm{q}\left(\Gamma_{\underline{k}_\mathrm{O}|\underline{k}_\mathrm{O}}\right)^{k-\underline{k}_\mathrm{O}}.$$

As a consequence, for all $\epsilon > 0$, there exists $\mathrm{t}\left(\epsilon, \left\|\boldsymbol{\eta}_{\underline{k}_\mathrm{O}|\underline{k}_\mathrm{O}}\right\|, \Gamma_{\underline{k}_\mathrm{O}|\underline{k}_\mathrm{O}}\right) \ge 0$ such that $\left\|\boldsymbol{\eta}_{k|k}\right\| < \epsilon$ for all $k - \underline{k}_\mathrm{O} > \mathrm{t}\left(\epsilon, \left\|\boldsymbol{\eta}_{\underline{k}_\mathrm{O}|\underline{k}_\mathrm{O}}\right\|, \Gamma_{\underline{k}_\mathrm{O}|\underline{k}_\mathrm{O}}\right)$.

When $\mathrm{a}\left(\Gamma_{\underline{k}_\mathrm{O}|\underline{k}_\mathrm{O}}\right)\mathrm{q}\left(\Gamma_{\underline{k}_\mathrm{O}|\underline{k}_\mathrm{O}}\right)\left\|\boldsymbol{\eta}_{\underline{k}_\mathrm{O}|\underline{k}_\mathrm{O}}\right\| < \epsilon$, we have $\mathrm{t}\left(\epsilon, \left\|\boldsymbol{\eta}_{\underline{k}_\mathrm{O}|\underline{k}_\mathrm{O}}\right\|, \Gamma_{\underline{k}_\mathrm{O}|\underline{k}_\mathrm{O}}\right) = 0$. On the other hand, the residence time is expressed as

$$\mathrm{t}(\epsilon, \|\boldsymbol{\eta}_{\underline{k}_\mathrm{O}|\underline{k}_\mathrm{O}}\|, \Gamma_{\underline{k}_\mathrm{O}|\underline{k}_\mathrm{O}}) = \log_{\mathrm{q}\left(\Gamma_{\underline{k}_\mathrm{O}|\underline{k}_\mathrm{O}}\right)}\left(\epsilon\left(\mathrm{a}\left(\Gamma_{\underline{k}_\mathrm{O}|\underline{k}_\mathrm{O}}\right)\left\|\boldsymbol{\eta}_{\underline{k}_\mathrm{O}|\underline{k}_\mathrm{O}}\right\|\right)^{-1}\right).$$

Furthermore, the upper bound of $\left\|\boldsymbol{\eta}_{k|k}\right\|$ is given as follows:

$$\left\|\boldsymbol{\eta}_{k|k}\right\| \leq \mathrm{a}\left(\Gamma_{\underline{k}_{\mathrm{O}}|\underline{k}_{\mathrm{O}}}\right) \mathrm{q}\left(\Gamma_{\underline{k}_{\mathrm{O}}|\underline{k}_{\mathrm{O}}}\right) \left\|\boldsymbol{\eta}_{\underline{k}_{\mathrm{O}}|\underline{k}_{\mathrm{O}}}\right\|, \quad \text{for all } k \in (\underline{k}_{\mathrm{O}}, \bar{k}_{\mathrm{O}}]$$

which concludes the proof. □

### 3.5.3 Boundedness of the mean estimation error under switches among observable and unobservable modes

Based on Proposition 2 and Proposition 3, the boundedness of the mean estimation error when the SMM switches among observable and unobservable modes is summarized in Proposition 4.

The main concept of Proposition 4 is given as follows. For a freeway section, denote as $(\underline{k}_{\mathrm{U}}^r, \bar{k}_{\mathrm{U}}^r]$ and $(\underline{k}_{\mathrm{O}}^r, \bar{k}_{\mathrm{O}}^r]$ the $r^{\text{th}}$ unobservable and observable time intervals, respectively. Consider a freeway section that switches from an observable mode at $\bar{k}_{\mathrm{O}}^{r-1} = \underline{k}_{\mathrm{U}}^r$ to an unobservable mode at $\underline{k}_{\mathrm{U}}^r + 1$, and remains unobservable through $\bar{k}_{\mathrm{U}}^r$. An upper bound for the 2-norm of the mean estimation error, which is uniform over $(\underline{k}_{\mathrm{U}}^r, \bar{k}_{\mathrm{U}}^r]$, can be obtained through Proposition 2 based on the error covariance and the upper bound of the mean error at time $\underline{k}_{\mathrm{U}}^r$. When the section switches back to the set of observable modes at time $\bar{k}_{\mathrm{U}}^r + 1 = \underline{k}_{\mathrm{O}}^r + 1$ and remains observable through $\bar{k}_{\mathrm{O}}^r$, the mean estimation error has been increased during the unobservable time interval, and may continue to increase initially before decreasing while the section is observable. Based on Proposition 3, the minimum residence time $\bar{k}_{\mathrm{O}}^r - \underline{k}_{\mathrm{O}}^r$ the section must remain observable to offset the increase of the mean estimation error, as well as the upper bound of the mean error during the observable interval $(\underline{k}_{\mathrm{O}}^r, \bar{k}_{\mathrm{O}}^r]$ are derived. The minimum residence time ensures that when the section switches back to an unobservable mode, the mean estimation error is smaller than a given upper bound (denoted by $\epsilon$). Based on this upper bound and the error covariance at time $\bar{k}_{\mathrm{O}}^r = \underline{k}_{\mathrm{U}}^{r+1}$, we can apply Proposition 2 again and obtain the upper bound for the 2-norm of the mean estimation error during the unobservable time interval starting at time $\underline{k}_{\mathrm{U}}^{r+1} + 1$. We continue the induction and derive the minimum residence time for each observable time interval, as well as the upper bounds of the 2-norm of the mean estimation error for all the observable and unobservable time intervals.

**Proposition 4** (Error bounds of the KF under switches among observable and unobservable modes of SMM)**.** *For a freeway section in Figure 2.2, denote as* $(\underline{k}_{\mathrm{U}}^r, \bar{k}_{\mathrm{U}}^r]$ *the* $r^{th}$ *time interval while the section switches inside the unobservable mode of the SMM, and* $(\underline{k}_{\mathrm{O}}^r, \bar{k}_{\mathrm{O}}^r]$ *the* $r^{th}$ *time interval while the section switches among observable modes. Hence* $\underline{k}_{\mathrm{U}}^1 = 0$ *(resp.* $\underline{k}_{\mathrm{O}}^1 = 0$*) when the section is unobservable (resp. observable) at time* 0*. Let* $\epsilon > 0$ *be an arbitrary positive constant, and suppose the following condition on the residence time for the observable time intervals holds:*

$$\bar{k}_{\mathrm{O}}^r - \underline{k}_{\mathrm{O}}^r > \begin{cases} \mathrm{t}\left(\epsilon, \mathrm{e}\left(\epsilon, \Gamma_{\bar{k}_{\mathrm{O}}^{r-1}|\bar{k}_{\mathrm{O}}^{r-1}}\right), \Gamma_{\underline{k}_{\mathrm{O}}^r|\underline{k}_{\mathrm{O}}^r}\right) & r \geq 2 \\ \mathrm{t}\left(\epsilon, \mathrm{e}_0\left(\Gamma_{0|0}\right), \Gamma_{\underline{k}_{\mathrm{O}}^1|\underline{k}_{\mathrm{O}}^1}\right) & r = 1 \text{ and } \underline{k}_{\mathrm{U}}^1 = 0 \\ \mathrm{t}\left(\epsilon, \sqrt{n}\varrho_{\mathrm{m}}, \Gamma_{0|0}\right) & r = 1 \text{ and } \underline{k}_{\mathrm{O}}^1 = 0, \end{cases} \tag{3.23}$$

*where for* $M \in \mathbb{R}^{n\times n}$*,*

$$\begin{aligned} \mathrm{e}_0(M) &= \sqrt{n}\left(\sqrt{n}\varrho_{\mathrm{m}}\left(c_0 + (n-2)\,\mathrm{c}(M)\right) + \varrho_{\mathrm{m}}\right) \\ \mathrm{e}(\epsilon, M) &= \sqrt{n}\left(\varrho_{\mathrm{m}} + \epsilon\left(c_0 + (n-2)\,\mathrm{c}(M_2)\right)\right), \end{aligned}$$

*with* $c_0$ *and* $\mathrm{c}(\cdot)$ *defined in* (3.19)*. Also recall* $\mathrm{a}(\cdot)$ *and* $\mathrm{q}(\cdot)$ *defined in* (3.21)*.*

*When* $r \geq 2$*, the mean error is upper bounded a follows:*

$$\left\|\boldsymbol{\eta}_{k|k}\right\| \leq \begin{cases} \textit{(a) for } k \in (\underline{k}_{\mathrm{U}}^r, \bar{k}_{\mathrm{U}}^r]\textit{:} \;\; \mathrm{e}\left(\epsilon, \Gamma_{\underline{k}_{\mathrm{U}}^r|\underline{k}_{\mathrm{U}}^r}\right), \\ \textit{(b) for } k \in (\underline{k}_{\mathrm{O}}^r, \bar{k}_{\mathrm{O}}^r]\textit{:} \;\; \mathrm{a}\left(\Gamma_{\underline{k}_{\mathrm{O}}^r|\underline{k}_{\mathrm{O}}^r}\right)\mathrm{q}\left(\Gamma_{\underline{k}_{\mathrm{O}}^r|\underline{k}_{\mathrm{O}}^r}\right)\mathrm{e}\left(\epsilon, \Gamma_{\bar{k}_{\mathrm{O}}^{r-1}|\bar{k}_{\mathrm{O}}^{r-1}}\right). \end{cases}$$

*When* $r = 1$ *and* $\underline{k}_{\mathrm{U}}^1 = 0$*, the mean estimation error satisfies*

$$\left\|\boldsymbol{\eta}_{k|k}\right\| \leq \begin{cases} \textit{(a) for } k \in (\underline{k}_{\mathrm{U}}^1, \bar{k}_{\mathrm{U}}^1]\textit{:} \;\; \mathrm{e}_0\left(\Gamma_{0|0}\right), \\ \textit{(b) for } k \in (\underline{k}_{\mathrm{O}}^1, \bar{k}_{\mathrm{O}}^1]\textit{:} \;\; \mathrm{a}\left(\Gamma_{\underline{k}_{\mathrm{O}}^1|\underline{k}_{\mathrm{O}}^1}\right)\mathrm{q}\left(\Gamma_{\underline{k}_{\mathrm{O}}^1|\underline{k}_{\mathrm{O}}^1}\right)\mathrm{e}_0\left(\Gamma_{0|0}\right). \end{cases}$$

*When* $r = 1$ *and* $\underline{k}_{\mathrm{O}}^1 = 0$*, the mean estimation error satisfies*

$$\left\|\boldsymbol{\eta}_{k|k}\right\| \leq \begin{cases} \textit{(a) for } k \in (\underline{k}_{\mathrm{U}}^1, \bar{k}_{\mathrm{U}}^1]\textit{:} \;\; \mathrm{e}\left(\epsilon, \Gamma_{\underline{k}_{\mathrm{U}}^1|\underline{k}_{\mathrm{U}}^1}\right), \\ \textit{(b) for } k \in (\underline{k}_{\mathrm{O}}^1, \bar{k}_{\mathrm{O}}^1]\textit{:} \;\; \mathrm{a}\left(\Gamma_{0|0}\right)\mathrm{q}\left(\Gamma_{0|0}\right)\sqrt{n}\varrho_{\mathrm{m}}. \end{cases}$$

*Proof.* The proof can be done by a straightforward application of the results in Propositions 2 and 3. Note that when the section is unobservable at time 0 (i.e., $\underline{k}_{\mathrm{U}}^1 = 0$), we have

$\underline{k}_{\mathrm{U}}^{r+1} = \bar{k}_{\mathrm{O}}^{r}$ and $\bar{k}_{\mathrm{U}}^{r} = \underline{k}_{\mathrm{O}}^{r}$ for all $r \in \mathbb{Z}^+$. When the section is observable at time 0 (i.e., $\underline{k}_{\mathrm{O}}^{1} = 0$), we have $\underline{k}_{\mathrm{O}}^{r+1} = \bar{k}_{\mathrm{U}}^{r}$ and $\bar{k}_{\mathrm{O}}^{r} = \underline{k}_{\mathrm{U}}^{r}$ for all $r \in \mathbb{Z}^+$.

**Step 1**: When $r \geq 2$.

*(a) For the $r^{th}$ unobservable time interval $k \in (\underline{k}_{\mathrm{U}}^{r}, \bar{k}_{\mathrm{U}}^{r}]$*: When the observable time interval right before $(\underline{k}_{\mathrm{U}}^{r}, \bar{k}_{\mathrm{U}}^{r}]$ is sufficiently long such that condition (3.23) is satisfied, the estimation error at time $\underline{k}_{\mathrm{U}}^{r}$ satisfies $\left\|\boldsymbol{\eta}_{\underline{k}_{\mathrm{U}}^{r}|\underline{k}_{\mathrm{U}}^{r}}\right\| \leq \epsilon$ based on Proposition 3. As a consequence, Proposition 2 gives

$$\begin{aligned}
\boldsymbol{\rho}_{k|k}^{l} &> -\epsilon\left(c_0 + (n-2)\,\mathrm{c}\left(\Gamma_{\underline{k}_{\mathrm{U}}^{r}|\underline{k}_{\mathrm{U}}^{r}}\right)\right), \\
\boldsymbol{\rho}_{k|k}^{l} &< \varrho_{\mathrm{m}} + \epsilon\left(c_0 + (n-2)\,\mathrm{c}\left(\Gamma_{\underline{k}_{\mathrm{U}}^{r}|\underline{k}_{\mathrm{U}}^{r}}\right)\right),
\end{aligned}$$

for all $l \in \{1, \cdots, n\}$ and $k \in (\underline{k}_{\mathrm{U}}^{r}, \bar{k}_{\mathrm{U}}^{r}]$. Consequently, the estimation error satisfies $\left\|\boldsymbol{\eta}_{k|k}\right\| \leq \mathrm{e}\left(\epsilon, \Gamma_{\underline{k}_{\mathrm{U}}^{r}|\underline{k}_{\mathrm{U}}^{r}}\right)$ for all $k \in (\underline{k}_{\mathrm{U}}^{r}, \bar{k}_{\mathrm{U}}^{r}]$.

*(b) For the $r^{th}$ observable time interval $k \in (\underline{k}_{\mathrm{O}}^{r}, \bar{k}_{\mathrm{O}}^{r}]$*: Note that the unobservable time interval right before $(\underline{k}_{\mathrm{O}}^{r}, \bar{k}_{\mathrm{O}}^{r}]$ is written as $(\underline{k}_{\mathrm{U}}^{r}, \bar{k}_{\mathrm{U}}^{r}] = (\bar{k}_{\mathrm{O}}^{r-1}, \underline{k}_{\mathrm{O}}^{r}]$ when the section is unobservable at time 0, and is written as $(\underline{k}_{\mathrm{U}}^{r-1}, \bar{k}_{\mathrm{U}}^{r-1}] = (\bar{k}_{\mathrm{O}}^{r-1}, \underline{k}_{\mathrm{O}}^{r}]$ when the section is observable at time 0. Similar to Case $(a)$ in Step 1, when $\bar{k}_{\mathrm{O}}^{r-1} - \underline{k}_{\mathrm{O}}^{r-1}$ satisfies condition (3.23), the estimation error at time $\underline{k}_{\mathrm{O}}^{r}$ satisfies

$$\left\|\boldsymbol{\eta}_{\underline{k}_{\mathrm{O}}^{r}|\underline{k}_{\mathrm{O}}^{r}}\right\| \leq \mathrm{e}\left(\epsilon, \Gamma_{\bar{k}_{\mathrm{O}}^{r-1}|\bar{k}_{\mathrm{O}}^{r-1}}\right).$$

Applying Proposition 3, it is concluded that for $k \in (\underline{k}_{\mathrm{O}}^{r}, \bar{k}_{\mathrm{O}}^{r}]$,

$$\left\|\boldsymbol{\eta}_{k|k}\right\| \leq \mathrm{a}\left(\Gamma_{\underline{k}_{\mathrm{O}}^{r}|\underline{k}_{\mathrm{O}}^{r}}\right)\mathrm{q}\left(\Gamma_{\underline{k}_{\mathrm{O}}^{r}|\underline{k}_{\mathrm{O}}^{r}}\right)\mathrm{e}\left(\epsilon, \Gamma_{\bar{k}_{\mathrm{O}}^{r-1}|\bar{k}_{\mathrm{O}}^{r-1}}\right).$$

**Step 2**: When $r = 1$ and $\underline{k}_{\mathrm{U}}^{1} = 0$.

*(a) For the $1^{st}$ unobservable time interval $k \in (\underline{k}_{\mathrm{U}}^{1}, \bar{k}_{\mathrm{U}}^{1}]$*: In this case, the section is unobservable at time 0. Since $\boldsymbol{\rho}_{0|0}^{l} \in [0, \varrho_{\mathrm{m}}]$, the initial estimation error satisfies $\left\|\boldsymbol{\eta}_{0|0}\right\| \leq \sqrt{n}\varrho_{\mathrm{m}}$. According to Proposition 2, we have

$$\begin{aligned}
\boldsymbol{\rho}_{k|k}^{l} &> -\sqrt{n}\varrho_{\mathrm{m}}\left(c_0 + (n-2)\,\mathrm{c}\left(\Gamma_{0|0}\right)\right) \\
\boldsymbol{\rho}_{k|k}^{l} &< \varrho_{\mathrm{m}} + \sqrt{n}\varrho_{\mathrm{m}}\left(c_0 + (n-2)\,\mathrm{c}\left(\Gamma_{0|0}\right)\right),
\end{aligned}$$

for all $l \in \{1, \cdots, n\}$ and $k \in (\underline{k}_{\mathrm{U}}^1, \bar{k}_{\mathrm{U}}^1]$. It follows that

$$\left\|\boldsymbol{\eta}_{k|k}\right\| \leq \sqrt{n}\left(\sqrt{n}\varrho_{\mathrm{m}}\left(c_0 + (n-2)\,\mathrm{c}\left(\Gamma_{0|0}\right)\right) + \varrho_{\mathrm{m}}\right) = \mathrm{e}_0\left(\Gamma_{0|0}\right), \quad \text{for } k \in (\underline{k}_{\mathrm{U}}^1, \bar{k}_{\mathrm{U}}^1].$$

*(b) For the* $1^{st}$ *observable time interval* $k \in (\underline{k}_{\mathrm{O}}^1, \bar{k}_{\mathrm{O}}^1]$: When the section switches from an unobservable mode at time $\underline{k}_{\mathrm{O}}^1$ to an observable mode at time $\underline{k}_{\mathrm{O}}^1 + 1$, it is shown in Case $(a)$ of Step 2 that the mean error is upper bounded by

$$\left\|\eta_{\underline{k}_{\mathrm{O}}^1|\underline{k}_{\mathrm{O}}^1}\right\| \leq \mathrm{e}_0\left(\Gamma_{0|0}\right).$$

Applying Proposition 3, it follows that

$$\left\|\boldsymbol{\eta}_{k|k}\right\| \leq \mathrm{a}\left(\Gamma_{\underline{k}_{\mathrm{O}}^1|\underline{k}_{\mathrm{O}}^1}\right)\mathrm{q}\left(\Gamma_{\underline{k}_{\mathrm{O}}^1|\underline{k}_{\mathrm{O}}^1}\right)\mathrm{e}_0\left(\Gamma_{0|0}\right),, \quad \text{for } k \in (\underline{k}_{\mathrm{O}}^1, \bar{k}_{\mathrm{O}}^1].$$

**Step 3**: When $r = 1$ and $\underline{k}_{\mathrm{O}}^1 = 0$.

*(a) For the* $1^{st}$ *unobservable time interval* $k \in (\underline{k}_{\mathrm{U}}^1, \bar{k}_{\mathrm{U}}^1]$: In this case, the section is observable at time 0. When $\bar{k}_{\mathrm{O}}^1 - \underline{k}_{\mathrm{O}}^1$ is larger than the third residence time listed in (3.23), the estimation error at time $\bar{k}_{\mathrm{O}}^1$ satisfies $\left\|\boldsymbol{\eta}_{\bar{k}_{\mathrm{O}}^1|\bar{k}_{\mathrm{O}}^1}\right\| \leq \epsilon$ based on Proposition 3. As a consequence, Proposition 2 gives

$$\begin{aligned}
\boldsymbol{\rho}_{k|k}^l &> -\epsilon\left(c_0 + (n-2)\,\mathrm{c}\left(\Gamma_{\underline{k}_{\mathrm{U}}^1|\underline{k}_{\mathrm{U}}^1}\right)\right), \\
\boldsymbol{\rho}_{k|k}^l &< \varrho_{\mathrm{m}} + \epsilon\left(c_0 + (n-2)\,\mathrm{c}\left(\Gamma_{\underline{k}_{\mathrm{U}}^1|\underline{k}_{\mathrm{U}}^1}\right)\right),
\end{aligned}$$

for all $l \in \{1, \cdots, n\}$ and $k \in (\underline{k}_{\mathrm{U}}^1, \bar{k}_{\mathrm{U}}^1]$. Consequently, the estimation error satisfies $\left\|\boldsymbol{\eta}_{k|k}\right\| \leq \mathrm{e}\left(\epsilon, \Gamma_{\underline{k}_{\mathrm{U}}^1|\underline{k}_{\mathrm{U}}^1}\right)$ for all $k \in (\underline{k}_{\mathrm{U}}^1, \bar{k}_{\mathrm{U}}^1]$.

*(b) For the* $1^{st}$ *observable time interval* $k \in (\underline{k}_{\mathrm{O}}^1, \bar{k}_{\mathrm{O}}^1]$: Since the section is observable at time 0, it holds that $\underline{k}_{\mathrm{O}}^1 = 0$. In this case, we have $\Gamma_{\underline{k}_{\mathrm{O}}^1|\underline{k}_{\mathrm{O}}^1} = \Gamma_{0|0}$ and $\left\|\boldsymbol{\eta}_{\underline{k}_{\mathrm{O}}^1|\underline{k}_{\mathrm{O}}^1}\right\| = \left\|\boldsymbol{\eta}_{0|0}\right\| \leq \sqrt{n}\varrho_{\mathrm{m}}$. Then we can directly apply Proposition 3 and conclude that

$$\left\|\boldsymbol{\eta}_{k|k}\right\| \leq \mathrm{a}\left(\Gamma_{0|0}\right)\mathrm{q}\left(\Gamma_{0|0}\right)\sqrt{n}\varrho_{\mathrm{m}}, \quad \text{for } k \in (\underline{k}_{\mathrm{O}}^1, \bar{k}_{\mathrm{O}}^1].$$

We conclude the proof by combining the above three steps.

□

**Remark 4.** *The minimum residence time in Proposition 4 shares a similar concept with the definition of (average) dwell time (e.g. [90, 91]), in the sense that both impose conditions on sufficiently long time spent in modes that are globally asymptotically stable (or observable in our case). However, several main differences between the two exist. For example, there is no condition imposed in this work regarding the ratio between the total time spent in observable and unobservable modes, while the analysis using an average dwell time (e.g., [91]) requires a sufficient large ratio between the total time spent in stable and unstable modes. Moreover, since this work derives switching conditions to ensure bounded estimation error provided by an online filter, the minimum residence times are also computed online, which depend on the estimation error covariances at the beginning of the observable time intervals. This also differs from the stability analysis based on the (average) dwell time where the timing conditions on the switching sequences are computed offline.*

# CHAPTER 4

# ERROR BOUNDS OF THE KALMAN FILTER ON TRAFFIC NETWORKS WITH JUNCTIONS

## 4.1 Introduction

In this chapter, we extend the analysis in Chapter 3 to traffic networks with junctions. The new contributions of this chapter are summarized below.

- **Developing the switching mode model with junctions.** We combine a switched linear representation of the CTM with the junction solver proposed in [92], yielding a switched linear model incorporating junction dynamics, namely the *switching mode model with junctions* (SMM-J). The SMM-J is an extension of the SMM, which describes the traffic density evolution on a freeway section with a junction. The SMM, on the other hand, only deals with one-dimensional freeway sections. Like the SMM, we also summarize the properties of the state transition matrices of the SMM-J, which assume important roles in deriving the error bounds of the KF under the SMM-J.

- **Observability analysis of the SMM-J.** We provide the observability result on each mode of the SMM-J, and show that nearly all modes are unobservable due to the irreversibility of the conservation laws in the presence of shocks and junctions. Compared to the one-dimensional road sections, the issue of non-observability is more frequently encountered when junctions exists, further motivating attention to the error bounds under unobservable scenarios.

- **Uniform upper bound of the mean error under the unobservable modes of the SMM-J.** We extend Proposition 1 and Proposition 2 to the SMM-J, following a similar line of analysis (i.e., exploring the interaction between the intrinsic properties embedded in the SMM-J and the information update of the KF). This gives us a uniform upper bound of the mean estimation error during the unobservable time

intervals of the system. To this end, we also discuss the extension of the error bounds under switches among observable and unobservable modes of the SMM-J.

The work in this chapter complements the results in Chapter 3. Thus, when estimating the traffic conditions in a large-scale road network, we partition the traffic network into local sections which are either one-dimensional, or having a junction inside. The traffic condition in each local section is estimated by a local estimator based on the KF and the SMM-J (or the SMM). Under this distributed computing manner, the estimation errors for the sections without junctions reside below the bounds derived in Chapter 3, and the error bounds studied in this chapter are used to justify the estimation accuracy in the sections with junctions.

This chapter is organized as follows. Section 4.2.1 reviews the junction solver developed in [92], based on which the SMM-J is derived in Section 4.2.2. Section 4.3 analyzes the performance of the KF on the unobservable modes of the SMM-J, where Section 4.3.1 extends Proposition 1 to show the ultimate boundedness of the mean error, and Section 4.3.2 generalized the results in Proposition 2 to obtain a uniform upper bound of the mean error. We conclude this chapter by some remarks on extending the results to systems that switch among the observable and unobservable modes of the SMM-J.

## 4.2 Macroscopic scalar traffic models on junctions

In this section, we derive the switched linear model describing traffic density evolutions on a road section with a junction, namely the *switching mode model with junctions*. The SMM-J combines a switched linear system representation of the CTM (i.e., the CTM where the flux function is the triangular fundamental diagram) with a junction solver. This section starts with a review of the applied junction solver. Next, we introduce the SMM-J and provide examples regarding its explicit formulas. Finally, the observability of the SMM-J is discussed.

### 4.2.1 Junction solver on traffic networks

This subsection introduces the junction solver proposed in [92]. As shown in Figure 4.1a, the junction solver computes flux $\mathrm{f}(\rho_k^l, \rho_k^i)$ and $\mathrm{f}(\rho_k^l, \rho_k^j)$ between the connecting cells $l$, $i$

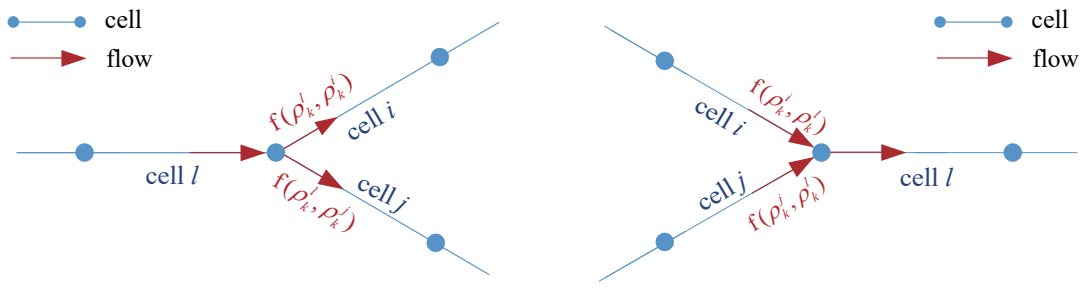


(a) Diverge junction (b) Merge junction

Figure 4.1: A diverge and a merge junction connected by three cells indexed by $i$, $j$, and $l$.

and $j$ forming a diverge junction. In the merge junction shown in Figure 4.1b, the junction solver computes $\mathrm{f}(\rho_k^i, \rho_k^l)$ and $\mathrm{f}(\rho_k^j, \rho_k^l)$ between the connecting cells. This solver is applied in Section 4.2.2 to develop the SMM-J.

#### 4.2.1.1 Diverge junction

At a diverge junction in Figure 4.1a, the junction solver is governed by the following rules:

(R.1): The mass across the junction is conserved.

(R.2): The throughput flow $\mathrm{f}(\rho_k^l, \rho_k^i) + \mathrm{f}(\rho_k^l, \rho_k^j)$, i.e., the outgoing flow of cell $l$, is maximized subject to the maximum flow that can be sent or received on each connecting cell.

(R.3): The distribution of flux $\mathrm{f}(\rho_k^l, \rho_k^i)$ and $\mathrm{f}(\rho_k^l, \rho_k^j)$ satisfies $\mathrm{f}(\rho_k^l, \rho_k^j) = \alpha_\mathrm{d} \mathrm{f}(\rho_k^l, \rho_k^i)$, where $\alpha_\mathrm{d}$ is the prescribed distribution parameter that models the routing preference to the downstream cells. When (R.3) conflicts (R.2), i.e., the flow solution that satisfies the distribution ratio does not maximize the throughput, then (R.3) is relaxed, such that the solution satisfies (R.2) and minimizes the deviation from the distribution parameter, e.g., $|\mathrm{f}(\rho_k^l, \rho_k^j)/\mathrm{f}(\rho_k^l, \rho_k^i) - \alpha_\mathrm{d}|$.

The diverge junction solver is posed as a convex program with a carefully constructed objective function to accommodate the throughput maximization (R.2) and the flow distribution (R.3). The mathematical formula of the diverge junction solver is given below (see [92, Section 3.2] for more details).

**Definition 2** (Convex program for the diverge junction solver)**.** *Define the objective function* $\mathrm{J}(f_1, f_2)$ *as:*

$$\mathrm{J}(f_1, f_2) = (1-\lambda)(f_1 + f_2) - \lambda (f_2 - \alpha_{\mathrm{d}} f_1)^2,$$

*where* $0 < \lambda < 1$ *and* $\lambda$ *is chosen such that* $\frac{\partial \mathrm{J}}{\partial f_1} > 0$ *and* $\frac{\partial \mathrm{J}}{\partial f_2} > 0$[1]*. The conditions on* $\lambda$ *is used to prioritize maximizing the throughput* $\mathrm{f}(\rho_k^l, \rho_k^i) + \mathrm{f}(\rho_k^l, \rho_k^j)$ *(as stated in (R.2)), then minimizing the deviation from the prescribed distribution parameter* $\alpha_{\mathrm{d}}$ *(as stated in (R.3)). The fluxes* $\mathrm{f}(\rho_k^l, \rho_k^i)$ *and* $\mathrm{f}(\rho_k^l, \rho_k^j)$ *are obtained by solving the following convex program:*

$$\begin{aligned} \mathrm{f}(\rho_k^l, \rho_k^i),\ \mathrm{f}(\rho_k^l, \rho_k^j) \ &= \ \underset{f_1, f_2}{\arg\max}\ \mathrm{J}(f_1, f_2) \\ s.t. \quad & f_1 \le \mathrm{r}(\rho_k^i) && (4.1) \\ & f_2 \le \mathrm{r}(\rho_k^j) && (4.2) \\ & f_1 + f_2 \le \mathrm{s}(\rho_k^l). && (4.3) \end{aligned}$$

Figure 4.2 provides a graphical illustration for the solutions of the convex program defined in Definition 2. The blue vertical solid line denotes the receiving capacity of cell $i$, i.e., $\mathrm{r}(\rho_k^i)$, and the blue horizontal solid line denotes the receiving capacity of cell $j$, i.e., $\mathrm{r}(\rho_k^j)$. The intercepts of the blue dashed line (with slope -1) denote the sending capacity of cell $l$, i.e., $\mathrm{s}(\rho_k^l)$. The shaded area denotes the feasible values of the flux from cell $l$ to $i$ and the flux from cell $l$ to $j$, the feasible area is obtained based on (4.1)-(4.3). The slope of the black dotted line is the prescribed distribution ratio $\alpha_{\mathrm{d}}$. The fluxes computed by the junction solver in Definition 2 is marked by the red dot, whose horizontal axis and vertical axis values are the obtained $\mathrm{f}(\rho_k^l, \rho_k^i)$ and $\mathrm{f}(\rho_k^l, \rho_k^j)$, respectively.

According to the convex program in Definition 2, to obtain $\mathrm{f}(\rho_k^l, \rho_k^i)$ and $\mathrm{f}(\rho_k^l, \rho_k^j)$ we need to find the solution point (i.e., the red dot) in Figure 4.2 that satisfies the following requirements:

- The point lies in the shaded feasible area, so that conditions (4.1)-(4.3) are satisfied;
- The point is as close as possible to the blue dashed line (with slope -1), so that the

[1] One possible choice of $\lambda$ is $\lambda = \min\left\{(1 + 2\alpha_a^2 q_{\mathrm{m}} + \epsilon)^{-1}, (1 + 2q_{\mathrm{m}} + \epsilon)^{-1}\right\}$, where $\epsilon > 0$ can be any positive value.

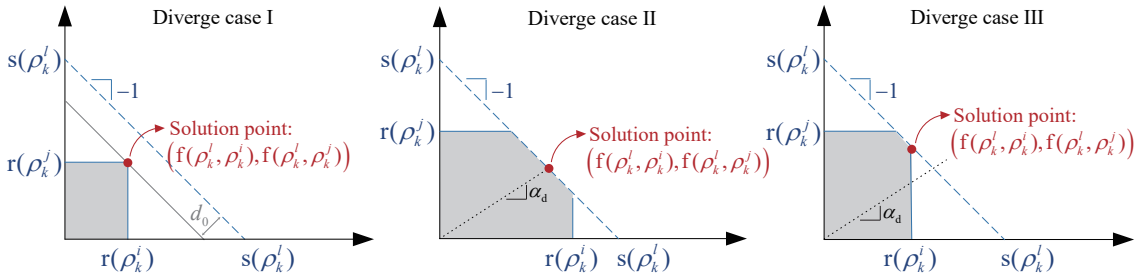


Figure 4.2: Three scenarios in the junction solver [92] for the diverge junction shown in Figure 4.1a, where cell $l$ diverges to cell $i$ and cell $j$. Note that in diverge case II and diverge case III, the receiving capacities of cell $i$ and cell $j$ are not necessarily smaller than the sending capacity of cell $l$, and the graphical illustration of the flux solutions is also applicable for $\mathrm{r}(\rho_k^i) \geq \mathrm{s}(\rho_k^l)$ and/or $\mathrm{r}(\rho_k^j) \geq \mathrm{s}(\rho_k^l)$.

throughput $\mathrm{f}(\rho_k^l, \rho_k^i)+\mathrm{f}(\rho_k^l, \rho_k^j)$ is maximized; this is due to the fact that the distance $d_0$ between the point and the blue dashed line is proportional to the disparity between the sending capacity of cell $l$ and the throughput, i.e., $|\mathrm{s}(\rho_k^l)-(\mathrm{f}(\rho_k^l, \rho_k^i)+\mathrm{f}(\rho_k^l, \rho_k^j))| = \sqrt{2}d_0$ (as illustrated in diverge case I of Figure 4.2);

- Conditioned on prioritizing maximizing the throughput, the point is as close as possible to the black dotted line (with slope $\alpha_\mathrm{d}$), so that the distribution ratio is respected; this means that when maximizing the throughput conflicts with the distribution ratio, the requirement $\mathrm{f}(\rho_k^l, \rho_k^j) = \alpha_\mathrm{d}\mathrm{f}(\rho_k^l, \rho_k^i)$ can be relaxed.

As shown in Figure 4.2, there are in total three scenarios depending on the values of $\mathrm{s}(\rho_k^l)$, $\mathrm{r}(\rho_k^i)$ and $\mathrm{r}(\rho_k^j)$. The three scenarios are: $(i)$ diverge case I, when $\mathrm{s}(\rho_k^l) \geq \mathrm{r}(\rho_k^i) + \mathrm{r}(\rho_k^j)$; $(ii)$ diverge case II, when $\mathrm{s}(\rho_k^l) < \mathrm{r}(\rho_k^i) + \mathrm{r}(\rho_k^j)$, and the prescribed distribution ratio $\alpha_\mathrm{d}$ can be followed exactly; and $(iii)$ diverge case III, when $\mathrm{s}(\rho_k^l) < \mathrm{r}(\rho_k^i) + \mathrm{r}(\rho_k^j)$, but (due to throughput maximization) the prescribed distribution ratio $\alpha_\mathrm{d}$ cannot be followed exactly.

Under diverge case I, the fluxes $\mathrm{f}(\rho_k^l, \rho_k^i)$ and $\mathrm{f}(\rho_k^l, \rho_k^j)$ are computed by:

$$\mathrm{f}(\rho_k^l, \rho_k^i) = \mathrm{r}(\rho_k^i), \quad \mathrm{f}(\rho_k^l, \rho_k^j) = \mathrm{r}(\rho_k^j). \tag{4.4}$$

Under diverge case II, the fluxes $\mathrm{f}(\rho_k^l, \rho_k^i)$ and $\mathrm{f}(\rho_k^l, \rho_k^j)$ are given as follows:

$$\mathrm{f}(\rho_k^l, \rho_k^i) = \frac{1}{\alpha_\mathrm{d}+1}\mathrm{s}(\rho_k^l), \quad \mathrm{f}(\rho_k^l, \rho_k^j) = \frac{\alpha_\mathrm{d}}{\alpha_\mathrm{d}+1}\mathrm{s}(\rho_k^l). \tag{4.5}$$

Under diverge case III, the junction solver first finds the two vertices of the shaded area that lie on the blue dashed line, and next define the point closer to the black dotted line as the flux solutions $\mathrm{f}(\rho_k^l, \rho_k^i)$ and $\mathrm{f}(\rho_k^l, \rho_k^j)$. Hence, depending on the magnitude of $\mathrm{s}(\rho_k^l)$, $\mathrm{r}(\rho_k^i)$ and $\mathrm{r}(\rho_k^j)$, the solutions could be either

$$\mathrm{f}(\rho_k^l, \rho_k^i) = \mathrm{r}(\rho_k^i), \quad \mathrm{f}(\rho_k^l, \rho_k^j) = \mathrm{s}(\rho_k^l) - \mathrm{r}(\rho_k^i), \tag{4.6}$$

or

$$\mathrm{f}(\rho_k^l, \rho_k^i) = \mathrm{s}(\rho_k^l) - \mathrm{r}(\rho_k^j), \quad \mathrm{f}(\rho_k^l, \rho_k^j) = \mathrm{r}(\rho_k^j). \tag{4.7}$$

Note that the diverge case III shown in Figure 4.2 illustrates the flux solutions presented in (4.6).

**Remark 5.** *The diverge junction solver described above is a non-First-In-First-Out (FIFO) model [25, 33]. The FIFO diverge model maximizes the outgoing flow of cell $l$ subject to the distribution ratio $\mathrm{f}(\rho_k^l, \rho_k^j) = \alpha_d \mathrm{f}(\rho_k^l, \rho_k^i)$. Although the FIFO model circumvents the conflicts between throughput maximization and flow distribution, it produces unrealistic solutions in some circumstances. Several diverge junction models have been proposed to resolve this issue [30, 31, 32]. In the same spirit of these models, the diverge junction solver applied in this work is developed to produce similar traffic condition dependent solutions without introducing additional complexity on the traffic dynamics [92]. As a related note, the results proved in this work can be extended to FIFO models with minor changes to the proof.*

#### 4.2.1.2 Merge junction

At a merge junction in Figure 4.1b, the junction solver conserves mass, and maximizes the throughput while minimizing the deviation from a prescribed priority parameter $\alpha_\mathrm{p}$ denoting the flow assignment ratio $\mathrm{f}(\rho_k^j, \rho_k^l) = \alpha_\mathrm{p} \mathrm{f}(\rho_k^i, \rho_k^l)$. This priority equation is relaxed if it conflicts with flow maximization. The reader is referred to [33, 35] for a detailed description of the merge model.

The structure of the diverge and merge models are similar, in the sense that both maximize the throughput while minimizing the deviation from the prescribed distribution or priority parameters. Therefore, the remainder of this chapter focuses on deriving the linear

traffic model and analyzing the performance of the KF on the road section with a diverge junction. The analysis can be transferred to the merge case via combining the merge junction solver with the switched linear representation of the CTM, exploring the properties of the resulting state transition matrices (as in the diverge case), and analyzing the effect of these properties on the boundedness of the Kalman gain and the mean estimation error.

### 4.2.2 The switching mode model with junctions

As stated in Section 4.1, when monitoring traffic on large-scale networks, the road network is partitioned into local sections which are either one-dimensional, or having a junction inside. The traffic states on the one-dimensional local sections evolve according to the SMM, and the SMM-J is used to describe the evolution of traffic states on local sections with junctions. As shown in Figure 4.3, consider a local section with $n$ cells, three links and a junction. The number of cells on each link is $n_1$, $n_2$, and $n_3$, respectively, with $n_1 + n_2 + n_3 = n$. The state variable at time $k \in \mathbb{N}$ is constructed as $\rho_k = \left(\rho_k^1, \cdots, \rho_k^{n_1}, \rho_k^{n_1+1}, \cdots, \rho_k^{n_1+n_2}, \rho_k^{n_1+n_2+1}, \cdots, \rho_k^n\right)^\top$. The SMM-J describes the evolution of $\rho_k$ using a switched linear model, and is derived under the following assumptions:

(Asm.7): For each local section, there is at most one transition between freeflow and congestion in each of the three links.

(Asm.8): The three connecting cells forming the junction (i.e., cell $n_1$, $n_1+1$ and $n_1+n_2+1$ in Figure 4.3) are either all in freeflow or all in congestion.

(Asm.7) is practically meaningful since the local sections are usually partitioned to be sufficiently short such that at most one queue is growing or dissipating within each link, which is also a commonly used assumption in the SMM [15, 28, 45, 46]. (Asm.8) is imposed to simplify the model by reducing the number of modes considered. Note that when (Asm.8) is relaxed, the number of modes is greatly increased, but without yielding new insights into the estimation performance at junctions. The analysis in this chapter still holds, the only difference is to consider an enormously increased number of modes.

Given the assumptions stated above, on each freeway section with a junction, the SMM-J may switch among 32 modes (defined in Table 4.1) depending on ($i$) the freeflow/congestion

Table 4.1: Mode definition and observability of the SMM-J

| Mode | F/C[1] status of cell(s) | | | | Transition[3] on link | | | Diverge | Obser– |
|---|---|---|---|---|---|---|---|---|---|
| | 1 | $n_1+n_2$ | $n$ | near junction[2] | 1 | 2 | 3 | case | vability[4] |
| 1 | F | F | F | F | none | none | none | II | UCO |
| 2 | F | F | F | C | Sh. | Ep. | Ep. | I | Unobservable |
| 3 | F | F | F | C | Sh. | Ep. | Ep. | II | Unobservable |
| 4 | F | F | F | C | Sh. | Ep. | Ep. | III | Unobservable |
| 5 | C | C | C | C | none | none | none | I | Unobservable |
| 6 | C | C | C | C | none | none | none | II | Unobservable |
| 7 | C | C | C | C | none | none | none | III | Unobservable |
| 8 | C | C | C | F | Ep. | Sh. | Sh. | II | Unobservable |
| 9 | F | C | C | C | Sh. | none | none | I | Unobservable |
| 10 | F | C | C | C | Sh. | none | none | II | Unobservable |
| 11 | F | C | C | C | Sh. | none | none | III | Unobservable |
| 12 | F | C | C | F | none | Sh. | Sh. | II | Unobservable |
| 13 | C | C | F | C | none | none | Ep. | I | Unobservable |
| 14 | C | C | F | C | none | none | Ep. | II | Unobservable |
| 15 | C | C | F | C | none | none | Ep. | III | Unobservable |
| 16 | C | C | F | F | Ep. | Sh. | none | II | Unobservable |
| 17 | C | F | C | C | none | Ep. | none | I | Unobservable |
| 18 | C | F | C | C | none | Ep. | none | II | Unobservable |
| 19 | C | F | C | C | none | Ep. | none | III | Unobservable |
| 20 | C | F | C | F | Ep. | none | Sh. | II | Unobservable |
| 21 | C | F | F | F | Ep. | none | none | II | UCO |
| 22 | C | F | F | C | none | Ep. | Ep. | I | Unobservable |
| 23 | C | F | F | C | none | Ep. | Ep. | II | Unobservable |
| 24 | C | F | F | C | none | Ep. | Ep. | III | Unobservable |
| 25 | F | C | F | F | none | Sh. | none | II | Unobservable |
| 26 | F | C | F | C | Sh. | none | Ep. | I | Unobservable |
| 27 | F | C | F | C | Sh. | none | Ep. | II | Unobservable |
| 28 | F | C | F | C | Sh. | none | Ep. | III | Unobservable |
| 29 | F | F | C | F | none | none | Sh. | II | Unobservable |
| 30 | F | F | C | C | Sh. | Ep. | none | I | Unobservable |
| 31 | F | F | C | C | Sh. | Ep. | none | II | Unobservable |
| 32 | F | F | C | C | Sh. | Ep. | none | III | Unobservable |

[1] F and C stand for freeflow and congestion, respectively.

[2] Cells indexed by $n_1$, $n_1+1$ and $n_1+n_2+1$.

[3] "Sh." and "Ep." stand for shock and expansion fan (i.e., transition from congestion to freeflow), respectively.

[4] The observability results are derived under sensor locations shown in Figure 4.3.

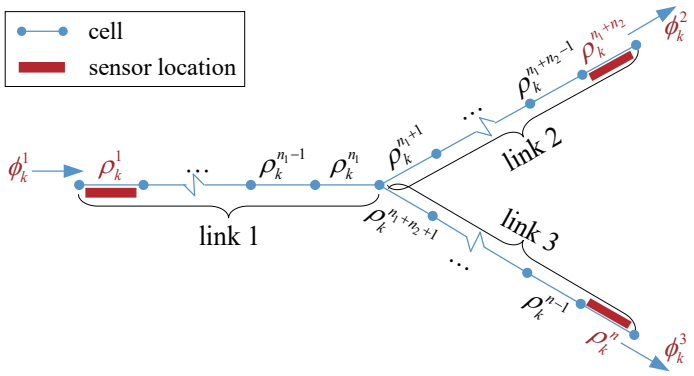


Figure 4.3: A local section with $n$ cells, three links and a junction.

status of the boundary cells and the connecting cells near the junction, and $(ii)$ the flux solution of the junction solver characterized by the three scenarios shown in Figure 4.2.

#### 4.2.2.1 Explicit formula of the SMM-J

In the SMM-J, the density update scheme for the interior cells in each link (i.e., cells indexed by $l \in \{2, \cdots, n_1 - 1\} \cup \{n_1 + 2, \cdots, n_1 + n_2 - 1\} \cup \{n_1 + n_2 + 2, \cdots, n - 1\}$) is given by (2.7), where the flow between two adjacent cells is computed according to (2.8). For the three boundary cells, their density updates are given as follows:

$$\begin{aligned}
\rho_{k+1}^{1} &= \rho_k^1 + \frac{\Delta t}{\Delta x}\left(\phi_k^1 - \mathrm{f}(\rho_k^1, \rho_k^2)\right), \\
\rho_{k+1}^{n_1+n_2} &= \rho_k^{n_1+n_2} + \frac{\Delta t}{\Delta x}\left(\mathrm{f}(\rho_k^{n_1+n_2-1}, \rho_k^{n_1+n_2}) - \phi_k^2\right), \\
\rho_{k+1}^{n} &= \rho_k^n + \frac{\Delta t}{\Delta x}\left(\mathrm{f}(\rho_k^{n-1}, \rho_k^n) - \phi_k^3\right),
\end{aligned}$$

where $\mathrm{f}(\rho_k^1, \rho_k^2)$, $\mathrm{f}(\rho_k^{n_1+n_2-1}, \rho_k^{n_1+n_2})$ and $\mathrm{f}(\rho_k^{n-1}, \rho_k^n)$ are also obtained from (2.8). The density update scheme for the three cells near the junction reads:

$$\begin{aligned}
\rho_{k+1}^{n_1} &= \rho_k^{n_1} + \frac{\Delta t}{\Delta x}\left(\mathrm{f}(\rho_k^{n_1-1}, \rho_k^{n_1}) - \mathrm{f}(\rho_k^{n_1}, \rho_k^{n_1+1}) - \mathrm{f}(\rho_k^{n_1}, \rho_k^{n_1+n_2+1})\right), \\
\rho_{k+1}^{n_1+1} &= \rho_k^{n_1+1} + \frac{\Delta t}{\Delta x}\left(\mathrm{f}(\rho_k^{n_1}, \rho_k^{n_1+1}) - \mathrm{f}(\rho_k^{n_1+1}, \rho_k^{n_1+2})\right), \\
\rho_{k+1}^{n_1+n_2+1} &= \rho_k^{n_1+n_2+1} + \frac{\Delta t}{\Delta x}\left(\mathrm{f}(\rho_k^{n_1}, \rho_k^{n_1+n_2+1}) - \mathrm{f}(\rho_k^{n_1+n_2+1}, \rho_k^{n_1+n_2+2})\right),
\end{aligned}$$

where the flows within the links $\mathrm{f}(\rho_k^{n_1-1}, \rho_k^{n_1})$, $\mathrm{f}(\rho_k^{n_1+1}, \rho_k^{n_1+2})$, and $\mathrm{f}(\rho_k^{n_1+n_2+1}, \rho_k^{n_1+n_2+2})$ are computed by (2.8), and the flows between neighboring cells around the junction (i.e., $\mathrm{f}(\rho_k^{n_1}, \rho_k^{n_1+1})$ and $\mathrm{f}(\rho_k^{n_1}, \rho_k^{n_1+n_2+1})$) are computed based on the junction solver discussed in Section 4.2.1.

When applying the triangular fundamental diagram (2.10) to compute the flow across the cells, the traffic state $\rho_k$ in a section evolves with linear dynamics in each mode stated in Table 4.1, forming a switched system:

$$\rho_{k+1} = A_k \rho_k + B_k^{\rho} \mathbf{1} \varrho_{\mathrm{m}} + B_k^{q} \mathbf{1} q_{\mathrm{m}} + B_k^{\phi} \phi_k, \tag{4.8}$$

where $\mathbf{1}$ is the vector of all ones, the vector $\phi_k = (\phi_k^1, \phi_k^2, \phi_k^3)^\top$, and $A_k \in \mathbb{R}^{n\times n}$, $B_k^{\rho} \in \mathbb{R}^{n\times n}$, $B_k^{q} \in \mathbb{R}^{n\times n}$, $B_k^{\phi} \in \mathbb{R}^{n\times 3}$ are constructed based on the current mode of the section, the locations of the shocks and expansion fans (if they exist), and the moving direction of the shocks.

The next two examples demonstrate the construction of matrices $A_k$, $B_k^{\rho}$, $B_k^{q}$ and $B_k^{\phi}$. Specifically, the construction of matrices $A_k$ provides insights on the properties of the state transition matrices of the SMM-J that reflect the intrinsic physical properties of the traffic model. These properties are critical in proving the estimation error bounds of the KF on traffic networks. Before showing the examples, first recall the notation $\Theta_p(i,j)$, $\Delta_p(i,j)$, $E_{p_1,p_2}^{p_3,p_4}$, $\tilde{\Theta}_p(i,j)$, $\tilde{\Delta}_p(i,j)$ introduced in Section 2.3.2.1, which will be used as elements of the matrices to be constructed.

**Example 1** (System dynamics of the SMM-J under Mode 1)**.** *Consider the road section in Figure 4.3 where all the cells are in freeflow. Within a single link, the flux between two neighboring cells indexed by $i$ and $i+1$ is given by $\mathrm{f}(\rho_k^i, \rho_k^{i+1}) = v_{\mathrm{m}} \rho_k^i$. At the junction, it holds that $\mathrm{s}(\rho_k^{n_1}) = v_{\mathrm{m}} \rho_k^{n_1} < \mathrm{r}(\rho_k^{n_1+1}) + \mathrm{r}(\rho_k^{n_1+n_2+1}) = 2q_{\mathrm{m}}$. Also note that $\mathrm{s}(\rho_k^{n_1}) \le \mathrm{r}(\rho_k^{n_1+1}) = q_{\mathrm{m}}$ and $\mathrm{s}(\rho_k^{n_1}) \le \mathrm{r}(\rho_k^{n_1+n_2+1}) = q_{\mathrm{m}}$, the distribution ratio $\alpha_d$ can be followed exactly. Hence, the state is under Mode 1 at time $k$, and the junction solver computes fluxes $\mathrm{f}(\rho_k^{n_1}, \rho_k^{n_1+1})$ and $\mathrm{f}(\rho_k^{n_1}, \rho_k^{n_1+n_2+1})$ according to diverge case II (4.5) as follows:*

$$\mathrm{f}(\rho_k^{n_1}, \rho_k^{n_1+1}) = \frac{\rho_k^{n_1} v_{\mathrm{m}}}{1+\alpha_{\mathrm{d}}}, \quad \mathrm{f}(\rho_k^{n_1}, \rho_k^{n_1+n_2+1}) = \frac{\alpha_{\mathrm{d}} \rho_k^{n_1} v_{\mathrm{m}}}{1+\alpha_{\mathrm{d}}}.$$

*Substituting the flows computed above into the update scheme of the traffic density on each*

*cell, it follows that the explicit forms of* $A_k$, $B_k^\rho$, $B_k^q$, *and* $B_k^\phi$ *in* (4.8) *are*

$$A_k = \begin{pmatrix} \Theta_{n_1} & & \\ \frac{v_m \Delta t}{(1+\alpha_d)\Delta x} E^{1,n_1}_{n_2,n_1} & \tilde{\Theta}_{n_2} & \\ \frac{\alpha_d v_m \Delta t}{(1+\alpha_d)\Delta x} E^{1,n_1}_{n_3,n_1} & & \tilde{\Theta}_{n_3} \end{pmatrix}, \quad B_k^\rho = B_k^q = \mathbf{0}_{n,n}, \tag{4.9}$$

$$B_k^\phi = \frac{\Delta t}{\Delta x}\left(E^{1,1}_{n,3} - E^{n_1+n_2,2}_{n,3} - E^{n,3}_{n,3}\right)$$

*in Mode 1. Note that in the above definitions and for the remainder of this subsection, blocks in the matrices which are left blank are zeros everywhere.* □

**Example 2** (System dynamics of the SMM-J under Modes 2-4)**.** *Consider the road section in Figure 4.3 where the three boundary cells indexed by* 1, $n_1+n_2$ *and* $n$ *are all in freeflow, and the three cells near the junction, i.e., the cells indexed by* $n_1$, $n_1+1$ *and* $n_1+n_2+1$ *are in congestion. Given the assumption that there is at most one transition between freeflow and congestion in each of the three links connecting the junction, it can be concluded that there is a shock on link 1, while link 2 and link 3 each has an expansion fan. Let* $l_1$ *be the location of the shock on link 1, i.e., the transition from freeflow to congestion on link 1 occurs between cell* $l_1$ *and* $l_1+1$*. Moreover, we define*

$$\tilde{l}_1 = \begin{cases} l_1 & \text{if the shock has positive velocity (or is stationary)} \\ l_1 - 1 & \text{if the shock has negative velocity,} \end{cases}$$

*and* $\hat{l}_1 = n_1 - 1 - \tilde{l}_1$*, which are later used to simplify the notations to define matrices* $A_k$, $B_k^\rho$, $B_k^q$, *and* $B_k^\phi$*. Similarly, denote as* $l_2$ *(resp.* $l_3$*) the location of the expansion fan on link 2 (resp. link 3), i.e., the transition from congestion to freeflow on link 2 (resp. link 3) occurs between cells* $l_2$ *and* $l_2+1$ *(resp. cells* $l_3$ *and* $l_3+1$*). To simplify the notation, we also define*

$$\tilde{l}_2 = l_2 - n_1, \quad \hat{l}_2 = n_2 - \tilde{l}_2, \quad \tilde{l}_3 = l_3 - n_1 - n_2, \quad \hat{l}_3 = n_3 - \tilde{l}_3.$$

*At the junction, the sending capacity of cell* $n_1$ *is* $\mathrm{s}(\rho_k^{n_1}) = q_m$*, and the receiving capacities of cell* $n_1+1$ *and cell* $n_1+n_2+1$ *are* $\mathrm{r}(\rho_k^{n_1+1}) = w(\varrho_m - \rho_k^{n_1+1})$ *and* $\mathrm{r}(\rho_k^{n_1+n_2+1}) = w(\varrho_m - \rho_k^{n_1+n_2+1})$*, respectively. Depending on the magnitudes of* $\mathrm{s}(\rho_k^{n_1})$, $\mathrm{r}(\rho_k^{n_1+1})$, *and* $\mathrm{r}(\rho_k^{n_1+n_2+1})$*, the junction solver follows one of the three possible scenarios shown in Figure*

*4.2.*

1. *Diverge case I: when* $\mathrm{s}(\rho_k^{n_1}) \geq \mathrm{r}(\rho_k^{n_1+1}) + \mathrm{r}(\rho_k^{n_1+n_2+1})$. *In this case, the state is under Mode 2 at time* $k$, *and the junction solver computes fluxes* $\mathrm{f}(\rho_k^{n_1}, \rho_k^{n_1+1})$ *and* $\mathrm{f}(\rho_k^{n_1}, \rho_k^{n_1+n_2+1})$ *according to diverge case I* (4.4) *as follows:*

$$\begin{aligned}\mathrm{f}(\rho_k^{n_1}, \rho_k^{n_1+1}) &= \mathrm{r}(\rho_k^{n_1+1}) = w(\varrho_{\mathrm{m}} - \rho_k^{n_1+1}),\\ \mathrm{f}(\rho_k^{n_1}, \rho_k^{n_1+n_2+1}) &= \mathrm{r}(\rho_k^{n_1+n_2+1}) = w(\varrho_{\mathrm{m}} - \rho_k^{n_1+n_2+1}).\end{aligned}$$

*Hence in Mode 2, the explicit forms of* $A_k$, $B_k^\rho$, $B_k^q$, *and* $B_k^\phi$ *in* (4.8) *are*

$$A_k = \begin{pmatrix} \Theta_{\tilde{l}_1} & & & & & & & \\ \frac{v_{\mathrm{m}}\Delta t}{\Delta x} E_{1,\tilde{l}_1}^{1,\tilde{l}_1} & 1 & \frac{w\Delta t}{\Delta x} E_{1,\hat{l}_1}^{1,1} & & & & & \\ & & \Delta_{\hat{l}_1} & \frac{w\Delta t}{\Delta x} E_{\hat{l}_1,\tilde{l}_2}^{\hat{l}_1,1} & & \frac{w\Delta t}{\Delta x} E_{\hat{l}_1,\tilde{l}_3}^{\hat{l}_1,1} & & \\ & & & \Delta_{\tilde{l}_2} & & & & \\ & & & & \tilde{\Theta}_{\hat{l}_2} & & & \\ & & & & & \Delta_{\tilde{l}_3} & & \\ & & & & & & \tilde{\Theta}_{\hat{l}_3} & \end{pmatrix},$$

$$\begin{aligned}B_k^\rho &= \frac{w\Delta t}{\Delta x}\left(-E_{n,n}^{\tilde{l}_1+1,\tilde{l}_1+2} - E_{n,n}^{n_1,n_1+n_2+1} + E_{n,n}^{l_2,l_2} + E_{n,n}^{l_3,l_3}\right),\\ B_k^q &= \frac{\Delta t}{\Delta x}\left(-E_{n,n}^{l_2.l_2} + E_{n,n}^{l_2+1,l_2} - E_{n,n}^{l_3,l_3} + E_{n,n}^{l_3+1,l_3}\right),\\ B_k^\phi &= \frac{\Delta t}{\Delta x}\left(E_{n,3}^{1,1} - E_{n,3}^{n_1+n_2,2} - E_{n,3}^{n,3}\right).\end{aligned}$$

2. *Diverge case II: when* $\mathrm{s}(\rho_k^{n_1}) < \mathrm{r}(\rho_k^{n_1+1}) + \mathrm{r}(\rho_k^{n_1+n_2+1})$, *and the prescribed distribution ratio* $\alpha_{\mathrm{d}}$ *can be followed exactly. In this case, the state is under Mode 3 at time* $k$, *and the junction solver computes fluxes* $\mathrm{f}(\rho_k^{n_1}, \rho_k^{n_1+1})$ *and* $\mathrm{f}(\rho_k^{n_1}, \rho_k^{n_1+n_2+1})$ *according to diverge case II* (4.5) *as follows:*

$$\begin{aligned}\mathrm{f}(\rho_k^{n_1}, \rho_k^{n_1+1}) &= \frac{1}{\alpha_{\mathrm{d}}+1}\mathrm{s}(\rho_k^{n_1}) = \frac{1}{\alpha_{\mathrm{d}}+1} q_{\mathrm{m}},\\ \mathrm{f}(\rho_k^{n_1}, \rho_k^{n_1+n_2+1}) &= \frac{\alpha_{\mathrm{d}}}{\alpha_{\mathrm{d}}+1}\mathrm{s}(\rho_k^{n_1}) = \frac{\alpha_{\mathrm{d}}}{\alpha_{\mathrm{d}}+1} q_{\mathrm{m}}.\end{aligned}$$

*In Mode 3, the explicit forms of $A_k$, $B_k^\rho$, $B_k^q$, and $B_k^\phi$ in* (4.8) *are*

$$A_k = \begin{pmatrix} \Theta_{\tilde{l}_1} & & & & & & & \\ \frac{v_{\mathrm{m}}\Delta t}{\Delta x}E_{1,\tilde{l}_1}^{1,\tilde{l}_1} & 1 & \frac{w\Delta t}{\Delta x}E_{1,\hat{l}_1}^{1,1} & & & & & \\ & & \Delta_{\hat{l}_1} & & & & & \\ & & & \tilde{\Delta}_{\tilde{l}_2} & & & & \\ & & & & \tilde{\Theta}_{\hat{l}_2} & & & \\ & & & & & \tilde{\Delta}_{\tilde{l}_3} & & \\ & & & & & & \tilde{\Theta}_{\hat{l}_3} & \end{pmatrix},$$

$$\begin{aligned} B_k^\rho =& \frac{w\Delta t}{\Delta x}\left(-E_{n,n}^{\tilde{l}_1+1,\tilde{l}_1+2} + E_{n,n}^{n_1,n_1} - E_{n,n}^{n_1+1,n_1+2} + E_{n,n}^{l_2,l_2} - E_{n,n}^{n_1+n_2+1,n_1+n_2+2} + E_{n,n}^{l_3,l_3}\right), \\ B_k^q =& \frac{\Delta t}{\Delta x}\left(-E_{n,n}^{n_1+n_1} + \frac{1}{1+\alpha_d}E_{n,n}^{n_1+1,n_1} + \frac{\alpha_d}{1+\alpha_d}E_{n,n}^{n_1+n_2+1,n_1}\right. \\ & \left. -E_{n,n}^{l_2,l_2} + E_{n,n}^{l_2+1,l_2} - E_{n,n}^{l_3,l_3} + E_{n,n}^{l_3+1,l_3}\right), \\ B_k^\phi =& \frac{\Delta t}{\Delta x}\left(E_{n,3}^{1,1} - E_{n,3}^{n_1+n_2,2} - E_{n,3}^{n,3}\right). \end{aligned}$$

3. *Diverge case III: when* $\mathrm{s}(\rho_k^{n_1}) < \mathrm{r}(\rho_k^{n_1+1}) + \mathrm{r}(\rho_k^{n_1+n_2+1})$*, but the prescribed distribution ratio* $\alpha_d$ *cannot be followed exactly. In this case, the state is under Mode 4 at time* $k$*. Depending on the magnitudes of* $\mathrm{s}(\rho_k^{n_1})$*,* $\mathrm{r}(\rho_k^{n_1+1})$ *and* $\mathrm{r}(\rho_k^{n_1+n_2+1})$*, the fluxes* $\mathrm{f}(\rho_k^{n_1}, \rho_k^{n_1+1})$ *and* $\mathrm{f}(\rho_k^{n_1}, \rho_k^{n_1+n_2+1})$ *computed by the junction solver are either obtained from* (4.6)*, i.e.,*

$$\begin{aligned} &\mathrm{f}(\rho_k^{n_1}, \rho_k^{n_1+1}) = \mathrm{r}(\rho_k^{n_1+1}) = w(\varrho_{\mathrm{m}} - \rho_k^{n_1+1}), \\ &\mathrm{f}(\rho_k^{n_1}, \rho_k^{n_1+n_2+1}) = \mathrm{s}(\rho_k^{n_1}) - \mathrm{r}(\rho_k^{n_1+1}) = q_{\mathrm{m}} - w(\varrho_{\mathrm{m}} - \rho_k^{n_1+1}), \end{aligned} \tag{4.10}$$

*or obtained from* (4.7)*, i.e.,*

$$\begin{aligned} &\mathrm{f}(\rho_k^{n_1}, \rho_k^{n_1+1}) = \mathrm{s}(\rho_k^{n_1}) - \mathrm{r}(\rho_k^{n_1+n_2+1}) = q_{\mathrm{m}} - w(\varrho_{\mathrm{m}} - \rho_k^{n_1+n_2+1}), \\ &\mathrm{f}(\rho_k^{n_1}, \rho_k^{n_1+n_2+1}) = \mathrm{r}(\rho_k^{n_1+n_2+1}) = w(\varrho_{\mathrm{m}} - \rho_k^{n_1+n_2+1}). \end{aligned} \tag{4.11}$$

*For conciseness of the presentation, we provide next the explicit formulas of* $A_k$*,* $B_k^\rho$*,* $B_k^q$*, and* $B_k^\phi$ *when the fluxes are computed according to* (4.10)*, and the construction*

*of the system dynamics when the fluxes are given by* (4.11) *can be done in a similar fashion. The matrices* $A_k$, $B_k^\rho$, $B_k^q$, *and* $B_k^\phi$ *read*

$$A_k = \begin{pmatrix} \Theta_{\tilde{l}_1} & & & & & & \\ \frac{v_m \Delta t}{\Delta x} E^{1,\tilde{l}_1}_{1,\tilde{l}_1} & 1 & \frac{w\Delta t}{\Delta x} E^{1,1}_{1,\hat{l}_1} & & & & \\ & & \Delta_{\hat{l}_1} & \frac{w\Delta t}{\Delta x} E^{\hat{l}_1,1}_{\hat{l}_1,\tilde{l}_2} & & & \\ & & & \Delta_{\tilde{l}_2} & & & \\ & & & & \tilde{\Theta}_{\hat{l}_2} & & \\ & & & \frac{w\Delta t}{\Delta x} E^{1,1}_{\tilde{l}_3,\tilde{l}_2} & & \tilde{\Delta}_{\tilde{l}_3} & \\ & & & & & & \tilde{\Theta}_{\hat{l}_3} \end{pmatrix},$$

$$\begin{aligned} B_k^\rho =& \frac{w\Delta t}{\Delta x}\left(-E^{\tilde{l}_1+1,\tilde{l}_1+2}_{n,n} + E^{l_2,l_2}_{n,n} - E^{n_1+n_2+1,n_1+n_2+2}_{n,n} - E^{n_1+n_2+1,n_1+1}_{n,n} + E^{l_3,l_3}_{n,n}\right), \\ B_k^q =& \frac{\Delta t}{\Delta x}\left(-E^{l_2.l_2}_{n,n} + E^{l_2+1,l_2}_{n,n} + E^{n_1+n_2+1,n_1+1}_{n,n} - E^{l_3,l_3}_{n,n} + E^{l_3+1,l_3}_{n,n}\right), \\ B_k^\phi =& \frac{\Delta t}{\Delta x}\left(E^{1,1}_{n,3} - E^{n_1+n_2,2}_{n,3} - E^{n,3}_{n,3}\right). \end{aligned}$$

□

#### 4.2.2.2 Properties of the state transition matrices of the SMM-J

Some properties of the state transition matrix $A_k$ of the SMM-J are summarized below. Similar to the SMM, the properties listed below 3.4.1 assume important roles in proving the boundedness of the Kalman gain when using the KF to estimate traffic conditions based on the SMM-J (see the proof of Lemma 7).

(P.3): For $A_k$ in all modes, each element satisfies

$$0 \leq A_k(r,c) \leq 1, \quad \text{for all } k \in \mathbb{N} \text{ and } r, c \in \{1, 2, \cdots, n\}.$$

This property is the same as property (P.1) of the SMM, which is due to the CFL condition (2.9) in the discretization scheme (2.7).

(P.4): When $A_k$ is derived under diverge case I and diverge case II, the sum of the elements

in $A_k$ at the same column $c$ satisfies

$$\sum_{r=1}^{n} A_k(r,c) \leq 1, \quad \text{for all } k \in \mathbb{N} \text{ and } c \in \{1,2,\cdots,n\}.$$

This property is due to the CFL condition as in (P.3) and the conservation law embedded in the traffic model.

(P.5): When $A_k$ is derived under diverge case III, the sum of the elements in $A_k$ at the same column $c$ satisfies

$$\sum_{r=1}^{n} A_k(r,c) \leq 1, \quad \text{for all } k \in \mathbb{N} \text{ and } c \in \{c | c \in \{1,2,\cdots,n\}, c \neq \ell\},$$

where $\ell = n_1 + 1$ if $\mathrm{f}(\rho_k^{n_1}, \rho_k^{n_1+1}) = \mathrm{r}(\rho_k^{n_1+1})$ and $\ell = n_1 + n_2 + 1$ if $\mathrm{f}(\rho_k^{n_1}, \rho_k^{n_1+1}) = \mathrm{s}(\rho_k^{n_1}) - \mathrm{r}(\rho_k^{n_1+n_2+1})$. Moreover, it also holds that for $A_k$ under diverge case III,

$$A_k(r,c) = 0, \quad \text{for all } k \in \mathbb{N},\ r \in \{n_1+1,\cdots,n\} \text{ and } c \in \{1,\cdots n_1\}.$$

This is due to the facts that $(i)$ in diverge case III, the flows from cell $n_1$ at the junction to the two downstream cells (i.e., cell $n_1+1$ and cell $n_1+n_2+1$) do not depend on the densities of the cells on link 1, as shown in (4.10)-(4.11), and $(ii)$ the internal flows between adjacent cells on link 2 and link 3 are also independent of the densities of the cells on link 1.

Based on the above properties, the following lemma derives the bounds on each entry of the product of the state transition matrices, which is important in proving the boundedness of the Kalman gain (see Lemma 7).

**Lemma 8** (Product of the state transition matrices of SMM-J)**.** *Consider the road section in Figure 4.3 that switches inside a SMM-J mode while $k \in (\underline{k}, \bar{k}]$, where $0 \leq \underline{k} < \bar{k} \leq +\infty$. Recall from* (2.5) *that the product of the state transition matrices is defined as*

$$\Xi_{k+1,\underline{k}+1} = \prod_{\kappa=k}^{\underline{k}+1} A_\kappa, \quad \textit{for } k \in (\underline{k}, \bar{k}]. \tag{4.12}$$

*The* $(i,j)^{th}$ *entry of* $\Xi_{k+1,\underline{k}+1}$ *satisfies*

$$0 \leq \Xi_{k+1,\underline{k}+1}(i,j) \leq 1 \quad \textit{for all } k \in (\underline{k}, \bar{k}] \textit{ and } i,j \in \{1,2,\cdots,n\}. \tag{4.13}$$

*Proof.* The proof applies (P.3)-(P.5), and is reported in Appendix C.6. □

#### 4.2.2.3 Observability of the SMM-J

Incorporating model noise in the SMM-J (4.8) yields:

$$\rho_{k+1} = A_k \rho_k + u_k + \omega_k, \quad \rho_k \in \mathbb{R}^n, \tag{4.14}$$

where $\omega_k \sim \mathbf{N}(0, Q_k)$ is the white Gaussian model noise, and define the deterministic system input as: $u_k = B_k^{\rho}\mathbf{1}\varrho_{\mathrm{m}} + B_k^{q}\mathbf{1}q_{\mathrm{m}} + B_k^{\phi}\phi_k$.

From an estimation point of view, the following assumption is made for the sensor locations:

(Asm.9): the sensors are located on the far ends of the three links connecting the junction (as illustrated in Figure 4.3), measuring the densities of the boundary cells of the local section (i.e., $\rho_k^1$, $\rho_k^{n_1+n_2}$ and $\rho_k^n$).

Hence, the sensor measurements are modeled as follows:

$$z_k = H_k \rho_k + v_k, \quad z_k \in \mathbb{R}^3, \tag{4.15}$$

where the observation matrix

$$H_k = E_{3,n}^{1,1} + E_{3,n}^{2,n_1+n_2} + E_{3,n}^{3,n}, \tag{4.16}$$

and $v_k \sim \mathbf{N}(0, R_k)$ is the white Gaussian measurement noise. Hence, as shown in (4.14)-(4.15), the system dynamics of the SMM-J is rewritten in the form of (2.1)-(2.2).

The observability of system (4.14)-(4.16) under different modes are listed in Table 4.1. According to Table 4.1, most of the modes are not observable except $(i)$ when all cells in the local section are in freeflow, and $(ii)$ when an expansion fan sits on link 1 and no other transitions between freeflow and congestion exist in the local section. From a physical

viewpoint, the non-observability of the SMM-J is due to the irreversibility of the vehicle conservation law given the available sensor measurements in the presence of shocks, and the presence of the junction. It is indicated that compared to the observability of the SMM [15], the issue of non-observability is more critical when junctions exist. For example, a one-dimensional road section where the traffic is in congestion everywhere is observable given measurements of the upstream boundary cell [15], while a congested road section with a junction is not observable even with the measurements of all the three boundary cells (as shown by the cases for Modes 5-7). The performance of the KF under uniformly completely observable systems is widely studied (as summarized in Lemma 2). In this chapter, we focus on analyzing the theoretical performance of the KF under the unobservable modes of the SMM-J.

## 4.3 Performance analysis of the KF on traffic networks with junctions

In this section, we show that the performance analysis of the KF under the SMM can be extended to the SMM-J. As stated in Section 4.2.2.3, since the unobservable scenarios are much more frequently encountered in the SMM-J, we study the error bounds for the KF under the unobservable modes. The essence of the proofs for the SMM-J under unobservable scenarios is similar to the SMM, and the major difference in the SMM-J is to compute the flows across the junction based on the junction solver introduced in Section 4.2.1. The analysis under the observable modes of the SMM-J follows very closely with the analysis for the SMM, and we discuss briefly at the end of this section regarding the extension of the results when the system switches among the unobservable and observable modes.

### 4.3.1 Ultimately bounded mean estimation error

In this subsection, we extend the results in Proposition 1 to show that in an unobservable road section with a junction, the mean estimates of all the cells are ultimately bounded inside the physically meaningful interval.

Like the analysis for the SMM, the first step to ensure the boundedness of the mean estimation error is showing the boundedness of the Kalman gain under unobservable sce-

narios. This is already justified in Lemma 7, which derives the uniform upper bound of the infinity norm of the Kalman gain for both the SMM and the SMM-J. The next proposition presents the ultimate boundedness of the mean error for the SMM-J when the system is unobservable.

**Proposition 5** (Ultimate bounded mean error under the unobservable modes of SMM-J)**.** *Consider a road section shown in Figure 4.3 that switches inside an unobservable mode of the SMM-J while $k \in (\underline{k}_{\mathrm{U}}, \infty)$. For all $\epsilon > 0$, a finite time $\tilde{\mathrm{t}}(\epsilon)$ exists such that $\boldsymbol{\rho}^l_{k|k} \in (-\epsilon, \varrho_{\mathrm{m}}+\epsilon)$ for all $k > \underline{k}_{\mathrm{U}} + \tilde{\mathrm{t}}(\epsilon)$ and for all $l \in \{1, 2, \cdots, n\}$, independent of the initial estimate. Moreover, the mean estimation error satisfies $\|\boldsymbol{\eta}_{k|k}\| < \sqrt{n}(\varrho_m + \epsilon)$ for all $k > \underline{k}_{\mathrm{U}} + \tilde{\mathrm{t}}(\epsilon)$, independent of the initial estimate.*

*Proof.* Denote as $\boldsymbol{\eta}^b_{k|k} = (\boldsymbol{\eta}^1_{k|k}, \boldsymbol{\eta}^{n_1+n_2}_{k|k}, \boldsymbol{\eta}^n_{k|k})^\top$ the mean error of the three boundary cells. Since the three boundary cells are all inside the observable subsystem, it follows that $\left\|\boldsymbol{\eta}^b_{k|k}\right\| \to 0$ as $k \to \infty$.

The proof is by induction. In Step 1, we use an induction from cell 1 to the downstream cells to show that if the estimate of cell 1 converges to the true state, then the estimate of all cells will ultimately be greater than $-\epsilon$ for all $\epsilon > 0$. In Step 2, we use an induction from the two downstream boundary cells (i.e., cell $n_1 + n_2$ and cell $n$) to their upstream cells to show that if the estimates of the two downstream boundary cells converge to the true state, then the estimate of all cells will ultimately be smaller than $\varrho_{\mathrm{m}} + \epsilon$ for all $\epsilon > 0$. In Step 3, we combine Step 1 and Step 2 to derive an ultimate bound for the mean estimation error.

**Step 1**: We use induction to show that for all $\epsilon > 0$ and $l \in \{1, \cdots, n\}$, there exists a finite time $\tilde{\mathrm{t}}^l_1(\epsilon)$ such that $\boldsymbol{\rho}^l_{k|k} > -\epsilon$ for all $k > \underline{k}_{\mathrm{U}} + \tilde{\mathrm{t}}^l_1(\epsilon)$.

Since the upstream boundary cell (i.e., cell 1) is in the observable subsystem, we have $\boldsymbol{\eta}^1_{k|k} \to 0$ and $\boldsymbol{\rho}^1_{k|k} \to \rho^1_k$, where $\rho^1_k \geq 0$. Hence a finite time $\tilde{\mathrm{t}}^1_1(\epsilon)$ exists such that $\boldsymbol{\rho}^1_{k|k} > -\frac{\epsilon}{n}$ for all $k > \underline{k}_{\mathrm{U}} + \tilde{\mathrm{t}}^1_1(\epsilon)$.

For all interior cells on link 1, i.e., cells indexed by $l \in \{2, 3, \cdots, n_1\}$, suppose $\boldsymbol{\rho}^{l-1}_{k|k} > -\frac{(l-1)\epsilon}{n}$, if $\boldsymbol{\rho}^l_{k|k} < -\frac{(l-1)\epsilon}{n}$, we obtain from (2.8) that

$$\mathrm{f}\left(\boldsymbol{\rho}^{l-1}_{k|k}, \boldsymbol{\rho}^l_{k|k}\right) > -v_{\mathrm{m}}\frac{(l-1)\epsilon}{n}, \;\; \mathrm{f}\left(\boldsymbol{\rho}^l_{k|k}, \boldsymbol{\rho}^{l+1}_{k|k}\right) \leq v_{\mathrm{m}}\boldsymbol{\rho}^l_{k|k}. \tag{4.17}$$

It follows that the estimate of cell $l$ satisfies

$$\begin{aligned}\boldsymbol{\rho}^l_{k+1|k+1} &= \boldsymbol{\rho}^l_{k|k} + \tfrac{\Delta t}{\Delta x}\left(\mathrm{f}\left(\boldsymbol{\rho}^{l-1}_{k|k}, \boldsymbol{\rho}^l_{k|k}\right) - \mathrm{f}\left(\boldsymbol{\rho}^l_{k|k}, \boldsymbol{\rho}^{l+1}_{k|k}\right)\right)\\ &\quad -K_{k+1}(l,1)\boldsymbol{\eta}^1_{k+1|k} - K_{k+1}(l,2)\boldsymbol{\eta}^{n_1+n_2}_{k+1|k} - K_{k+1}(l,3)\boldsymbol{\eta}^n_{k+1|k}\\ &> \boldsymbol{\rho}^l_{k|k} + \tfrac{v_{\mathrm{m}}\Delta t}{\Delta x}\left|\boldsymbol{\rho}^l_{k|k} + \tfrac{(l-1)\epsilon}{n}\right| - \mathrm{k}\left(\Gamma_{\underline{k}_{\mathrm{U}}|\underline{k}_{\mathrm{U}}}\right)\left\|\boldsymbol{\eta}^b_{k|k}\right\|_\infty,\end{aligned} \tag{4.18}$$

where the inequality is due to $\|K_k\|_\infty \leq \mathrm{k}(\Gamma_{\underline{k}_{\mathrm{U}}|\underline{k}_{\mathrm{U}}})$ given in Lemma 7. Thus there exists a scalar $\tilde{v}_1 > \frac{\Delta x \mathrm{k}\left(\Gamma_{\underline{k}_{\mathrm{U}}|\underline{k}_{\mathrm{U}}}\right)}{v_{\mathrm{m}}\Delta t}$ such that

$$\boldsymbol{\rho}^l_{k+1|k+1} - \boldsymbol{\rho}^l_{k|k} > \tilde{v}_0\left|\boldsymbol{\rho}^l_{k|k} + \frac{(l-1)\epsilon}{n}\right|, \text{ for all } \left|\boldsymbol{\rho}^l_{k|k} + \frac{(l-1)\epsilon}{n}\right| \geq \tilde{v}_1\left\|\boldsymbol{\eta}^b_{k|k}\right\|_\infty, \tag{4.19}$$

where $\tilde{v}_0 = \frac{v_{\mathrm{m}}\Delta t}{\Delta x} - \frac{\mathrm{k}\left(\Gamma_{\underline{k}_{\mathrm{U}}|\underline{k}_{\mathrm{U}}}\right)}{\tilde{v}_1} > 0$. Also note that $\left\|\boldsymbol{\eta}^b_{k|k}\right\|_\infty \to 0$ as $k \to \infty$, which indicates that the one-step change of the estimates is ultimately positive, and large enough so that a finite time $\tilde{\mathrm{t}}^l_1(\epsilon)$ exists such that $\boldsymbol{\rho}^l_{k|k} > -\frac{l\epsilon}{n} > -\epsilon$ for all $k > \underline{k}_{\mathrm{U}} + \tilde{\mathrm{t}}^l_1(\epsilon)$ [89].

We now show that for the two cells on the downstream side of the junction, i.e., cell $n_1+1$ and cell $n_1+n_2+1$, there exist finite times $\tilde{\mathrm{t}}^{n_1+1}_1(\epsilon)$ and $\tilde{\mathrm{t}}^{n_1+n_2+1}_1(\epsilon)$ such that $\boldsymbol{\rho}^{n_1+1}_{k|k} > -\frac{(n_1+1)\epsilon}{n} > -\epsilon$ for all $k > \underline{k}_{\mathrm{U}} + \tilde{\mathrm{t}}^{n_1+1}_1(\epsilon)$ and $\boldsymbol{\rho}^{n_1+n_2+1}_{k|k} > -\frac{(n_1+1)\epsilon}{n} > -\epsilon$ for all $k > \underline{k}_{\mathrm{U}} + \tilde{\mathrm{t}}^{n_1+n_2+1}_1(\epsilon)$. Suppose $\boldsymbol{\rho}^{n_1}_{k|k} > -\frac{n_1\epsilon}{n}$, if $\boldsymbol{\rho}^{n_1+1}_{k|k} < -\frac{n_1\epsilon}{n}$, the junction solver follows diverge case II or diverge case III. Hence, the flow from cell $n_1$ to cell $n_1+1$ satisfies:

$$\mathrm{f}\left(\boldsymbol{\rho}^{n_1}_{k|k}, \boldsymbol{\rho}^{n_1+1}_{k|k}\right) = \begin{cases} \frac{1}{\alpha_{\mathrm{d}}+1}\mathrm{s}\left(\boldsymbol{\rho}^{n_1}_{k|k}\right) > -v_{\mathrm{m}}\frac{n_1\epsilon}{n} & \text{diverge case II} \\ \mathrm{s}\left(\boldsymbol{\rho}^{n_1}_{k|k}\right) - \mathrm{r}\left(\boldsymbol{\rho}^{n_1+n_2+1}_{k|k}\right) > -v_{\mathrm{m}}\frac{n_1\epsilon}{n} & \text{diverge case III,}\end{cases}$$

where the last inequality is due to the fact that $\mathrm{r}\left(\boldsymbol{\rho}^{n_1+n_2+1}_{k|k}\right) \leq 0$ in diverge case III (otherwise the solution for the junction solver follows diverge case II). The outgoing flows for cell $n_1+1$ satisfies:

$$\mathrm{f}\left(\boldsymbol{\rho}^{n_1+1}_{k|k}, \boldsymbol{\rho}^{n_1+2}_{k|k}\right) \leq v_{\mathrm{m}}\boldsymbol{\rho}^{n_1+1}_{k|k}.$$

Following the similar arguments as in (4.18)-(4.19), it can be concluded that there exist a finite time $\tilde{\mathrm{t}}^{n_1+1}_1(\epsilon)$ such that $\boldsymbol{\rho}^{n_1+1}_{k|k} > -\frac{(n_1+1)\epsilon}{n} > -\epsilon$ for all $k > \underline{k}_{\mathrm{U}} + \tilde{\mathrm{t}}^{n_1+1}_1(\epsilon)$. Applying the same analysis for cell $n_1+n_2+1$, it can be concluded that there exist a finite time

$\tilde{\mathrm{t}}_1^{n_1+n_2+1}(\epsilon)$ such that $\boldsymbol{\rho}_{k|k}^{n_1+n_2+1} > -\frac{(n_1+1)\epsilon}{n} > -\epsilon$ for all $k > \underline{k}_{\mathrm{U}} + \tilde{\mathrm{t}}_1^{n_1+n_2+1}(\epsilon)$. Continuing the induction on link 2 from cell $n_1+1$ to cell $n_1+n_2$, we obtain that for all $\epsilon > 0$ and $l \in \{n_1+1, n_1+2, \cdots, n_1+n_2\}$, there exists a finite time $\tilde{\mathrm{t}}_1^l(\epsilon)$ such that $\boldsymbol{\rho}_{k|k}^l > -\frac{l\epsilon}{n} > -\epsilon$ for all $k > \underline{k}_{\mathrm{U}} + \tilde{\mathrm{t}}_1^l(\epsilon)$. As for the cells on link 3, we process the same induction from cell $n_1+n_2+1$ to cell $n$, which yields that for all $\epsilon > 0$ and $l \in \{n_1+n_2+1, n_1+n_2+2, \cdots, n\}$, there exists a finite time $\tilde{\mathrm{t}}_1^l(\epsilon)$ such that $\boldsymbol{\rho}_{k|k}^l > -\frac{(l-n_2)\epsilon}{n} > -\epsilon$ for all $k > \underline{k}_{\mathrm{U}} + \tilde{\mathrm{t}}_1^l(\epsilon)$.

Let $\tilde{\mathrm{t}}_1(\epsilon) = \max_{l\in\{1,\cdots,n\}}\{\tilde{\mathrm{t}}_1^l(\epsilon)\}$, it is concluded that $\boldsymbol{\rho}_{k|k}^l > -\epsilon$ for all $k > \underline{k}_{\mathrm{U}} + \tilde{\mathrm{t}}_1(\epsilon)$ and $l \in \{1, \cdots, n\}$. This proves the ultimate lower bound of the estimates.

**Step 2**: We use induction to show that for all $\epsilon > 0$ and $l \in \{1, \cdots, n\}$, there exists a finite time $\tilde{\mathrm{t}}_2^l(\epsilon)$ such that $\boldsymbol{\rho}_{k|k}^l < \varrho_{\mathrm{m}} + \epsilon$ for all $k > \underline{k}_{\mathrm{U}} + \tilde{\mathrm{t}}_2^l(\epsilon)$.

Since the two downstream boundary cells (indexed by $n_1+n_2$ and $n$) are in the observable subsystem, we have $\boldsymbol{\eta}_{k|k}^{n_1+n_2} \to 0$ and $\boldsymbol{\rho}_{k|k}^{n_1+n_2} \to \rho_k^{n_1+n_2}$, as well as $\boldsymbol{\eta}_{k|k}^n \to 0$ and $\boldsymbol{\rho}_{k|k}^n \to \rho_k^n$. Given the facts that $\rho_k^{n_1+n_2} \le \varrho_{\mathrm{m}}$ and $\rho_k^n \le \varrho_{\mathrm{m}}$, there exist finite times $\tilde{\mathrm{t}}_2^{n_1+n_2}(\epsilon)$ and $\tilde{\mathrm{t}}_2^n(\epsilon)$ such that $\boldsymbol{\rho}_{k|k}^{n_1+n_2} < \varrho_{\mathrm{m}} + \frac{\epsilon}{n}$ for all $k > \underline{k}_{\mathrm{U}} + \tilde{\mathrm{t}}_2^{n_1+n_2}(\epsilon)$, and $\boldsymbol{\rho}_{k|k}^n < \varrho_{\mathrm{m}} + \frac{\epsilon}{n}$ for all $k > \underline{k}_{\mathrm{U}} + \tilde{\mathrm{t}}_2^n(\epsilon)$.

For all interior cells on link 3, i.e., cells indexed by $l \in \{n_1+n_2+1, n_1+n_2+2, \cdots, n-1\}$, suppose $\boldsymbol{\rho}_{k|k}^{l+1} < \varrho_{\mathrm{m}} + \frac{(n-l)\epsilon}{n}$, if $\boldsymbol{\rho}_{k|k}^l > \varrho_{\mathrm{m}} + \frac{(n-l)\epsilon}{n}$, we obtain from (2.8) that

$$\mathrm{f}\left(\boldsymbol{\rho}_{k|k}^{l-1}, \boldsymbol{\rho}_{k|k}^l\right) \le w\left(\varrho_{\mathrm{m}} - \boldsymbol{\rho}_{k|k}^l\right), \tag{4.20}$$

$$\mathrm{f}\left(\boldsymbol{\rho}_{k|k}^l, \boldsymbol{\rho}_{k|k}^{l+1}\right) = w\left(\varrho_{\mathrm{m}} - \boldsymbol{\rho}_{k|k}^{l+1}\right) > w\left(-\frac{(n-l)\epsilon}{n}\right). \tag{4.21}$$

It follows that the estimate of cell $l$ satisfies

$$\begin{aligned}\boldsymbol{\rho}_{k+1|k+1}^l = \boldsymbol{\rho}_{k|k}^l &+ \tfrac{\Delta t}{\Delta x}\left(\mathrm{f}\left(\boldsymbol{\rho}_{k|k}^{l-1}, \boldsymbol{\rho}_{k|k}^l\right) - \mathrm{f}\left(\boldsymbol{\rho}_{k|k}^l, \boldsymbol{\rho}_{k|k}^{l+1}\right)\right)\\ &-K_{k+1}(l,1)\boldsymbol{\eta}_{k+1|k}^1 - K_{k+1}(l,2)\boldsymbol{\eta}_{k+1|k}^{n_1+n_2} - K_{k+1}(l,3)\boldsymbol{\eta}_{k+1|k}^n\\ &< \boldsymbol{\rho}_{k|k}^l - \tfrac{w\Delta t}{\Delta x}\left|\boldsymbol{\rho}_{k|k}^l - \varrho_{\mathrm{m}} - \tfrac{(n-l)\epsilon}{n}\right| + \mathrm{k}\left(\Gamma_{\underline{k}_{\mathrm{U}}|\underline{k}_{\mathrm{U}}}\right)\left\|\boldsymbol{\eta}_{k|k}^b\right\|_\infty.\end{aligned} \tag{4.22}$$

Thus there exists scalar $\tilde{w}_1$ such that $\frac{\Delta x \mathrm{k}\left(\Gamma_{\underline{k}_{\mathrm{U}}|\underline{k}_{\mathrm{U}}}\right)}{w\Delta t} < \tilde{w}_1$, and

$$\begin{aligned}\boldsymbol{\rho}_{k+1|k+1}^l - \boldsymbol{\rho}_{k|k}^l < &-\tilde{w}_0\left|\boldsymbol{\rho}_{k|k}^l - \varrho_{\mathrm{m}} - \frac{(n-l)\epsilon}{n}\right|,\\ &\text{for all } \left|\boldsymbol{\rho}_{k|k}^l - \varrho_{\mathrm{m}} - \frac{(n-l)\epsilon}{n}\right| \ge \tilde{w}_1\left\|\boldsymbol{\eta}_{k|k}^b\right\|_\infty.\end{aligned} \tag{4.23}$$

Also note that $\left\|\boldsymbol{\eta}^b_{k|k}\right\|_\infty \to 0$ as $k \to \infty$, which indicates that the one-step change of the estimates is ultimately negative, and large enough so that a finite time $\tilde{\mathrm{t}}_2^l(\epsilon)$ exists such that $\boldsymbol{\rho}^l_{k|k} < \varrho_{\mathrm{m}} + \frac{(n-l+1)\epsilon}{n} < \varrho_{\mathrm{m}} + \epsilon$ for all $k > \underline{k}_{\mathrm{U}} + \tilde{\mathrm{t}}_2^l(\epsilon)$.

The above arguments can be generalized for all cells on link 2. Hence for all $\epsilon > 0$ and $l \in \{n_1+1, n_1+2, \cdots, n_1+n_2-1\}$, there exists a finite time $\tilde{\mathrm{t}}_2^l(\epsilon)$ such that $\boldsymbol{\rho}^l_{k|k} < \varrho_{\mathrm{m}} + \frac{(n_1+n_2-l+1)\epsilon}{n} < \varrho_{\mathrm{m}} + \epsilon$ for all $k > \underline{k}_{\mathrm{U}} + \tilde{\mathrm{t}}_2^l(\epsilon)$.

We now show that for the cell on the upstream side of the junction, i.e., cell $n_1$, there exists finite time $\tilde{\mathrm{t}}_2^{n_1}(\epsilon)$ such that $\boldsymbol{\rho}^{n_1}_{k|k} < \varrho_{\mathrm{m}} + \frac{(n-n_1+1)\epsilon}{n} < \varrho_{\mathrm{m}} + \epsilon$ for all $k > \underline{k}_{\mathrm{U}} + \tilde{\mathrm{t}}_2^{n_1}(\epsilon)$. Suppose $\boldsymbol{\rho}^{n_1+1}_{k|k} < \varrho_{\mathrm{m}} + \frac{n_2\epsilon}{n}$ and $\boldsymbol{\rho}^{n_1+n_2+1}_{k|k} < \varrho_{\mathrm{m}} + \frac{n_3\epsilon}{n}$, if $\boldsymbol{\rho}^{n_1}_{k|k} > \varrho_{\mathrm{m}} + \frac{(n-n_1)\epsilon}{n} = \varrho_{\mathrm{m}} + \frac{(n_2+n_3)\epsilon}{n}$, the incoming and outgoing flows of cell $n_1$ satisfy

$$\mathrm{f}\left(\boldsymbol{\rho}^{n_1-1}_{k|k}, \boldsymbol{\rho}^{n_1}_{k|k}\right) \le w\left(\varrho_{\mathrm{m}} - \boldsymbol{\rho}^{n_1}_{k|k}\right),$$

and

$$\begin{aligned}
&\mathrm{f}\left(\boldsymbol{\rho}^{n_1}_{k|k}, \boldsymbol{\rho}^{n_1+1}_{k|k}\right) + \mathrm{f}\left(\boldsymbol{\rho}^{n_1}_{k|k}, \boldsymbol{\rho}^{n_1+n_2+1}_{k|k}\right) \\
&= \begin{cases} \mathrm{s}\left(\boldsymbol{\rho}^{n_1}_{k|k}\right) = q_{\mathrm{m}} > w\left(-\frac{n_2+n_3}{n}\epsilon\right) & \text{diverge case II or III} \\ \mathrm{r}\left(\boldsymbol{\rho}^{n_1+1}_{k|k}\right) + \mathrm{r}\left(\boldsymbol{\rho}^{n_1+n_2+1}_{k|k}\right) > w\left(-\frac{n_2+n_3}{n}\epsilon\right) & \text{diverge case I.} \end{cases}
\end{aligned}$$

Following the similar arguments as in (4.22)-(4.23) it can be concluded that there exist finite time $\tilde{\mathrm{t}}_2^{n_1}(\epsilon)$ such that $\boldsymbol{\rho}^{n_1}_{k|k} < \varrho_{\mathrm{m}} + \frac{(n-n_1+1)\epsilon}{n} < \varrho_{\mathrm{m}} + \epsilon$ for all $k > \underline{k}_{\mathrm{U}} + \tilde{\mathrm{t}}_2^{n_1}(\epsilon)$. Continuing the induction from cell $n_1$ to cell 1, it follows that for all $l \in \{1, 2, \cdots, n_1\}$ there exists a finite time $\tilde{\mathrm{t}}_2^l(\epsilon)$ such that $\boldsymbol{\rho}^l_{k|k} < \varrho_{\mathrm{m}} + \frac{(n-l+1)\epsilon}{n} \le \varrho_{\mathrm{m}} + \epsilon$ for all $k > \underline{k}_{\mathrm{U}} + \tilde{\mathrm{t}}_2^l(\epsilon)$.

Let $\tilde{\mathrm{t}}_2(\epsilon) = \max_{l\in\{1,\cdots,n\}}\{\tilde{\mathrm{t}}_2^l(\epsilon)\}$, we obtain $\boldsymbol{\rho}^l_{k|k} < \varrho_{\mathrm{m}} + \epsilon$ for all $k > \underline{k}_{\mathrm{U}} + \tilde{\mathrm{t}}_2(\epsilon)$ and $l \in \{1, \cdots, n\}$. This proves the ultimate upper bound of the estimates.

**Step 3**: Combining Steps 1 and 2, and define $\tilde{\mathrm{t}}(\epsilon) = \max_l\{\tilde{\mathrm{t}}_1(\epsilon), \tilde{\mathrm{t}}_2(\epsilon)\}$, we obtain $\boldsymbol{\rho}^l_{k|k} \in (-\epsilon, \varrho_{\mathrm{m}} + \epsilon)$ for all $l \in \{1, \cdots, n\}$ and $k > \underline{k}_{\mathrm{U}} + \tilde{\mathrm{t}}(\epsilon)$. Consequently, $\|\boldsymbol{\eta}_{k|k}\| < \sqrt{n}(\varrho_{\mathrm{m}} + \epsilon)$ for all $k > \underline{k}_{\mathrm{U}} + \tilde{\mathrm{t}}(\epsilon)$. □

Proposition 5 indicates that when the mean estimation error of the three boundary cells converges to zero, it will drive the state estimate of all the interior cells inside $[0, \varrho_{\mathrm{m}}]$ due to the conservation law and the flow-density relationship embedded in the traffic model. For example, when the state estimate $\boldsymbol{\rho}^l_{k|k}$ is smaller than zero, the sending capacity of cell $l$ is

much smaller than the receiving capacity of cell $l$ (as shown in (4.17)). Consequently, the update equation of the estimate (4.18) ensures that the one-step change of the state estimate of cell $l$ is always positive, and the magnitude of the one-step change is proportional to the distance between zero and the current state estimate $\boldsymbol{\rho}^l_{k|k}$. This ensures that the estimate of cell $l$ is constantly pushed towards zero unless it is sufficiently close to zero. The ultimate upper bound is also derived under the same fashion.

### 4.3.2 Uniform upper bound of the mean estimation error

In the next proposition, we extend the results in Proposition 2 and prove a uniform upper bound of the mean estimation error when the system is not observable. Deriving the uniform upper bound under the SMM-J follows the same line of analysis with Proposition 2, but contains more detailed analysis of the traffic flows across the junction. Fortunately, the flows across the junction required to derive the next proposition can be obtained from some minor modifications based on the proof of Proposition 5.

**Proposition 6** (Uniform upper bound of the mean error under the unobservable modes of SMM-J)**.** *Consider a road section shown in Figure 4.3 that switches inside an unobservable mode of the SMM-J while $k \in (\underline{k}_{\mathrm{U}}, \bar{k}_{\mathrm{U}}]$, where $0 \leq \underline{k}_{\mathrm{U}} < \bar{k}_{\mathrm{U}} \leq +\infty$. Let*

$$\begin{aligned} \tilde{c}_0 &= \max\left\{1, \check{a}_3 \check{c}_2 q_1^{-1} \sqrt{\check{c}_2 \check{c}_1^{-1}}\right\}, \\ \tilde{\mathrm{c}}\left(\Gamma_{\underline{k}_{\mathrm{U}}|\underline{k}_{\mathrm{U}}}\right) &= \tilde{c}_0 \Delta x \left(1 + \check{a}_3 \mathrm{k}\left(\Gamma_{\underline{k}_{\mathrm{U}}|\underline{k}_{\mathrm{U}}}\right)\right) \left(\Delta t \min\left\{v_{\mathrm{m}}, w\right\}\right)^{-1}, \end{aligned} \tag{4.24}$$

*where $\check{c}_1$, $\check{c}_2$ are defined in* (3.14)*, $\check{a}_3$ is defined in* (3.13)*, and $\mathrm{k}(\cdot)$ is given in* (3.15)*. For all $\epsilon > 0$, if $\left\|\boldsymbol{\eta}_{\underline{k}_{\mathrm{U}}|\underline{k}_{\mathrm{U}}}\right\| < \epsilon$, then $\|\boldsymbol{\eta}_{k|k}\| < \tilde{\mathrm{h}}(\epsilon, \Gamma_{\underline{k}_{\mathrm{U}}|\underline{k}_{\mathrm{U}}})$ for all $k \in (\underline{k}_{\mathrm{U}}, \bar{k}_{\mathrm{U}}]$, where*

$$\tilde{\mathrm{h}}(\epsilon, \Gamma_{\underline{k}_{\mathrm{U}}|\underline{k}_{\mathrm{U}}}) = \sqrt{n}\left(\varrho_{\mathrm{m}} + \epsilon\left(\tilde{c}_0 + (n-2)\tilde{\mathrm{c}}\left(\Gamma_{\underline{k}_{\mathrm{U}}|\underline{k}_{\mathrm{U}}}\right)\right)\right).$$

*Proof.* The proof is by induction.

**Step 1**: Denote as $\check{\boldsymbol{\eta}}^{(1)}_{k|k}$ the mean error of the observable subsystem. The error covariance of the observable subsystem $\check{\Gamma}^{(1)}_{k|k}$ satisfies $\check{c}_1 I < \check{\Gamma}^{(1)}_{k|k} < \check{c}_2 I$ and $\quad \check{\Gamma}^{(1)}_{k|k-1} > q_1 I$ for all $k \in (\underline{k}_{\mathrm{U}}, \bar{k}_{\mathrm{U}}]$. Let $\check{A}^{(1)}_k$ be the state transition matrix associated with the observable subsystem,

it follows that

$$\left\|\check{\boldsymbol{\eta}}^{(1)}_{\underline{k}_{\mathrm{U}}+1|\underline{k}_{\mathrm{U}}+1}\right\| \leq \left\|\left(I-\check{K}^{(1)}_{\underline{k}_{\mathrm{U}}+1}\check{H}^{(1)}\right)\check{A}^{(1)}_{k}\right\|\left\|\check{\boldsymbol{\eta}}^{(1)}_{\underline{k}_{\mathrm{U}}|\underline{k}_{\mathrm{U}}}\right\|$$
$$=\left\|\check{\Gamma}^{(1)}_{\underline{k}_{\mathrm{U}}+1|\underline{k}_{\mathrm{U}}+1}\left(\check{\Gamma}^{(1)}_{\underline{k}_{\mathrm{U}}+1|\underline{k}_{\mathrm{U}}}\right)^{-1}\check{A}^{(1)}_{k}\right\|\left\|\check{\boldsymbol{\eta}}^{(1)}_{\underline{k}_{\mathrm{U}}|\underline{k}_{\mathrm{U}}}\right\| < \check{a}_3\check{c}_2 q_1^{-1}\left\|\check{\boldsymbol{\eta}}^{(1)}_{\underline{k}_{\mathrm{U}}|\underline{k}_{\mathrm{U}}}\right\|.$$

Define the Lyapunov function of the observable subsystem as

$$\check{V}_k=\left(\check{\boldsymbol{\eta}}^{(1)}_{k|k}\right)^{\top}\left(\check{\Gamma}^{(1)}_{k|k}\right)^{-1}\check{\boldsymbol{\eta}}^{(1)}_{k|k},$$

then $\check{c}_2^{-1}\left\|\check{\boldsymbol{\eta}}^{(1)}_{k|k}\right\|^2 < \check{V}_k < \check{c}_1^{-1}\left\|\check{\boldsymbol{\eta}}^{(1)}_{k|k}\right\|^2$ and $\check{V}_{k+1} < \check{V}_k$ for all $k \in (\underline{k}_{\mathrm{U}}, \bar{k}_{\mathrm{U}})$ due to [53, Lemma 3]. Consequently,

$$\left\|\check{\boldsymbol{\eta}}^{(1)}_{k|k}\right\| < \left(\check{c}_2\check{V}_k\right)^{\frac{1}{2}} < \left(\check{c}_2\check{V}_{\underline{k}_{\mathrm{U}}+1}\right)^{\frac{1}{2}} < \sqrt{\check{c}_2\check{c}_1^{-1}}\left\|\check{\boldsymbol{\eta}}^{(1)}_{\underline{k}_{\mathrm{U}}+1|\underline{k}_{\mathrm{U}}+1}\right\|,$$

for all $k \in (\underline{k}_{\mathrm{U}}+1, \bar{k}_{\mathrm{U}}]$. It follows that for all $k \in (\underline{k}_{\mathrm{U}}, \bar{k}_{\mathrm{U}}]$,

$$\left\|\check{\boldsymbol{\eta}}^{(1)}_{k|k}\right\| < \check{a}_3\check{c}_2 q_1^{-1}\sqrt{\check{c}_2\check{c}_1^{-1}}\left\|\check{\boldsymbol{\eta}}^{(1)}_{\underline{k}_{\mathrm{U}}|\underline{k}_{\mathrm{U}}}\right\| < \check{a}_3\check{c}_2 q_1^{-1}\sqrt{\check{c}_2\check{c}_1^{-1}}\epsilon \leq \tilde{c}_0\epsilon. \tag{4.25}$$

Since the three boundary cells are in the observable subsystem, it is concluded that $\left\|\boldsymbol{\eta}^{l}_{k|k}\right\| \leq \tilde{c}_0\epsilon$ for $l \in \{1, n_1+n_2, n\}$ and $k \in (\underline{k}_{\mathrm{U}}, \bar{k}_{\mathrm{U}}]$.

**Step 2**: Now we use induction from upstream to downstream side to show that $\boldsymbol{\rho}^{l}_{k|k} \geq -\epsilon(\tilde{c}_0 + (n-2)\tilde{\mathrm{c}}(\Gamma_{\underline{k}_{\mathrm{U}}|\underline{k}_{\mathrm{U}}}))$ for all $k \in (\underline{k}_{\mathrm{U}}, \bar{k}_{\mathrm{U}}]$.

*(a) Cells on link 1:* Since $|\boldsymbol{\eta}^{1}_{k|k}| < \tilde{c}_0\epsilon$ for all $k \in (\underline{k}_{\mathrm{U}}, \bar{k}_{\mathrm{U}}]$, it holds that $\boldsymbol{\rho}^{1}_{k|k} > -\tilde{c}_0\epsilon = -\tilde{c}_0\epsilon - (1-1)\tilde{\mathrm{c}}\left(\Gamma_{\underline{k}_{\mathrm{U}}|\underline{k}_{\mathrm{U}}}\right)\epsilon$. Hence when $l=1$, $\boldsymbol{\rho}^{1}_{k|k} > -\tilde{c}_0\epsilon - (l-1)\tilde{\mathrm{c}}\left(\Gamma_{\underline{k}_{\mathrm{U}}|\underline{k}_{\mathrm{U}}}\right)\epsilon$ holds for all $k \in (\underline{k}_{\mathrm{U}}, \bar{k}_{\mathrm{U}}]$. For all interior cells on link 1, i.e., cells indexed by $l \in \{2, 3, \cdots, n_1-1\}$, suppose $\boldsymbol{\rho}^{l}_{k|k} > -\tilde{c}_0\epsilon - (l-1)\tilde{\mathrm{c}}\left(\Gamma_{\underline{k}_{\mathrm{U}}|\underline{k}_{\mathrm{U}}}\right)\epsilon$ for all $k \in (\underline{k}_{\mathrm{U}}, \bar{k}_{\mathrm{U}}]$. If $\boldsymbol{\rho}^{l+1}_{k|k} < -\tilde{c}_0\epsilon - l\tilde{\mathrm{c}}\left(\Gamma_{\underline{k}_{\mathrm{U}}|\underline{k}_{\mathrm{U}}}\right)\epsilon$, we obtain from (2.8) that

$$\mathrm{f}\left(\boldsymbol{\rho}^{l}_{k|k}, \boldsymbol{\rho}^{l+1}_{k|k}\right) > v_{\mathrm{m}}\left(-\tilde{c}_0\epsilon - (l-1)\tilde{\mathrm{c}}\left(\Gamma_{\underline{k}_{\mathrm{U}}|\underline{k}_{\mathrm{U}}}\right)\epsilon\right), \quad \mathrm{f}\left(\boldsymbol{\rho}^{l+1}_{k|k}, \boldsymbol{\rho}^{l+2}_{k|k}\right) \leq v_{\mathrm{m}}\boldsymbol{\rho}^{l+1}_{k|k}.$$

It follows that the estimate of cell $l+1$ satisfies

$$\begin{aligned}
\boldsymbol{\rho}_{k+1|k+1}^{l+1} &= \boldsymbol{\rho}_{k|k}^{l+1} + \tfrac{\Delta t}{\Delta x}\left(\mathrm{f}\left(\boldsymbol{\rho}_{k|k}^{l}, \boldsymbol{\rho}_{k|k}^{l+1}\right) - \mathrm{f}\left(\boldsymbol{\rho}_{k|k}^{l+1}, \boldsymbol{\rho}_{k|k}^{l+2}\right)\right) \\
&\quad -K_{k+1}(l+1,1)\boldsymbol{\eta}_{k+1|k}^{1} - K_{k+1}(l+1,2)\boldsymbol{\eta}_{k+1|k}^{n_1+n_2} - K_{k+1}(l+1,3)\boldsymbol{\eta}_{k+1|k}^{n} \\
&> \boldsymbol{\rho}_{k|k}^{l+1} + \tfrac{v_{\mathrm{m}}\Delta t}{\Delta x}\left|\boldsymbol{\rho}_{k|k}^{l+1} + \tilde{c}_0\epsilon + (l-1)\tilde{\mathrm{c}}\left(\Gamma_{\underline{k}_{\mathrm{U}}|\underline{k}_{\mathrm{U}}}\right)\epsilon\right| - \mathrm{k}\left(\Gamma_{\underline{k}_{\mathrm{U}}|\underline{k}_{\mathrm{U}}}\right)\check{a}_3\tilde{c}_0\epsilon \\
&= \boldsymbol{\rho}_{k|k}^{l+1} + \tfrac{v_{\mathrm{m}}\Delta t}{\Delta x}\left|\boldsymbol{\rho}_{k|k}^{l+1} + \tilde{c}_0\epsilon + l\tilde{\mathrm{c}}\left(\Gamma_{\underline{k}_{\mathrm{U}}|\underline{k}_{\mathrm{U}}}\right)\epsilon\right| \\
&\quad + \tfrac{v_{\mathrm{m}}\Delta t}{\Delta x}\tilde{\mathrm{c}}\left(\Gamma_{\underline{k}_{\mathrm{U}}|\underline{k}_{\mathrm{U}}}\right)\epsilon - \mathrm{k}\left(\Gamma_{\underline{k}_{\mathrm{U}}|\underline{k}_{\mathrm{U}}}\right)\check{a}_3\tilde{c}_0\epsilon \\
&\geq \boldsymbol{\rho}_{k|k}^{l+1} + \tfrac{v_{\mathrm{m}}\Delta t}{\Delta x}\left|\boldsymbol{\rho}_{k|k}^{l+1} + \tilde{c}_0\epsilon + l\tilde{\mathrm{c}}\left(\Gamma_{\underline{k}_{\mathrm{U}}|\underline{k}_{\mathrm{U}}}\right)\epsilon\right|,
\end{aligned} \tag{4.26}$$

where the first inequality is due to $\|K_k\|_\infty \leq \mathrm{k}(\Gamma_{\underline{k}_{\mathrm{U}}|\underline{k}_{\mathrm{U}}})$ given in Lemma 7 and the fact that $\|\check{\boldsymbol{\eta}}_{k+1|k}^{(1)}\| = \|\check{A}_k^{(1)}\check{\boldsymbol{\eta}}_{k|k}^{(1)}\| = \check{a}_3\|\check{\boldsymbol{\eta}}_{k|k}^{(1)}\| < \check{a}_3\tilde{c}_0\epsilon$ for all $k \in (\underline{k}_{\mathrm{U}}, \bar{k}_{\mathrm{U}}]$, and the last inequality is obtained by $\frac{v_{\mathrm{m}}\Delta t}{\Delta x}\tilde{\mathrm{c}}(\Gamma_{\underline{k}_{\mathrm{U}}|\underline{k}_{\mathrm{U}}})\epsilon - \mathrm{k}(\Gamma_{\underline{k}_{\mathrm{U}}|\underline{k}_{\mathrm{U}}})\check{a}_3\tilde{c}_0\epsilon \geq \left(1 + \check{a}_3\mathrm{k}(\Gamma_{\underline{k}_{\mathrm{U}}|\underline{k}_{\mathrm{U}}})\right)\tilde{c}_0\epsilon - \mathrm{k}(\Gamma_{\underline{k}_{\mathrm{U}}|\underline{k}_{\mathrm{U}}})\check{a}_3\tilde{c}_0\epsilon \geq 0$. Also since $\boldsymbol{\rho}_{\underline{k}_{\mathrm{U}}|\underline{k}_{\mathrm{U}}}^{l+1} > -\epsilon \geq -\tilde{c}_0\epsilon > -\tilde{c}_0\epsilon - l\tilde{\mathrm{c}}(\Gamma_{\underline{k}_{\mathrm{U}}|\underline{k}_{\mathrm{U}}})\epsilon$, it is concluded that $\boldsymbol{\rho}_{k|k}^{l+1} > -\tilde{c}_0\epsilon - l\tilde{\mathrm{c}}(\Gamma_{\underline{k}_{\mathrm{U}}|\underline{k}_{\mathrm{U}}})\epsilon$ for all $k \in (\underline{k}_{\mathrm{U}}, \bar{k}_{\mathrm{U}}]$. Continuing the induction along the cells on link 1, we obtain $\boldsymbol{\rho}_{k|k}^{n_1} > -\tilde{c}_0\epsilon - (n_1-1)\tilde{\mathrm{c}}(\Gamma_{\underline{k}_{\mathrm{U}}|\underline{k}_{\mathrm{U}}})\epsilon > -\tilde{c}_0\epsilon - (n-2)\tilde{\mathrm{c}}(\Gamma_{\underline{k}_{\mathrm{U}}|\underline{k}_{\mathrm{U}}})\epsilon$ for all $k \in (\underline{k}_{\mathrm{U}}, \bar{k}_{\mathrm{U}}]$.

*(b) Cells on link 2 and link 3:* Now we have shown that $\boldsymbol{\rho}_{k|k}^{n_1} > -\tilde{c}_0\epsilon - (n_1-1)\tilde{\mathrm{c}}\left(\Gamma_{\underline{k}_{\mathrm{U}}|\underline{k}_{\mathrm{U}}}\right)\epsilon$ for all $k \in (\underline{k}_{\mathrm{U}}, \bar{k}_{\mathrm{U}}]$. If $\boldsymbol{\rho}_{k|k}^{n_1+1} < -\tilde{c}_0\epsilon - n_1\tilde{\mathrm{c}}\left(\Gamma_{\underline{k}_{\mathrm{U}}|\underline{k}_{\mathrm{U}}}\right)\epsilon$, the junction solver follows diverge case II or diverge case III. Hence, the flow from cell $n_1$ to cell $n_1+1$ satisfies:

$$\begin{aligned}
\mathrm{f}\left(\boldsymbol{\rho}_{k|k}^{n_1}, \boldsymbol{\rho}_{k|k}^{n_1+1}\right) &= \begin{cases} \frac{1}{\alpha_{\mathrm{d}}+1}\mathrm{s}\left(\boldsymbol{\rho}_{k|k}^{n_1}\right) & \text{diverge case II} \\ \mathrm{s}\left(\boldsymbol{\rho}_{k|k}^{n_1}\right) - \mathrm{r}\left(\boldsymbol{\rho}_{k|k}^{n_1+n_2+1}\right) \geq \mathrm{s}\left(\boldsymbol{\rho}_{k|k}^{n_1}\right) & \text{diverge case III} \end{cases} \\
&> -v_{\mathrm{m}}\left(-\tilde{c}_0\epsilon - (n_1-1)\tilde{\mathrm{c}}\left(\Gamma_{\underline{k}_{\mathrm{U}}|\underline{k}_{\mathrm{U}}}\right)\epsilon\right),
\end{aligned}$$

where the inequality in diverge case III is due to the fact that $\mathrm{r}\left(\boldsymbol{\rho}_{k|k}^{n_1+n_2+1}\right) \leq 0$ if the junction solver is in diverge case III (otherwise the junction solver follows diverge case II). Meanwhile, the flow going out of cell $n_1+1$ satisfies:

$$\mathrm{f}\left(\boldsymbol{\rho}_{k|k}^{n_1+1}, \boldsymbol{\rho}_{k|k}^{n_1+2}\right) \leq v_{\mathrm{m}}\boldsymbol{\rho}_{k|k}^{n_1+1}.$$

Following the similar arguments as in (4.26), it can be concluded that $\boldsymbol{\rho}_{k|k}^{n_1+1} > -\tilde{c}_0\epsilon -$

$n_1\tilde{\mathrm{c}}(\Gamma_{\underline{k}_\mathrm{U}|\underline{k}_\mathrm{U}})\epsilon > -\tilde{c}_0\epsilon - (n-2)\tilde{\mathrm{c}}(\Gamma_{\underline{k}_\mathrm{U}|\underline{k}_\mathrm{U}})\epsilon$ for all $k \in (\underline{k}_\mathrm{U}, \bar{k}_\mathrm{U}]$. Applying the same analysis for cell $n_1+n_2+1$, it can be concluded that $\boldsymbol{\rho}^{n_1+n_2+1}_{k|k} > -\tilde{c}_0\epsilon - n_1\tilde{\mathrm{c}}(\Gamma_{\underline{k}_\mathrm{U}|\underline{k}_\mathrm{U}})\epsilon > -\tilde{c}_0\epsilon - (n-2)\tilde{\mathrm{c}}(\Gamma_{\underline{k}_\mathrm{U}|\underline{k}_\mathrm{U}})\epsilon$ for all $k \in (\underline{k}_\mathrm{U}, \bar{k}_\mathrm{U}]$. Continuing the induction on link 2 from cell $n_1+1$ to cell $n_1+n_2-1$, we obtain that $\boldsymbol{\rho}^{l}_{k|k} > -\tilde{c}_0\epsilon - (l-1)\tilde{\mathrm{c}}(\Gamma_{\underline{k}_\mathrm{U}|\underline{k}_\mathrm{U}})\epsilon > -\tilde{c}_0\epsilon - (n-2)\tilde{\mathrm{c}}(\Gamma_{\underline{k}_\mathrm{U}|\underline{k}_\mathrm{U}})\epsilon$ for all $l \in \{n_1+1, \cdots, n_1+n_2-1\}$ and $k \in (\underline{k}_\mathrm{U}, \bar{k}_\mathrm{U}]$. As for the cells in link 3, we process the same induction from cell $n_1+n_2+1$ to cell $n-1$, which yields that $\boldsymbol{\rho}^{l}_{k|k} > -\tilde{c}_0\epsilon - (l-n_2-1)\tilde{\mathrm{c}}(\Gamma_{\underline{k}_\mathrm{U}|\underline{k}_\mathrm{U}})\epsilon > -\tilde{c}_0\epsilon - (n-2)\tilde{\mathrm{c}}(\Gamma_{\underline{k}_\mathrm{U}|\underline{k}_\mathrm{U}})\epsilon$ for all $l \in \{n_1+n_2+1, \cdots, n-1\}$ and $k \in (\underline{k}_\mathrm{U}, \bar{k}_\mathrm{U}]$. This proves the uniform lower bound of the state estimates.

**Step 3**: Now we use induction from downstream to upstream side to show that $\boldsymbol{\rho}^{l}_{k|k} \leq \varrho_\mathrm{m} + \epsilon(\tilde{c}_0 + (n-2)\tilde{\mathrm{c}}(\Gamma_{\underline{k}_\mathrm{U}|\underline{k}_\mathrm{U}}))$ for all $k \in (\underline{k}_\mathrm{U}, \bar{k}_\mathrm{U}]$.

*(a) Cells on link 3:* Since the downstream boundary cell on link 3 (i.e., cell indexed by $n$) are in the observable subsystem, it follows from (4.25) that $\boldsymbol{\rho}^{n}_{k|k} \leq \varrho_\mathrm{m} + \tilde{c}_0\epsilon = \varrho_\mathrm{m} + \epsilon(\tilde{c}_0 + (n-n)\tilde{\mathrm{c}}(\Gamma_{\underline{k}_\mathrm{U}|\underline{k}_\mathrm{U}}))$ for all $k \in (\underline{k}_\mathrm{U}, \bar{k}_\mathrm{U}]$. Hence for $k \in (\underline{k}_\mathrm{U}, \bar{k}_\mathrm{U}]$, the inequality $\boldsymbol{\rho}^{l}_{k|k} \leq \varrho_\mathrm{m} + \epsilon(\tilde{c}_0 + (n-l)\tilde{\mathrm{c}}(\Gamma_{\underline{k}_\mathrm{U}|\underline{k}_\mathrm{U}})) < \epsilon(\tilde{c}_0 + (n-2)\tilde{\mathrm{c}}(\Gamma_{\underline{k}_\mathrm{U}|\underline{k}_\mathrm{U}}))$ holds for $l = n$.

For the interior cells on link 3, i.e., $l \in \{n, n-2, \cdots, n_1+n_2+2\}$, suppose $\boldsymbol{\rho}^{l}_{k|k} < \varrho_\mathrm{m} + \tilde{c}_0\epsilon + (n-l)\tilde{\mathrm{c}}\left(\Gamma_{\underline{k}_\mathrm{U}|\underline{k}_\mathrm{U}}\right)\epsilon$ for all $k \in (\underline{k}_\mathrm{U}, \bar{k}_\mathrm{U}]$. If $\boldsymbol{\rho}^{l-1}_{k|k} > \varrho_\mathrm{m} + \tilde{c}_0\epsilon + (n-l+1)\tilde{\mathrm{c}}\left(\Gamma_{\underline{k}_\mathrm{U}|\underline{k}_\mathrm{U}}\right)\epsilon$, we obtain from (2.8) that

$$
\begin{aligned}
&\mathrm{f}\left(\boldsymbol{\rho}^{l-2}_{k|k}, \boldsymbol{\rho}^{l-1}_{k|k}\right) \leq w\left(\varrho_\mathrm{m} - \boldsymbol{\rho}^{l-1}_{k|k}\right),\\
&\mathrm{f}\left(\boldsymbol{\rho}^{l-1}_{k|k}, \boldsymbol{\rho}^{l}_{k|k}\right) = w\left(\varrho_\mathrm{m} - \boldsymbol{\rho}^{l}_{k|k}\right) > w\left(-\tilde{c}_0\epsilon + (n-l)\tilde{\mathrm{c}}\left(\Gamma_{\underline{k}_\mathrm{U}|\underline{k}_\mathrm{U}}\right)\epsilon\right).
\end{aligned}
$$

If follows that

$$
\begin{aligned}
\boldsymbol{\rho}^{l-1}_{k+1|k+1} &< \boldsymbol{\rho}^{l-1}_{k|k} - \frac{w\Delta t}{\Delta x}\left|\boldsymbol{\rho}^{l-1}_{k|k} - \varrho_\mathrm{m} - \tilde{c}_0\epsilon - (n-l)\tilde{\mathrm{c}}\left(\Gamma_{\underline{k}_\mathrm{U}|\underline{k}_\mathrm{U}}\right)\epsilon\right| + \mathrm{k}\left(\Gamma_{\underline{k}_\mathrm{U}|\underline{k}_\mathrm{U}}\right)\check{a}_3\tilde{c}_0\epsilon\\
&= \boldsymbol{\rho}^{l-1}_{k|k} - \frac{w\Delta t}{\Delta x}\left|\boldsymbol{\rho}^{l-1}_{k|k} - \varrho_\mathrm{m} - \tilde{c}_0\epsilon - (n-l+1)\tilde{\mathrm{c}}\left(\Gamma_{\underline{k}_\mathrm{U}|\underline{k}_\mathrm{U}}\right)\epsilon\right|\\
&\quad - \frac{w\Delta t}{\Delta x}\tilde{\mathrm{c}}\left(\Gamma_{\underline{k}_\mathrm{U}|\underline{k}_\mathrm{U}}\right)\epsilon + \mathrm{k}\left(\Gamma_{\underline{k}_\mathrm{U}|\underline{k}_\mathrm{U}}\right)\check{a}_3\tilde{c}_0\epsilon\\
&\leq \boldsymbol{\rho}^{l-1}_{k|k} - \frac{w\Delta t}{\Delta x}\left|\boldsymbol{\rho}^{l-1}_{k|k} - \varrho_\mathrm{m} - \tilde{c}_0\epsilon - (n-l+1)\tilde{\mathrm{c}}\left(\Gamma_{\underline{k}_\mathrm{U}|\underline{k}_\mathrm{U}}\right)\epsilon\right|.
\end{aligned}
$$

Also since $\boldsymbol{\rho}^{l-1}_{\underline{k}_\mathrm{U}|\underline{k}_\mathrm{U}} < \varrho_\mathrm{m} + \epsilon \leq \varrho_\mathrm{m} + \tilde{c}_0\epsilon < \varrho_\mathrm{m} + \tilde{c}_0\epsilon + (n-l+1)\tilde{\mathrm{c}}\left(\Gamma_{\underline{k}_\mathrm{U}|\underline{k}_\mathrm{U}}\right)\epsilon$, it is concluded that $\boldsymbol{\rho}^{l-1}_{k|k} < \varrho_\mathrm{m} + \tilde{c}_0\epsilon + (n-l+1)\tilde{\mathrm{c}}\left(\Gamma_{\underline{k}_\mathrm{U}|\underline{k}_\mathrm{U}}\right)\epsilon$ for all $k \in (\underline{k}_\mathrm{U}, \bar{k}_\mathrm{U}]$. Hence, the estimates on link 3 satisfies $\boldsymbol{\rho}^{l}_{k|k} < \varrho_\mathrm{m} + \tilde{c}_0\epsilon + (n-l)\tilde{\mathrm{c}}\left(\Gamma_{\underline{k}_\mathrm{U}|\underline{k}_\mathrm{U}}\right)\epsilon < \varrho_\mathrm{m} + \tilde{c}_0\epsilon + (n-2)\tilde{\mathrm{c}}\left(\Gamma_{\underline{k}_\mathrm{U}|\underline{k}_\mathrm{U}}\right)\epsilon$ for all

$l \in \{n-1, n-2, \cdots, n_1+n_2+1\}$ and $k \in (\underline{k}_{\mathrm{U}}, \bar{k}_{\mathrm{U}}]$.

*(b) Cells on link 2:* The above arguments can be generalized for all cells on link 2. Since the boundary cell on link 2 is indexed by $n_1+n_2$, the estimates on link 3 satisfies $\boldsymbol{\rho}^{l}_{k|k} < \varrho_{\mathrm{m}} + \tilde{c}_0\epsilon + (n_1+n_2-l)\tilde{\mathrm{c}}\left(\Gamma_{\underline{k}_{\mathrm{U}}|\underline{k}_{\mathrm{U}}}\right)\epsilon < \varrho_{\mathrm{m}} + \tilde{c}_0\epsilon + (n-2)\tilde{\mathrm{c}}\left(\Gamma_{\underline{k}_{\mathrm{U}}|\underline{k}_{\mathrm{U}}}\right)\epsilon$ for all $l \in \{n_1+n_2-1, n_1+n_2-2, \cdots, n_1+1\}$ and $k \in (\underline{k}_{\mathrm{U}}, \bar{k}_{\mathrm{U}}]$.

*(c) Cells on link 1:* We first derive the uniform upper bound for the cell on the upstream side of the junction, i.e., cell $n_1$. Recall that we have shown in part(a) and part(b) that $\boldsymbol{\rho}^{n_1+1}_{k|k} < \varrho_{\mathrm{m}} + \tilde{c}_0\epsilon + (n_2-1)\tilde{\mathrm{c}}\left(\Gamma_{\underline{k}_{\mathrm{U}}|\underline{k}_{\mathrm{U}}}\right)\epsilon$ and $\boldsymbol{\rho}^{n_1+n_2+1}_{k|k} < \varrho_{\mathrm{m}} + \tilde{c}_0\epsilon + (n_3-1)\tilde{\mathrm{c}}\left(\Gamma_{\underline{k}_{\mathrm{U}}|\underline{k}_{\mathrm{U}}}\right)\epsilon$ for $k \in (\underline{k}_{\mathrm{U}}, \bar{k}_{\mathrm{U}}]$. If $\boldsymbol{\rho}^{n_1}_{k|k} > \varrho_{\mathrm{m}} + \tilde{c}_0\epsilon + (n_2+n_3-1)\tilde{\mathrm{c}}\left(\Gamma_{\underline{k}_{\mathrm{U}}|\underline{k}_{\mathrm{U}}}\right)\epsilon$, the incoming flow of cell $n_1$ satisfy

$$\mathrm{f}\left(\boldsymbol{\rho}^{n_1-1}_{k|k}, \boldsymbol{\rho}^{n_1}_{k|k}\right) \leq w\left(\varrho_{\mathrm{m}} - \boldsymbol{\rho}^{n_1}_{k|k}\right).$$

The outgoing flow of cell $n_1$ is the sum of the flow from cell $n_1$ to cell $n_1+1$ and the flow from cell $n_1$ to cell $n_1+n_2+1$, which (depending on the densities of cells $n_1$, $n_1+1$ and $n_1+n_2+1$) satisfies the following inequality:

$$\begin{aligned}
&\mathrm{f}\left(\boldsymbol{\rho}^{n_1}_{k|k}, \boldsymbol{\rho}^{n_1+1}_{k|k}\right) + \mathrm{f}\left(\boldsymbol{\rho}^{n_1}_{k|k}, \boldsymbol{\rho}^{n_1+n_2+1}_{k|k}\right) \\
=&\begin{cases} \mathrm{s}\left(\boldsymbol{\rho}^{n_1}_{k|k}\right) = q_{\mathrm{m}} & \text{diverge case II or III} \\ \mathrm{r}\left(\boldsymbol{\rho}^{n_1+1}_{k|k}\right) + \mathrm{r}\left(\boldsymbol{\rho}^{n_1+n_2+1}_{k|k}\right) > w\left(-\frac{n_2+n_3}{n}\epsilon\right) & \text{diverge case I,} \end{cases} \\
>&w\left(-2\tilde{c}_0\epsilon - (n_2+n_3-2)\tilde{\mathrm{c}}\left(\Gamma_{\underline{k}_{\mathrm{U}}|\underline{k}_{\mathrm{U}}}\right)\epsilon\right).
\end{aligned}$$

This indicates that the disparity between the inflow and outflow of cell $n_1$ will drive the decrease of the density estimate of cell $n_1$ in the model prediction step of the Kalman filter, as shown in the following inequalities:

$$\begin{aligned}
\boldsymbol{\rho}^{n_1}_{k+1|k+1} &< \boldsymbol{\rho}^{n_1}_{k|k} - \frac{w\Delta t}{\Delta x}\left|\boldsymbol{\rho}^{n_1}_{k|k} - \varrho_{\mathrm{m}} - 2\tilde{c}_0\epsilon - (n_2+n_3-2)\tilde{\mathrm{c}}\left(\Gamma_{\underline{k}_{\mathrm{U}}|\underline{k}_{\mathrm{U}}}\right)\epsilon\right| + \mathrm{k}\left(\Gamma_{\underline{k}_{\mathrm{U}}|\underline{k}_{\mathrm{U}}}\right)\check{a}_3\tilde{c}_0\epsilon \\
&= \boldsymbol{\rho}^{n_1}_{k|k} - \frac{w\Delta t}{\Delta x}\left|\boldsymbol{\rho}^{n_1}_{k|k} - \varrho_{\mathrm{m}} - \tilde{c}_0\epsilon - (n_2+n_3-1)\tilde{\mathrm{c}}\left(\Gamma_{\underline{k}_{\mathrm{U}}|\underline{k}_{\mathrm{U}}}\right)\epsilon\right| \\
&\quad - \frac{w\Delta t}{\Delta x}\tilde{\mathrm{c}}\left(\Gamma_{\underline{k}_{\mathrm{U}}|\underline{k}_{\mathrm{U}}}\right)\epsilon + \frac{w\Delta t}{\Delta x}\tilde{c}_0\epsilon + \mathrm{k}\left(\Gamma_{\underline{k}_{\mathrm{U}}|\underline{k}_{\mathrm{U}}}\right)\check{a}_3\tilde{c}_0\epsilon \\
&\leq \boldsymbol{\rho}^{n_1}_{k|k} - \frac{w\Delta t}{\Delta x}\left|\boldsymbol{\rho}^{n_1}_{k|k} - \varrho_{\mathrm{m}} - \tilde{c}_0\epsilon - (n_2+n_3-1)\tilde{\mathrm{c}}\left(\Gamma_{\underline{k}_{\mathrm{U}}|\underline{k}_{\mathrm{U}}}\right)\epsilon\right|.
\end{aligned}$$

Also note that $\boldsymbol{\rho}^{n_1}_{\underline{k}_{\mathrm{U}}|\underline{k}_{\mathrm{U}}} < \varrho_{\mathrm{m}} + \epsilon \leq \varrho_{\mathrm{m}} + \tilde{c}_0\epsilon < \varrho_{\mathrm{m}} + \tilde{c}_0\epsilon + (n_2 + n_3 - 1)\tilde{\mathrm{c}}\left(\Gamma_{\underline{k}_{\mathrm{U}}|\underline{k}_{\mathrm{U}}}\right)\epsilon$, it is concluded that $\boldsymbol{\rho}^{n_1}_{k|k} < \varrho_{\mathrm{m}} + \tilde{c}_0\epsilon + (n - n_1)\tilde{\mathrm{c}}\left(\Gamma_{\underline{k}_{\mathrm{U}}|\underline{k}_{\mathrm{U}}}\right)\epsilon$ for all $k \in (\underline{k}_{\mathrm{U}}, \bar{k}_{\mathrm{U}}]$. Following the argument in part(a) of Step 3 and continue the induction from cell $n_1$ to cell 2, it follows that $\boldsymbol{\rho}^{l}_{k|k} < \varrho_{\mathrm{m}} + \tilde{c}_0\epsilon + (n-l)\tilde{\mathrm{c}}\left(\Gamma_{\underline{k}_{\mathrm{U}}|\underline{k}_{\mathrm{U}}}\right)\epsilon \leq \varrho_{\mathrm{m}} + \tilde{c}_0\epsilon + (n-2)\tilde{\mathrm{c}}\left(\Gamma_{\underline{k}_{\mathrm{U}}|\underline{k}_{\mathrm{U}}}\right)\epsilon$ for all $l \in \{2, 3, \cdots, n_1\}$ and $k \in (\underline{k}_{\mathrm{U}}, \bar{k}_{\mathrm{U}}]$.

**Step 4**: Combining Steps 1 and 2, we obtain $\boldsymbol{\rho}^{l}_{k|k} \in (-\epsilon(\tilde{c}_0 + (n-2)\tilde{\mathrm{c}}(\Gamma_{\underline{k}_{\mathrm{U}}|\underline{k}_{\mathrm{U}}})), \varrho_{\mathrm{m}} + \epsilon(\tilde{c}_0 + (n-2)\tilde{\mathrm{c}}(\Gamma_{\underline{k}_{\mathrm{U}}|\underline{k}_{\mathrm{U}}})))$ for all $l \in \{1, \cdots, n\}$ and $k \in (\underline{k}_{\mathrm{U}}, \bar{k}_{\mathrm{U}}]$. Consequently, $\|\boldsymbol{\eta}_{k|k}\| < \sqrt{n}(\varrho_{\mathrm{m}} + \epsilon(\tilde{c}_0 + (n-2)\tilde{\mathrm{c}}(\Gamma_{\underline{k}_{\mathrm{U}}|\underline{k}_{\mathrm{U}}}))) = \tilde{\mathrm{h}}(\epsilon, \Gamma_{\underline{k}_{\mathrm{U}}|\underline{k}_{\mathrm{U}}})$ for all $k \in (\underline{k}_{\mathrm{U}}, \bar{k}_{\mathrm{U}}]$. □

We conclude this section by some remarks on extending the results to systems that switch among the observable and unobservable modes of the SMM-J. Given the fact that the uniform upper bound of the mean error under the unobservable scenarios is available in Proposition 6, similar to the analysis for the SMM in Section 3.5.3, the next step is to leverage the convergence rate of the mean error under observable scenarios, and derive the minimum residence time required in the observable modes to offset the error increase in the unobservable modes. After this, we can combine the results for the observable and unobservable modes to obtain the error bounds under switches among these two kinds of modes.

The convergence rate of the mean estimation error under the observable modes of the SMM-J can be derived in the similar fashion as in Lemma 6. As in Lemma 6, the critical precondition is to obtain the upper and lower bounds of the error covariance $\Gamma_{k|k}$ uniform across the observable time interval. To compute this lower and upper bounds, we can follow the same analysis as in Lemma 3-Lemma 5 to derive the bounds for the SMM-J. This involves leveraging the properties (P.3)-(P.5) of the SMM-J to determine relevant norms for the state transition matrices, the bounds for the information matrix, etc., for the observable time intervals of the SMM-J.

When the system is unobservable, the uniform error bound for each unobservable mode of the SMM-J varies with the dimensionality and state transition matrix of the observable subsystem in the unobservable mode. Hence, given the fact that there are in total 30 unobservable modes in the SMM-J, deriving the explicit formula of the error bound for each mode is much more tedious compared to the SMM. Hence, we present in this chapter the general formula of the error bound which is applicable for all the unobservable modes

of the SMM-J. Like the SMM, the uniform upper bound of the mean error also quantifies the maximum increase of the mean error when the SMM-J switches inside an unobservable mode.

Finally, given the maximum increase of the mean error under each unobservable mode, and the convergence rate of the mean error when the system is observable, we can follow the similar analysis as in Section 3.5.3 to combine the above results to derive the minimum residence time for each observable time interval, as well as the upper bounds of the 2-norm of the mean estimation error for all the observable and unobservable time intervals.

# CHAPTER 5

# DISTRIBUTED CONSENSUS-BASED FILTERING IN LARGE-SCALE ESTIMATION

## 5.1 Introduction

In this chapter, we consider distributed estimation schemes on large-scale networks (not limited to transportation networks) to reduce state-space dimensionality. The entire state to be estimated is partitioned into local sections, with each section estimated by its own local agent. Each agent shares sensor data and state estimates with neighbors. To ensure estimation consistency among neighboring agents, the network is partitioned such that overlapping regions exist among the local sections, and a consensus term is added to promote agreement among neighboring agents on the estimates of their shared overlapping regions. The new contributions of this chapter are summarized as follows.

- **Redesign of the consensus term.** Based on the *distributed local Kalman consensus filter* (DLKCF) first introduced in author's earlier work [47], we redesign the consensus term to make it scalable both in terms of communication (i.e., each agent only communicates with its one-hop neighbors, and the global communication topology is not needed) and computation.

- **Global asymptotic stability of the DLKCF.** We show that when the subsystems on all the local states are uniformly completely observable, the redesigned DLKCF has *globally asymptotic stable* (GAS) mean error dynamics. This indicates that adding the consensus term to promote neighbor agreement preserves the unbiasedness of the filter.

- **Error bounds of the DLKCF for traffic estimation.** We extend the results in Chapter 3 to derive the bounds on the mean error of the DLKCF when it is used to estimate traffic conditions based on the SMM. The results for the SMM-J can also be

obtained in the same fashion.

This chapter is organized as follows. Section 5.2 introduces the DLKCF. In Section 5.3, we show the GAS of the mean error dynamics of the DLKCF under uniformly completely observable systems. Section 5.4 derives the error bounds of the DLKCF in the context of traffic estimation problems, specifically, when the systems switch among the observable and unobservable modes of the SMM. Finally, numerical experiments in Section 5.5 show the effect of the consensus term on reducing disagreement among estimates given by neighboring agents.

## 5.2 Distributed local Kalman consensus filter

Consider a large-scale system that is partitioned into $N$ overlapping local sections. The system dynamics of section $i$ reads

$$\rho_{i,k+1} = A_{i,k}\rho_k + u_{i,k} + \omega_{i,k}, \quad \rho_k \in \mathbb{R}_i^n, \tag{5.1}$$

where $A_{i,k}$ is the state transition matrix, and $\omega_{i,k}$ is the white Gaussian model noise associated with section $i$.

Define $\mathcal{N}_i$ as the set of neighbors of section $i$, and denote as $\mathcal{J}_i = \mathcal{N}_i \cup \{i\}$. The observation equation modeled at agent $i$ that corresponds to the sensor data obtained by the sensors directly connected to agent $j$ is given by:

$$z_{j,k}^i = H_{j,k}^i \rho_{i,k} + v_{j,k}^i, \; z_{j,k}^i \in \mathbb{R}^{m_j^i}, j \in \mathcal{J}_i, \tag{5.2}$$

where $v_{j,k}^i \sim \mathbf{N}(0, R_{j,k}^i)$. Note that the sensor data $z_{j,k}^i$ for $j \in \mathcal{N}_i$ is obtained through receiving measurements from agent $j$. Consequently, through communication each agent possesses columnized sensor data $z_{i,k} = \mathrm{col}_{j\in\mathcal{J}_i}(z_{j,k}^i)$ with noise $v_{i,k} = \mathrm{col}_{j\in\mathcal{J}_i}(v_{j,k}^i)$ and a corresponding columnized output matrix $H_{i,k} = \mathrm{col}_{j\in\mathcal{J}_i}(H_{j,k}^i)$, as well as a block diagonal measurement error covariance $R_{i,k} = \mathrm{diag}_{j\in\mathcal{J}_i}(R_{j,k}^i)$.

For $j \in \mathcal{N}_i$, denote the dimension of the overlap between section $i$ and $j$ as $n_{i,j}$. When the cells on section $i$ indexed by $l, \cdots, l + n_{i,j} - 1$ overlap with section $j$, define matrix $\hat{I}_{i,j}$ as the projection such that the quantity $\hat{I}_{i,j}\rho_{i,k}$ selects the state of section $i$ that overlaps

with section $j$, i.e.,

$$\hat{I}_{i,j} = \left(\mathbf{0}_{n_{i,j},l-1} \;\; I_{n_{i,j}} \;\; \mathbf{0}_{n_{i,j},n_i-n_{i,j}-l+1}\right).$$

In the DLKCF, a consensus term is added to the correction step to promote agreement on estimates among neighboring agents. The time and information updates of the DLKCF for agent $i$ read

$$\text{Time update:} \begin{cases} \rho_{i,k|k-1} = A_{i,k-1}\rho_{i,k-1|k-1} + u_{i,k-1} \\ \Gamma_{i,k|k-1} = A_{i,k-1}\Gamma_{i,k-1|k-1}A_{i,k-1}^{\top} + Q_{i,k-1} \end{cases} \tag{5.3}$$

$$\text{Information update:} \begin{cases} \rho_{i,k|k} = \rho_{i,k|k-1} + K_{i,k}\left(z_{i,k} - H_{i,k}\rho_{i,k|k-1}\right) \\ \quad + \sum_{j\in\mathcal{N}_i} C_{i,k}^{j}\left(\hat{I}_{j,i}\rho_{j,k|k-1} - \hat{I}_{i,j}\rho_{i,k|k-1}\right) \\ \Gamma_{i,k|k} = \Gamma_{i,k|k-1} - K_{i,k}H_{i,k}\Gamma_{i,k|k-1} \\ K_{i,k} = \Gamma_{i,k|k-1}H_{i,k}^{\top}(R_{i,k} + H_{i,k}\Gamma_{i,k|k-1}H_{i,k}^{\top})^{-1}, \end{cases} \tag{5.4}$$

where define

$$\delta_{i,k}^{j} = \hat{I}_{j,i}\rho_{j,k|k-1} - \hat{I}_{i,j}\rho_{i,k|k-1}$$

as the disagreement between sections $i$ and $j$ on their estimates of their shared region. Our choice of the consensus gain is given by:

$$C_{i,k}^{j} = \gamma_{i,k}^{j}\Gamma_{i,k|k-1}\hat{I}_{i,j}^{\top} \tag{5.5}$$

where $\gamma_{i,k}^{j} = \gamma_{j,k}^{i}$ is a sufficiently small scaling factor, with $\gamma_{i,k}^{j} < \gamma_{i,k}^{*}$ for all $i$, $j \in \mathcal{N}_i$ and $k$. The explicit form of $\gamma_{i,k}^{*}$ will be given in Proposition 7 to ensure the unbiasedness of the DLKCF. According to (5.4)-(5.5), the consensus term is designed based on the belief of the current estimation accuracy and the disparity among neighbors on the prior estimate, thus promoting agreement on the state estimates. Although an arbitrary convex combination of the estimates between neighboring agents may considerably reduce disagreement, it may largely increase the estimation error. Hence, the scaling factor needs to be carefully designed to ensure stability of the DLKCF.

Before analyzing the performance of the estimator, the following assumptions are made for the DLKCF:

(Asm.10): the noise models satisfy $q_1 I < Q_{i,k} < q_2 I$ and $r_1 I < R_{i,k} < r_2 I$ for all $i$ and $k$, where $q_1$, $q_2$, $r_1$ and $r_2$ are positive constants;

(Asm.11): the initial error covariances are positive definite, i.e., $\Gamma_{i,0|0} > \mathbf{0}$ for all $i$;

(Asm.12): the state transition matrices $A_{i,k}$ are nonsingular for all $i$ and $k$;

(Asm.13): the scaling factor satisfies $\gamma_{i,k}^j \leq \hat{\gamma}_{i,k}^j = \hat{c}\,|\mathcal{N}_i|^{-1}\,\|\Gamma_{i,k|k-1}\hat{I}_{i,j}^\top \delta_{i,k}^j\|^{-1}$ in addition to $\gamma_{i,k}^j < \gamma_{i,k}^*$ for all $i$, $j \in \mathcal{N}_i$ and $k$. Here $|\mathcal{N}_i|$ is the number of neighbors of agent $i$, and $\hat{c} > 0$ is a constant predefined to set an upper bound for the magnitude of the consensus term.

Also note that the upper bound $\hat{\gamma}_{i,k}^j$ can be computed locally and online by each agent. In this case, the 2-norm of the consensus term is upper bounded as follows:

$$\left\| \sum_{j \in \mathcal{N}_i} \gamma_{i,k}^j \Gamma_{i,k|k-1} \hat{I}_{i,j}^\top \delta_{i,k}^j \right\| \leq \hat{c}, \quad \text{for all } i \text{ and } k. \tag{5.6}$$

**Remark 6.** *Given the consensus gain* (5.5)*, one may derive the optimal Kalman gain $K_{i,k}$ through minimizing tr$(\Gamma_{i,k|k})$ in a similar way as Theorem 1 in [53], thus yielding an optimal DLKCF which incorporates the cross-correlations among different agents in the estimation error covariance. However, the optimal DLKCF has large communication requirements (i.e., the cross covariance $\Gamma_{i,k|k}^j$ between section $i$ and $j$ needs to be computed by agent $i$ for all $j \in \{1, \cdots, N\}$) that conflicts the goal of designing a scalable estimation algorithm. Moreover, when cross-correlation terms are included, a section which is always observable can have an unbounded error covariance if the neighboring section is unobservable, as detailed in [88, Appendix A]. Instead, the Kalman gain $K_{i,k}$ in the DLKCF is non-interacting, resulting in a suboptimal filter. Nevertheless, it is shown in Proposition 7 that the GAS property of the error dynamics is not affected by neglecting the cross-correlation terms. To check whether the filter-calculated error covariance matches the error covariance of the DLKCF, we explore the average normalized (state) estimation error squared (NEES) measure [93] in Section 5.5.2.*

## 5.3 Stability of the DLKCF under observable scenarios

In this section, we show that when the subsystems on all the local sections are uniformly completely observable, the mean estimation error of each section is globally asymptotically stable. Define the prior and posterior estimation error for section $i$ as $\eta_{i,k|k-1} = \rho_{i,k|k-1} - \rho_{i,k}$ and $\eta_{i,k|k} = \rho_{i,k|k} - \rho_{i,k}$. The global estimation error $\eta_{1:N,k|k}$ is constructed by $\eta_{1:N,k|k} = \mathrm{col}(\eta_{1,k|k}, \cdots, \eta_{N,k|k})$. According to (5.3)-(5.4), the mean of the estimation error in section $i$ evolves as follows:

$$\boldsymbol{\eta}_{i,k|k} = F_{i,k} A_{i,k-1} \boldsymbol{\eta}_{i,k-1|k-1} + \sum_{j \in \mathcal{N}_i} C_{i,k}^j \boldsymbol{\delta}_{i,k}^j, \tag{5.7}$$

where $F_{i,k} = I - K_{i,k} H_{i,k}$. We choose a *common Lyapunov function* candidate

$$V_k = \sum_{i=1}^{N} \boldsymbol{\eta}_{i,k|k}^\top \Gamma_{i,k|k}^{-1} \boldsymbol{\eta}_{i,k|k}, \tag{5.8}$$

and compute its one-step change $\Delta V_k = V_k - V_{k-1}$ by applying (5.7) as follows:

$$\begin{aligned} \Delta V_k = & \textstyle\sum_{i=1}^{N} \boldsymbol{\eta}_{i,k-1|k-1}^\top \left( A_{i,k-1}^\top F_{i,k}^\top \Gamma_{i,k|k}^{-1} F_{i,k} A_{i,k-1} - \Gamma_{i,k-1|k-1}^{-1} \right) \boldsymbol{\eta}_{i,k-1|k-1} \\ & + 2 \textstyle\sum_{i=1}^{N} \left( \boldsymbol{\eta}_{i,k|k-1}^\top F_{i,k}^\top \Gamma_{i,k|k}^{-1} \sum_{j \in \mathcal{N}_i} C_{i,k}^j \boldsymbol{\delta}_{i,k}^j \right) \\ & + \textstyle\sum_{i=1}^{N} \left( \sum_{j \in \mathcal{N}_i} C_{i,k}^j \boldsymbol{\delta}_{i,k}^j \right)^\top \Gamma_{i,k|k}^{-1} \left( \sum_{j \in \mathcal{N}_i} C_{i,k}^j \boldsymbol{\delta}_{i,k}^j \right). \end{aligned} \tag{5.9}$$

When all the local sections are uniformly completely stable, it follows from Lemma 2 that the error covariance satisfies $c_{i,1} I_{n_i} < \Gamma_{i,k|k} < c_{i,2} I_{n_i}$ for all $i$ and $k$, where $c_{i,1}$ and $c_{i,2}$ are positive constants. Hence, the common Lyapunov function 5.8 is radially unbounded, which is a necessary condition to ensure the feasibility of the Lyapunov function. Now we are ready to show the GAS of the mean error dynamics.

**Proposition 7** (Global asymptotic stability of the DLKCF)**.** *Consider the DLKCF in* (5.3) *and* (5.4) *with the consensus gain in* (5.5)*. Suppose all sections are uniformly completely observable. Then, the mean estimation error* $\boldsymbol{\eta}_{1:N,k|k} = \mathbb{E}[\eta_{1:N,k|k}]$ *is GAS for sufficiently small* $\gamma_{i,k}^j$*.*

*Proof.* We show $\Delta V_k$ in (5.9) is negative definite when $\boldsymbol{\eta}_{1:N,k-1|k-1} \neq 0$. For notation

simplicity and ease of understanding, we consider the case where

$$\mathcal{N}_i = \begin{cases} \{i+1\} & \text{if } i = 1 \\ \{i-1, i+1\} & \text{if } i \neq 1, \text{ and } i \neq N \\ \{i-1\} & \text{if } i = N, \end{cases} \tag{5.10}$$

and the overlapping regions are located at the boundaries of each section, i.e.,

$$\hat{I}_{i,j} = \begin{cases} \begin{pmatrix} I_{n_{i,j}} & \mathbf{0}_{n_{i,j}, n_i - n_{i,j}} \end{pmatrix} & \text{if } j = i-1 \\ \begin{pmatrix} \mathbf{0}_{n_{i,j}, n_i - n_{i,j}} & I_{n_{i,j}} \end{pmatrix} & \text{if } j = i+1. \end{cases} \tag{5.11}$$

The proof can be directly extended to any distributions of neighbors and overlapping regions.

**Step 1.** Negative definiteness of the first term in (5.9).

The proof for the first term follows closely from [53] with minor changes. Here we only show the result and introduce the matrices needed in this proof. Note that $A_{i,k}$ is invertible for all $i$ and $k$. Each element in the first term in (5.9) can be equivalently written as:

$$\begin{aligned} &\boldsymbol{\eta}_{i,k-1|k-1}^\top \left( A_{i,k-1}^\top F_{i,k}^\top \Gamma_{i,k|k}^{-1} F_{i,k} A_{i,k-1} - \Gamma_{i,k-1|k-1}^{-1} \right) \boldsymbol{\eta}_{i,k-1|k-1} \\ &= -\boldsymbol{\eta}_{i,k|k-1}^\top \left( \left( A_{i,k-1} \Gamma_{i,k-1|k-1} A_{i,k-1}^\top \right)^{-1} - F_{i,k}^\top \Gamma_{i,k|k}^{-1} F_{i,k} \right) \boldsymbol{\eta}_{i,k|k-1} \\ &= -\boldsymbol{\eta}_{i,k|k-1}^\top \left( \left( A_{i,k-1} \Gamma_{i,k-1|k-1} A_{i,k-1}^\top \right)^{-1} - \left( A_{i,k-1} \Gamma_{i,k-1|k-1} A_{i,k-1}^\top + W_{i,k-1} \right)^{-1} \right) \boldsymbol{\eta}_{i,k|k-1} \\ &= -\boldsymbol{\eta}_{i,k|k-1}^\top \Lambda_{i,k-1} \boldsymbol{\eta}_{i,k|k-1}, \end{aligned}$$

where the second equation is due to Lemma 2 in [53], with $\Lambda_{i,k}$ defined as

$$\Lambda_{i,k} = \left( A_{i,k} \Gamma_{i,k|k} A_{i,k}^\top \right)^{-1} - \left( A_{i,k} \Gamma_{i,k|k} A_{i,k}^\top + W_{i,k} \right)^{-1},$$

where

$$W_{i,k} = Q_{i,k} + \Gamma_{i,k+1|k} S_{i,k+1} \Gamma_{i,k+1|k} > 0,$$

and $S_{i,k} = H_{i,k}^\top R_{i,k}^{-1} H_{i,k}$. Due to the matrix inversion lemma,

$$\begin{aligned}
&\Gamma_{i,k|k} A_{i,k}^\top \Lambda_{i,k} A_{i,k} \Gamma_{i,k|k} \\
=&\Gamma_{i,k|k} - \Gamma_{i,k|k} A_{i,k}^\top \left( A_{i,k} \Gamma_{i,k|k} A_{i,k}^\top + W_{i,k} \right)^{-1} A_{i,k} \Gamma_{i,k|k}, \\
=&\left( \Gamma_{i,k|k}^{-1} + A_{i,k}^\top W_{i,k}^{-1} A_{i,k} \right)^{-1} > 0,
\end{aligned}$$

hence $\Lambda_{i,k} > 0$. Consequently, the first term in (5.9) is negative definite.

**Step 2.** Negative semidefiniteness of the second term in (5.9).

Due to Lemma 2(i) in [53] we have $F_{i,k} = \Gamma_{i,k|k} \Gamma_{i,k|k-1}^{-1}$, hence the consensus gain is equivalent to

$$C_{i,k}^j = \gamma_{i,k}^j \Gamma_{i,k|k-1} \hat{I}_{i,j}^\top = \gamma_{i,k}^j \Gamma_{i,k|k} \left( F_{i,k}^\top \right)^{-1} \hat{I}_{i,j}^\top.$$

Let $\hat{i} \in \{1, \cdots, N-1\}$ be the index of the overlapping regions, and define

$$\hat{\boldsymbol{\eta}}_{\hat{i},k|k-1} = (\boldsymbol{\eta}_{\hat{i},k|k-1}^\top \hat{I}_{\hat{i},\hat{i}+1}^\top, \boldsymbol{\eta}_{\hat{i}+1,k|k-1}^\top \hat{I}_{\hat{i}+1,\hat{i}}^\top)^\top.$$

The second term in (5.9) can be written as

$$\begin{aligned}
&2 \textstyle\sum_{i=1}^N \left( \boldsymbol{\eta}_{i,k|k-1}^\top F_{i,k}^\top \Gamma_{i,k|k}^{-1} \sum_{j \in \mathcal{N}_i} C_{i,k}^j \boldsymbol{\delta}_{i,k}^j \right) \\
=&\, 2 \textstyle\sum_{\hat{i}=1}^{N-1} \gamma_{\hat{i},k}^{\hat{i}+1} \left( \boldsymbol{\eta}_{\hat{i},k|k-1}^\top \hat{I}_{\hat{i},\hat{i}+1}^\top \boldsymbol{\delta}_{\hat{i},k}^{\hat{i}+1} + \boldsymbol{\eta}_{\hat{i}+1,k|k-1}^\top \hat{I}_{\hat{i}+1,\hat{i}}^\top \boldsymbol{\delta}_{\hat{i}+1,k}^{\hat{i}} \right) \\
=&\, -2 \textstyle\sum_{\hat{i}=1}^{N-1} \gamma_{\hat{i},k}^{\hat{i}+1} \hat{\boldsymbol{\eta}}_{\hat{i},k|k-1}^\top \hat{L}_{\hat{i}} \hat{\boldsymbol{\eta}}_{\hat{i},k|k-1} \leq 0,
\end{aligned}$$

where

$$\hat{L}_{\hat{i}} = \begin{pmatrix} 1 & -1 \\ -1 & 1 \end{pmatrix} \otimes I_{n_{\hat{i},\hat{i}+1}},$$

and the last inequality holds due to the quadratic property of the Laplacian matrix [94].

**Step 3.** Upper bound of the third term in (5.9).

Given the choice of consensus gain in (5.5), the third term in (5.9) can be written as

$$\begin{aligned}&\textstyle\sum_{i=1}^{N}\left(\sum_{j\in\mathcal{N}_i}C_{i,k}^{j}\boldsymbol{\delta}_{i,k}^{j}\right)^{\top}\Gamma_{i,k|k}^{-1}\left(\sum_{j\in\mathcal{N}_i}C_{i,k}^{j}\boldsymbol{\delta}_{i,k}^{j}\right)\\=&\textstyle\sum_{i=1}^{N}\left(\sum_{j\in\mathcal{N}_i}\hat{I}_{i,j}^{\top}\gamma_{i,k}^{j}\boldsymbol{\delta}_{i,k}^{j}\right)^{\top}G_{i,k}\left(\sum_{j\in\mathcal{N}_i}\hat{I}_{i,j}^{\top}\gamma_{i,k}^{j}\boldsymbol{\delta}_{i,k}^{j}\right),\end{aligned}$$

where we define $G_{i,k}=A_{i,k-1}\Gamma_{i,k-1|k-1}A_{i,k-1}^{\top}+Q_{i,k-1}+\Gamma_{i,k|k-1}S_{i,k}\Gamma_{i,k|k-1}$. Recall that $\mathcal{J}_i=\mathcal{N}_i\cup\{i\}$, and define $\boldsymbol{\eta}_{\mathcal{J}_i,k|k-1}=\mathrm{col}_{j\in\mathcal{J}_i}\left(\boldsymbol{\eta}_{j,k|k-1}\right)$ where $j$ are sorted in ascending order. Columnizing $\boldsymbol{\delta}_{i,k}^{j}$ over all neighbors $j\in\mathcal{N}_i$ within section $i$ yields

$$\boldsymbol{\delta}_{\mathcal{N}_i,k}=\mathrm{col}_{j\in\mathcal{N}_i}\left(\gamma_{i,k}^{j}\boldsymbol{\delta}_{i,k}^{j}\right)=\tilde{L}_i\tilde{I}_i\boldsymbol{\eta}_{\mathcal{J}_i,k|k-1},\tag{5.12}$$

where $j$ are sorted in ascending order, $\tilde{L}_i$ is defined as

$$\tilde{L}_i=\begin{cases}\begin{pmatrix}-\hat{I}_{i,i+1} & \hat{I}_{i+1,i}\end{pmatrix} & \text{if } i=1\\ \begin{pmatrix}\hat{I}_{i-1,i} & -\hat{I}_{i,i-1}\end{pmatrix} & \text{if } i=n\\ \begin{pmatrix}\hat{I}_{i-1,i} & -\hat{I}_{i,i-1} & \mathbf{0}_{n_{i-1,i},n_{i+1}}\\ \mathbf{0}_{n_{i,i+1},n_{i-1}} & -\hat{I}_{i,i+1} & \hat{I}_{i+1,i}\end{pmatrix} & \text{otherwise,}\end{cases}$$

and

$$\begin{aligned}\tilde{I}_i=&\mathrm{diag}(I_{n_{i-1}-n_{i-1,i}},\gamma_{i,k}^{i-1}I_{n_{i-1,i}},\gamma_{i,k}^{i-1}I_{n_{i-1,i}},\\&I_{n_i-n_{i-1,i}-n_{i+1,i}},\gamma_{i,k}^{i+1}I_{n_{i+1,i}},\gamma_{i,k}^{i+1}I_{n_{i+1,i}},I_{n_{i+1}-n_{i+1,i}})\end{aligned}$$

Further define

$$\tilde{H}_i=\begin{cases}\hat{I}_{i,i+1} & \text{if } i=1\\ \hat{I}_{i,i-1} & \text{if } i=n\\ \begin{pmatrix}\hat{I}_{i,i-1}^{\top} & \hat{I}_{i,i+1}^{\top}\end{pmatrix} & \text{otherwise.}\end{cases}$$

The third term in (5.9) is equivalent to

$$\begin{aligned}&\textstyle\sum_{i=1}^{N}\left(\sum_{j\in\mathcal{N}_i}\hat{I}_{i,j}^{\top}\gamma_{i,k}^{j}\boldsymbol{\delta}_{i,k}^{j}\right)^{\top}G_{i,k}\left(\sum_{j\in\mathcal{N}_i}\hat{I}_{i,j}^{\top}\gamma_{i,k}^{j}\boldsymbol{u}_{i,k}^{j}\right)\\=&\textstyle\sum_{i=1}^{N}\boldsymbol{\eta}_{\mathcal{J}_i,k|k-1}^{\top}\tilde{I}_i\tilde{L}_i^{\top}\tilde{H}_i^{\top}G_{i,k}\tilde{H}_i\tilde{L}_i\tilde{I}_i\boldsymbol{\eta}_{\mathcal{J}_i,k|k-1}\\\leq&\textstyle\sum_{i=1}^{N}\left(\gamma_{i,k}^{\max}\right)^{2}\lambda_{\max}\left(\tilde{L}_i^{\top}\tilde{H}_i^{\top}G_{i,k}\tilde{H}_i\tilde{L}_i\right)\|\boldsymbol{\eta}_{\mathcal{J}_i,k|k-1}\|^{2},\end{aligned}$$

where $\gamma_{i,k}^{\max} = \max_{j\in\mathcal{N}_i} \gamma_{i,k}^{j}$ and $\lambda_{\max}$ (resp. $\lambda_{\min}$) is the maximum (resp. minimum) eigenvalue of a matrix.

**Step 4.** The negative definiteness of (5.9).

Note that given Step 1, the first term of (5.9) can be equivalently written as

$$\textstyle\sum_{i=1}^{N} -\boldsymbol{\eta}_{i,k|k-1}^{\top}\Lambda_{i,k-1}\boldsymbol{\eta}_{i,k|k-1} = \sum_{i=1}^{N} -\boldsymbol{\eta}_{\mathcal{J}_i,k|k-1}^{\top}\Lambda_{\mathcal{J}_i,k-1}\boldsymbol{\eta}_{\mathcal{J}_i,k|k-1},$$

where $\Lambda_{\mathcal{J}_i,k} = \mathrm{diag}_{j\in\mathcal{J}_i}(\mu_i^j\Lambda_{j,k})$ with the indexes $j$ sorted by ascending order, and the scaling factors are pre-defined and satisfy $\sum_{j\in\mathcal{J}_i}\mu_j^i = 1$ for all $i$. Given Steps 1-3, $\Delta V_k$ satisfies

$$\begin{aligned}\Delta V_k \leq\ & -2\textstyle\sum_{\hat{i}=1}^{N-1}\gamma_{\hat{i},k}^{\hat{i}+1}\hat{\boldsymbol{\eta}}_{\hat{i},k|k-1}^{\top}\hat{L}_{\hat{i}}\hat{\boldsymbol{\eta}}_{\hat{i},k|k-1} \\ & + \textstyle\sum_{i=1}^{N}\left(\left(\gamma_{i,k}^{\max}\right)^2\lambda_{\max}\left(\tilde{L}_i^{\top}\tilde{H}_i^{\top}G_{i,k}\tilde{H}_i\tilde{L}_i\right) - \lambda_{\min}\left(\Lambda_{\mathcal{J}_i,k-1}\right)\right)\|\boldsymbol{\eta}_{\mathcal{J}_i,k|k-1}\|^2.\end{aligned} \tag{5.13}$$

Therefore by choosing $\gamma_{i,k}^{j}$ sufficiently small we can render $\Delta V_k < 0$ for all $k \geq 0$ and for all $\boldsymbol{\eta}_{1:N,k-1|k-1} \neq 0$. Precisely, we need $\gamma_{i,k}^{j} < \gamma_{i,k}^{*}$ where $\gamma_{i,k}^{*}$ is defined by

$$\gamma_{i,k}^{*} = \left(\frac{\lambda_{\min}\left(\Lambda_{\mathcal{J}_i,k-1}\right)}{\lambda_{\max}\left(\tilde{L}_i^{\top}\tilde{H}_i^{\top}G_{i,k}\tilde{H}_i\tilde{L}_i\right)}\right)^{\frac{1}{2}}.$$

Note that to compute $\gamma_{i,k}^{*}$, only information from one-hop neighbors is needed, and global communication topology is not required compared to [53]. Hence, $\Delta V_k < 0$ for all $k \geq 0$ and $\boldsymbol{\eta}_{1:N,k-1|k-1} \neq 0$, and therefore $\boldsymbol{\eta}_{1:N,k|k} = 0$ is GAS for the mean error dynamics of the DLKCF. Consequently, all estimators reach consensus on the shared states. □

Indeed, when the consensus gain is zero, the mean error dynamics of each local agent is also GAS when all the sections are UCO. However, due to different model errors and innovation sequences, the estimates provided by neighboring agents on their shared overlapping regions inevitably disagree in any realization of the filter. Hence, the consensus term is designed to promote agreement while preserving the unbiasedness of the filter. Moreover, when $\gamma_{i,k}^{j} < \gamma_{i,k}^{*}$, it can be deduced from (5.13) that $\Delta V_k < -\sqrt{2}\sum_{\hat{i}=1}^{N-1}\gamma_{\hat{i},k}^{\hat{i}+1}\|\boldsymbol{u}_{\hat{i},k}^{\hat{i}+1}\|^2$ (derived in [88, Appendix E]). This indicates that $V_k$ strictly decreases at the rate proportional to the total disagreement until the neighboring disagreements on all the overlapping regions converge to zero (also holds for any distributions of neighbors and overlapping regions), which is a property cannot be achieved without the consensus term.

## 5.4 Error bounds of the DLKCF for traffic estimation

In this section, we analyze the performance of the DLKCF in the context of traffic estimation problems, and derive the error bounds for the DLKCF on a local section when the section switches among observable and unobservable modes of the SMM.

First note that when either of two neighboring sections is unobservable, the consensus term between the two sections is turned off. This choice is made to ensure that the consensus term would not destabilize the estimation error or degrade the estimation accuracy under unobservable scenarios. Under this setting, the error bound of the DLKCF under each unobservable road section is the same as the KF. Also note that the update scheme of the error covariance is the same for the DLKCF and the KF, this implies that the upper and lower bounds of the error covariance given by the DLKCF under UCO systems coincide with the KF.

In the performance analysis of the DLKCF, the elements that are affected by the introduction of the consensus term are the minimum residence time in the observable time intervals, and the formula of the error bounds under switches among observable and unobservable modes. For the remainder of this section, we extend the results in Proposition 3 and Proposition 4 to derive the error bounds of the DLKCF under the SMM. The error bounds of the DLKCF under the SMM-J can be obtained in the same manner.

**Proposition 8** (Residence time and error bounds of DLKCF in the observable modes of SMM)**.** *Consider a local road section (shown in Figure 2.2) in a large-scale transportation network. Suppose the local section switches arbitrarily among the observable modes of the SMM while* $k \in (\underline{k}_{\mathrm{O}}, \bar{k}_{\mathrm{O}}]$*, where* $0 \leq \underline{k}_{\mathrm{O}} < \bar{k}_{\mathrm{O}} \leq +\infty$*. The traffic state on the local road section is estimated by a local agent based on the DLKCF. Define*

$$\begin{aligned} \mathrm{a}\left(\Gamma_{\underline{k}_{\mathrm{O}}|\underline{k}_{\mathrm{O}}}\right) &= \left(\mathrm{c}_2\left(\Gamma_{\underline{k}_{\mathrm{O}}|\underline{k}_{\mathrm{O}}}\right)\left(\mathrm{c}_1\left(\Gamma_{\underline{k}_{\mathrm{O}}|\underline{k}_{\mathrm{O}}}\right)\right)^{-1}\right)^{\frac{1}{2}}, \\ \mathrm{q}\left(\Gamma_{\underline{k}_{\mathrm{O}}|\underline{k}_{\mathrm{O}}}\right) &= \left(1-\mathrm{c}_3\left(\Gamma_{\underline{k}_{\mathrm{O}}|\underline{k}_{\mathrm{O}}}\right)\left(\mathrm{c}_2\left(\Gamma_{\underline{k}_{\mathrm{O}}|\underline{k}_{\mathrm{O}}}\right)\right)^{-1}\right)^{\frac{1}{2}}, \end{aligned} \tag{5.14}$$

*where* $\mathrm{c}_1(\cdot)$*,* $\mathrm{c}_2(\cdot)$ *are the bounds from* (3.7)*, and*

$$\mathrm{c}_3\left(\Gamma_{\underline{k}_{\mathrm{O}}|\underline{k}_{\mathrm{O}}}\right) = \mathrm{d}\left(\mathrm{c}_1\left(\Gamma_{\underline{k}_{\mathrm{O}}|\underline{k}_{\mathrm{O}}}\right), \mathrm{c}_2\left(\Gamma_{\underline{k}_{\mathrm{O}}|\underline{k}_{\mathrm{O}}}\right)\right),$$

*with* $\mathrm{d}(\cdot,\cdot)$ *defined in Lemma 6.*

*For all $\epsilon > 0$, there exists* $\hat{\mathrm{t}}\left(\epsilon, \left\|\boldsymbol{\eta}_{\underline{k}_{\mathrm{O}}|\underline{k}_{\mathrm{O}}}\right\|, \Gamma_{\underline{k}_{\mathrm{O}}|\underline{k}_{\mathrm{O}}}\right)$ *such that if*

$$\bar{k}_{\mathrm{O}} - \underline{k}_{\mathrm{O}} > \hat{\mathrm{t}}\left(\epsilon, \left\|\boldsymbol{\eta}_{\underline{k}_{\mathrm{O}}|\underline{k}_{\mathrm{O}}}\right\|, \Gamma_{\underline{k}_{\mathrm{O}}|\underline{k}_{\mathrm{O}}}\right),$$

*the mean error at time* $\bar{k}_{\mathrm{O}}$ *satisfies* $\left\|\boldsymbol{\eta}_{\bar{k}_{\mathrm{O}}|\bar{k}_{\mathrm{O}}}\right\| < \epsilon + \hat{c} + \frac{\hat{c}\mathrm{a}\left(\Gamma_{\underline{k}_{\mathrm{O}}|\underline{k}_{\mathrm{O}}}\right)\mathrm{q}\left(\Gamma_{\underline{k}_{\mathrm{O}}|\underline{k}_{\mathrm{O}}}\right)}{1-\mathrm{q}\left(\Gamma_{\underline{k}_{\mathrm{O}}|\underline{k}_{\mathrm{O}}}\right)}$. *Explicitly,*

$$\hat{\mathrm{t}}\left(\epsilon, \left\|\boldsymbol{\eta}_{\underline{k}_{\mathrm{O}}|\underline{k}_{\mathrm{O}}}\right\|, \Gamma_{\underline{k}_{\mathrm{O}}|\underline{k}_{\mathrm{O}}}\right) = \begin{cases} 0, & \text{if } \mathrm{a}\left(\Gamma_{\underline{k}_{\mathrm{O}}|\underline{k}_{\mathrm{O}}}\right)\mathrm{q}\left(\Gamma_{\underline{k}_{\mathrm{O}}|\underline{k}_{\mathrm{O}}}\right)\left\|\boldsymbol{\eta}_{\underline{k}_{\mathrm{O}}|\underline{k}_{\mathrm{O}}}\right\| \leq \frac{\hat{c}\mathrm{a}\left(\Gamma_{\underline{k}_{\mathrm{O}}|\underline{k}_{\mathrm{O}}}\right)\mathrm{q}\left(\Gamma_{\underline{k}_{\mathrm{O}}|\underline{k}_{\mathrm{O}}}\right)}{1-\mathrm{q}\left(\Gamma_{\underline{k}_{\mathrm{O}}|\underline{k}_{\mathrm{O}}}\right)}, \\ \log_{\mathrm{q}\left(\Gamma_{\underline{k}_{\mathrm{O}}|\underline{k}_{\mathrm{O}}}\right)}\left(\epsilon\left(\mathrm{a}\left(\Gamma_{\underline{k}_{\mathrm{O}}|\underline{k}_{\mathrm{O}}}\right)\left\|\boldsymbol{\eta}_{\underline{k}_{\mathrm{O}}|\underline{k}_{\mathrm{O}}}\right\| - \frac{\hat{c}\mathrm{a}\left(\Gamma_{\underline{k}_{\mathrm{O}}|\underline{k}_{\mathrm{O}}}\right)}{1-\mathrm{q}\left(\Gamma_{\underline{k}_{\mathrm{O}}|\underline{k}_{\mathrm{O}}}\right)}\right)^{-1}\right), & o.w. \end{cases} \tag{5.15}$$

*Furthermore, for all* $k \in (\underline{k}_{\mathrm{O}}, \bar{k}_{\mathrm{O}}]$,

$$\begin{aligned} \left\|\boldsymbol{\eta}_{k|k}\right\| \leq \max\Big\{ & \hat{c} + \mathrm{a}\left(\Gamma_{\underline{k}_{\mathrm{O}}|\underline{k}_{\mathrm{O}}}\right)\mathrm{q}\left(\Gamma_{\underline{k}_{\mathrm{O}}|\underline{k}_{\mathrm{O}}}\right)\left\|\boldsymbol{\eta}_{\underline{k}_{\mathrm{O}}|\underline{k}_{\mathrm{O}}}\right\|, \\ & \hat{c} + \hat{c}\mathrm{a}\left(\Gamma_{\underline{k}_{\mathrm{O}}|\underline{k}_{\mathrm{O}}}\right)\mathrm{q}\left(\Gamma_{\underline{k}_{\mathrm{O}}|\underline{k}_{\mathrm{O}}}\right)\left(1-\mathrm{q}\left(\Gamma_{\underline{k}_{\mathrm{O}}|\underline{k}_{\mathrm{O}}}\right)\right)^{-1}\Big\}. \end{aligned}$$

*Proof.* The proposition is derived based on the extensions from the proof of Proposition 3, which is reported in Appendix D.1. □

The next proposition leverages the analysis in Proposition 4, and derives the minimum residence time of all the observable time intervals as well as the error bounds for the DLKCF under switches among observable and unobservable modes.

**Proposition 9** (Error bounds of the DLKCF under switches among observable and unobservable modes of SMM)**.** *Consider a local road section (shown in Figure 2.2) in a large-scale transportation network. Denote as* $(\underline{k}^r_{\mathrm{U}}, \bar{k}^r_{\mathrm{U}}]$ *(resp.* $(\underline{k}^r_{\mathrm{O}}, \bar{k}^r_{\mathrm{O}}]$*) the* $r^{th}$ *time interval while the local section switches among unobservable (resp. observable) modes of the SMM. Hence* $\underline{k}^1_{\mathrm{U}} = 0$ *(resp.* $\underline{k}^1_{\mathrm{O}} = 0$*) when the local section is unobservable (resp. observable) at time* 0*. Let* $\epsilon > 0$ *be an arbitrary positive constant, and suppose the following conditions on the residence time for the observable time intervals hold:*

$$\bar{k}^r_{\mathrm{O}} - \underline{k}^r_{\mathrm{O}} > \begin{cases} \hat{\mathrm{t}}\left(\epsilon, \hat{\mathrm{e}}\left(\epsilon, \Gamma_{\underline{k}^{r-1}_{\mathrm{O}}|\underline{k}^{r-1}_{\mathrm{O}}}, \Gamma_{\bar{k}^{r-1}_{\mathrm{O}}|\bar{k}^{r-1}_{\mathrm{O}}}\right), \Gamma_{\underline{k}^r_{\mathrm{O}}|\underline{k}^r_{\mathrm{O}}}\right) & r \geq 2 \\ \hat{\mathrm{t}}\left(\epsilon, \hat{\mathrm{e}}_0\left(\Gamma_{0|0}\right), \Gamma_{\underline{k}^1_{\mathrm{O}}|\underline{k}^1_{\mathrm{O}}}\right) & r = 1 \text{ and } \underline{k}^1_{\mathrm{U}} = 0 \\ \hat{\mathrm{t}}\left(\epsilon, \sqrt{n}\varrho_{\mathrm{m}}, \Gamma_{0|0}\right) & r = 1 \text{ and } \underline{k}^1_{\mathrm{O}} = 0, \end{cases} \tag{5.16}$$

*where* $\hat{\mathrm{e}}_0(M) = \sqrt{n}\left(\sqrt{n}\varrho_{\mathrm{m}}\left(c_0 + (n-2)\,\mathrm{c}(M)\right) + \varrho_{\mathrm{m}}\right)$ *for* $M \in \mathbb{R}^{n\times n}$, *and*

$$\hat{\mathrm{e}}(\epsilon, M_1, M_2) = \sqrt{n}\left(\varrho_{\mathrm{m}} + \left(\epsilon + \hat{c} + \tfrac{\hat{c}\mathrm{a}(M_1)\mathrm{q}(M_1)}{1-\mathrm{q}(M_1)}\right) \times \left(c_0 + (n-2)\,\mathrm{c}(M_2)\right)\right),$$

*for* $M_1, M_2 \in \mathbb{R}^{n\times n}$, *with* $\hat{c}$ *given in* (5.6), $c_0$ *and* $\mathrm{c}(\cdot)$ *defined in* (3.19), $\mathrm{a}(\cdot)$ *and* $\mathrm{q}(\cdot)$ *defined in* (5.14).

*When* $r \geq 2$, *the mean error is upper bounded as follows:*

$$\left\|\boldsymbol{\eta}_{k|k}\right\| \leq \begin{cases} (a)\ \textit{for}\ k \in (\underline{k}^r_{\mathrm{U}}, \bar{k}^r_{\mathrm{U}}]\textit{:}\ \hat{\mathrm{e}}\left(\epsilon, \Gamma_{\bar{k}^{r-1}_{\mathrm{U}}|\bar{k}^{r-1}_{\mathrm{U}}}, \Gamma_{\underline{k}^r_{\mathrm{U}}|\underline{k}^r_{\mathrm{U}}}\right), \\ (b)\ \textit{for}\ k \in (\underline{k}^r_{\mathrm{O}}, \bar{k}^r_{\mathrm{O}}]\textit{:}\ \max\Big\{\hat{c} + \mathrm{a}\left(\Gamma_{\underline{k}^r_{\mathrm{O}}|\underline{k}^r_{\mathrm{O}}}\right) \times \\ \qquad \mathrm{q}\left(\Gamma_{\underline{k}^r_{\mathrm{O}}|\underline{k}^r_{\mathrm{O}}}\right)\hat{\mathrm{e}}\left(\epsilon, \Gamma_{\underline{k}^{r-1}_{\mathrm{O}}|\underline{k}^{r-1}_{\mathrm{O}}}, \Gamma_{\bar{k}^{r-1}_{\mathrm{O}}|\bar{k}^{r-1}_{\mathrm{O}}}\right), \\ \qquad \hat{c} + \hat{c}\mathrm{a}\left(\Gamma_{\underline{k}^r_{\mathrm{O}}|\underline{k}^r_{\mathrm{O}}}\right) \times \\ \qquad \mathrm{q}\left(\Gamma_{\underline{k}^r_{\mathrm{O}}|\underline{k}^r_{\mathrm{O}}}\right)\left(1 - \mathrm{q}\left(\Gamma_{\underline{k}^r_{\mathrm{O}}|\underline{k}^r_{\mathrm{O}}}\right)\right)^{-1}\Big\}. \end{cases}$$

*When* $r = 1$ *and* $\underline{k}^1_{\mathrm{U}} = 0$, *the mean estimation error satisfies*

$$\left\|\boldsymbol{\eta}_{k|k}\right\| \leq \begin{cases} (a)\ \textit{for}\ k \in (\underline{k}^1_{\mathrm{U}}, \bar{k}^1_{\mathrm{U}}]\textit{:}\ \hat{\mathrm{e}}_0\left(\Gamma_{0|0}\right), \\ (b)\ \textit{for}\ k \in (\underline{k}^1_{\mathrm{O}}, \bar{k}^1_{\mathrm{O}}]\textit{:}\ \max\Big\{\hat{c} + \mathrm{a}\left(\Gamma_{\underline{k}^1_{\mathrm{O}}|\underline{k}^1_{\mathrm{O}}}\right) \times \\ \qquad \mathrm{q}\left(\Gamma_{\underline{k}^1_{\mathrm{O}}|\underline{k}^1_{\mathrm{O}}}\right)\hat{\mathrm{e}}_0\left(\Gamma_{0|0}\right),\ \ \hat{c} + \hat{c}\mathrm{a}\left(\Gamma_{\underline{k}^1_{\mathrm{O}}|\underline{k}^1_{\mathrm{O}}}\right) \times \\ \qquad \mathrm{q}\left(\Gamma_{\underline{k}^1_{\mathrm{O}}|\underline{k}^1_{\mathrm{O}}}\right)\left(1 - \mathrm{q}\left(\Gamma_{\underline{k}^1_{\mathrm{O}}|\underline{k}^1_{\mathrm{O}}}\right)\right)^{-1}\Big\}. \end{cases}$$

*When* $r = 1$ *and* $\underline{k}^1_{\mathrm{O}} = 0$, *the mean estimation error satisfies*

$$\left\|\boldsymbol{\eta}_{k|k}\right\| \leq \begin{cases} (a)\ \textit{for}\ k \in (\underline{k}^1_{\mathrm{U}}, \bar{k}^1_{\mathrm{U}}]\textit{:}\ \hat{\mathrm{e}}\left(\delta, \Gamma_{0|0}, \Gamma_{\underline{k}^1_{\mathrm{U}}|\underline{k}^1_{\mathrm{U}}}\right), \\ (b)\ \textit{for}\ k \in (\underline{k}^1_{\mathrm{O}}, \bar{k}^1_{\mathrm{O}}]\textit{:}\ \max\left\{\hat{c} + \mathrm{a}\left(\Gamma_{0|0}\right) \times \right. \\ \qquad \left. \mathrm{q}\left(\Gamma_{0|0}\right)\sqrt{n}\varrho_{\mathrm{m}},\ \ \hat{c} + \hat{c}\mathrm{a}\left(\Gamma_{0|0}\right) \times \right. \\ \qquad \left. \mathrm{q}\left(\Gamma_{0|0}\right)\left(1 - \mathrm{q}\left(\Gamma_{0|0}\right)\right)^{-1}\right\}. \end{cases}$$

*Proof.* The proof is done by combining Proposition 2 and Proposition 8, which is detailed in Appendix 9. □

## 5.5 Numerical experiments

In this section, we present simulation results of the DLKCF in the context of traffic estimation problems. The numerical experiments focus on (*i*) demonstrating the effect of the consensus term in promoting neighbor agreements on the estimates of their shared states, (*ii*) showing that neglecting the cross-covariance terms in the error covariance will not significantly affect the accuracy of the computed error covariance in the DLKCF, and (*iii*) showing that the DLKCF considerably reduces the computational complexity compared to a central estimator.

### 5.5.1 Effect of inter-agent communication

In this section, we show the critical role the consensus term plays in reducing the disagreement between agents. Consider a traffic network which is a stretch of highway divided into 136 cells and 7 local sections. We apply normalized parameters for the triangular fundamental diagram. The true solution is set to be a combination of an expansion fan and a shock propagating upstream, with a sinusoidal upstream boundary condition (Figure 5.1a), which is computed based on the CTM. Parameter values and elements of the experimental setup not detailed here can be found in the README documentation for the supplementary source code https://github.com/yesun/DLKCF.

Disagreement and error on state estimates can be generated for various reasons, here we consider the combining effects of the following two causes: (*i*) *heterogeneous sensors* (HS), with some of the sensors having large measurement errors; (*ii*) *inconsistent agents* (IA), with some agents assuming incorrect noise models for the low quality sensors. In this experiment, we put a large-error sensor (with the measurement error standard deviation of 0.3, compared to 0.03 for all other sensors) once every three sensors starting from the downstream sensor of the first section. Moreover, agents associated with sections indexed by even numbers are unable to recognize the large-error sensors they are directly connected to (thus still applying 0.03 as the measurement error standard deviation for these sensors). We also apply perturbations of 10-20% on the model parameters (i.e., $\varrho_{\mathrm{m}}$, $\varrho_{\mathrm{c}}$, and $v_{\mathrm{m}}$) on different sections.

We explore the effects of the above two causes on the disagreement and error of estimates

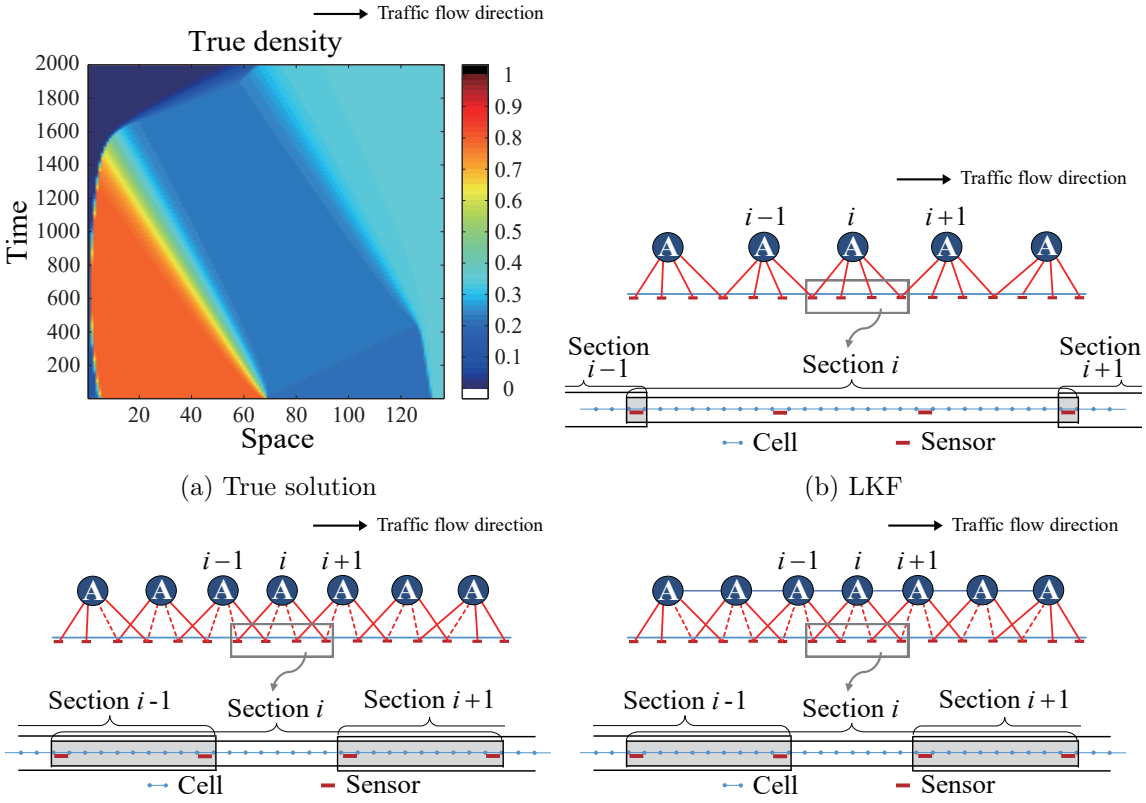


(a) True solution

(b) LKF

(c) DLKCF-0

(d) DLKCF

Figure 5.1: (a) True Solution; (b-d) Freeway network setup and communication topology for: (b) the LKF; (c) the DLKCF-0; and (d) the DLKCF. The red solid lines represent the direct connection between agents (labeled A in circles) and sensors (red rectangles), and the red dashed lines represent connection between agents and sensors obtained through receiving shared measurements and sensor models from neighbors. The lines connecting agents stand for the existence of consensus terms between agents. In the zoomed-in parts, the freeway is discretized by cells and localized by sections. Overlapping regions are represented by the shaded areas.

Table 5.1: Disagreement and error of estimate

| Causes | | Disagreement $\bar{\delta}^{\mathrm{t,a}}$ | | | Error $\bar{\eta}^{\mathrm{t,a}}$ ($\times 10^{-2}$) | | |
|---|---|---|---|---|---|---|---|
| HS | IA | LKF | DLKCF-0 | DLKCF | LKF | DLKCF-0 | DLKCF |
| False | – | – | 0.294 | 0.119 | 0.423 | 0.349 | 0.308 |
| True | False | – | 0.336 | 0.119 | 0.562 | 0.503 | 0.468 |
| True | True | – | 7.361 | 4.664 | 2.941 | 2.670 | 2.633 |

for ($i$) the *local KF* (LKF), where each local agent runs the KF described in Section 3.2 independently based on measurements from the sensors it is directly connected to (e.g., $z^i_{i,k}$ for agent $i$), without sharing measurements or estimates; ($ii$) the *DLKCF with zero consensus gain* (DLKCF-0), where the time and information updates are given by (5.3)-(5.4) (i.e., neighboring agents share sensor data and sensor models) with consensus gains set to zero (i.e., $C^j_{i,k} = \mathbf{0}_{n_i,n_{i,j}}$ for all $i$, $j \in \mathcal{N}_i$ and $k$); and ($iii$) the DLKCF with consensus gain as given in (5.5) (where $\gamma^j_{i,k} = 0.99 \min\{\gamma^*_{i,k}, \gamma^*_{j,k}, \hat{\gamma}^j_{i,k}\}$ with $\hat{c} = 0.01$). Figure 5.1 shows the network setup and the communication topology for the LKF (Figure 5.1b), the DLKCF-0 (Figure 5.1c) and DLKCF (Figure 5.1d). At time $k$, the agent-wise average disagreement $\bar{\delta}^{\mathrm{a}}_{k|k}$ of the posterior estimate is computed by $\bar{\delta}^{\mathrm{a}}_{k|k} = \frac{1}{N-1}\sum_{i=1}^{N-1} \frac{\|\delta^{i+1}_{i,k}\|_2^2}{n_{i,i+1}}$ with, and the average estimation error across agents is given by $\bar{\eta}^{\mathrm{a}}_{k|k} = \frac{1}{N}\sum_{i=1}^{N} \frac{\|\eta_{i,k|k}\|_2^2}{n_i}$.

Table 5.1 reports the average disagreement and estimation error (across time and agents) of the three filters, where $\bar{\delta}^{\mathrm{t,a}} = \sum_{k=1}^{k_{\max}} \bar{\delta}^{\mathrm{a}}_{k|k}$ and $\bar{\eta}^{\mathrm{t,a}} = \sum_{k=1}^{k_{\max}} \eta^{\mathrm{a}}_{k|k}$ with $k_{\max}$ denoting the total number of time steps. Since the neighboring sections in the LKF have no overlapping cells except the shared boundary cells with sensor measurements, the neighbor disagreement for the LKF is not considered. It is shown that the estimation accuracy of the LKF is vulnerable to inconsistent error models, since the inconsistent agents can never identify the high-error sensors they are connected to, while in the DLKCF-0 and DLKCF some of the inconsistent agents apply the correct measurement error covariance matrices when they share sensor data and sensor models with neighbors. Moreover, compared to the DLKCF-0, adding the consensus term in the DLKCF considerably reduces the neighbor disagreement (regardless of the existence of heterogeneous sensors or inconsistent agents). Hence, the DLKCF outperforms the other filters with respect to agreement and accuracy on estimates.

Table 5.2: Number of times (out of 2000) NEES surpasses the 95% region.

| | Section index | | | | | | |
|---|---|---|---|---|---|---|---|
| | 0 | 1 | 2 | 3 | 4 | 5 | 6 |
| NEES>upper limit | 31 | 5 | 11 | 49 | 35 | 14 | 8 |
| NEES<lower limit | 8 | 36 | 24 | 11 | 16 | 10 | 19 |

Table 5.3: Runtime comparison of the central KF and DLKCF (per agent)

| Central KF | | DLKCF | | | | |
|---|---|---|---|---|---|---|
| $n$ | runtime $t_{\mathrm{c}}$ (sec) | $n$ | $n_l$ | $\hat{n}$ | $N$ | runtime $t_{\mathrm{d}}$ (sec) |
| 100 | 104 | 100 | 28 | 10 | 5 | 6.2 |
| 210 | 512 | 210 | 50 | 10 | 5 | 24.6 |
| 210 | 512 | 210 | 58 | 20 | 5 | 42.2 |

### 5.5.2 Accuracy of the computed error covariance

As stated in Remark 6, we remove the existence of inconsistent agents and perform an NEES check [93] of the DLKCF across 50 Monte Carlo runs, thus accessing the validity of dropping the cross-correlations among different agents in the estimation error covariance. When the number of Monte Carlo runs is 50, the two-sided 95% probability concentration region is [1.484, 2.6]. Hence, the percentage of time steps that the NEES is greater than the upper limit 2.6 or smaller than the lower limit 1.484 should not exceed 2.5%. The precise percentage of time steps the NEES of each local section is greater than the upper limit (or smaller than the lower limit) is detailed in Table 5.2. It is shown that the percentage of time steps the NEES falls out of the 95% region meets the criteria given above, thus the filter-calculated error covariance matches the mean square error of the DLKCF.

### 5.5.3 Computational complexity

For the $i^{\mathrm{th}}$ local agent of the DLKCF, the computational complexity of conducting the time update, as well as updating the posterior error covariance in the correction step, is $O(n_i^3)$ at each estimation step. As for computing the posterior estimate, the computational complexity also depends on the required operations to obtain $\gamma_{i,k}^*$ in the consensus term. Recall Proposition 7 that the value of $\gamma_{i,k}^*$ is obtained by computing the minimum eigenvalue of $\Lambda_{\mathcal{J}_i,k}$ and the maximum eigenvalue of $\tilde{L}_i^\top \tilde{H}_i^\top G_{i,k} \tilde{H}_i \tilde{L}_i$ whose dimension is closely related to the size of the local sections and the overlapping regions. For simplicity let $n_i = n_l$ for

all $i$, denote as $|\mathcal{N}_i|$ the number of neighbors of agent $i$, and let $\hat{n}$ be the uniform size of the overlapping regions. Then the dimensions of the corresponding matrices are $G_{i,k} \in \mathbb{R}^{n_l \times n_l}$, $\tilde{H}_i \in \mathbb{R}^{|\mathcal{N}_i|\hat{n} \times n_l}$, and $\tilde{L}_i \in \mathbb{R}^{|\mathcal{N}_i|\hat{n} \times (|\mathcal{N}_i|+1)n_l}$. The complexity of computing $\lambda_{\min}(\Lambda_{\mathcal{J}_i,k})$ is $O(n_l^3)$ (each agent only needs to compute diagonal block $\lambda_{\min}(\Lambda_{i,k})$ locally and share it with its neighbors). Given the structure of $\tilde{H}_i$ and $\tilde{L}_i$ shown in Step 3 of the proof of Proposition 7, the complexity of computing the maximum eigenvalue of $\tilde{L}_i^\top \tilde{H}_i G_{i,k} \tilde{H}_i^\top \tilde{L}_i$ is $O((|\mathcal{N}_i|\,\hat{n})^3)$. Hence, the computational complexity of the DLKCF for each local agent is $O(n_l^3 + (|\mathcal{N}_i|\,\hat{n})^3)$. This implies that we need $\hat{n} < n_l |\mathcal{N}_i|^{-1}$ to have a consensus term with computational complexity less than the local KF.

Table 5.3 reports the runtime per agent of the DLKCF and the central KF (i.e., using one KF to estimate the entire state space) to complete 2000 estimation steps tracking a shockwave on a stretch of freeway, which we denote as $t_{\mathrm{d}}$ and $t_{\mathrm{c}}$, respectively. It is evident that compared to the central KF, the runtime of the DLKCF is considerably reduced. Moreover, given a fixed network dimension and a fixed number of agents, the computation load increases with the size of the overlapping regions.

# CHAPTER 6

# ONLINE ESTIMATION WITH SENSOR SCHEDULERS FOR DATA TRANSMISSION REDUCTION

## 6.1 Introduction

In this chapter, we study filtering algorithms embedded with event-triggered sensor scheduling schemes to reduce data transmission while preserving estimation accuracy. When a sensor is embedded with a sensor scheduler, it sends data to the estimator only when the sensor scheduler triggers data transmission, and the data transmission decision is made based on the sensor scheduling scheme that determines whether the sensor data is "informative enough" to the estimator. Same as in Chapter 5, the estimation problem considered in this chapter is not limited to traffic monitoring problems, but general estimation problems in the *cyber-physical system* (CPS) which requires economical data assimilation (i.e., transmit only the most informative part of the sensor measurements to the estimator). The new contributions of this chapter are listed as follows.

- **Design of the Kalman filter with synthetic measurements.** We propose a *Kalman filter with synthetic measurements* (KF-SM) which extracts the implicit information embedded in the sensor scheduling scheme to update both the state estimate and the error covariance when data transmission is declined. The existing algorithms, on the other hand, update only the error covariance when data transmission is not triggered.

- **Optimality of the KF-SM.** In the KF-SM, the state estimate is updated using the synthetic measurements obtained based on the estimated distribution of the true measurements, which introduces an positive semidefinite extra term in the error covariance. However, under the proposed update scheme of the KF-SM and the synthetic measurement generation algorithm, this extra term is shown to be small and is dominated by the reduction of the error covariance obtained from the implicit

information embedded in the sensor scheduler. Hence, the boundedness of the error covariance is secured. Moreover, the KF-SM is shown to be an *minimum mean square error* (MMSE) estimator that incorporates the randomeness of the synthetic measurements.

- **Input-to-state stability of the KF-SM.** We show that the estimation error dynamics of the KF-SM is *input-to-state stable* (ISS) when treating the synthetic measurement error (with respect to the true measurement) as an input to the error dynamics (i.e., the estimation error of the KF-SM is small if the synthetic measurement is close to the true measurement, which is ensured by sensor scheduling scheme of the KF-SM).

This chapter is organized as follows. Section 6.2 introduces the motivation of using synthetic measurements to correct state estimates when data transmission is not triggered. In Section 6.3, we review the existing Kalman filtering algorithms embedded with threshold-based event-triggered sensor schedulers, which are closely related to the proposed KF-SM. Section 6.4 present the KF-SM algorithm. The performance analysis of the KF-SM is given in Section 6.5, including the optimality (Section 6.5.1) and input-to-state stability of the estimator (Section 6.5.2). Finally, Section 6.6 presents numerical studies which shows that the KF-SM outperforms state-of-the art estimators in terms of estimation accuracy.

## 6.2 Motivation and system setup

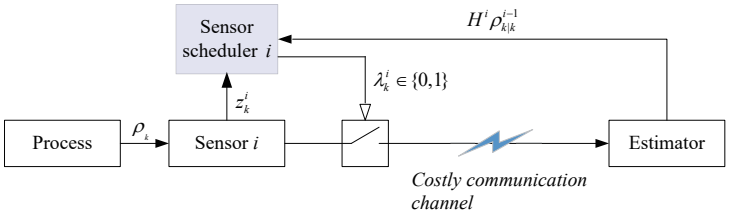


Figure 6.1: Remote estimation with an event-triggered sensor scheduler, shown for a single sensor $i$.

Consider a remote estimation problem with a central estimator and multiple remote sensors, and the communication topology for a single sensor is illustrated in Figure 6.1.

It is assumed that data transmission from the sensors to the estimator is costly, while broadcasting estimates from the estimator to the sensors is relatively cheap. The true state evolves as the time-varying system

$$\rho_{k+1} = A_k \rho_k + u_k + \omega_k, \quad \rho_k \in \mathbb{R}^n. \tag{6.1}$$

Let $S$ be the total number of sensors in the system. For $i \in \mathcal{S} = \{1, \cdots, S\}$, the sensor measurement $z_k^i$ from sensor $i$ at time step $k$ is modeled by

$$z_k^i = H^i \rho_k + v_k^i, \quad z_k^i \in \mathbb{R}^{m^i}, \tag{6.2}$$

where $H^i$ is the time-invariant[1] observation matrix of sensor $i$, and $v_k^i \sim \mathbf{N}(\mathbf{0}, R^i)$ is the white Gaussian measurement noise with covariance $R^i > \mathbf{0}$, and is independent of the model noise. The observation equation that models the measurements given by the entire sensor set reads

$$z_k = H \rho_k + v_k, \tag{6.3}$$

where the sensor data $z_k = \underset{s \in \mathcal{S}}{\text{col}} \left(z_k^s\right)$, the observation matrix $H = \underset{s \in \mathcal{S}}{\text{col}} \left(H^s\right)$, the sensor error $v_k = \left({v_k^1}^\top, \cdots, {v_k^S}^\top\right)^\top \sim \mathbf{N}(\mathbf{0}, R)$ with $R = \text{diag}\left(R^1, \cdots, R^S\right)$.

For $i \in \mathcal{S}$, denote as $\rho_{k|k}^i$ the state estimate of $\rho_k$ after the information from sensor $i$ at time $k$ (either the sensor measurement or the fact that data transmission did not occur) is processed by the estimator, and $\Gamma_{k|k}^i$ the error covariance associated with $\rho_{k|k}^i$. Denote as $\rho_{k|k-1}$ the state estimate of $\rho_k$ before any information obtained at time $k$ from the sensors is processed, and $\Gamma_{k|k-1}$ the error covariance of $\rho_{k|k-1}$. The scheduler at sensor $i$ makes a data transmission decision based on the normalized disparity between $H^i \rho_{k|k}^{i-1}$ (the predicted measurement of sensor $i$ given $\rho_{k|k}^{i-1}$) broadcast from the estimator and $y_k^i$ measured at sensor $i$. The disparity $y_k^i = z_k^i - H^i \rho_{k|k}^{i-1}$ is defined as the *innovation*. If $y_k^i$ (after being normalized) exceeds a given threshold, sensor data $z_k^i$ is transmitted to the central estimator through

[1]The time-invariance of the observation equation for each sensor is motivated by the practical concern that information transmission from the sensors to the estimator is expensive. When the observation equation is time-varying, even if sensor data $y_k^i$ is not sent, sensor $i$ still needs to send costly information on $H_k^i$ and $R_k^i$ to the estimator at each time step $k$ (so that the estimator can update the estimation error covariance), which conflicts with the original goal of sensor scheduling to reduce communication cost.

the costly communication channel. The decision variable $\lambda_k^i \in \{0,1\}$ indicates if $y_k^i$ is sent ($\lambda_k^i = 1$) or not sent ($\lambda_k^i = 0$). Sensor schedulers provide additional implicit information to the central estimator when no data is sent. The state-of-the-art filtering algorithms [80, 81, 82, 83] developed to solve the remote estimation problem illustrated in Figure 6.1 leverage this implicit information and compute the estimate according to the following framework:

**Framework 1.**

$$\textit{Time update:} \begin{cases} \textit{Update the state estimate } \rho^S_{k-1|k-1} \to \rho_{k|k-1} \\ \textit{Update the error covariance } \Gamma^S_{k-1|k-1} \to \Gamma_{k|k-1}, \end{cases} \tag{6.4}$$

$$\textit{Information update:} \begin{cases} \textit{Let } \rho^0_{k|k} = \rho_{k|k-1} \textit{ and } \Gamma^0_{k|k} = \Gamma_{k|k-1} \\ \textit{For } i = 1 \textit{ to } S \textit{ do} \\ \quad \textit{Sensor scheduler } i \textit{ computes sensor decision } \lambda_k^i \\ \quad \textit{If } \lambda_k^i = 1 \\ \quad\quad \textit{Update } \rho^{i-1}_{k|k} \to \rho^i_{k|k} \textit{ and } \Gamma^{i-1}_{k|k} \to \Gamma^i_{k|k} \\ \quad\quad \textit{via minimum mean square estimates} \\ \quad \textit{Else} \\ \quad\quad \textit{Set } \rho^i_{k|k} = \rho^{i-1}_{k|k} \\ \quad\quad \textit{Update the error covariance } \Gamma^{i-1}_{k|k} \to \Gamma^i_{k|k}. \end{cases} \tag{6.5}$$

In summary, at each time step $k$, the central estimator processes the information from each sensor sequentially (i.e., the measurements from multiple sensors are processed one sensor at a time within the same time step $k$). When a sensor indexed by $i$ sends measurement, the state estimates and the error covariance are both updated (i.e., update $\rho^{i-1}_{k|k} \to \rho^i_{k|k}$ and $\Gamma^{i-1}_{k|k} \to \Gamma^i_{k|k}$). On the other hand, if sensor $i$ does not send data, only the error covariance is updated (i.e., $\Gamma^{i-1}_{k|k} \to \Gamma^i_{k|k}$), with the precise update formula depending on the formula of the sensor scheduler. The state estimate, however, is not updated (i.e., $\rho^i_{k|k} = \rho^{i-1}_{k|k}$)[2].

[2]Note that with a slight abuse of notation, in the previous chapters $\rho^l_{k|k}$ denotes the $l^{\text{th}}$ entry of vector $\rho^l_{k|k}$. Later in this chapter, we use $x(l)$ to denote the $l^{\text{th}}$ entry of vector $x$.

### 6.2.1 Motivation for synthetic measurements

In [82, 83], the threshold applied in the sensor scheduler for each sensor is drawn (at the sensor's side) from the standard uniform distribution at each time step, and the value of the threshold is not known by the estimator. As a consequence, the Gaussian distribution of the estimation error is preserved, and the filtering algorithm proposed in [82, 83], termed the *Kalman filter with a stochastic threshold-based sensor scheduler* (KF-ST)[3], is an exact MMSE estimator. However, for the stochastic threshold, a potential issue occurs when the estimation error is already quite large, but the sensor scheduler still declines sending measurements since the threshold randomly drawn from the uniform distribution is also large. On the contrary, the filter proposed in [80, 81], termed the *Kalman filter with a deterministic threshold-based sensor scheduler* (KF-DT)[4], applies a deterministic threshold in each sensor scheduler (i.e., the applied threshold is fixed and known by the estimator). In this case, data transmission is guaranteed to be triggered when the normalized innovation (which also reflects the magnitude of the estimation error) exceeds a given threshold. However, this also implies that data transmission is sure to be stopped when the normalized innovation decreases to a given threshold, after which the estimation error cannot continue to decrease due to the fact that the state estimate is not corrected without data transmission. The above concerns on the KF-ST and KF-DT are illustrated in more detail in Example 3.

Moreover, in many applications, the sensors altogether measure only a subset of the state variables, thus the sensor schedulers may not serve as a sufficient indicator of the estimation accuracy. For example, consider a physical system tracked by a set of sensors which are distributed sparsely compared to the dimension of the state. Even though data transmission is not triggered, the estimate of the full state vector may still be inaccurate and needs to be corrected in the information update.

In order to further improve the estimation accuracy on the basis of the KF-ST and KF-DT, we propose a filtering algorithm which always corrects the state estimate in the information update, even without data transmission. Specifically, when data transmission

[3]When the filtering algorithm is first introduced in [82] for the single sensor case, it is named the KF under a closed-loop stochastic event-triggered scheduling rule (CLSET-KF). In the multiple sensor extension [83], the filter is referred to as the MMSE estimator under the incorporated sensor scheduler. In this chapter, the abbreviation "KF-ST" is introduced to simplify the name.

[4]The filter proposed in [80, 81] is referred to as an approximate MMSE under the incorporated sensor scheduler with a deterministic threshold, while the abbreviation "KF-DT" is introduced in this chapter to simplify the name.

is triggered, the state estimate is corrected by the true measurement in the information update. When $z_k^i$ is not sent, the state estimate is corrected via a synthetic measurement $\tilde{z}_k^i$ (generated based on the estimated distribution of the true measurement) as follows:

$$\rho_{k|k}^i = \rho_{k|k}^{i-1} + \tilde{K}_k^i \left( \tilde{z}_k^i - H^i \rho_{k|k}^{i-1} \right), \tag{6.6}$$

where $\tilde{K}_k^i$ is the synthetic gain associated with $\tilde{z}_k^i$. To ensure that data transmission is guaranteed to be triggered when the normalized innovation exceeds a given value (as opposed to the KF-ST), the proposed filter applies deterministic thresholds in the sensor schedulers. The deterministic threshold also ensures that the disparity between the synthetic and the true measurements is always within a bound set by the sensor scheduler. Given the synthetic measurements, the estimation error can continue to decrease even without data transmission. This addresses the concern of the KF-DT that the estimation error stops decreasing when the normalized innovation reaches a lower bound. As a consequence, the estimation error can reach values closer to zero compared to the KF-DT (see more detail in Example 3). In summary, the update framework of the proposed filter reads:

**Framework 2.**

*Time update: See* (6.4)

$$\textit{Information update:} \begin{cases} \textit{Let } \rho_{k|k}^0 = \rho_{k|k-1} \textit{ and } \Gamma_{k|k}^0 = \Gamma_{k|k-1} \\ \textit{For } i = 1 \textit{ to } S \textit{ do} \\ \quad \textit{Sensor scheduler } i \textit{ computes sensor decision } \lambda_k^i \\ \quad \textit{If } \lambda_k^i = 1 \\ \quad\quad \textit{Update } \rho_{k|k}^{i-1} \to \rho_{k|k}^i \textit{ and } \Gamma_{k|k}^{i-1} \to \Gamma_{k|k}^i \\ \quad\quad \textit{via minimum mean square estimates} \\ \quad \textit{Else} \\ \quad\quad \textit{Generate synthetic measurement } \tilde{z}_k^i \\ \quad\quad \textit{Update } \rho_{k|k}^{i-1} \to \rho_{k|k}^i \textit{ via } \tilde{z}_k^i \textit{ based on } (6.6) \\ \quad\quad \textit{Update the error covariance } \Gamma_{k|k}^{i-1} \to \Gamma_{k|k}^i, \end{cases} \tag{6.7}$$

To the best of our knowledge, this framework has not been studied in the existing literature. Although [95] also propose to compute $\rho_{k|k}^i$ according to (6.6) based on a virtual

measurement as a supplement to the true measurement when $\lambda_k^i = 0$, the proposed virtual measurement is deterministic and is set as $\tilde{z}_k^i = H^i \rho_{k|k}^{i-1}$. This implies that there is no difference between the virtual measurement and the predicted measurement given the latest estimate $\rho_{k|k}^{i-1}$, thus the resulting $\rho_{k|k}^i$ computed from (6.6) is exactly the same as $\rho_{k|k}^{i-1}$. Consequently, the estimator in [95] fits Framework 1.

## 6.3 Preliminaries

### 6.3.1 The sequential processing form of the Kalman filter

Denote as $\lambda_k = \left(\lambda_k^1, \cdots, \lambda_k^S\right)^\top$ the decision variables at time $k$, and let $\mathcal{T}_k = \{i | \lambda_k^i = 1, i \in \mathcal{S}\}$ be the set of sensors that transmit data at time $k$. Moreover, define the columnized sensor data $z_{\mathcal{T}_k} = \mathrm{col}_{i \in \mathcal{T}_k}\left(z_k^i\right)$. The information set containing the decision variables and sensor measurements up to time $k-1$ is denoted by $\mathcal{Z}_{k-1} = \{\lambda_0, \cdots, \lambda_{k-1}, z_{\mathcal{T}_0}, \cdots, z_{\mathcal{T}_{k-1}}\}$. Furthermore, define the information set obtained by the estimator at time $k$ based on data from the first $i$ sensors and all the past data as

$$\mathcal{Z}_k^i = \begin{cases} \mathcal{Z}_k^{i-1} \cup \{\lambda_k^i\} & \text{if } \lambda_k^i = 0, \\ \mathcal{Z}_k^{i-1} \cup \{\lambda_k^i, z_k^i\} & \text{if } \lambda_k^i = 1, \end{cases} \qquad \text{for } i \in \mathcal{S} \text{ with } \mathcal{Z}_k^0 = \mathcal{Z}_{k-1}, \text{ where } \mathcal{Z}_{-1} = \emptyset.$$

The central estimator computes the MMSE estimate of the state given the past information transmitted from the sensors. The *prior estimate* and *posterior estimate* of the state at time $k$ can be expressed as $\rho_{k|k-1} = \mathbb{E}[\rho_k | \mathcal{Z}_{k-1}]$ and $\rho_{k|k} = \mathbb{E}[\rho_k | \mathcal{Z}_k]$, respectively. When the estimator conducts sequential processing of the sensor data, the intermediate estimates are defined as $\rho_{k|k}^i = \mathbb{E}[\rho_k | \mathcal{Z}_k^i]$ for $i \in \mathcal{S}$, and the posterior estimate is then given by $\rho_{k|k} = \rho_{k|k}^S$. The estimation errors and the estimation error covariance matrices associated with the corresponding estimates defined above are given by

$$\begin{cases} \eta_{k|k-1} = \rho_{k|k-1} - \rho_k \\ \Gamma_{k|k-1} = \mathbb{E}\left[\left(\rho_{k|k-1} - \rho_k\right)\left(\rho_{k|k-1} - \rho_k\right)^\top \middle| \mathcal{Z}_{k-1}\right], \end{cases}$$

$$\begin{cases} \eta_{k|k}^i = \rho_{k|k}^i - \rho_k \\ \Gamma_{k|k}^i = \mathbb{E}\left[\left(\rho_{k|k}^i - \rho_k\right)\left(\rho_{k|k}^i - \rho_k\right)^\top \middle| \mathcal{Z}_k^i\right], \text{for } i \in \mathcal{S}, \end{cases}$$

$$\begin{cases} \eta_{k|k} = \rho_{k|k} - \rho_k \\ \Gamma_{k|k} = \mathbb{E}\left[ \left(\rho_{k|k} - \rho_k\right) \left(\rho_{k|k} - \rho_k\right)^\top \middle| \mathcal{Z}_k \right], \end{cases}$$

where the initial estimates on the state and the error covariance are given by $\rho_{0|-1}$ and $\Gamma_{0|-1}$, respectively.

Recall that when $\lambda_k^i = 1$ for all $i \in \mathcal{S}$ and $k \geq 0$, the standard KF is obtained. The reader is referred to [18] for the following form of the KF, which is equivalent to (3.1)-(3.2) and the estimate is updated sequentially (i.e., the measurements from multiple sensors are processed one sensor at a time within the same time step $k$) over the sensor data in the information update step:

$$\text{Time update: } \begin{cases} \rho_{k|k-1} = A_{k-1}\rho_{k-1|k-1} \\ \Gamma_{k|k-1} = A_{k-1}\Gamma_{k-1|k-1}A_{k-1}^\top + Q_{k-1} \end{cases} \tag{6.8}$$

$$\text{Information update: } \begin{cases} \text{Let } \rho_{k|k}^0 = \rho_{k|k-1}, \text{ and } \Gamma_{k|k}^0 = \Gamma_{k|k-1} \\ \text{For } i = 1 \text{ to } S \text{ do} \\ \quad \rho_{k|k}^i = \rho_{k|k}^{i-1} + K_k^i \left( z_k^i - H^i \rho_{k|k}^{i-1} \right) \\ \quad \Gamma_{k|k}^i = \Gamma_{k|k}^{i-1} - K_k^i H^i \Gamma_{k|k}^{i-1} \\ \quad \text{where } K_k^i = \Gamma_{k|k}^{i-1} {H^i}^\top \left( R^i + H^i \Gamma_{k|k}^{i-1} {H^i}^\top \right)^{-1} \\ \rho_{k|k} = \rho_{k|k}^S. \end{cases} \tag{6.9}$$

### 6.3.2 Kalman filter with a deterministic threshold-based sensor scheduler

In the deterministic threshold-based sensor scheduler proposed in [80, 81], the sensor decision is computed as a function of the innovation $y_k^i = z_k^i - H^i \rho_{k|k}^{i-1}$ as follows:

$$\lambda_k^i = \begin{cases} 0 & \text{if } \varphi_1(y_k^i) < \zeta^i \\ 1 & \text{if } \varphi_1(y_k^i) \geq \zeta^i, \end{cases} \tag{6.10}$$

where $\zeta^i$ is a pre-determined deterministic threshold, and the function $\varphi_1(y_k^i)$ is defined by the following equations:

$$\varphi_1(y_k^i) = \left\| D_k^i y_k^i \right\|_\infty = \left\| \varepsilon_k^i \right\|_\infty, \text{ where } D_k^i = \left( R^i + H^i \Gamma_{k|k}^{i-1} {H^i}^\top \right)^{-\frac{1}{2}}, \tag{6.11}$$

and $\varepsilon_k^i = D_k^i y_k^i$ is defined to be the normalized innovation. Hence, the sensor data $z_k^i$ can be expressed as

$$z_k^i = \left(D_k^i\right)^{-1} \varepsilon_k^i + H^i \rho_{k|k}^{i-1}. \tag{6.12}$$

The essence of a deterministic threshold-based sensor scheduler is that it assesses how much new information sensor data $z_k^i$ can provide to the estimator by comparing the normalized innovation with a deterministic threshold, thus determining if $z_k^i$ should be transmitted to the estimator.

Note that given the schedule policy (6.10) where $\zeta^i$ is deterministic and known by the estimator, it holds that the *probability density function* (PDF) satisfies $\mathrm{p}(z_k^i = z | \mathcal{Z}_k^{i-1}, \lambda_k^i = 0) = 0$ when $\varphi_1(z - H^i \rho_{k|k}^{i-1}) \geq \zeta^i$. This indicates that $\mathrm{p}(\rho_k | \mathcal{Z}_k^{i-1}, \lambda_k^i = 0)$ does not follow a Gaussian distribution since $z_k^i = H^i \rho_k + v_k^i$ as stated in (6.2). To avoid tracking a a general PDF, the following Gaussian approximation[5]

$$\mathrm{p}(\rho_k | \mathcal{Z}_k^{i-1}, \lambda_k^i = 0) \simeq \mathbf{N}(\rho_{k|k}^i, \Gamma_{k|k}^i), \quad \text{for } i \in \mathcal{S}$$

is widely used (see [80] and references therein). Equivalently, this approximation indicates

$$\mathrm{p}(\eta_{k|k}^i | \mathcal{Z}_k^{i-1}, \lambda_k^i = 0) \simeq \mathbf{N}(0, \Gamma_{k|k}^i), \quad \text{for } i \in \mathcal{S}. \tag{6.13}$$

It is shown in [80] that under approximation (6.13), the normalized innovation follows $\varepsilon_k^i \sim \mathbf{N}(\mathbf{0}, I_{m^i})$ before the sensor scheduler decides if $z_k^i$ is transmitted to the estimator, where $I_{m^i}$ is the identity matrix with dimension $m^i$. When the sensor scheduler decides not to send sensor data $z_k^i$, even though the measurement is not received, the estimator obtains additional information that $\|\varepsilon_k^i\|_\infty < \zeta^i$, and the distribution of $\varepsilon_k^i$ is updated from a normal distribution to a truncated normal distribution:

$$\mathrm{p}\left(\varepsilon_k^i = \varepsilon \,\middle|\, \|\varepsilon_k^i\|_\infty < \zeta^i\right) = \begin{cases} \frac{1}{\Pr(\|\xi\|_\infty < \zeta^i)} \mathrm{p}(\xi = \varepsilon) & \text{if } \|\varepsilon\|_\infty < \zeta^i \\ 0 & \text{otherwise,} \end{cases} \tag{6.14}$$

where $\xi \sim \mathbf{N}(\mathbf{0}, I_{m^i})$ and $\Pr(E)$ is defined as the probability of event $E$. In [80] and [81],

[5]The error covariance $\Gamma_{k|k}^i$ in (6.13) is computed given the fact that $\lambda_k^i = 0$, with explicit formula given in (6.15).

the Kalman filter with a deterministic threshold-based sensor scheduler is derived based on the updated distribution (6.14), and is shown to be an approximate MMSE estimator, with the update equations given in the following definition.

**Definition 3.** *The Kalman filter with a deterministic threshold-based sensor scheduler (KF-DT) applies sensor scheduler* (6.10)-(6.11)*, with update equations*

$$
\begin{aligned}
&\textit{Time update: See } (6.8),\\
&\textit{Information update:} \begin{cases}
\textit{Let } \rho^0_{k|k} = \rho_{k|k-1}, \textit{ and } \Gamma^0_{k|k} = \Gamma_{k|k-1}\\
\textit{For } i = 1 \textit{ to } S \textit{ do}\\
\quad \textit{Sensor scheduler } i \textit{ computes } \lambda^i_k \textit{ based on } (6.10)\\
\quad \textit{If } \lambda^i_k = 1\\
\qquad \textit{Compute } \rho^i_{k|k} \textit{ and } \Gamma^i_{k|k} \textit{ according to } (6.9)\\
\quad \textit{Else}\\
\qquad \rho^i_{k|k} = \rho^{i-1}_{k|k}\\
\qquad \Gamma^i_{k|k} = \Gamma^{i-1}_{k|k} - K^i_k H^i \Gamma^{i-1}_{k|k}\\
\qquad \textit{where } K^i_k = \mathrm{x}\left(\zeta^i\right) \Gamma^{i-1}_{k|k} {H^i}^\top \left(R^i + H^i \Gamma^{i-1}_{k|k} {H^i}^\top\right)^{-1}\\
\rho_{k|k} = \rho^S_{k|k},
\end{cases}
\end{aligned}
\tag{6.15}
$$

*where* $0 < \mathrm{x}(\zeta) < 1$ *is given by*

$$
\mathrm{x}(\zeta) = \sqrt{\frac{2}{\pi}} \zeta \exp\left(-\frac{\zeta^2}{2}\right) \left(1 - 2\mathrm{x}_0\left(\zeta\right)\right)^{-1}, \tag{6.16}
$$

*and* $\mathrm{x}_0(\zeta) = \int_\zeta^\infty \frac{1}{\sqrt{2\pi}} \exp\left(-\frac{t^2}{2}\right) dt$.

### 6.3.3 Kalman filter with a stochastic threshold-based sensor scheduler

In order to make the Gaussian property stated in (6.13) hold exactly, the estimator must be unaware of the thresholds applied by the sensors to compute the decision variables $\lambda^i_k$. A stochastic threshold-based sensor scheduler is proposed in [82], where for all $i$ and $k$ the threshold $\zeta^i_k$ is a random variable drawn independently from a uniform distribution over

$[0,1]$, and $\lambda_k^i$ is computed by

$$\lambda_k^i = \begin{cases} 0 & \text{if } \varphi_2(y_k^i) \geq \zeta_k^i \\ 1 & \text{if } \varphi_2(y_k^i) < \zeta_k^i, \end{cases} \tag{6.17}$$

where the function $\varphi_2(y_k^i)$ is defined as

$$\varphi_2(y_k^i) = \exp\left(-\frac{1}{2}\left(y_k^i\right)^\top Y^i y_k^i\right), \tag{6.18}$$

and $Y_k^i > \mathbf{0}$ is a matrix to adjust data transmission rate. Under scheduler (6.17)-(6.18), the Gaussian condition in (6.13) is preserved, leading to an exact MMSE estimator defined as follows [82, 83].

**Definition 4.** *The Kalman filter with a stochastic threshold-based sensor scheduler (KF-ST) applies sensor scheduler* (6.17)-(6.18)*, with update schemes*

*Time update: See* (6.8)*,*

$$\textit{Information update:} \begin{cases} \textit{Let } \rho_{k|k}^0 = \rho_{k|k-1}, \textit{ and } \Gamma_{k|k}^0 = \Gamma_{k|k-1} \\ \textit{For } i = 1 \textit{ to } S \textit{ do} \\ \quad \textit{Sensor scheduler } i \textit{ computes } \lambda_k^i \textit{ based on } (6.17) \\ \quad \textit{If } \lambda_k^i = 1 \\ \quad\quad \textit{Compute } \rho_{k|k}^i \textit{ and } \Gamma_{k|k}^i \textit{ according to } (6.9) \\ \quad \textit{Else} \\ \quad\quad \rho_{k|k}^i = \rho_{k|k}^{i-1} \\ \quad\quad \Gamma_{k|k}^i = \Gamma_{k|k}^{i-1} - K_k^i H^i \Gamma_{k|k}^{i-1} \\ \quad\quad \textit{where } K_k^i = \Gamma_{k|k}^{i-1} {H^i}^\top \left(\left(Y^i\right)^{-1} + R^i + H^i \Gamma_{k|k}^{i-1} {H^i}^\top\right)^{-1} \\ \rho_{k|k} = \rho_{k|k}^S. \end{cases} \tag{6.19}$$

## 6.4 Kalman filter with synthetic measurements

For the KF-DT and KF-ST, state estimate $\rho_{k|k}^i$ is not corrected in the information update when $\lambda_k^i = 0$. In this section, we propose a filtering algorithm that corrects both the

state estimate and the estimation error covariance in the information update when data transmission does not occur. Although the sensor scheduler (6.17)-(6.18) in the KF-ST allows for the analytical form of an exact MMSE estimator, when data transmission is not triggered, the estimator has very limited knowledge on the estimation error since the threshold in the sensor scheduler is stochastic and not known by the estimator. Hence, we apply scheduler (6.10)-(6.11), which enables the estimator to draw synthetic measurements whose distance from the true measurements is guaranteed to be upper bounded by a function of the deterministic threshold $\zeta^i$. Moreover, under a fixed threshold, data transmission is guaranteed to be triggered when the normalized innovation exceeds a fixed value.

When sensor data $z_k^i$ is not sent, the KF-SM updates the state estimate by (6.6), where the synthetic measurement $\tilde{z}_k^i$ is consistent with $\lambda_k^i = 0$ (i.e., the sensor scheduler would not trigger data transmission if the true measurement is $\tilde{z}_k^i$). The same Gaussian assumption (6.13) is made for the KF-SM. Based on this assumption, the normalized innovation $\varepsilon_k^i$ follows distribution (6.14) when $\lambda_k^i = 0$. In the synthetic generation procedure presented in Algorithm 1, we first draw a synthetic normalized innovation $\tilde{\varepsilon}_k^i$ from distribution (6.14), as shown in Steps 1-7 of Algorithm 1. Next, the synthetic measurement $\tilde{z}_k^i$ is computed based on the relationship between the sensor measurement and normalized innovation given in (6.12), i.e.,

$$\tilde{z}_k^i = \left(D_k^i\right)^{-1} \tilde{\varepsilon}_k^i + H^i \rho_{k|k}^{i-1},$$

which is completed in Steps 8-9 of Algorithm 1.

**Algorithm 1** Synthetic Measurement Generation

**Input:** threshold $\zeta^i$ in (6.10), matrix $D_k^i$ defined in (6.11), vector $H^i \rho_{k|k}^{i-1}$
**Output:** synthetic measurement $\tilde{z}_k^i$
1. **for** $l = 1, \cdots, m^i$ **do**
2. Draw $\tilde{\varepsilon}_k^i(l)$ from $\mathbf{N}(0,1)$
3. **while** $|\tilde{\varepsilon}_k^i(l)| \geq \zeta^i$ **do**
4. Redraw $\tilde{\varepsilon}_k^i(l)$ from $\mathbf{N}(0,1)$
5. **end while**
6. **end for**
7. Construct the synthetic normalized innovation as $\tilde{\varepsilon}_k^i = \left(\tilde{\varepsilon}_k^i(1), \cdots, \tilde{\varepsilon}_k^i(m_i)\right)^\top$
8. Compute the synthetic innovation $\tilde{y}_k^i = \left(D_k^i\right)^{-1} \tilde{\varepsilon}_k^i$
9. **return** synthetic measurement $\tilde{z}_k^i = \tilde{y}_k^i + H^i \rho_{k|k}^{i-1}$

One may note that $\tilde{\varepsilon}_k^i$ and $\tilde{y}_k^i$ in Algorithm 1 are zero mean, which ensures that the KF-SM is unbiased. Let

$$\tilde{\delta}_k^i = \tilde{z}_k^i - z_k^i \tag{6.20}$$

be the disparity between the synthetic measurement and the true measurement. Algorithm 1 ensures that $\|\tilde{\varepsilon}_k^i\|_\infty < \zeta^i$, and consequently the disparity satisfies $\left\|\tilde{\delta}_k^i\right\| < 2\zeta^i \left\|D_k^i\right\|^{-1} (m^i)^{\frac{1}{2}}$. Before defining the KF-SM, the next lemma expresses the covariance of $\tilde{\varepsilon}_k^i$ as a function of $\zeta^i$ when $\tilde{\varepsilon}_k^i$ is drawn according to Algorithm 1, which is necessary to compute the error covariance of the KF-SM analytically.

**Lemma 9** (Lemma A.1 in [80])**.** *The synthetic normalized innovation $\tilde{\varepsilon}_k^i$ in Algorithm 1 satisfies $\mathbb{E}\left[\tilde{\varepsilon}_k^i\right] = \mathbf{0}$, and $Cov\left(\tilde{\varepsilon}_k^i\right) = \mathbb{E}\left[\tilde{\varepsilon}_k^i \left(\tilde{\varepsilon}_k^i\right)^\top\right] = \left(1 - \mathrm{x}\left(\zeta^i\right)\right) I_{m^i}$, with $\mathrm{x}\left(\zeta^i\right)$ defined in* (6.16)*.*

The KF-SM is defined below.

**Definition 5.** *The Kalman filter with synthetic measurements (KF-SM) applies a deterministic sensor scheduler shown in* (6.10)-(6.11)*, with update equations given as follows:*

*Time update:* *See* (6.8)*,*

$$\textit{Information update:} \begin{cases} \textit{Let } \rho_{k|k}^0 = \rho_{k|k-1}, \textit{ and } \Gamma_{k|k}^0 = \Gamma_{k|k-1} \\ \textit{For } i = 1 \textit{ to } S \textit{ do} \\ \quad \textit{Sensor scheduler } i \textit{ computes } \lambda_k^i \textit{ based on } (6.10) \\ \quad \textit{If } \lambda_k^i = 1 \\ \quad\quad \textit{Compute } \rho_{k|k}^i \textit{ and } \Gamma_{k|k}^i \textit{ according to } (6.9) \\ \quad \textit{Else} \\ \quad\quad \textit{Generate } \tilde{z}_k^i \textit{ according to Algorithm 1} \\ \quad\quad \rho_{k|k}^i = \rho_{k|k}^{i-1} + \tilde{K}_k^i \left(\tilde{z}_k^i - H^i \rho_{k|k}^{i-1}\right) \\ \quad\quad \Gamma_{k|k}^i = \Gamma_{k|k}^{i-1} - K_k^i H^i \Gamma_{k|k}^{i-1} \\ \quad\quad\quad\quad + \tilde{K}_k^i \left(D_k^i\right)^{-1} Cov\left(\tilde{\varepsilon}_k^i\right) \left(D_k^i\right)^{-1} \left(\tilde{K}_k^i\right)^\top \\ \quad\quad\quad \textit{where } K_k^i = \mathrm{x}\left(\zeta^i\right) \Gamma_{k|k}^{i-1} {H^i}^\top \left(R^i + H^i \Gamma_{k|k}^{i-1} {H^i}^\top\right)^{-1} \\ \rho_{k|k} = \rho_{k|k}^S, \end{cases} \tag{6.21}$$

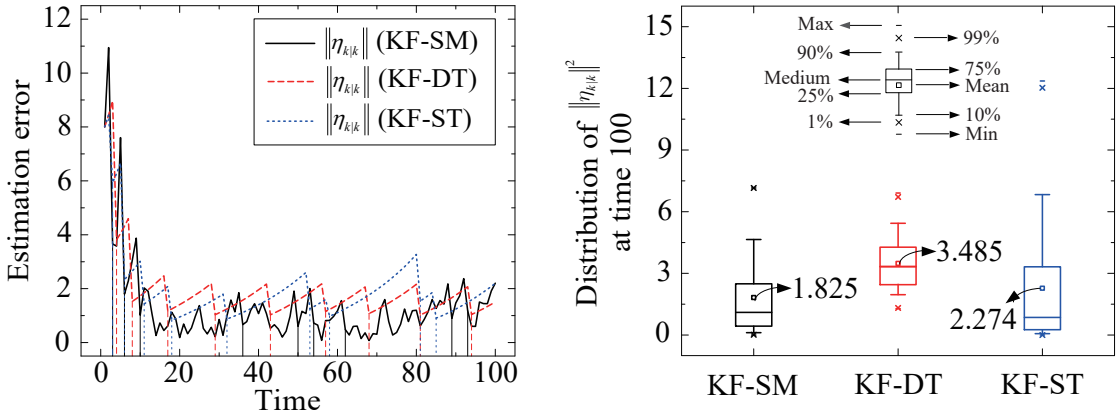


(a) Estimation error for a single run

(b) Distribution of estimation error

Figure 6.2: Performance of the KF-SM, KF-DT and KF-ST in Example 3. (a) The 2-norm of the estimation error given by the KF-SM, KF-DT and KF-ST for a single realization, where the vertical lines indicate the time steps when the sensor data is sent (with solid, dashed and dotted vertical lines representing the KF-SM, KF-DT, and KF-ST, respectively); (b) The distribution of $\left\|\eta_{k|k}\right\|^2$ for the KF-SM, KF-DT and KF-DT at time step $k = 100$.

*where* $\mathrm{x}(\cdot)$ *is given in* (6.16), $Cov\left(\tilde{\varepsilon}_k^i\right) = \left(1 - \mathrm{x}\left(\zeta^i\right)\right) I_{m^i}$ *according to Lemma 9, and the gain* $\tilde{K}_k^i$ *associated with synthetic measurement* $\tilde{z}_k^i$ *is set to be* $\tilde{K}_k^i = K_k^i$.

In the KF-SM, when $\lambda_k^i = 0$, the state estimate is updated using $\tilde{z}_k^i$. On the right hand side of the error covariance update equation, the second term is the reduction of the error covariance computed based on the fact that the normalized innovation is below the deterministic threshold required for data transmission, and the third term is the inflation of the error covariance due to the randomness generated from the synthetic measurements. Later, we show this extra term characterizing the inflation is at most one fourth of the error covariance reduction given in the second term.

**Remark 7.** *For the KF-SM, the choice* $\tilde{K}_k^i = K_k^i$ *is made to ensure that the correction of the state estimate based on the synthetic measurement is sufficiently large, while satisfying the following two conditions (detailed in Section 6.5.1 and Section 6.5.2): (i) the extra term in the error covariance update equation introduced by the synthetic measurements is controlled under a small upper bound; (ii) the error dynamics of the KF-SM is stabilized.*

Before analyzing the performance of the filter, we briefly provide Example 3 to highlight the intuition behind the effect of the KF-SM on improving the estimation accuracy com-

pared to the KF-ST and KF-DT. It also illustrates the concerns on the performance of the KF-ST and KF-DT (as stated in Section 6.2.1) that motivates the KF-SM.

**Example 3.** *Consider the KF-SM, KF-DT and KF-ST applied to track a linear system where for all* $k \geq 0$

$$A_k = \begin{pmatrix} 1.05 & 0 \\ 0.1 & 0.9 \end{pmatrix}, \quad Q_k = \begin{pmatrix} 0.01 & 0 \\ 0 & 1 \end{pmatrix}, \tag{6.22}$$
$$H = \begin{pmatrix} 0 & 1 \end{pmatrix}, \quad R = 0.01.$$

*The sensor-to-estimator communication rate is defined by:*

$$r_{\mathrm{c}} = \frac{1}{k_{\max}|\mathcal{S}|} \sum_{k=1}^{k_{\max}} \sum_{i \in \mathcal{S}} \lambda_k^i, \tag{6.23}$$

*where* $k_{\max}$ *is the total number of time steps. For all the three filters, the communication rate* $r_c$ *is set to be 0.09, where the total number of time steps* $k_{\max} = 100$*.*

*Figure 6.2a illustrates the evolution of the estimation error given by the three filters for a single realization. Since the stochastic threshold is randomly drawn in the sensor scheduler, at step 80, the estimation error is already quite large, but the sensor scheduler still declines sending the measurement. Hence, the estimation error of the KF-ST exceeds* $\left\|\eta_{k|k}\right\| = 3$ *at step 80, which is a value that cannot be reached by the estimation error of the other two filters after around step 20. For the KF-DT and the KF-SM, data transmission is guaranteed to be triggered when the normalized innovation exceeds the fixed threshold, hence (after around step 20) the estimation error is guaranteed to start decreasing once its 2-norm exceeds a fixed value around* $\left\|\eta_{k|k}\right\| = 2$*. However, since data transmission is sure to be declined when the normalized innovation is below the fixed threshold and the state estimate of the KF-DT is not corrected without data transmission, the 2-norm of the estimation error given by the KF-DT also cannot reach a smaller value than* $\left\|\eta_{k|k}\right\| = 1$*. On the other hand, the synthetic measurements can drive the estimation error of the KF-SM closer to zero compared to the KF-DT.*

*Figure 6.2b shows the distribution (across 100 realizations) of* $\left\|\eta_{k|k}\right\|^2$ *given by the three filters at time* $k = 100$*. Here, the small square in each box shows the sample mean square error (with its value labeled in Figure 6.2b) of each filter. Compared to the KF-DT, although*

*the error distribution of the KF-SM has larger spread due to the randomness of the synthetic measurements, there are more realizations close to zero. Moreover, the maximum values of the magnitude of the estimation error given by the KF-SM and KF-DT are close. Due to the stochastic threshold, the estimation error of the KF-ST reaches larger magnitude, and has larger spread compared to the other two filters. Consequently, the KF-SM outperforms the KF-DT and KF-ST in terms of estimation accuracy for this system.*

## 6.5 Performance analysis of the KF-SM

### 6.5.1 Approximate MMSE estimator

Under Gaussian approximation (6.13), it is indicated that to minimize the trace of the error covariance, a necessary condition is $\tilde{K}_k^i = \mathbf{0}$ (if $\tilde{K}_k^i$ is a decision variable). However, the synthetic measurement does not help correct the state estimate if $\tilde{K}_k^i = \mathbf{0}$. Hence, as shown in the next proposition, the error covariance with the minimum trace is derived under the condition that $\tilde{K}_k^i$ is assumed to be given first (i.e., the gain $\tilde{K}_k^i$ is not treated as a variable to be optimized to obtain the MMSE estimator).

**Proposition 10** (Optimality of the KF-SM)**.** *Under the Gaussian approximation shown in* (6.13)*, the KF-SM given in Definition 5 is a MMSE estimator for any choice of* $\tilde{K}_k^i$*.*

*Proof.* When $\lambda_k^i = 1$, the information update of the KF-SM is the same as the standard KF, which is a MMSE estimator. Hence, we prove for the case when $\lambda_k^i = 0$.

The update of the state estimate given the synthetic measurement $\tilde{z}_k^i$ reads:

$$\rho_{k|k}^i = \rho_{k|k}^{i-1} + \tilde{K}_k^i \left( \tilde{z}_k^i - H^i \rho_{k|k}^{i-1} \right) = \rho_{k|k}^{i-1} + \tilde{K}_k^i \left( D_k^i \right)^{-1} \tilde{\varepsilon}_k^i.$$

Hence the estimation error and the error covariance of the KF-SM reads

$$\begin{aligned}
\eta_{k|k}^i &= \rho_{k|k}^i - \rho_k = \rho_{k|k}^{i-1} - \rho_k + \tilde{K}_k^i \left( D_k^i \right)^{-1} \tilde{\varepsilon}_k^i, \\
\Gamma_{k|k}^i &= \mathbb{E}\left[ \left( \rho_{k|k}^{i-1} - \rho_k \right) \left( \rho_{k|k}^{i-1} - \rho_k \right)^\top \left| \mathcal{Z}_k^{i-1}, \lambda_k^i = 0 \right. \right] \\
&\qquad + \mathbb{E}\left[ \left( \tilde{K}_k^i \left( D_k^i \right)^{-1} \tilde{\varepsilon}_k^i \right) \left( \tilde{K}_k^i \left( D_k^i \right)^{-1} \tilde{\varepsilon}_k^i \right)^\top \left| \mathcal{Z}_k^{i-1}, \lambda_k^i = 0 \right. \right],
\end{aligned}$$

where the second equation is due to the fact that $\tilde{\varepsilon}_k^i$ is drawn independently of $\rho_k$, and the fact that $\mathbb{E}\left[\rho_{k|k}^{i-1} - \rho_k \left| \mathcal{Z}_k^{i-1}, \lambda_k^i = 0 \right.\right] = \mathbf{0}$. Also note that since $D_k^i$ is deterministic given $\mathcal{Z}_k^{i-1}$ and $\lambda_k^i = 0$, the error covariance can be further simplified to

$$\begin{aligned}\Gamma_{k|k}^i = \mathbb{E}\left[\left(\rho_{k|k}^{i-1} - \rho_k\right)\left(\rho_{k|k}^{i-1} - \rho_k\right)^\top \left| \mathcal{Z}_k^{i-1}, \lambda_k^i = 0 \right.\right] \\ + \tilde{K}_k^i \left(D_k^i\right)^{-1} \mathrm{Cov}\left(\tilde{\varepsilon}_k^i\right) \left(D_k^i\right)^{-1} \left(\tilde{K}_k^i\right)^\top.\end{aligned} \tag{6.24}$$

Notice that the second term in (6.24) is fixed conditioned on $\mathcal{Z}_k^{i-1}$, $\lambda_k^i = 0$, $\tilde{K}_k^i$, and any synthetic measurement generation algorithm generating $\tilde{\varepsilon}_k^i$. Hence, minimizing the error covariance of the KF-SM is equivalent to minimizing the first term in (6.24). According to [80, 81], under Gaussian assumption (6.13), minimizing the first term in (6.24) yields the error covariance update in the analysis step of the KF-DT (6.15). This error covariance update in the KF-DT coincides with the first two terms of the error covariance update equation of the KF-SM in (6.21). Also note that the third term of the error covariance update equation of the KF-SM in (6.21) is the same as the second term in (6.24). Hence, under the Gaussian approximation (6.13), the KF-SM is a MMSE estimator for any choice[6] of $\tilde{K}_k^i$. □

For the remainder of this subsection, we analyze the upper bound of the third term in the error covariance update equation in (6.21), and show that this extra term is very small and will not affect the boundedness of the error covariance given by the KF-SM.

#### 6.5.1.1 Extra term of the error covariance due to synthetic measurements

When $\lambda_k^i = 0$, recall that the gain associated with the synthetic measurement is chosen to be $\tilde{K}_k^i = K_k^i$, and $\mathrm{Cov}\left(\tilde{\varepsilon}_k^i\right) = \left(1 - \mathrm{x}\left(\zeta^i\right)\right) I_{m^i}$. Hence, the error covariance update equation of the KF-SM in (6.21) can be rewritten as

$$\Gamma_{k|k}^i \leq \Gamma_{k|k}^{i-1} - K_k^i H^i \Gamma_{k|k}^{i-1} + \mathrm{x}\left(\zeta^i\right)\left(1 - \mathrm{x}\left(\zeta^i\right)\right) K_k^i H^i \Gamma_{k|k}^{i-1}, \tag{6.25}$$

[6] When $\tilde{K}_k^i = \mathbf{0}$, the KF-SM is equivalent to the KF-DT.

where $\mathrm{x}\left(\zeta^i\right)\left(1-\mathrm{x}\left(\zeta^i\right)\right) \leq 0.25$ since $\mathrm{x}\left(\zeta^i\right)$ is between 0 and 1. In summary, when $\lambda_k^i = 0$, the error covariance of the KF-SM satisfies

$$\Gamma_{k|k}^i \leq \Gamma_{k|k}^{i-1} - K_k^i H^i \Gamma_{k|k}^{i-1} + 0.25 K_k^i H^i \Gamma_{k|k}^{i-1},$$

after incorporating the randomness originating from the synthetic measurement. This indicates that the increase of the error covariance caused by the synthetic measurement is at most one fourth of the reduction of the error covariance given the fact that the normalized innovation is below the threshold required for data transmission.

#### 6.5.1.2 Boundedness of the error covariance given by the KF-SM

In the next lemma, the boundedness of the error covariance of the KF-SM is shown by extending the stability result for the KF-DT discussed in Proposition 2 in [81].

**Lemma 10.** *Consider the KF-SM tracking a target described by* (6.1)*, where the dynamical system constructed by* (6.1) *and* (6.3) *is uniformly completely observable and uniformly completely controllable*[7] *. Under Gaussian approximation* (6.13)*, there exists a critical threshold* $\zeta^c$ *such that if* $\zeta^i < \zeta^c$ *for all* $i$*, the error covariance satisfies* $\sup_k \mathbb{E}\left[\Gamma_{k|k}\right] < \infty$ *for all* $\Gamma_{0|-1} \geq \mathbf{0}$*.*

*Proof.* Based on (6.25) and recall that when $\lambda_k^i = 0$ it holds that

$$K_k^i = \mathrm{x}\left(\zeta^i\right) \Gamma_{k|k}^{i-1} {H^i}^\top (R^i + H^i \Gamma_{k|k}^{i-1} {H^i}^\top)^{-1},$$

the error covariance of the KF-SM satisfies

$$\Gamma_{k|k}^i \leq \Gamma_{k|k}^{i-1} - \mathrm{g}(\lambda_k^i, \zeta^i) \Gamma_{k|k}^{i-1} {H^i}^\top (R^i + H^i \Gamma_{k|k}^{i-1} {H^i}^\top)^{-1} H^i \Gamma_{k|k}^{i-1},$$

where

$$\mathrm{g}(\lambda_k^i, \zeta^i) = \lambda_k^i + \left(1-\lambda_k^i\right) \mathrm{x}\left(\zeta^i\right)\left(1-\mathrm{x}\left(\zeta^i\right)\left(1-\mathrm{x}\left(\zeta^i\right)\right)\right).$$

[7] The dynamical system constructed by (6.1) and (6.3) is uniformly completely controllable if there exists a positive integer $T$ and positive constants $\alpha$ and $\beta$ such that $\alpha I_n < \mathcal{C}_{k,k-T} < \beta I_n$ for all $k \geq T$. The matrix $\mathcal{C}_{\underline{k},\bar{k}}$ is the controllability matrix for time interval $k \in [\underline{k}, \bar{k}]$ defined as $\mathcal{I}_{\underline{k},\bar{k}} = \sum_{k=\underline{k}}^{\bar{k}} \Xi_{\bar{k},k} Q_k \Xi_{\bar{k},k}^\top$, with $\Xi_{\bar{k},k}$ defined in (2.5). The uniform complete observability is defined in Definition 1

Taking the derivative of $\mathrm{g}(\lambda_k^i, \zeta^i)$ with respect to $\zeta^i$, we obtain that $\mathrm{g}(\lambda_k^i, \zeta^i)$ is a decreasing function in $\zeta^i$. The remainder of the proof follows from Proposition 2 in [81], which combines the i.i.d. property of $\mathrm{g}(\lambda_k^i, \zeta^i)$ with Theorem 2 in [96] to show the boundedness of the error covariance. □

Motivated by Lemma 10, for the remainder of this chapter we analyze the performance of the KF-SM under the following assumptions:

(Asm.14): the dynamical system constructed by (6.1) and (6.3) is uniformly completely observable and uniformly completely controllable (this assumption is also very important when proving the ISS of the KF-SM in Proposition 11, as stated in the paragraph following the proof of Proposition 11);

(Asm.15): the threshold $\zeta^i$ is small enough for all $i$ to secure the boundedness of the error covariance.

### 6.5.2 Input-to-state stability of the KF-SM

This subsection shows that the estimation error dynamics of the KF-SM is *input-to-state stable* (ISS), if we treat the error of the synthetic measurements (with respect to the true measurements) as an input to the estimation error dynamics. Because the KF-SM is ISS, the estimation error of the KF-SM is guaranteed to be bounded if the disparity between the synthetic measurements and the true measurements is bounded.

When $\lambda_k^i = 0$, the estimate $\rho_{k|k}^i$ and the estimation error $\eta_{k|k}^i$ after processing the $i^{\text{th}}$ information update step reads

$$\begin{aligned}
\rho_{k|k}^i &= \rho_{k|k}^{i-1} + \tilde{K}_k^i \left( z_k^i - H^i \rho_{k|k}^{i-1} \right) + \tilde{K}_k^i \left( \tilde{z}_k^i - z_k^i \right), \\
\eta_{k|k}^i &= \left( I - \tilde{K}_k^i H^i \right) \eta_{k|k}^{i-1} + \tilde{K}_k^i \tilde{\delta}_k^i + \tilde{K}_k^i v_k^i.
\end{aligned}$$

Recall that in the KF-SM the synthetic gain is chosen as $\tilde{K}_k^i = K_k^i$ when $\lambda_k^i = 0$. Combining the above equation with time update (6.8) and the $S$ iteration steps stated in (6.21), the

error dynamics of $\eta_{k|k}$ is written as

$$\begin{aligned}\eta_{k|k} = &\prod_{i=0}^{S-1}\left(I - K_k^{S-i}H^{S-i}\right)A_{k-1}\eta_{k-1|k-1}\\ &+\sum_{i\in\mathcal{T}_k^c}\prod_{l=0}^{S-i-1}\left(I - K_k^{S-l}H^{S-l}\right)K_k^i\tilde{\delta}_k^i\\ &+\sum_{i=1}^{S}\prod_{l=0}^{S-i-1}\left(I - K_k^{S-l}H^{S-l}\right)K_k^i v_k^i\\ &-\omega_{k-1}\end{aligned} \tag{6.26}$$

where $\mathcal{T}_k^c$ is the complement of $\mathcal{T}_k$ (i.e., $\mathcal{T}_k^c$ is the set of sensors that do not transmit measurements at time $k$). Note that the perturbations from the model and measurement noise (i.e., the last two terms in the right hand side of (6.26)) will not destabilize the error dynamics (6.26). Hence for the remainder of this work, we study the following unperturbed error dynamics given by the KF-SM:

$$\begin{aligned}\eta_{k|k} = &\prod_{i=0}^{S-1}\left(I - K_k^{S-i}H^{S-i}\right)A_{k-1}\eta_{k-1|k-1}\\ &+\sum_{i\in\mathcal{T}_k^c}\prod_{l=0}^{S-i-1}\left(I - K_k^{S-l}H^{S-l}\right)K_k^i\tilde{\delta}_k^i,\end{aligned} \tag{6.27}$$

where the second term in the right hand side can potentially destabilize the system. Consequently, it is treated as an input to the error dynamics (6.27) rather than perturbation.

**Remark 8.** *Note that the evolution of the estimation error* (6.27) *depends on the set of sensors that send measurements, which is in turn correlated with the estimation error. To address the correlation, equation* (6.27) *is treated as the evolution equation of the estimation error conditioned on* $\mathcal{T}_k^c$*. Hence, if error dynamics* (6.27) *is shown to be input-to-state stable under all* $\mathcal{T}_k^c$*, its ISS property is obtained.*

**Proposition 11** (ISS of the KF-SM)**.** *Consider the KF-SM tracking a target described by* (6.1)*. The estimation error dynamics* (6.27) *of the KF-SM is input-to-state stable, where the second term on the right hand side of* (6.27) *is treated as an input to the error dynamics.*

*Proof.* For all $\mathcal{T}_k^c$, the unforced system of (6.27) (i.e., system (6.27) after setting $\tilde{\delta}_k^i = 0$ for all $i$ and $k$) is given by

$$\eta_{k|k} = \prod_{i=0}^{S-1}\left(I - K_k^{S-i}H^{S-i}\right)A_{k-1}\eta_{k-1|k-1}. \tag{6.28}$$

We need to show that the unforced system (6.28) is *globally exponentially stable* (GES).

Due to Lemma 4.6 in [89], the global exponential stability of the unforced system (6.28) is a sufficient condition of the ISS of system (6.27).

Due to Lemma 2(i) in [53], it holds that

$$I - K_k^i H^i = \hat{\Gamma}_{k|k}^i \left(\Gamma_{k|k}^{i-1}\right)^{-1}, \tag{6.29}$$

where

$$\hat{\Gamma}_{k|k}^i = \Gamma_{k|k}^{i-1} - K_k^i H^i \Gamma_{k|k}^{i-1}.$$

Given the information update (6.21) of the KF-SM, the matrix $\hat{\Gamma}_{k|k}^i$ can also be written as

$$\hat{\Gamma}_{k|k}^i = \Gamma_{k|k}^i - X_k^i, \tag{6.30}$$

with $X_k^i \geq 0$ defined as

$$X_k^i = \begin{cases} K_k^i \left(D_k^i\right)^{-1} \mathrm{Cov}\left(\tilde{\varepsilon}_k^i\right) \left(D_k^i\right)^{-1} \left(K_k^i\right)^\top & \text{if } \lambda_k^i = 0 \\ \mathbf{0} & \text{if } \lambda_k^i = 1. \end{cases}$$

Construct $\hat{K}_k^i$ such that

$$\hat{K}_k^i = \Gamma_{k|k}^{i-1} {H^i}^\top \left(\hat{R}_k^i + H^i \Gamma_{k|k}^{i-1} {H^i}^\top\right)^{-1},$$

with $\hat{R}_k^i$ defined by

$$\hat{R}_k^i = \begin{cases} \frac{1}{\mathrm{x}(\zeta^i)} R^i + \left(\frac{1}{\mathrm{x}(\zeta^i)} - 1\right) H^i \Gamma_{k|k}^{i-1} {H^i}^\top & \text{if } \lambda_k^i = 0 \\ R^i & \text{if } \lambda_k^i = 1. \end{cases}$$

Hence $\hat{K}_k^i = K_k^i$ for all $i$, and $\hat{\Gamma}_{k|k}^i$ can be considered as the estimation error covariance of the state estimate given by

$$\hat{\rho}_{k|k}^i = \rho_{k|k}^{i-1} + \hat{K}_k^i \left(\hat{z}_k^i - H^i \rho_{k|k}^{i-1}\right),$$

where $\hat{z}_k^i \sim \mathbf{N}(H^i \rho_{k|k}^{i-1}, \hat{R}_k^i)$. Thus it holds that

$$\hat{\Gamma}_{k|k}^i = \hat{F}_k^i \Gamma_{k|k}^{i-1} \left(\hat{F}_k^i\right)^\top + \hat{K}_k^i \hat{R}_k^i \left(\hat{K}_k^i\right)^\top, \tag{6.31}$$

where (recall that $\Gamma_{k|k}^0 = \Gamma_{k|k-1}$)

$$\hat{F}_k^i = \hat{\Gamma}_{k|k}^i \left(\Gamma_{k|k}^{i-1}\right)^{-1}.$$

Given (6.29), the evolution of the estimation error $\eta_{k|k}^i$ can be expressed as

$$\eta_{k|k}^i = \hat{\Gamma}_{k|k}^i \left(\Gamma_{k|k}^{i-1}\right)^{-1} \eta_{k|k}^{i-1}, \tag{6.32}$$

Based on (6.32), the error dynamics for the unforced system (6.28) can be rewritten as

$$\eta_{k|k} = \textstyle\prod_{i=0}^{S-1} \hat{F}_k^{S-i} A_{k-1} \eta_{k-1|k-1} = \hat{F}_k A_{k-1} \eta_{k-1|k-1}, \tag{6.33}$$

where $\hat{F}_k = \prod_{i=0}^{S-1} \hat{F}_k^{S-i}$.

To show the estimation error of the system (6.28) (equivalently system (6.33)) is GES, we need to show that a Lyapunov function of the estimation error exists such that its one-step change is negative definite. Consider the following Lyapunov function candidate

$$V_k = \eta_{k|k}^\top \Gamma_{k|k}^{-1} \eta_{k|k}, \tag{6.34}$$

and its one step-change is given by

$$\begin{aligned} V_k - V_{k-1} &= \eta_{k|k}^\top \Gamma_{k|k}^{-1} \eta_{k|k} - \eta_{k-1|k-1}^\top \Gamma_{k-1|k-1}^{-1} \eta_{k-1|k-1} \\ &= -\eta_{k-1|k-1}^\top \left(\Gamma_{k-1|k-1}^{-1} - A_{k-1}^\top \hat{F}_k^\top \Gamma_{k|k}^{-1} \hat{F}_k A_{k-1}\right) \eta_{k-1|k-1}, \end{aligned} \tag{6.35}$$

where the last equation is due to (6.33). Substituting (6.31) into (6.30), we obtain

$$\begin{aligned} \Gamma_{k|k}^i &= \hat{F}_k^i \Gamma_{k|k}^{i-1} \left(\hat{F}_k^i\right)^\top + \hat{K}_k^i \hat{R}_k^i \left(\hat{K}_k^i\right)^\top + X_k^i \\ &= \hat{F}_k^i \Gamma_{k|k}^{i-1} \left(\hat{F}_k^i\right)^\top + \hat{\Lambda}_k^i, \end{aligned} \tag{6.36}$$

where define $\hat{\Lambda}_k^i = \hat{K}_k^i \hat{R}_k^i \left(\hat{K}_k^i\right)^\top + X_k^i$. Hence $\Gamma_{k|k}$ can be computed from $\Gamma_{k|k-1}$ by recur-

sively applying (6.36), which reads

$$\begin{aligned}\Gamma_{k|k} &= \hat{F}_k \Gamma_{k|k-1} \hat{F}_k^\top + \textstyle\sum_{i=1}^{S-1} \prod_{l=1}^{S-i} \hat{F}_k^{S-l+1} \hat{\Lambda}_k^i \left( \prod_{l=1}^{S-i} \hat{F}_k^{S-l+1} \right)^\top + \hat{\Lambda}_k^S \\ &= \hat{F}_k \left( A_{k-1} \Gamma_{k-1|k-1} A_{k-1}^\top + W_{k-1} \right) \hat{F}_k^\top,\end{aligned} \tag{6.37}$$

where

$$W_{k-1} = Q_{k-1} + \textstyle\sum_{i=1}^{S-1} \prod_{l=1}^{i} \left( \hat{F}_k^l \right)^{-1} \hat{\Lambda}_k^i \left( \left( \hat{F}_k^l \right)^{-1} \right)^\top + \hat{F}_k^{-1} \hat{\Lambda}_k^S \left( \hat{F}_k^{-1} \right)^\top > \mathbf{0}.$$

Substituting (6.37) into (6.35), the one-step change of the Lyapunov function candidate is written as

$$\Delta V_k = -\eta_{k-1|k-1}^\top \left( \Gamma_{k-1|k-1}^{-1} - A_{k-1}^\top (A_{k-1} \Gamma_{k-1|k-1} A_{k-1}^\top + W_{k-1})^{-1} A_{k-1} \right) \eta_{k-1|k-1}.$$

Following the arguments of Lemma 3 in [53] where the matrix inversion lemma is applied to show the negative definiteness of one-step change of the Lyapunov function, we obtain

$$\Gamma_{k-1|k-1}^{-1} - A_{k-1}^\top (A_{k-1} \Gamma_{k-1|k-1} A_{k-1}^\top + W_{k-1})^{-1} A_{k-1} > \mathbf{0},$$

which yields $\Delta V_k < 0$. This concludes that the unforced system (6.28) is GES. Consequently, system (6.27) is input-to-state stable for all $\mathcal{T}_k^c$, and the estimation error dynamics of the KF-SM is input-to-state stable. □

In the proof of the ISS property, we apply the Lyapunov method to show the stability of the unforced system (6.28). The uniform complete observability and controllability of the dynamical system (6.1), (6.3) assume a critical role, in the sense that they ensure the boundedness of the error covariance matrix (as stated in Lemma 10), which is necessary for the feasibility (i.e., radial unboundedness) of the Lyapunov function (6.34). Note that each sensor individually is not enough to ensure the observability of the system, thus we have to study the combinatorial effect of all the sensors together. Moreover, directly proving the stability of matrix $\prod_{i=0}^{S-1} \left( I - K_k^{S-i} H^{S-i} \right) A_{k-1}$ after it converges (as in the classical filtering theory) is also problematic, since the dynamical system (6.1) is time varying, which means that matrix $\prod_{i=0}^{S-1} \left( I - K_k^{S-i} H^{S-i} \right) A_{k-1}$ in the unforced system (6.28) will not converge to a fixed value, thus it is not possible to study the poles of the converged

matrix to show stability.

The ISS property of the KF-SM implies that if the error of the synthetic measurement $\tilde{\delta}_k^i$ is bounded, the estimation error of the KF-SM is also guaranteed to be bounded, as shown in the next corollary.

**Corollary 1** (Ultimate boundedness of the KF-SM)**.** *The estimation error of the KF-SM in the unperturbed error dynamics* (6.27) *is ultimately bounded.*

*Proof.* Since the error covariance $\Gamma_{k|k}$ is bounded for all $k$, it follows that $K_k^i$ and $D_k^i$ are bounded for all $i$ and $k$. Also recall from Section 6.4 that $\left\|\tilde{\delta}_k^i\right\| < 2\zeta^i \left\|D_k^i\right\|^{-1} (m^i)^{\frac{1}{2}}$, where $m^i$ is the dimension of sensor data $y_k^i$. Hence, there exists a class $\mathcal{K}_\infty$ function[8] $\mathrm{z}_0(\cdot)$ such that the second term in (6.27) satisfies

$$\left\| \sum_{i \in \mathcal{T}_k^c} \prod_{l=0}^{S-i-1} \left( I - K_k^{S-l} H^{S-l} \right) K_k^i \tilde{\delta}_k^i \right\| < \mathrm{z}_0 \left( \zeta_{\max} \right), \tag{6.38}$$

where $\zeta_{\max} = \max_{i \in \mathcal{S}} \zeta^i$. Given the exponential stability of the unforced system (6.28), the estimation error (6.27) of the KF-SM satisfies

$$\|\eta_{k|k}\| \leq \tilde{a}\tilde{q}^k \|\eta_{0|0}\| + \mathrm{z}\left( \sup_{0 \leq \kappa \leq k} \left\| \sum_{i \in \mathcal{T}_\kappa^c} \prod_{l=0}^{S-i-1} \left( I - K_\kappa^{S-l} H^{S-l} \right) K_\kappa^i \tilde{\delta}_\kappa^i \right\| \right),$$

where $\tilde{a} > 0$, $0 < \tilde{q} < 1$, and $\mathrm{z}(\cdot)$ is a class $\mathcal{K}$ function. Substituting (6.38) in the above equation, we obtain

$$\|\eta_{k|k}\| \leq \tilde{a}\tilde{q}^k \|\eta_{0|0}\| + \mathrm{z}\left( \mathrm{z}_0 \left( \zeta_{\max} \right) \right).$$

which yields the ultimate boundedness of the estimation error. □

## 6.6 Numerical examples

In this section, we assess the performance of the KF-SM (Definition 5) in terms of both the mean and variance of the estimation error, and compare it with the KF-DT (Definition 3) and KF-ST (Definition 4). First, we compare the performance of the three filters estimating

[8] Recall that a continuous function $\alpha : [0, a) \to [0, \infty)$ is said to belong to class $\mathcal{K}$ if it is strictly increasing and $\alpha(0) = 0$. It belongs to class $\mathcal{K}_\infty$ if $\alpha(r) \to \infty$ as $r \to \infty$.

a time-varying divergent system. Next, we consider the system where a target modeled by a discrete advection equation is tracked by sparsely distributed sensors. The numerical results show an advantage of the KF-SM on improving the estimation accuracy under various low communication rates.

### 6.6.1 A two-dimensional divergent system

In this subsection, we investigate the relationship between the estimation accuracy and the communication rate, and explore the randomness of the estimation error introduced by the synthetic measurements. The target to be estimated is a two-dimensional time-varying dynamical system. For all $k \geq 0$

$$\begin{aligned} &A_k \in \{A^{(1)}, A^{(2)}\}, \quad Q_k = \begin{pmatrix} 1 & 2 \\ 2 & 9 \end{pmatrix}, \\ &H = \begin{pmatrix} 0 & 1 \end{pmatrix}, \quad R = 0.01, \end{aligned} \tag{6.39}$$

where

$$A^{(1)} = \begin{pmatrix} 1.05 & 0 \\ 0.1 & 0.9 \end{pmatrix}, \quad A^{(2)} = \begin{pmatrix} 1.05 & 0 \\ 0.2 & 0.8 \end{pmatrix},$$

and $\Pr(A_{k+1} = A_k) = 0.5$. In this system, the estimation error is sure to increase (due to the model prediction in the time update step) if the state estimate is not corrected in the information update step. Each filter is run for 100 times to access the overall estimation accuracy of the different filters. The initial state $\rho_0 = (2 \quad 1)^\top$, and the initial estimate is set to be $\rho_{0|-1} = (10 \quad 1.05)^\top + \omega_{0|-1}$ with $\omega_{0|-1} \sim \mathbf{N}(\mathbf{0}, 100 I_2)$.

Define $\bar{\eta}^{\mathrm{t,r}} = \frac{1}{k_{\max}} \sum_{k=1}^{k_{\max}} \left\| \bar{\eta}^{\mathrm{r}}_{k|k} \right\|$ where $\bar{\eta}^{\mathrm{r}}_{k|k} = \frac{1}{100} \sum_{\tau=1}^{100} \eta^{\tau}_{k|k}$, with $\eta^{\tau}_{k|k}$ denoted as the estimation error given by the $\tau^{\mathrm{th}}$ run at time $k$. Moreover, define $\bar{\sigma}^{\mathrm{t,r}} = \frac{1}{k_{\max}} \sum_{k=1}^{k_{\max}} \bar{\sigma}^{\mathrm{r}}_{k|k}$, where $\bar{\sigma}^{\mathrm{r}}_{k|k} = \sqrt{\frac{1}{100} \sum_{\tau=1}^{100} \| \eta^{\tau}_{k|k} - \bar{\eta}^{\mathrm{r}}_{k|k} \|^2}$ quantifies the variance of the estimation error over different runs. Recall that the sensor-to-estimator communication rate $r_{\mathrm{c}}$ for each run is defined in (6.23), and denote as $\bar{r}_{\mathrm{c}}$ the average of $r$ over 100 runs. Table 6.1 reports the mean $\bar{\eta}^{\mathrm{t,r}}$ and variance $\bar{\sigma}^{\mathrm{t,r}}$ of the estimation error given by the KF-SM, KF-DT and KF-ST under different communication rates $\bar{r}_{\mathrm{c}}$. The cases for $\bar{r}_{\mathrm{c}} > 0.5$ are omitted since for each filter, the values of $\bar{\eta}^{\mathrm{t,r}}$ and $\bar{\sigma}^{\mathrm{t,r}}$ change little when $\bar{r}_{\mathrm{c}}$ is inside the interval $(0.5, 1]$. The

Table 6.1: Estimation error of the KF-SM, KF-DT and KF-ST tracking system (6.39) under different communication rates

| | KF-SM | | KF-DT | | KF-ST | |
|---|---|---|---|---|---|---|
| $\bar{r}_{\mathrm{c}}$ | $\bar{\eta}^{\mathrm{t,r}}$ | $\bar{\eta}^{\mathrm{t,r}}+\bar{\sigma}^{\mathrm{t,r}}$ $(\bar{\sigma}^{\mathrm{t,r}})$ | $\bar{\eta}^{\mathrm{t,r}}$ | $\bar{\eta}^{\mathrm{t,r}}+\bar{\sigma}^{\mathrm{t,r}}$ $(\bar{\sigma}^{\mathrm{t,r}})$ | $\bar{\eta}^{\mathrm{t,r}}$ | $\bar{\eta}^{\mathrm{t,r}}+\bar{\sigma}^{\mathrm{t,r}}$ $(\bar{\sigma}^{\mathrm{t,r}})$ |
| 0.1 | 1.329 | 4.943(3.614) | 3.265 | 6.744(3.479) | 2.119 | 5.937(3.818) |
| 0.2 | 0.969 | 2.924(1.955) | 1.398 | 3.314(1.916) | 1.100 | 3.209(2.109) |
| 0.3 | 0.715 | 2.264(1.549) | 0.936 | 2.471(1.535) | 1.054 | 2.678(1.624) |
| 0.4 | 0.611 | 2.085(1.474) | 0.873 | 2.326(1.453) | 0.868 | 2.398(1.530) |
| 0.5 | 0.526 | 1.966(1.440) | 0.836 | 2.272(1.436) | 0.793 | 2.242(1.449) |

parameters for the sensor schedulers in each filter are chosen[9] according to Figure 6.3a to obtain different $\bar{r}_{\mathrm{c}}$. It is shown that under the same communication rate, the KF-SM always has the smallest average estimation error $\bar{\eta}^{\mathrm{t,r}}$, and this advantage is particularly apparent when the communication rate is low. Although the variance $\bar{\sigma}^{\mathrm{t,r}}$ for the KF-SM is slightly larger than the KF-DT since the synthetic measurements increase the randomness of the estimation error across different runs, the value of $\bar{\eta}^{\mathrm{t,r}}+\bar{\sigma}^{\mathrm{t,r}}$ given by the KF-SM is still the smallest. The deterministic thresholds applied in the sensor schedulers for the KF-SM and KF-DT decrease as $\bar{r}_{\mathrm{c}}$ increases, which reduces the variance of the estimation error for the KF-SM. The values of $\bar{\sigma}^{\mathrm{t,r}}$ for the KF-SM and KF-DT become similar as $\bar{r}_{\mathrm{c}}$ increases.

Figure 6.3b plots the evolution of $\|\bar{\eta}^{\mathrm{r}}_{k|k}\|$ and $\|\bar{\eta}^{\mathrm{r}}_{k|k}\|+\bar{\sigma}^{\mathrm{r}}_{k|k}$ given by the three filters for $\bar{r}_{\mathrm{c}}=0.1$, and Figure 6.3c-6.3d illustrate the corresponding trajectories of $\|\eta_{k|k}\|$ for a single run to provide more insight on the results observed in Table 6.1. After step 30, the estimation error covariances for the three filters become stabilized. In the deterministic sensor scheduler, the innovation is normalized by an approximately constant value (see (6.11)), and compared with a threshold which is fixed as well. Therefore, data transmission for the KF-SM and KF-DT will be stopped by the sensor schedulers when the estimation error reaches to an approximately constant value (e.g., around $\| \eta_{k|k} \|= 2$ for the KF-DT as shown in Figure 6.3c). For the KF-DT, the estimation error increases when the sensor stops sending data. Comparatively, the estimation error of the KF-SM can continue to decrease although data transmission does not occur, which is due to the feedback provided by the synthetic measurements (as shown in Figure 6.3c). Since the KF-ST applies a

[9]In this numerical experiment, we first fix a communication rate and choose the parameters to obtain this communication rate. This setup is different from the parameter selection problem in [82] where the parameter is optimized to minimize the communication rate (constrained on the upper bound of the error covariance).

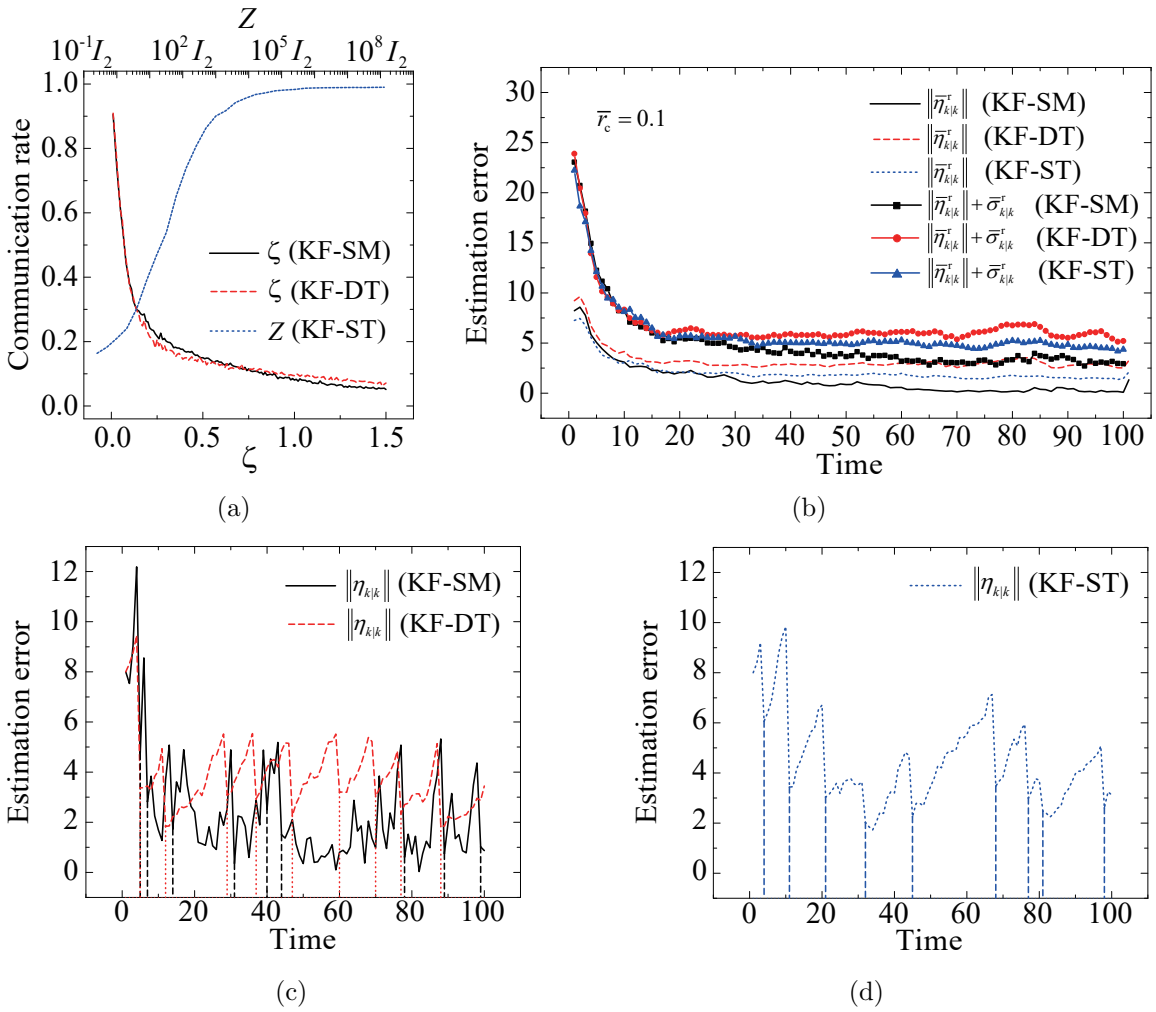


Figure 6.3: Performance of the KF-SM, KF-DT and KF-ST tracking system (6.39). (a) The relationship between the parameters of the sensor schedulers and the communication rates; (b) The 2-norm of the average estimation error and the variance of the estimation error given by the KF-SM, KF-DT and KF-ST over 100 runs; (c) The 2-norm of the estimation error given by the KF-SM and KF-DT for a single run, where the vertical lines indicate the time steps when the sensor data is sent (with dashed and dotted vertical lines representing the KF-SM and KF-DT, respectively); (d) The 2-norm of the estimation error given by the KF-ST for a single run, where the vertical lines indicate the time steps when the sensor data is sent.

stochastic threshold in the sensor scheduler, the fact that the estimation error is large does not guarantee that data transmission can be triggered (as shown in Figure 6.3d). In the KF-SM, the sensor is guaranteed to send measurements when $\|\eta_{k|k}\| > 5$ (see Figure 6.3c). Consequently, the KF-SM has the smallest average estimation error $\|\bar{\eta}^{\mathrm{r}}_{k|k}\|$, as depicted in Figure 6.3b.

Figure 6.3c-6.3d also indicate why the variances $\bar{\sigma}^{\mathrm{r}}_{k|k}$ of the estimation error of the KF-SM and KF-ST are slightly larger than the KF-DT. The randomness of the estimation error for the KF-DT is given by the modeling error and measurement noise, while for the KF-SM it is given by the modeling error, measurement noise, and the synthetic measurement. This is shown in Figure 6.3c, where the estimation error of the KF-SM directly depends on the synthetic measurement. For the KF-ST in Figure 6.3d, the estimation error also varies with the stochastic thresholds in addition to the model and measurement noise. Nevertheless, it is shown in Figure 6.3b and Table 6.1 that the reduction on $\|\bar{\eta}^{\mathrm{r}}_{k|k}\|$ for the KF-SM dominates the increase in $\bar{\sigma}^{\mathrm{r}}_{k|k}$.

### 6.6.2 A system modeled by a discrete advection equation

In this subsection, we investigate the performance of the KF-SM, KF-DT and KF-ST under a system motivated by CPS estimation problems, where a scalar field is modeled by a discrete advection equation, and the sensor is sparsely distributed.

Consider the advection equation of a scalar field $\psi(t, x)$ where $t$ and $x$ represent time and space, respectively, and the propagation speed is a positive constant $v_{\mathrm{c}} > 0$:

$$\frac{\partial \psi}{\partial t} + v_{\mathrm{c}} \frac{\partial \psi}{\partial x} = 0, \tag{6.40}$$

with boundary inflow at the upstream side given by $\mathrm{f}(t)$. Consider a discretization grid defined by a space step $\triangle x$ and a time step $\triangle t$, and denote as $\rho_k(l)$ the average of $\psi(k\triangle t, x)$ for $l\triangle x \leq x < (l+1)\triangle x$. Construct the state vector at the $k^{\mathrm{th}}$ time step as $\rho_k = (\rho_k(1), \cdots, \rho_k(l), \cdots, \rho_k(n))^\top$, the discrete counterpart of (6.40) can be modeled by

$$\rho_{k+1} = A_k \rho_k + u_k, \tag{6.41}$$

where the upstream inflow $u_k = (\mathrm{f}(k\triangle t), \cdots, 0, \cdots, 0)^\top$, and

$$A_k = \begin{pmatrix} 1 - v_{\mathrm{c}}\frac{\triangle t}{\triangle s} & & & \\ v_{\mathrm{c}}\frac{\triangle t}{\triangle s} & 1 - v_{\mathrm{c}}\frac{\triangle t}{\triangle s} & & \\ & \ddots & \ddots & \\ & & v_{\mathrm{c}}\frac{\triangle t}{\triangle s} & 1 - v_{\mathrm{c}}\frac{\triangle t}{\triangle s} \end{pmatrix}, \quad \forall k > 0.$$

Given the CFL condition (2.9) for numerical stability, it holds that $0 < v_{\mathrm{c}}\frac{\triangle t}{\triangle s} \leq 1$. Consider the case where the dimension of the state vector $n = 10$, the propagation speed $v_{\mathrm{c}} = 1$, the space step $\triangle x = 1$, and the time step $\triangle t = 1$. Hence, the matrix $A_k$ in (6.41) is given by

$$A_k = \begin{pmatrix} 0 & & & \\ 1 & 0 & & \\ & \ddots & \ddots & \\ & & 1 & 0 \end{pmatrix}, \quad \forall k > 0.$$

The upstream inflow is given by the following sinusoidal function:

$$\mathrm{f}(k\triangle t) = \mathrm{f}(k) = 0.01 + 0.01 \sin\left(\frac{k\pi}{4000} + \pi\right),$$

which is neither known by the estimators nor measured by the sensors. Therefore, the target model applied by the estimators is still given by

$$\rho_{k+1} = \hat{A}_k \rho_k + \omega_k, \quad \omega_k \sim \mathbf{N}(\mathbf{0}, Q_k),$$

where for all $k > 0$:

$$\hat{A}_k = \begin{pmatrix} 1 & & & \\ 1 & 0 & & \\ & \ddots & \ddots & \\ & & 1 & 0 \end{pmatrix}, \quad Q_k = \begin{pmatrix} 100 & 25 & & & \\ 25 & 100 & 25 & & \\ & \ddots & \ddots & \ddots & \\ & & 25 & 100 & 25 \\ & & & 25 & 100 \end{pmatrix} \times 10^{-4}.$$

One may note that the model applied in the filters is slightly different from the true model

(6.41). This is done to reflect realistic differences between the true system to be estimated and the model assumed in the estimator encountered in field deployments. It thereby counteracts an overly optimistic performance of the filter in simulation, known as the *inverse crime* setting [97].

The state is measured by two sensors with $H^1 = (0, \cdots, 0, 1)$, $H^2 = (1, 0, \cdots, 0)$, $R^1 = R^2 = 0.01$, and is estimated by the KF-SM, KF-DT and KF-ST. One may note that the sensors altogether measure only a small subset of the state variable. In this case, even if the normalized innovations for the two sensors are both below the threshold required for data transmission, the estimate of the full state vector may still be inaccurate and needs to be corrected in the information update. As in the previous subsection, each filter is run for 100 times. The $l^{\text{th}}$ element of the initial state $\rho_0$ is given by

$$\rho_0(l) = \begin{cases} 0.25 & \text{if } 1 \leq l \leq 5 \\ 0.5 & \text{if } 6 \leq l \leq 10, \end{cases}$$

and the $l^{\text{th}}$ entry of the initial estimate is set to be $\rho_{0|-1}(l) = 0.5 + 0.075(l-1)$ and $\Gamma_{0|-1} = \mathbf{0}$.

Figure 6.4a plots the 2-norm of the mean of the estimation error $\|\bar{\eta}^{\text{r}}_{k|k}\|$ given by the three filters under communication rate $\bar{r}_{\text{c}} = 0.05$. The parameters in the sensor schedulers applied in the three filters are given in Table 6.2. Similar to the previous subsection, Figure 6.4a shows that the average estimation error of the KF-SM is always the smallest compared to the KF-DT and KF-ST. To explain this result, we also plot the evolution of the estimation errors of individual state variables given by the three filters for one single run. Figure 6.4b-6.4d show the absolute estimation errors of the state variables directly measured by the two sensors (i.e., $|\eta_{k|k}(1)|$ and $|\eta_{k|k}(10)|$), as well as the state variables with the largest or smallest absolute estimation error (i.e., $\eta^{\max}_{k|k} = \max_{l \in \{1,\cdots,10\}} |\eta_{k|k}(l)|$ and $\eta^{\min}_{k|k} = \min_{l \in \{1,\cdots,10\}} |\eta_{k|k}(l)|$). The dashed (resp. solid) vertical lines represent the time steps when sensor 1 (resp. sensor 2) sends data. Since the two sensors measure only the first and last entries of the state vector, data transmission is stopped once the estimation errors of the these two state variables are small, even though the estimation errors of other state variables are still large. During time intervals without data transmission, the estimation error of each state variable in the KF-DT and KF-ST cannot be reduced, until the large errors propagate to the sensor locations again to activate data transmission. However, due to

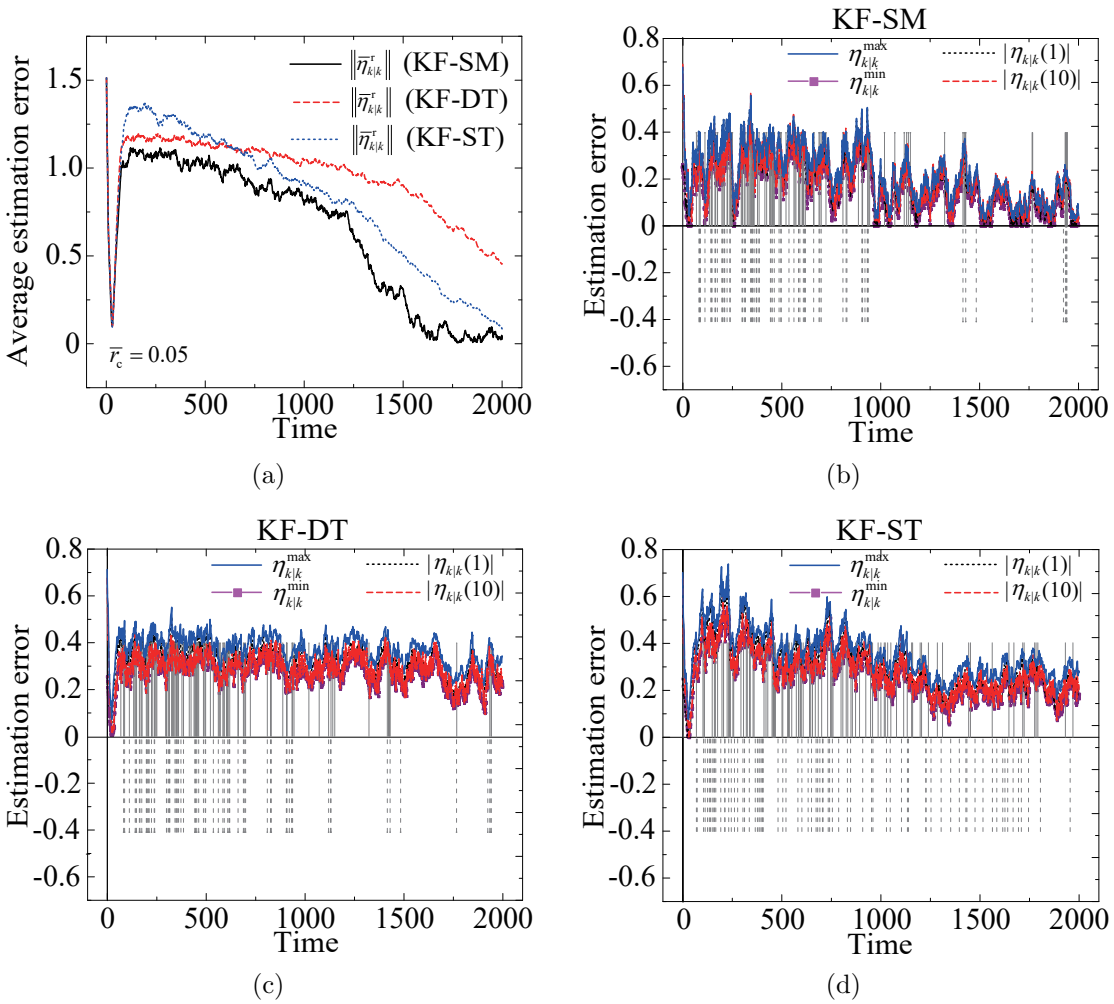


Figure 6.4: Performance of the KF-SM, KF-DT and KF-ST in the numerical experiment described in Section 6.6.2. (a) The 2-norm of the average estimation error given by the KF-SM, KF-DT, KF-ST and KF over 100 runs; (b)-(d) The absolute estimation error of individual state variables given by the KF-SM (b), KF-DT (c) and KF-ST (d) for a single run, where the vertical lines represent the time steps with data transmission.

Table 6.2: Parameters in the sensor schedulers used in the KF-SM, KF-DT and KF-ST tracking system (6.41)

| Parameter | Communication rate $\bar{r}_{\mathrm{c}}$ | | | | |
|---|---|---|---|---|---|
| | 0.05 | 0.10 | 0.20 | 0.35 | 0.50 |
| KF-SM and KF-DT: $\zeta^i$ for $i = 1, 2$ | 0.45 | 0.25 | 0.15 | 0.105 | 0.07 |
| KF-ST: $Y^i$ for $i = 1, 2$ | $0.5I$ | $2.5I$ | $12I$ | $36I$ | $80I$ |

Table 6.3: Estimation error of the KF-SM, KF-DT and KF-ST tracking system (6.41) under different communication rates

| | KF-SM | | | KF-DT | | | KF-ST | | |
|---|---|---|---|---|---|---|---|---|---|
| $\bar{r}_{\mathrm{c}}$ | $\bar{\eta}^{\mathrm{t,r}}$ | $\bar{\sigma}^{\mathrm{t,r}}$ | $\bar{\varsigma}^{\mathrm{t,r}}$ | $\bar{\eta}^{\mathrm{t,r}}$ | $\bar{\sigma}^{\mathrm{t,r}}$ | $\bar{\varsigma}^{\mathrm{t,r}}$ | $\bar{\eta}^{\mathrm{t,r}}$ | $\bar{\sigma}^{\mathrm{t,r}}$ | $\bar{\varsigma}^{\mathrm{t,r}}$ |
| 0.05 | 1.174 | 0.425 | 0.640 | 1.628 | 0.192 | 0.747 | 1.611 | 0.246 | 0.845 |
| 0.10 | 0.513 | 0.217 | 0.142 | 0.606 | 0.152 | 0.145 | 0.951 | 0.182 | 0.332 |
| 0.20 | 0.251 | 0.139 | 0.046 | 0.281 | 0.119 | 0.048 | 0.473 | 0.139 | 0.105 |
| 0.35 | 0.188 | 0.117 | 0.031 | 0.203 | 0.110 | 0.032 | 0.282 | 0.119 | 0.048 |
| 0.5 | 0.162 | 0.108 | 0.027 | 0.169 | 0.106 | 0.027 | 0.204 | 0.110 | 0.032 |

the synthetic measurements, the estimation error of the KF-SM can decrease even when data transmission is not triggered. Moreover, $\eta^{\min}_{k|k}$, $|\eta_{k|k}(1)|$, and $|\eta_{k|k}(10)|$ are nearly identical for all the three filters, implying that the state variables which are directly measured by the sensors have small estimation error compared to other state variables. For the KF-DT and KF-ST, the distance between $\eta^{\max}_{k|k}$ and $\eta^{\min}_{k|k}$ is more apparent. In the KF-SM, the synthetic measurements help correct the state estimate of the state variables which are not directly measured, thus reducing the disparity between $\eta^{\max}_{k|k}$ and $\eta^{\min}_{k|k}$. Consequently, feeding the synthetic measurements back into the state estimate is beneficial for reducing the estimation error of the state variables whose values are not directly measured by the sensors, even though the synthetic measurements are only a proxy for the true measurements.

Let $\bar{\varsigma}^{\mathrm{t,r}} = \frac{1}{k_{\max}} \sum_{k=1}^{k_{\max}} \bar{\varsigma}^{\mathrm{r}}_{k|k}$, where $\bar{\varsigma}^{\mathrm{r}}_{k|k} = \sqrt{\frac{1}{100} \sum_{\tau=1}^{100} \|\eta^{\tau}_{k|k}\|^2}$ is the sample mean square error across all runs at time $k$. Table 6.3 reports the values of $\bar{\eta}^{\mathrm{t,r}}$, $\bar{\sigma}^{\mathrm{t,r}}$ and $\bar{\varsigma}^{\mathrm{t,r}}$ given by the three filters under various communication rates. It is shown that the KF-SM always has the smallest average estimation error $\bar{\eta}^{\mathrm{t,r}}$. Although the synthetic measurements increase the variance $\bar{\sigma}^{\mathrm{t,r}}$ of the estimation error, the increase is dominated by the reduction on the average estimation error, especially under low communication rates. As a consequence, the sample mean square error $\bar{\varsigma}^{\mathrm{t,r}}$ given by the KF-SM is also the smallest.

# CHAPTER 7

# CONCLUSIONS AND OPEN PROBLEMS

The research presented in this dissertation addresses several critical issues in the real-time estimation of cyber-physical systems, with specific focus on large-scale traffic monitoring problems. In this chapter, we present the main contributions of this dissertation and discuss some open problems.

## 7.1 Main contributions

**Error bounds of the Kalman filter on one-dimensional freeway sections.** Although many traffic estimation algorithms in the existing literature are verified experimentally, very few results exist that theoretically analyze the performance of traffic estimators (e.g., bounds on the estimation error), especially under unobservable scenarios. In Chapter 3, we provide theoretical performance analysis of the KF on one-dimensional freeway sections, where the system dynamics is modeled by the SMM. We derive the error bounds of the KF, even when the system switches among the observable and unobservable modes of the SMM. This is done by exploring the combined effects of intrinsic properties of traffic models (i.e., flow-density relationship, conservation law), requirements to ensure the stability of the discretization scheme of the LWR PDE (i.e., the CFL condition), and the information update schemes of the KF. Specifically, we leverage the maximum increase of the mean error while the system is unobservable and the convergence rate of the mean error under the observable modes to derive the minimum residence time in the observable time intervals, as well as the upper bounds of the mean error in the observable and unobservable time intervals. This is the first result on the theoretical performance of any traffic filters under unobservable scenarios, as well as under switches among observable and unobservable modes.

**Extension of the error bounds for traffic networks with junctions.** In Chapter 4, we extend the results on the error bounds of the KF on one-dimensional freeway sections to freeway sections with junctions. First, we combine the CTM with a junction solver, and develop a switched linear model describing the evolution of traffic conditions on a freeway section with a junction inside. The newly developed model, namely the SMM-J, also reflects the intrinsic physical properties of the traffic flow and the stability effect of the discretization scheme. Compared to one-dimensional freeway sections, the issue of non-observability is more severe when junctions exist, and nearly all of the modes of the SMM-J are unobservable, motivating attentions on the unobservable modes. Hence, we extend the results proved in Chapter 3 and derive the error bounds of the KF when the system stays inside the unobservable modes of the SMM-J. The essence of the error bounds analysis in junctions follows closely with the cases on one-dimensional road sections, in the sens that both explore the interactions between the physical properties in the traffic models and the measurement feedback in the filter update. The error bounds under switches among observable and unobservable modes can be obtained similarly as in Chapter 3.

The above two contributions are complementary parts when estimating large-scale freeway networks. In a large-scale network, we partition the traffic network into local sections which are either one-dimensional, or having a junction inside. The traffic condition in each local section is estimated by a local estimator based on the KF and the SMM-J (or the SMM). Under this distributed computing manner, the estimation errors for the sections without junctions reside below the bounds derived in Chapter 3, and the error bounds studied in Chapter 4 are used to justify the estimation accuracy in the sections with junctions.

This dissertation also studies two important elements to improve scalability in estimation problems.

**Distributed consensus-based filtering in large-scale estimation.** In Chapter 5, a (spatially) distributed local Kalman consensus filter is designed and analyzed. To reduce state space dimensionality, the large-scale network (not limited to traffic networks) is partitioned into overlapping sections, with the local state on each state estimated by its own local agent (estimator). To promote agreement on the estimates of the shared states among

neighboring agents, we study the effect of adding consensus terms to each estimator. Compared to the author's previous work [47], the consensus is redesigned to make it scalable both in terms of computation and communication. Furthermore, it is shown that the redesigned consensus term maintains the unbiasedness of the mean error under observable scenarios. We also extend the results in Chapter 3 to analyze the performance of the DLKCF estimating traffic conditions based on the SMM, and derive the error bounds of the DLKCF when the system switches among the observable and unobservable modes. Numerical experiments illustrate the effect of the DLKDF on reducing the overall estimation error as well as promoting agreement among agents. The numerical results also show a considerable reduction on the runtime of the DLKCF compared to a central estimator.

**Online estimation with sensor schedulers for data transmission reduction.** In Chapter 6, we study Kalman filtering algorithms embedded with sensor schedulers, where the sensor schedulers are incorporated to select the most informative part of the data to transmit to the estimator, thus reducing data transmission while preserving estimation accuracy. Compared to existing algorithms which update only the error covariance when data transmission is not triggered, we design the KS-SM that extracts implicit information from the sensor schedulers to update both the error covariance and state estimate when sensor data is not transmitted. When data transmission is declined by the sensor scheduler, the KF-SM updates the state estimates using synthetic measurements generated based on the estimated distribution of the true measurements. It is shown that the KF-SM is an approximate MMSE estimator with bounded error covariance. Moreover, we show that the error dynamics of the KF-SM is ISS, indicating that the estimation error is small provided that the disparity between the synthetic and true measurements is small (which can be guaranteed by the scheduling policy of the sensor schedulers). Finally, numerical examples show an advantage of the KF-SM on reducing the estimation error based on the synthetic measurements under various communication rates.

## 7.2 Open problems

We discuss below some open problems that have been uncovered through this work, which may be the focus of future research efforts.

**More flexible sensor placement in traffic estimation.** When deriving the error bounds of the KF estimating traffic conditions based on the SMM and the SMM-J, we assume that the sensors do not move, and are placed at the boundaries of each freeway section, measuring the traffic densities in the boundary cells (i.e., (Asm.2) and (Asm.9)). Under these assumptions, the observable and unobservable subsystems remain unchanged in each unobservable mode (e.g., in the FC model of the SMM, the observable and unobservable subsystems remains the same no matter where the shock is located). If we add moving sensors (e.g., smartphones), the observable and unobservable subsystems will change when the SMM stays inside the unobservable mode, which makes the proof more involved in unobservable scenarios. One possible future work is to extend the analysis in this dissertation to handle these more general situations.

**Consensus terms in unobservable systems.** In the consensus term designed in Chapter 5, the consensus term is turned off when the system is unobservable. This is to make sure that the consensus term will not destabilize the estimation error or degrade the estimation accuracy under unobservable scenarios, and is also due to the fact that the state estimate is shown to be bounded even under the simple update schemes of the KF. Nevertheless, it would be interesting to see if better consensus structures can be designed that help the unobservable sections achieve better estimates by communicating with the observable neighbors.

**Application of the sensor scheduling schemes to traffic estimation problems.** Traffic estimation is very likely to benefit from sensor scheduling schemes due to the following properties: (*i*) although the amount of high fidelity data is rapidly increasing, data transmission still faces the concern of energy, bandwidth, and monetary constraints; (*ii*) due to physical properties of vehicle flows (e.g., conservation laws), model predictions in the estimation algorithms are sometimes sufficient to provide accurate estimate, thus it is unnecessary to send data at every time step from every sensor to correct the state estimates. Before applying sensor scheduling schemes to traffic estimation algorithms, it is important to study the analytical relationship between the parameters in the scheduling policy and the estimation error and/or error covariance, thus deriving the optimal parameters that help achieve the best trade-off between data transmission and estimation performance.

Moreover, since the non-observability issue is inevitable in traffic estimation, it is also important to find the suitable scheduling policies (and the corresponding update schemes of the estimators) when the system is unobservable.

# REFERENCES


[1] P. Corke, T. Wark, R. Jurdak, W. Hu, P. Valencia, and D. Moore, "Environmental wireless sensor networks," *Proceedings of the IEEE*, vol. 98, no. 11, pp. 1903–1917, 2010.

[2] L. Oliveira and J. Rodrigues, "Wireless sensor networks: a survey on environmental monitoring," *Journal of Communications*, vol. 6, no. 2, pp. 143–151, 2011.

[3] V. Roy, A. Simonetto, and G. Leus, "Spatio-temporal sensor management for environmental field estimation," *Signal Processing*, vol. 128, pp. 369–381, 2016.

[4] Y. Jin, M. Motani, W. Soh, and J. Zhang, "SparseTrack: Enhancing indoor pedestrian tracking with sparse infrastructure support," in *Proceedings of the 29th IEEE Conference on Computer Communications*, 2010, pp. 1–9.

[5] K. Park, H. Shin, and H. Cha, "Smartphone-based pedestrian tracking in indoor corridor environments," *Personal and Ubiquitous Computing*, vol. 17, no. 2, pp. 359–370, 2013.

[6] X. Zhu, Q. Li, and G. Chen, "Apt: Accurate outdoor pedestrian tracking with smartphones," in *2013 Proceedings IEEE INFOCOM*. IEEE, 2013, pp. 2508–2516.

[7] J. C. Herrera, D. B. Work, R. Herring, X. J. Ban, Q. Jacobson, and A. M. Bayen, "Evaluation of traffic data obtained via GPS-enabled mobile phones: The Mobile Century field experiment," *Transportation Research Part C: Emerging Technologies*, vol. 18, no. 4, pp. 568–583, 2010.

[8] L. Mihaylova, A. Hegyi, A. Gning, and R. Boel, "Parallelized particle and Gaussian sum particle filters for large-scale freeway traffic systems," *IEEE Transactions on Intelligent Transportation Systems*, vol. 13, no. 1, pp. 36 – 48, 2012.

[9] R. Wang, Y. Li, and D. B. Work, "Comparing traffic state estimators for mixed human and automated traffic flows," *Transportation Research Part C: Emerging Technologies*, vol. 78, pp. 95–110, 2017.

[10] L. Mihaylova, R. Boel, and A. Hegyi, "Freeway traffic estimation within recursive Bayesian framework," *Automatica*, vol. 43, no. 2, pp. 290–300, 2007.

[11] D. B. Work, S. Blandin, O.-P. Tossavainen, B. Piccoli, and A. Bayen, "A traffic model for velocity data assimilation," *Applied Mathematics Research eXpress*, vol. 2010, no. 1, pp. 1–35, 2010.

[12] H. Chen and H. A. Rakha, "Prediction of dynamic freeway travel times based on vehicle trajectory construction," in *Proceedings of the 15th IEEE Conference on Intelligent Transportation Systems*, 2012, pp. 576–581.

[13] Y. Yuan, J. van Lint, R. Wilson, F. van Wageningen-Kessels, and S. Hoogendoorn, "Real-time Lagrangian traffic state estimator for freeways," *IEEE Transactions on Intelligent Transportation Systems*, vol. 13, no. 1, pp. 59–70, 2012.

[14] S. Blandin, A. Couque, A. Bayen, and D. B. Work, "On sequential data assimilation for scalar macroscopic traffic flow models," *Physica D: Nonlinear Phenomena*, vol. 241, no. 17, pp. 1421–1440, 2012.

[15] L. Munoz, X. Sun, R. Horowitz, and L. Alvarez, "Piecewise-linearized cell transmission model and parameter calibration methodology," *Transportation Research Record*, no. 1965, pp. 183–191, 2006.

[16] Y. Sun and D. B. Work, "Scaling the Kalman filter for large-scale traffic estimation," *IEEE Transactions on Control of Network Systems (in press)*, 2017.

[17] Y. Sun and D. B. Work, "Error bounds for Kalman filters on traffic networks," *Networks and Heterogeneous Media (conditionally accepted)*, 2017.

[18] B. Anderson and J. Moore, *Optimal filtering*. Englewood Cliffs, N.J.: Prentice-Hall, inc, 1979.

[19] A. H. Jazwinski, *Stochastic process and filtering theory*. Academic Press, 1970.

[20] Z. Li, Y. Zhu, H. Zhu, and M. Li, "Compressive sensing approach to urban traffic sensing," in *Proceedings of the 31st International Conference on Distributed Computing Systems (ICDCS)*, 2011, pp. 889–898.

[21] R. Ambrosino, B. Sinopoli, and K. Poolla, "Optimal sensor scheduling for remote estimation over wireless sensor networks," in *Modelling, Estimation and Control of Networked Complex Systems*. Springer, 2009, pp. 127–142.

[22] P. I. Richards, "Shock waves on the highway," *Operations Research*, vol. 4, no. 1, pp. 42–51, 1956.

[23] M. Lighthill and G. Whitham, "On kinematic waves. II. A theory of traffic flow on long crowded roads," *Proceedings of the Royal Society of London. Series A, Mathematical and Physical Sciences*, vol. 229, no. 1178, pp. 317–345, 1955.

[24] C. F. Daganzo, "The cell transmission model: a dynamic representation of highway traffic consistent with the hydrodynamic theory," *Transportation Research Part B: Methodological*, vol. 28, no. 4, pp. 269–287, 1994.

[25] C. F. Daganzo, "The cell transmission model, part II: network traffic," *Transportation Research Part B: Methodological*, vol. 29, no. 2, pp. 79–93, 1995.

[26] J. P. Lebacque, "The Godunov scheme and what it means for first order traffic flow models," in *Proceedings of the 13th International Symposium on Transportation and Traffic Theory*, 1996, pp. 647–677.

[27] S. Godunov, "A difference method for the numerical calculation of discontinuous solutions of hydrodynamic equations," *Mathematics Sbornik*, vol. 47, no. 3, pp. 271–306, 1959.

[28] X. Sun, L. Munoz, and R. Horowitz, "Highway traffic state estimation using improved mixture Kalman filters for effective ramp metering control," in *Proceedings of the 42nd IEEE Conference on Decision and Control*, 2003, pp. 6333–6338.

[29] H. Holden and N. H. Risebro, "A mathematical model of traffic flow on a network of unidirectional roads," *SIAM Journal on Mathematical Analysis*, vol. 26, no. 4, pp. 999–1017, 1995.

[30] M. Herty and A. Klar, "Modeling, simulation, and optimization of traffic flow networks," *SIAM Journal on Scientific Computing*, vol. 25, no. 3, pp. 1066–1087, 2003.

[31] W.-L. Jin and H. M. Zhang, "On the distribution schemes for determining flows through a merge," *Transportation Research Part B: Methodological*, vol. 37, no. 6, pp. 521–540, 2003.

[32] J. P. Lebacque, "First-order macroscopic traffic flow models: intersection modeling, network modeling," in *Transportation and Traffic Theory. Flow, Dynamics and Human Interaction. 16th International Symposium on Transportation and Traffic Theory*, 2005.

[33] M. Garavello and B. Piccoli, *Traffic flow on networks*, A. Bressan, Ed. American Institute of Mathematical Sciences (AIMS), Springfield, MO, 2006.

[34] W.-L. Jin, "Continuous kinematic wave models of merging traffic flow," *Transportation Research Part B: Methodological*, vol. 44, no. 8, pp. 1084–1103, 2010.

[35] K. Han, B. Piccoli, and W. Szeto, "Continuous-time link-based kinematic wave model: formulation, solution existence, and well-posedness," *Transportmetrica B: Transport Dynamics*, vol. 4, no. 3, pp. 187–222, 2016.

[36] M. Garavello, K. Han, and B. Piccoli, *Models for vehicular traffic on networks*. American Institute of Mathematical Sciences (AIMS), Springfield, MO, 2016, vol. 9.

[37] W.-L. Jin, "A Riemann solver for a system of hyperbolic conservation laws at a general road junction," *Transportation Research Part B: Methodological*, vol. 98, pp. 21–41, 2017.

[38] R. Wang, S. Fan, and D. B. Work, "Efficient multiple model particle filtering for joint traffic state estimation and incident detection," *Transportation Research Part C: Emerging Technologies*, vol. 71, pp. 521–537, 2016.

[39] Y. Wang and M. Papageorgiou, "Real-time freeway traffic state estimation based on extended Kalman filter: a general approach," *Transportation Research Part B: Methodological*, vol. 39, no. 2, pp. 141–167, 2005.

[40] F. Morbidi, L. L. Ojeda, C. Canudas de Wit, and I. Bellicot, "A new robust approach for highway traffic density estimation," in *Proceedings of the 13th European Control Conference*, 2014, pp. 1–6.

[41] J. Thai and A. M. Bayen, "State estimation for polyhedral hybrid systems and applications to the godunov scheme for highway traffic estimation," *IEEE Transactions on Automatic Control*, vol. 60, no. 2, pp. 311–326, 2015.

[42] T. Seo, A. M. Bayen, T. Kusakabe, and Y. Asakura, "Traffic state estimation on highway: a comprehensive survey," *Annual Reviews in Control*, 2017.

[43] S. Jabari and H. Liu, "A stochastic model of traffic flow: Gaussian approximation and estimation," *Transportation Research Part B: Methodological*, vol. 47, pp. 15–41, 2013.

[44] S. Contreras, S. Agarwal, and P. Kachroo, "Quality of traffic observability on highways with lagrangian sensors," *IEEE Transactions on Automation Science and Engineering*, 2017.

[45] I. Morarescu and C. Canudas de Wit, "Highway traffic model-based density estimation," in *Proceedings of the American Control Conference*, vol. 3, 2011, pp. 2012–2017.

[46] C. Vivas, S. Siri, A. Ferrara, S. Sacone, G. Cavanna, and F. R. Rubio, "Distributed consensus-based switched observers for freeway traffic density estimation," in *Proceedings of the 54th IEEE Conference on Decision and Control*. IEEE, 2015, pp. 3445–3450.

[47] Y. Sun, "A distributed local kalman consensus filter for traffic estimation: design, analysis and validation," M.S. thesis, University of Illinois at Urbana-Champaign, 2015.

[48] A. A. Kurzhanskiy, "Set-valued estimation of freeway traffic density," *IFAC Proceedings Volumes*, vol. 42, no. 15, pp. 271–277, 2009.

[49] A. A. Kurzhanskiy and P. Varaiya, "Guaranteed prediction and estimation of the state of a road network," *Transportation Research Part C: Emerging Technologies*, vol. 21, no. 1, pp. 163–180, 2012.

[50] B. S. Y. Rao, H. F. Durrant-Whyte, and J. A. Scheen, "A fully dencentralized multisensor system for tracking and surveillance," *International Journal of Robotics Research*, vol. 12, no. 1, pp. 20–44, 1993.

[51] S. Grime and H. F. Durrant-Whyte, "Data fusion in decentralized sensor networks," *Control Engineering Practice*, vol. 2, no. 5, pp. 849–863, 1994.

[52] R. Olfati-Saber, "Distributed Kalman filtering for sensor networks," in *Proceedings of the 46th IEEE Conference on Decision and Control*, 2007, pp. 5492–5498.

[53] R. Olfati-Saber, "Kalman-consensus filter: optimality, stability, and performance," in *Proceedings of the 48th IEEE Conference on Decision and Control*, 2009, pp. 7036–7042.

[54] M. A. Demetriou, "Adaptive consensus filters of spatially distributed systems with limited connectivity," in *Proceedings of the 52nd IEEE Conference on Decision and Control*, 2013, pp. 442–447.

[55] H. Bai, R. A. Freeman, and K. M. Lynch, "Distributed Kalman filtering using the internal model average consensus estimator," in *Proceedings of the American Control Conference*, 2011, pp. 1500–1505.

[56] A. Kamal, J. Farrell, and A. Roy-Chowdhury, "Information weighted consensus filters and their application in distributed camera networks," *IEEE Transactions on Automatic Control*, vol. 58, no. 12, pp. 3112–3125, 2013.

[57] G. Battistelli, L. Chisci, G. Mugnai, A. Farina, and A. Graziano, "Consensus-based linear and nonlinear filtering," *IEEE Transactions on Automatic Control*, vol. 60, no. 5, pp. 1410–1415, 2015.

[58] U. A. Khan and J. M. F. Moura, "Distributing the Kalman filter for large-scale systems," *IEEE Transactions on Signal Processing*, vol. 56, no. 10, pp. 4919–4935, 2008.

[59] S. S. Stanković, M. S. Stanković, and D. M. Stipanović, "Consensus based overlapping decentralized estimator," *IEEE Transactions on Automatic Control*, vol. 54, no. 2, pp. 410–415, 2009.

[60] M. Farina, G. Ferrari-Trecate, and R. Scattolini, "Moving-horizon partition-based state estimation of large-scale systems," *Automatica*, vol. 46, no. 5, pp. 910–918, 2010.

[61] J. Cortés, "Distributed Kriged Kalman filter for spatial estimation," *IEEE Transactions on Automatic Control*, vol. 54, no. 12, pp. 2816–2827, 2009.

[62] M. Athans, "On the determination of optimal costly measurement strategies for linear stochastic systems," *Automatica*, vol. 8, pp. 397–412, 1972.

[63] J. S. Baras and A. Bensoussan, "Optimal sensor scheduling in nonlinear filtering of diffusion processes," *SIAM Journal on Control and Optimization*, vol. 27, pp. 786–813, 1989.

[64] A. V. Savkin, R. Evans, and E. Skafidas, "The problem of optimal robust sensor scheduling," *Systems & Control Letters*, vol. 43, pp. 149–157, 2001.

[65] J. S. Evans and V. Krishnamurthy, "Optimal sensor scheduling for hidden Markov model state estimation," *International Journal of Control*, vol. 74, no. 18, pp. 1737–1742, 2001.

[66] W. Wu and A. Arapostathis, "Optimal sensor querying: general Markovian and LQG models with controlled observations," *IEEE Transactions on Automatic Control*, vol. 53, no. 6, pp. 1392–1405, 2008.

[67] M. Miskowicz, "Asymptotic effectiveness of the event-based sampling according to the integral criterion," *Sensors*, vol. 7, pp. 16–37, 2007.

[68] J. W. Marck and J. Sijs, "Relevant sampling applied to event-based state-estimation," in *Proceedings of the 4th International Conference on Sensor Technologies and Applications*, 2010, pp. 618–624.

[69] D. Zhang, W. Cai, and Q.-G. Wang, "Energy-efficient $h_\infty$ filtering for networked systems with stochastic signal transmissions," *Signal Processing*, vol. 101, pp. 134–141, 2014.

[70] R. Cogill, S. Lall, and J. P. Hespanha, "A constant factor approximation algorithm for event-based sampling," in *Proceedings of the 2007 American Control Conference*, 2007, pp. 305 – 311.

[71] G. M. Lipsa and N. C. Martins, "Remote state estimation with communication costs for first-order LTI systems," *IEEE Transactions on Automatic Control*, vol. 56, no. 9, pp. 2013–2025, 2011.

[72] A. Nayyar, T. Basar, D. Teneketzis, and V. V. Veeravalli, "Optimal strategies for communication and remote estimation with an energy harvesting sensor," *IEEE Transactions on Automatic Control*, vol. 58, no. 9, pp. 2246–2260, 2013.

[73] L. Berbakov, C. Antón-Haro, and J. Matamoros, "Optimal transmission policy for cooperative transmission with energy harvesting and battery operated sensor nodes," *Signal Processing*, vol. 93, no. 11, pp. 3159–3170, 2013.

[74] Y. Li, D. E. Quevedo, V. Lau, S. Dey, and L. Shi, "Transmission power schedule for energy harvesting sensor in remote state estimation," in *Proceedings of the 19th IFAC World Congress*, 2014, pp. 122–127.

[75] O. C. Imer and T. Basar, "Optimal estimation with limited measurements," in *Proceedings of the 44th IEEE Conference on Decision and Control*, 2005, pp. 1029 – 1034.

[76] Y. Xu and J. P. Hespanha, "Optimal communication logics in networked control systems," in *Proceedings of the 43rd IEEE Conference on Decision and Control*, 2004, pp. 3527–3532.

[77] A. Molin and S. Hirche, "On LQG joint optimal scheduling and control under communication constraints," in *Proceedings of the 48th IEEE Conference on Decision and Control*, 2009, pp. 5832–5838.

[78] Y. Sun and D. B. Work, "Kalman filtering with synthetic measurements under an event-triggered sensor scheduler," in *Proceedings of the 15th European Control Conference*. IEEE, 2016, pp. 2533–2540.

[79] Y. Sun and D. B. Work, "Online estimation with synthetic measurements under an event-triggered sensor scheduler," *submitted to Signal Processing*, 2017.

[80] J. Wu, Q. Jia, K. H. Johansson, and L. Shi, "Event-based sensor data scheduing: trade-off between communication rate and estimation quality," *IEEE Transactions on Automatic Control*, vol. 58, no. 4, pp. 1041–1046, 2013.

[81] K. You and L. Xie, "Kalman filtering with scheduled measurements," *IEEE Transactions on Signal Processing*, vol. 61, no. 6, pp. 1520–1530, 2013.

[82] D. Han, Y. Mo, J. Wu, S. Weerakkody, B. Sinopoli, and L. Shi, "Stochastic event-triggered sensor schedule for remote state estimation," *IEEE Transactions on Automatic Control*, vol. 60, no. 10, pp. 2661–2675, 2015.

[83] S. Weerakkody, Y. Mo, B. Sinopoli, D. Han, and L. Shi, "Multi-sensor scheduling for state estimation with event-based, stochastic triggers," in *Proceedings of the 4th IFAC Workshop on Distributed Estimation and Control in Networked Systems*, 2013.

[84] S. Fan, Y. Sun, B. Piccoli, B. Seibold, and D. B. Work, "A collapsed generalized Aw-Rascle-Zhang model and its model accuracy," *arXiv preprint arXiv:1702.03624*, 2017.

[85] A. Y. L. Roux, "On the convergence of the Godounov's scheme for first order quasi linear equations," *Proceedings of the Japan Academy*, vol. 52, no. 9, pp. 488–491, 1976.

[86] G. Bretti, R. Natalini, and B. Piccoli, "Numerical approximations of a traffic flow model on networks," *NHM*, vol. 1, no. 1, pp. 57–84, 2006.

[87] R. E. Kalman et al., "A new approach to linear filtering and prediction problems," *Journal of Basic Engineering*, vol. 82, no. 1, pp. 35–45, 1960.

[88] Y. Sun and D. B. Work, "Scaling the Kalman filter for large-scale traffic estimation," *arXiv preprint arXiv:1608.00917*, 2016. [Online]. Available: http://arxiv.org/abs/1608.00917

[89] H. Khalil, *Nonlinear systems*, 3rd ed. Prentice Hall, 2002.

[90] D. Liberzon, *Switching in systems and control*. Springer Science & Business Media, 2012.

[91] D. Xie, H. Zhang, H. Zhang, and B. Wang, "Exponential stability of switched systems with unstable subsystems: a mode-dependent average dwell time approach," *Circuits, Systems, and Signal Processing*, vol. 32, no. 6, pp. 3093–3105, 2013.

[92] Y. Li, C. G. Claudel, B. Piccoli, and D. B. Work, "A convex formulation of traffic dynamics on transportation networks," *arXiv preprint arXiv:1702.03908*, 2016. [Online]. Available: https://arxiv.org/abs/1702.03908

[93] Y. Bar-Shalom, X. R. Li, and T. Kirubarajan, *Estimation with applications to tracking and navigation*, 1st ed. Wiley-Interscience, 2001.

[94] C. Godsil and G. Royle, *Algebraic graph theory*. Springer, 2001.

[95] G. Battistelli, A. Benavoli, and L. Chisci, "Data-driven communication for state estimation with sensor networks," *Automatica*, vol. 48, no. 5, pp. 926–935, 2012.

[96] B. Sinopoli, L. Schenato, M. Franceschetti, K. Poolla, M. Jordan, and S. Sastry, "Kalman filtering with intermittent observations," *IEEE Transactions on Automatic Control*, vol. 49, no. 9, pp. 1453–1464, 2004.

[97] J. Kaipio and E. Somersalo, *Statistical and computational inverse problems*. New York, NY: Springer, 2005.

[98] C. Chen, *Linear system theory and design*, 3rd ed. Oxford University Pressl, 1999.

[99] C. Chui and G. Chen, *Kalman filtering with real-time applications*, 4th ed. Springer, 2009.

# APPENDIX A

# EXAMPLE OF THE DIVERGENCE OF THE MEAN ERROR UNDER AN UNOBSERVABLE SYSTEM

Consider a linear discrete system describing the evolution of a moving object. The state vector is constructed as $\rho_k = \left(\rho_k^1, \rho_k^2, \rho_k^3\right)$, where $\rho_{k|k}^1$, $\rho_{k|k}^2$, and $\rho_{k|k}^3$ are the location, speed, and acceleration of the moving object at time $k \in \mathbb{N}$, respectively. The moving object travels with a constant acceleration. The system dynamics is given by

$$\rho_{k+1} = A_k \rho_k + \omega_k, \quad \rho_k \in \mathbb{R}^3, \tag{A.1}$$

where $\omega_k \sim \mathbf{N}(\mathbf{0}, Q_k)$, the state transition matrix and the model error covariance matrices are given as follows:

$$A_k = \begin{pmatrix} 1 & 1 & 0.5 \\ 0 & 1 & 1 \\ 0 & 0 & 1 \end{pmatrix}, \quad Q_k = \begin{pmatrix} 1 & 0 & 0 \\ 0 & 1 & 0 \\ 0 & 0 & 1 \end{pmatrix}, \quad \text{for all } k.$$

The initial state is $\rho_0 = (2, 1, 0.05)^\top$. The sensor measures the acceleration of the moving object, i.e., the measurement is modeled by

$$z_k = H_k \rho_k + v_k, \quad z_k \in \mathbb{R}, \tag{A.2}$$

where

$$H_k = \begin{pmatrix} 0 & 0 & 1 \end{pmatrix}, \quad v_k \sim \mathbf{N}(0, R_k) \text{ with } R_k = 1, \quad \text{for all } k.$$

We use the KF (3.1)-(3.2) to estimate the state, where the initial condition is set to be $\boldsymbol{\eta}_{0|0} = (3, 2, 0.2)^\top$ and $\Gamma_{0|0} = I_3$.

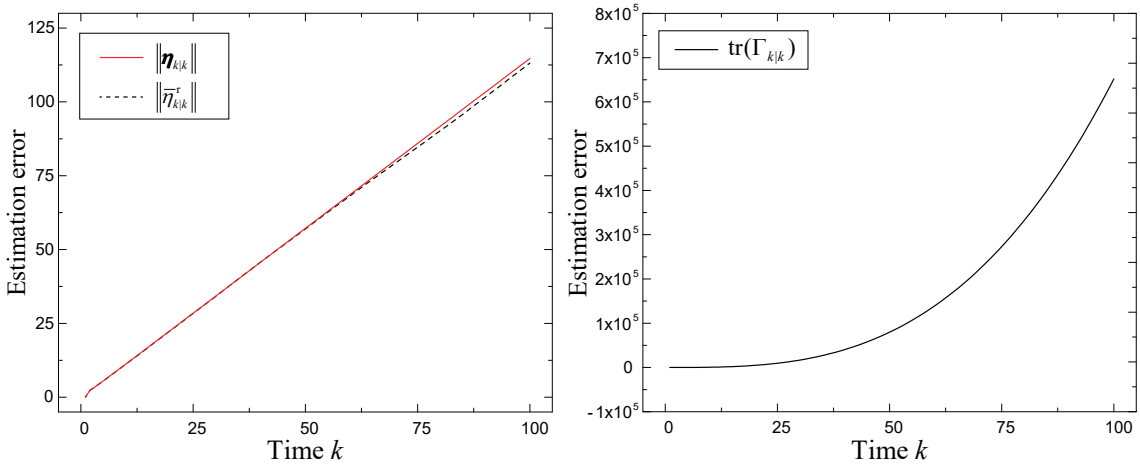


(a) Evolution of the estimation errors (b) Evolution of the error covariance (trace)

Figure A.1: Example: using the KF to track the unobservable system (A.1)-(A.2).

The system (A.1)-(A.2) is not observable, which can be concluded by computing its observability matrix [98, Theorem 6.O1], and showing that the observability matrix is not full rank. The mean estimation error evolves as the following equation:

$$\boldsymbol{\eta}_{k|k} = (I - K_k H_k)\, A_{k-1} \boldsymbol{\eta}_{k-1|k-1}. \tag{A.3}$$

In Figure A.1a, the solid curve shows the analytical evolution of $\left\|\boldsymbol{\eta}_{k|k}\right\|$ which follows (A.3). A Monte Carlo test of $N_r = 10,000$ realizations of the KF is also conducted, and the dashed curve in Figure A.1a shows the empirical evolution of the estimation error $\left\|\bar{\eta}^{r}_{k|k}\right\|$, where $\bar{\eta}^{r}_{k|k} = \frac{1}{N_r}\sum_{\tau=1}^{N_r} \eta^{\tau}_{k|k}$, and $\eta^{\tau}_{k|k}$ is the posterior estimation error at time $k$ on the $\tau^{\text{th}}$ realization. We also plot in Figure A.1b the trace of the estimation error covariance $\text{tr}(\Gamma_{k|k})$. It is shown that different from the observable scenario described in Lemma 2, the error covariance and the estimation error diverge as $k$ increases in this example, which is typical for unobservable linear systems.

# APPENDIX B

# OBSERVABLE AND UNOBSERVABLE SUBSYSTEMS IN THE UNOBSERVABLE MODES

In an unobservable mode, the SMM and the SMM-J can be transformed to the *Kalman observability canonical form*. The transformed state consists of the observable and the unobservable parts, i.e.,

$$\check{\rho}_k = U\rho_k = \begin{pmatrix} \check{\rho}_k^{(1)} \\ \check{\rho}_k^{(2)} \end{pmatrix},$$

where $U$ is an orthogonal matrix, $\check{\rho}_k^{(1)} \in \mathbb{R}^{d_1}$ and $\check{\rho}_k^{(2)} \in \mathbb{R}^{d_2}$ are the state in the observable and unobservable subsystems, respectively, with $d_1 + d_2 = n$. As a consequence, the system dynamics of the SMM and the SMM-J can be transformed to the following formula:

$$\begin{aligned} \check{\rho}_{k+1} &= \check{A}_k\rho_k + \check{u}_k + \check{\omega}_k, \quad \rho_k \in \mathbb{R}^n, \\ z_k &= \check{H}_k\check{\rho}_k + v_k, \quad z_k \in \mathbb{R}^m, \end{aligned}$$

where the transformed state transition matrix $\check{A}_k$ and the transformed observation matrix $\check{H}_k$ can also be partitioned according to the observable and unobservable subsystems, i.e.,

$$\check{A}_k = UA_kU^\top = \begin{pmatrix} \check{A}_k^{(1)} & \mathbf{0}_{d_1,d_2} \\ \check{A}_k^{(21)} & \check{A}_k^{(2)} \end{pmatrix}, \quad \check{H}_k = H_kU^\top = \begin{pmatrix} \check{H}_k^{(1)} & \mathbf{0} \end{pmatrix}, \tag{B.1}$$

with $\check{H}_k^{(1)} \in \mathbb{R}^{m\times d_1}$ defined as follows:

$$\check{H}_k^{(1)} = \begin{cases} I_m & \text{if } d_1 = m \\ \begin{pmatrix} I_m & \mathbf{0}_{m,d_1-m} \end{pmatrix} & \text{if } d_1 > m, \end{cases} \quad \text{for all } k.$$

Moreover, the transformed system input is given by $\check{u}_k = Uu_k$, and the transformed model noise is given by $\check{w}_k = Uw_k \sim \mathbf{N}(\mathbf{0}, \check{Q}_k)$, where the transformed model error covariance $\check{Q}_k$ can be partitioned to blocks corresponding to the observable and unobservable subsystems, i.e.,

$$\check{Q}_k = UQ_kU^\top = \begin{pmatrix} \check{Q}_k^{(1)} & \check{Q}_k^{(12)} \\ \check{Q}_k^{(21)} & \check{Q}_k^{(2)} \end{pmatrix}.$$

Divide the prior estimation error covariance matrix based on the observable and unobservable subsystems as follows:

$$\check{\Gamma}_{k|k-1} = \begin{pmatrix} \check{\Gamma}_{k|k-1}^{(1)} & \check{\Gamma}_{k|k-1}^{(12)} \\ \check{\Gamma}_{k|k-1}^{(21)} & \check{\Gamma}_{k|k-1}^{(2)} \end{pmatrix}.$$

In the KF, the prior error covariance matrix is computed recursively by the Riccati equation

$$\check{\Gamma}_{k+1|k} = \check{A}_k \left( \check{\Gamma}_{k|k-1} - \check{\Gamma}_{k|k-1}\check{H}_k^\top \left( \check{H}_k \check{\Gamma}_{k|k-1} \check{H}_k^\top + R_k \right)^{-1} \check{H}_k \check{\Gamma}_{k|k-1} \right) \check{A}_k^\top + \check{Q}_k, \tag{B.2}$$

Define

$$\check{\Upsilon}_k^{(1)} = \check{A}_k^{(1)} - \check{A}_k^{(1)} \check{\Gamma}_{k|k-1}^{(1)} \left( \check{H}_k^{(1)} \right)^\top \left( \check{H}_k \check{\Gamma}_{k|k-1} \check{H}_k^\top + R_k \right)^{-1} \check{H}_k^{(1)} = \check{A}_k^{(1)} - \check{A}_k^{(1)} \check{K}_k^{(1)} \check{H}_k^{(1)},$$

and apply partition into observable and unobservable subsystems to both sides of (B.2), we obtain the following two blocks of equations describing the evolutions of $\check{\Gamma}_{k+1|k}^{(1)}$ and $\check{\Gamma}_{k+1|k}^{(12)}$ :

$$\check{\Gamma}_{k+1|k}^{(1)} = \check{\Upsilon}_k^{(1)} \check{\Gamma}_{k|k-1}^{(1)} \left( \check{A}_k^{(1)} \right)^\top + \check{Q}_k^{(1)}, \tag{B.3}$$

$$\check{\Gamma}_{k+1|k}^{(12)} = \check{\Upsilon}_k^{(1)} \check{\Gamma}_{k|k-1}^{(12)} \left( \check{A}_k^{(2)} \right)^\top + \check{\Upsilon}_k^{(1)} \check{\Gamma}_{k|k-1}^{(1)} \left( \check{A}_k^{(21)} \right)^\top + \check{Q}_k^{(12)}. \tag{B.4}$$

We present below an example showing the observable and unobservable subsystems for the FC mode of the SMM.

**Example 4.** *We transform the state vector as follows:*

$$\check{\rho}_k = U\rho_k, \tag{B.5}$$

*where the* $(r,c)^{th}$ *entry of* $U$ *is defined as*

$$U(r,c) = \begin{cases} 1 & \text{if } r = r+1 \text{ and } i \geq 3 \\ 1 & \text{if } r = c = 1 \\ 1 & \text{if } r = 2 \text{ and } c = n \\ 0 & \text{otherwise.} \end{cases} \tag{B.6}$$

*Basically, the transformation* $U$ *makes*

$$\check{\rho}_k^2 = \rho_k^n, \quad \text{and } \check{\rho}_k^i = \rho_k^{i-1} \text{ for } i \in \{3, 4, \cdots, n\}.$$

*Hence, after transforming system* (2.13)-(2.16) *according to* (B.5) *and* (B.6)*, the observable subsystem* $\check{\rho}_k^{(1)}$ *consists of the densities of the first and last cells in the freeway section, and the unobservable subsystem* $\check{\rho}_k^{(2)}$ *is formed by the densities of the interior cells in the section.*

*As shown in Section 2.3.2.1, before transforming the state, the state transition matrix* $A_k \in \mathbb{R}^{n\times n}$ *takes the following form in an unobservable mode:*

$$A_\sigma^s = \begin{pmatrix} \Theta_{\tilde{s}} & \mathbf{0}_{\tilde{s},1} & \mathbf{0}_{\tilde{s},\bar{s}} \\ \frac{v_m \Delta t}{\Delta x} E_{1,\tilde{s}}^{1,\tilde{s}} & 1 & \frac{w\Delta t}{\Delta x} E_{1,\bar{s}}^{1,1} \\ \mathbf{0}_{\bar{s},\tilde{s}} & \mathbf{0}_{\bar{s},1} & \Delta_{\bar{s}} \end{pmatrix}.$$

*After state transformation,* $A_k$ *is transformed to* $\check{A}_k$ *as stated in* (B.1)*, where*

$$\check{A}^{(1)} = \begin{pmatrix} 1 - \frac{v_m \Delta t}{\Delta x} & \\ & 1 - \frac{w\Delta t}{\Delta x} \end{pmatrix} \in \mathbb{R}^{2\times 2}, \quad \check{A}^{(21)} = \begin{pmatrix} \frac{v_m \triangle t}{\triangle x} & 0 \\ 0 & 0 \\ \vdots & \vdots \\ 0 & 0 \\ 0 & \frac{w\triangle t}{\triangle x} \end{pmatrix} \in \mathbb{R}^{(n-2)\times 2},$$

*and*

$$\check{A}_k^{(2)} = \begin{pmatrix} \Theta_{d_1} & \mathbf{0}_{d_1,1} & \mathbf{0}_{d_1,\bar{d}_2} \\ \begin{pmatrix} \mathbf{0}_{1,d_1-1} & \frac{v_{\mathrm{m}}\Delta t}{\Delta x} \end{pmatrix} & 1 & \begin{pmatrix} \frac{w\Delta t}{\Delta x} & \mathbf{0}_{1,d_2-1} \end{pmatrix} \\ \mathbf{0}_{d_2,d_1} & \mathbf{0}_{d_2,1} & \Delta_{d_2} \end{pmatrix} \in \mathbb{R}^{(n-2)\times(n-2)}.$$

*The transformed observation matrix is given by* $\check{H} = \begin{pmatrix} \check{H}^{(1)} & \mathbf{0} \end{pmatrix}$*, where* $\check{H}^{(1)} = I_2$*.*

# APPENDIX C

# PROOF OF LEMMAS

## C.1 Proof of Lemma 1

In order to show the uniform complete observability, we first need to find a finite integer $T > 0$ such that rank $\left(\mathcal{I}_{\bar{k},\underline{k}}\right) = n$ for all $\bar{k} - \underline{k} \geq T$. The observability grammian matrix is defined as

$$\mathcal{G}_{\bar{k},\underline{k}} = \sum_{k=\underline{k}}^{\bar{k}} \Xi_{k,\underline{k}}^{\top} H_k^{\top} R_k^{-1} H_k \Xi_{k,\underline{k}} = \Xi_{\bar{k},\underline{k}}^{\top} \mathcal{I}_{\bar{k},\underline{k}} \Xi_{\bar{k},\underline{k}},$$

where $\Xi_{\cdot,\cdot}$ is defined in (2.5). Hence, the observability matrix $\mathcal{G}_{\bar{k},\underline{k}}$ and the information matrix defined in (2.4) have the same rank, and it is sufficient to find a $T$ such that rank $\left(\mathcal{G}_{\bar{k},\underline{k}}\right) = n$ for all $\bar{k} - \underline{k} \geq T$. Given the assumption that $r_1 I < R_k < r_2 I$ in (Asm.4), the observability grammian matrix satisfies

$$\mathcal{G}_{\bar{k},\underline{k}} > r_2^{-1} \sum_{k=\underline{k}}^{\bar{k}} \Xi_{k,\underline{k}}^{\top} H_b^{\top} H_b \Xi_{k,\underline{k}} = r_2^{-1} \tilde{\mathcal{G}}_{\bar{k},\underline{k}}^{\top} \tilde{\mathcal{G}}_{\bar{k},\underline{k}}, \tag{C.1}$$

where

$$\tilde{\mathcal{G}}_{\bar{k},\underline{k}} = \begin{pmatrix} H_b \\ H_b A_{\underline{k}} \\ H_b A_{\underline{k}+1} A_{\underline{k}} \\ \vdots \\ H_b \prod_{k=\bar{k}-1}^{\underline{k}} A_k \end{pmatrix}, \tag{C.2}$$

with $A_k \in \mathcal{A}_{\mathrm{O}} := \{A_{\mathrm{FF}}, A_{\mathrm{CC}}, A_{\mathrm{CF}}^s \,|s \in \{1, 2, \cdots, n-1\}\}$. It can be shown after some basic linear algebra that for $A_k \in \mathcal{A}_{\mathrm{O}}$

$$H_b \prod_{k=\underline{k}+\iota-1}^{\underline{k}} A_k = \begin{pmatrix} \tilde{g}_{1,1}^{\iota} & \cdots & \tilde{g}_{1,\iota_1}^{\iota} & 0 & 0 & \cdots & 0 \\ 0 & \cdots & 0 & 0 & \tilde{g}_{2,n-\iota_2+1}^{\iota} & \cdots & \tilde{g}_{2,n}^{\iota} \end{pmatrix} \in \mathbb{R}^{2\times n}, \tag{C.3}$$

where $\iota_1 \leq \iota + 1$, $\iota_2 \leq \iota + 1$ and $\iota_1 + \iota_2 \geq \iota + 2$, the elements $\tilde{g}_{\cdot,\cdot}^{\iota} > 0$ are functions of $A_k$ for $k \in [\underline{k}, \underline{k} + \iota)$. Recall that $M(r, c)$ denotes the $(r, c)$-th entry of matrix $M$. Given properties (P.1)-(P.2) of the state transition matrices we have

$$\underline{\theta}^{\iota} \leq \tilde{g}_{1,\kappa_1}^{\iota} \leq 1, \quad \underline{\theta}^{\iota} \leq \tilde{g}_{2,n-\kappa_2+1} \leq 1 \quad \text{for } \kappa_1 \in \{1, \cdots, \iota_1\} \text{ and } \kappa_2 \in \{1, \cdots, \iota_2\},$$

where $\underline{\theta} = \min\{v_{\mathrm{m}} \frac{\Delta t}{\Delta x}, 1 - v_{\mathrm{m}} \frac{\Delta t}{\Delta x}, w \frac{\Delta t}{\Delta x}, 1 - w \frac{\Delta t}{\Delta x}\}$. Consequently, the rank of the observability grammian matrix and the rank of the information matrix satisfy

$$\operatorname{rank}\left(\tilde{\mathcal{G}}_{\bar{k},\underline{k}}\right) = n = \operatorname{rank}\left(\mathcal{G}_{\bar{k},\underline{k}}\right) = \operatorname{rank}\left(\mathcal{I}_{\bar{k},\underline{k}}\right), \quad \text{when } \bar{k} - \underline{k} \geq \max\{1, n-2\}.$$

Hence, it can be concluded that $\mathcal{I}_{k,k-T_1} > \mathbf{0}$ for all $k \geq T_1$. Consequently, for $k \geq T_1$,

$$\mathcal{I}_{k,k-T_1} = \sum_{\iota=k-T_1}^{k} \Xi_{\iota,k}^{\top} H_{\iota}^{\top} R_{\iota}^{-1} H_{\iota} \Xi_{\iota,k} > r_2^{-1} \sum_{\iota=k-T_1}^{k} \Xi_{\iota,k}^{\top} H_b^{\top} H_b \Xi_{\iota,k} \geq \alpha_{\mathcal{I}} I > \mathbf{0}, \tag{C.4}$$

where $\alpha_{\mathcal{I}} > 0$ is defined in (2.18). Also note that the information matrix satisfies

$$\mathcal{I}_{k,k-T_1} = \sum_{\iota=k-T_1}^{k} \Xi_{\iota,k}^{\top} H_b^{\top} R_{\iota}^{-1} H_b \Xi_{\iota,k} < r_1^{-1} \sum_{\iota=k-T_1}^{k} \Xi_{\iota,k}^{\top} \Xi_{\iota,k} \leq \beta_{\mathcal{I}} I, \quad \text{for } k \geq T_1, \tag{C.5}$$

where $\beta_{\mathcal{I}} > 0$ is defined in (2.18). Combining (C.4) and (C.5), we obtain

$$\alpha_{\mathcal{I}} I < \mathcal{I}_{k,k-T_1} < \beta_{\mathcal{I}} I, \quad \text{for all } k \geq T_1 = \max\{1, n-2\}.$$

## C.2 Proof of Lemma 3

The proof can be done based on the uniform complete observability and controllability of the system under switches among the observable modes. The information matrix for time interval $k \in [\underline{k}, \bar{k}]$ is defined in (2.4), and we define below the controllability matrix for time interval $k \in [\underline{k}, \bar{k}]$:

$$\mathcal{C}_{\bar{k},\underline{k}} = \sum_{k=\underline{k}}^{\bar{k}-1} \Xi_{\bar{k},k+1} Q_{k+1} \Xi_{\bar{k},k+1}^{\top}.$$

When the system switches among the observable modes of the SMM, the state transition matrix satisfies:

$$A_k \in \mathcal{A}_{\mathrm{O}}, \quad \text{for all } k.$$

**Step 1**: The uniform complete observability of the system is analyzed in Lemma 1(see the proof in Appendix C.1), where it is shown that

$$\alpha_{\mathcal{I}} I < \mathcal{I}_{k,k-T_1} < \beta_{\mathcal{I}} I, \quad \text{for all } k \geq T_1 = \max\{1, n-2\}.$$

**Step 2**: Deriving the uniform complete controllability of the system. For $k \geq T_1 = \max\{1, n-2\}$, the controllability matrix is given by

$$\mathcal{C}_{k,k-T_1} = \sum_{\iota=k-T_1}^{k-1} \Xi_{k,\iota+1} Q_{\iota+1} \Xi_{k,\iota+1}^{\top} > \mathbf{0}.$$

It follows that

$$\mathbf{0} < \alpha_{\mathcal{C}} I < \mathcal{C}_{k,k-T_1} < \beta_{\mathcal{C}} I, \quad \text{for all } k \geq T_1 = \max\{1, n-2\},$$

with $0 < \alpha_{\mathcal{C}} < \beta_{\mathcal{C}}$ defined in (3.4).

**Step 3**: Combining Steps 1 and 2 we obtain that for all $k \geq T_1 = \max\{1, n-2\}$

$$\min\{\alpha_{\mathcal{I}}, \alpha_{\mathcal{C}}\} I < \mathcal{I}_{k,k-T_1} < \max\{\beta_{\mathcal{I}}, \beta_{\mathcal{C}}\} I,$$
$$\min\{\alpha_{\mathcal{I}}, \alpha_{\mathcal{C}}\} I < \mathcal{C}_{k,k-T_1} < \max\{\beta_{\mathcal{I}}, \beta_{\mathcal{C}}\} I.$$

Based on the assumption that $\Gamma_{0|0} > \mathbf{0}$, it is concluded according to Lemma 7.1 and Lemma 7.2 in [19] that

$$\mathbf{0} < \left( \frac{\min\{\alpha_{\mathcal{I}}, \alpha_{\mathcal{C}}\}}{1 + \min\{\alpha_{\mathcal{I}}, \alpha_{\mathcal{C}}\} \max\{\beta_{\mathcal{I}}, \beta_{\mathcal{C}}\}} \right) I < \Gamma_{k|k} < \left( \frac{1 + \min\{\alpha_{\mathcal{I}}, \alpha_{\mathcal{C}}\} \max\{\beta_{\mathcal{I}}, \beta_{\mathcal{C}}\}}{\min\{\alpha_{\mathcal{I}}, \alpha_{\mathcal{C}}\}} \right) I$$

for all $k \geq T_1 = \max\{1, n-2\}$, which concludes the proof.

## C.3 Proof of Lemma 4

We first derive some inequalities which will be used in deriving the upper bound of error covariance. Define

$$\bar{e}_\iota = \max_{M_\kappa \in \mathcal{A}_{\mathrm{O}}} \left\{ \sigma_{\max} \left( \prod_{\kappa=\iota-1}^{0} M_\kappa \prod_{\kappa=0}^{\iota-1} M_\kappa^\top \right) \right\}, \quad \text{for all } \iota \in \mathbb{Z}^+,$$

where $\sigma_{\max}(\cdot)$ and $\sigma_{\min}(\cdot)$ are the maximum and minimum singular values of a matrix. Due to properties (P.1)-(P.2) that

$$\begin{aligned} &0 \leq M(r,c) \leq 1, \quad \text{for all } M \in \mathcal{A}_{\mathrm{O}} \text{ and } r, c \in \{1, 2, \cdots, n\}, \\ &\sum_{r=1}^{n} M(r,c) \leq 1, \quad \text{for all } M \in \mathcal{A}_{\mathrm{O}} \text{ and } c \in \{1, 2, \cdots, n\}, \end{aligned}$$

and $M(r,c) = 0$ for all $M \in \mathcal{A}_{\mathrm{O}}$ when $|r-c| > 1$.

It is concluded that the $(r,c)$-th entry of $\prod_{\kappa=\iota-1}^{0} M_\kappa$ satisfies

$$\left( \prod_{\kappa=\iota-1}^{0} M_\kappa \right)(r,c) \begin{cases} = 0, & \text{if } |r-c| > \iota + 1, \\ \leq 1, & \text{otherwise.} \end{cases}$$

Hence the diagonal entries of $\prod_{\kappa=\iota-1}^{0} M_\kappa \prod_{\kappa=0}^{\iota-1} M_\kappa^\top$ satisfies

$$\left( \prod_{\kappa=\iota-1}^{0} M_\kappa \prod_{\kappa=0}^{\iota-1} M_\kappa^\top \right)(r,r) \leq 2\iota + 1, \quad \text{for all } r \in \{1, 2, \cdots, n\},$$

thus

$$\sigma_{\max} \left( \prod_{\kappa=\iota-1}^{0} M_\kappa \prod_{\kappa=0}^{\iota-1} M_\kappa^\top \right) < 2(2\iota + 1). \tag{C.6}$$

Consequently, it is concluded that

$$\bar{e}_\iota < 2(2\iota + 1). \tag{C.7}$$

**Step 1**: In this step, we derive an upper bound of $\Gamma_{k|k}$ for $k \in [0, \max\{1, n-2\})$. When $0 \le k < \max\{1, n-2\}$, the error covariance matrix satisfies

$$\begin{aligned}
\Gamma_{k|k} \le \Gamma_{k|k-1} &= A_{k-1}\Gamma_{k-1|k-1}A_{k-1}^\top + Q_{k-1} \\
&\le \left(\prod_{\kappa=k-1}^{0} A_\kappa\right)\Gamma_{0|0}\left(\prod_{\kappa=0}^{k-1} A_\kappa^\top\right) + Q_{k-1} + \sum_{\iota=1}^{k-1}\left(\prod_{\kappa=k-1}^{\iota} A_\kappa\right)Q_{\iota-1}\left(\prod_{\kappa=\iota}^{k-1} A_\kappa^\top\right) \\
&= \Xi_{k,0}\Gamma_{0|0}\Xi_{k,0}^\top + Q_{k-1} + \sum_{\iota=1}^{k-1}\Xi_{k,\iota}Q_{\iota-1}\Xi_{k,\iota}^\top \\
&< \left(\bar{e}_k\left\|\Gamma_{0|0}\right\| + q_2 + \sum_{\iota=1}^{k-1}\bar{e}_{k-\iota}q_2\right) I \\
&< \left(2\left(2k+1\right)\left\|\Gamma_{0|0}\right\| + q_2 + 2\sum_{\iota=1}^{k-1}\left(2\left(k-\iota\right)+1\right)q_2\right) I \quad \text{(due to (C.7))} \\
&= \left(2\left(2k+1\right)\left\|\Gamma_{0|0}\right\| + \left(2k^2-1\right)q_2\right) I.
\end{aligned}$$

Hence, the error covariance satisfies

$$\Gamma_{k|k} \le \begin{cases} \left(2\left(2n-5\right)\left\|\Gamma_{0|0}\right\| + \left(2\left(n-3\right)^2-1\right)q_2\right) I & \text{if } n \ge 4 \\ \left\|\Gamma_{0|0}\right\| I & \text{if } 2 \le n < 4. \end{cases}$$

**Step 2**: In this step, we derive a lower bound of $\Gamma_{k|k}$ for $k \in [0, \max\{1, n-2\})$. Consider a matrix sequence computed as follows

$$\underline{\Gamma}_{k+1|k} = \underline{A}_k\left(\underline{\Gamma}_{k|k-1} - \underline{\Gamma}_{k|k-1}\underline{H}_k^\top(\underline{H}_k\underline{\Gamma}_{k|k-1}\underline{H}_k^\top + \underline{R}_k)^{-1}\underline{H}_k\underline{\Gamma}_{k|k-1}\right)\underline{A}_k^\top + \underline{Q}_k,$$

where

$$\underline{A}_k = A_k, \quad \underline{H}_k = H_k, \quad \underline{R}_k = R_k, \quad \underline{Q}_k = Q_k, \quad \text{for all } k \ge 0, \quad \text{and } \underline{\Gamma}_{0|-1} = \mathbf{0}.$$

Due to Lemma 6.2 in [99], it holds that $\Gamma_{k+1|k} > \underline{\Gamma}_{k+1|k}$ if $\Gamma_{k|k-1} > \underline{\Gamma}_{k|k-1}$. By definition we have $\Gamma_{0|-1} \geq \Gamma_{0|0} > \underline{\Gamma}_{0|-1} = \mathbf{0}$, which implies that $\underline{\Gamma}_{k+1|k} < \Gamma_{k+1|k}$ for all $k \geq 0$. Also due to Section 4.4 in [18], we have $\underline{\Gamma}_{k+1|k} > \underline{\Gamma}_{k|k-1}$ for all $k \geq 0$ since $\underline{\Gamma}_{0|-1} = \mathbf{0}$. This yields

$$\Gamma_{k|k-1} > \underline{\Gamma}_{1|0} = \underline{A}_0 \underline{\Gamma}_{0|0} \underline{A}_0^\top + \underline{Q}_0 > q_1 I, \quad \text{for all } k \geq 1,$$

where the second inequality is due to the fact that $\underline{\Gamma}_{0|0} = \mathbf{0}$ given $\underline{\Gamma}_{0|-1} = \mathbf{0}$, and $\underline{Q}_0 > q_1 I$. It follows that

$$\begin{aligned}\Gamma_{k|k} &= \left(\Gamma_{k|k-1}^{-1} + H_k^\top R_k^{-1} H_k\right)^{-1} > \left(\underline{\Gamma}_{1|0}^{-1} + H_k^\top R_k^{-1} H_k\right)^{-1} \\ &> \left(q_1^{-1} I + r_1^{-1} H_k^\top H_k\right)^{-1} > \left(q_1^{-1} + r_1^{-1}\right)^{-1} I, \quad \text{for all } k \geq 1.\end{aligned}$$

It follows that

$$\Gamma_{k|k} \geq \min\left\{\lambda_{\min}\left(\Gamma_{0|0}\right), \left(q_1^{-1} + r_1^{-1}\right)^{-1}\right\} I, \quad \text{for all } 0 \leq k < \max\{1, n-2\}.$$

Combining Steps 1 and 2 concludes the proof.

## C.4 Proof of Lemma 6

Let $V_k = \boldsymbol{\eta}_{k|k}^\top \Gamma_{k|k}^{-1} \boldsymbol{\eta}_{k|k}$ be the Lyapunov function candidate of system (3.8). According to Lemma 3 in [53], the one-step change of $V_k$ is given by

$$\begin{aligned}&\Delta V_{k+1} = V_{k+1} - V_k \\ =& -\boldsymbol{\eta}_{k|k}^\top \left(A_k^\top F_{k+1}^\top \Gamma_{k+1|k+1}^{-1} F_{k+1} A_k - \Gamma_{k|k}^{-1}\right) \boldsymbol{\eta}_{k|k} \\ =& -\boldsymbol{\eta}_{k|k}^\top \left(\Gamma_{k|k}^{-1} - A_k^\top \left(A_k \Gamma_{k|k} A_k^\top + Q_k + \Gamma_{k+1|k} H_{k+1}^\top R_{k+1}^{-1} H_{k+1} \Gamma_{k+1|k}\right)^{-1} A_k\right) \boldsymbol{\eta}_{k|k} \\ =& -\boldsymbol{\eta}_{k|k}^\top \Gamma_{k|k}^{-1} \left(\Gamma_{k|k}^{-1} + A_k^\top \left(Q_k + \Gamma_{k+1|k} H_{k+1}^\top R_{k+1}^{-1} H_{k+1} \Gamma_{k+1|k}\right)^{-1} A_k\right)^{-1} \Gamma_{k|k}^{-1} \boldsymbol{\eta}_{k|k} \\ =& -\boldsymbol{\eta}_{k|k}^\top \left(\Gamma_{k|k} + \Gamma_{k|k} A_k^\top \left(Q_k + \Gamma_{k+1|k} H_{k+1}^\top R_{k+1}^{-1} H_{k+1} \Gamma_{k+1|k}\right)^{-1} A_k \Gamma_{k|k}\right)^{-1} \boldsymbol{\eta}_{k|k} \\ \leq& -\left\|\Gamma_{k|k} + \Gamma_{k|k} A_k^\top \left(Q_k + \Gamma_{k+1|k} H_{k+1}^\top R_{k+1}^{-1} H_{k+1} \Gamma_{k+1|k}\right)^{-1} A_k \Gamma_{k|k}\right\|^{-1} \left\|\boldsymbol{\eta}_{k|k}\right\|^2,\end{aligned} \tag{C.8}$$

where

$$\begin{aligned}
&\left\|\Gamma_{k|k}+\Gamma_{k|k}A_k^\top\left(Q_k+\Gamma_{k+1|k}H_{k+1}^\top R_{k+1}^{-1}H_{k+1}\Gamma_{k+1|k}\right)^{-1}A_k\Gamma_{k|k}\right\| \\
\leq&\left\|\Gamma_{k|k}\right\|+\left\|\Gamma_{k|k}A_k^\top\left(Q_k+\Gamma_{k+1|k}H_{k+1}^\top R_{k+1}^{-1}H_{k+1}\Gamma_{k+1|k}\right)^{-1}A_k\Gamma_{k|k}\right\| \\
<&c_2+q_1^{-1}\left\|\Gamma_{k|k}A_k^\top A_k\Gamma_{k|k}\right\| \\
\leq&c_2+q_1^{-1}\left\|\Gamma_{k|k}\right\|\left\|A_k^\top A_k\right\|\left\|\Gamma_{k|k}\right\| \\
\leq&c_2+q_1^{-1}c_2^2\max_{M\in\mathcal{A}_{\mathrm{O}}}\sigma_{\max}^2(M),
\end{aligned} \tag{C.9}$$

Combining (C.8) and (C.9), we obtain that for all $k\in[\underline{k}_{\mathrm{O}},+\infty)$,

$$\Delta V_{k+1}<-\left(c_2+q_1^{-1}c_2^2\max_{M\in\mathcal{A}_{\mathrm{O}}}\sigma_{\max}^2(M)\right)^{-1}\left\|\boldsymbol{\eta}_{k|k}\right\|^2=-\mathrm{d}(c_1,c_2)\left\|\boldsymbol{\eta}_{k|k}\right\|^2.$$

Since $\mathbf{0}<c_1I\leq\Gamma_{k|k}\leq c_2I$ for all $k\in[\underline{k}_{\mathrm{O}},+\infty)$, it follows that

$$c_2^{-1}\left\|\boldsymbol{\eta}_{k|k}\right\|^2\leq V_k\leq c_1^{-1}\left\|\boldsymbol{\eta}_{k|k}\right\|^2,\quad\text{for all } k\in[\underline{k}_{\mathrm{O}},+\infty). \tag{C.10}$$

Consequently, the 2-norm of $\boldsymbol{\eta}_{k|k}$ satisfies

$$\begin{aligned}
\left\|\boldsymbol{\eta}_{k|k}\right\|\leq(c_2V_k)^{\frac{1}{2}}<&\left(c_2V_{\eta,0}\left(1-\mathrm{d}(c_1,c_2)\,c_1\right)^k\right)^{\frac{1}{2}} \\
\leq&\left(c_1^{-1}c_2\left\|\boldsymbol{\eta}_{0|0}\right\|^2\left(1-\mathrm{d}(c_1,c_2)\,c_1\right)^{k-\underline{k}_{\mathrm{O}}}\right)^{\frac{1}{2}} \\
=&\left(c_1^{-1}c_2\right)^{\frac{1}{2}}\left(\left(1-\mathrm{d}(c_1,c_2)\,c_1\right)^{\frac{1}{2}}\right)^k\left\|\boldsymbol{\eta}_{0|0}\right\|,\quad\text{for all } k\in[\underline{k}_{\mathrm{O}},+\infty).
\end{aligned} \tag{C.11}$$

Combining (3.8) and (C.11), we obtain

$$\left\|\prod_{\kappa=k-1}^{0}F_{\kappa+1}A_\kappa\right\|\leq\hat{a}\hat{q}^k,\quad\text{for all } k\in[\underline{k}_{\mathrm{O}},+\infty).$$

where $\hat{a}=\left(c_1^{-1}c_2\right)^{\frac{1}{2}}\geq1$, $0<\hat{q}=\left(1-\mathrm{d}(c_1,c_2)\,c_1\right)^{\frac{1}{2}}<1$.

## C.5 Proof of Lemma 7

As detailed in Appendix B, we transform the state vector according to observable and unobservable subsystems, i.e.,

$$\check{\rho}_k = U\rho_k = \begin{pmatrix} \check{\rho}_k^{(1)} \\ \check{\rho}_k^{(2)} \end{pmatrix},$$

where $\check{\rho}_k^{(1)} \in \mathbb{R}^{d_1}$ and $\check{\rho}_k^{(2)} \in \mathbb{R}^{d_2}$ are the state in the observable and unobservable subsystems, respectively. The transformed Kalman gain is given by

$$\check{K}_k = UK_k = \begin{pmatrix} \check{K}_k^{(1)} \\ \check{K}_k^{(21)} \end{pmatrix}, \tag{C.12}$$

where $\check{K}_k^{(1)}$ and $\check{K}_k^{(21)}$ correspond to the observable and unobservable subsystems, respectively, with

$$\check{K}_k^{(1)} = \check{\Gamma}_{k|k-1}^{(1)} \left(\check{H}_k^{(1)}\right)^\top \left(R_k + \check{H}_k^{(1)} \check{\Gamma}_{k|k-1}^{(1)} \left(\check{H}_k^{(1)}\right)^\top\right)^{-1}, \tag{C.13}$$

$$\check{K}_k^{(21)} = \check{\Gamma}_{k|k-1}^{(21)} \left(\check{H}_k^{(1)}\right)^\top \left(R_k + \check{H}_k^{(1)} \check{\Gamma}_{k|k-1}^{(1)} \left(\check{H}_k^{(1)}\right)^\top\right)^{-1}. \tag{C.14}$$

The proof consists of the following five steps. Step 1 derives an upper bound for $\left\|K_{\underline{k}_\mathrm{U}+1}\right\|_\infty$. Step 2 derives an upper bound of $\left\|\check{K}_k^{(1)}\right\|_\infty$ for $k \in (\underline{k}_\mathrm{U}+1, \bar{k}_\mathrm{U}]$. In Step 3, we study the convergence rate of the error dynamics of the observable subsystem, which is also related to the boundedness of $\check{K}_k^{(21)}$. Based on the convergence rate obtained in Step 3, Step 4 derives an upper bound of $\left\|\check{K}_k^{(21)}\right\|_\infty$ for $k \in (\underline{k}_\mathrm{U}+1, \bar{k}_\mathrm{U}]$. Step 5 combines the above steps together and concludes the proof.

**Step 1**: At time step $\underline{k}_\mathrm{U}+1$, the Kalman gain is computed as follows:

$$K_{\underline{k}_\mathrm{U}+1} = \Gamma_{\underline{k}_\mathrm{U}+1|\underline{k}_\mathrm{U}} H_{\underline{k}_\mathrm{U}+1}^\top \left(R_{\underline{k}_\mathrm{U}+1} + H_{\underline{k}_\mathrm{U}+1} \Gamma_{\underline{k}_\mathrm{U}+1|\underline{k}_\mathrm{U}} H_{\underline{k}_\mathrm{U}+1}^\top\right)^{-1},$$

where $\Gamma_{\underline{k}_{\mathrm{U}}+1|\underline{k}_{\mathrm{U}}} = A_{\underline{k}_{\mathrm{U}}}\Gamma_{\underline{k}_{\mathrm{U}}|\underline{k}_{\mathrm{U}}}A_{\underline{k}_{\mathrm{U}}}^{\top} + Q_{\underline{k}_{\mathrm{U}}}$. Given that $\left\|\Gamma_{\underline{k}_{\mathrm{U}}|\underline{k}_{\mathrm{U}}}\right\|_{\infty} \leq \sqrt{n}\left\|\Gamma_{\underline{k}_{\mathrm{U}}|\underline{k}_{\mathrm{U}}}\right\|$, $\|Q_k\|_{\infty} < \sqrt{n}q_2$, and define

$$a_1 = \max_{k\in(\underline{k}_{\mathrm{U}},\bar{k}_{\mathrm{U}}]}\left\{\|A_k\|_{\infty}\right\}, \quad a_2 = \max_{k\in(\underline{k}_{\mathrm{U}},\bar{k}_{\mathrm{U}}]}\left\{\left\|A_k^{\top}\right\|_{\infty}\right\},$$

the prior error covariance at time $\underline{k}_{\mathrm{U}}+1$ satisfies

$$\left\|\Gamma_{\underline{k}_{\mathrm{U}}+1|\underline{k}_{\mathrm{U}}}\right\|_{\infty} \leq \left\|A_{\underline{k}_{\mathrm{U}}}\right\|_{\infty}\left\|\Gamma_{\underline{k}_{\mathrm{U}}|\underline{k}_{\mathrm{U}}}\right\|_{\infty}\left\|A_{\underline{k}_{\mathrm{U}}}^{\top}\right\|_{\infty} + \left\|Q_{\underline{k}_{\mathrm{U}}}\right\|_{\infty} < \sqrt{n}\left\|\Gamma_{\underline{k}_{\mathrm{U}}|\underline{k}_{\mathrm{U}}}\right\|a_1a_2 + \sqrt{n}q_2.$$

Moreover, since (recall that $m$ is the dimension of the sensor measurement $z_k$)

$$\begin{aligned}
&\left\|\left(R_{\underline{k}_{\mathrm{U}}+1} + H_{\underline{k}_{\mathrm{U}}+1}\Gamma_{\underline{k}_{\mathrm{U}}+1|\underline{k}_{\mathrm{U}}}H_{\underline{k}_{\mathrm{U}}+1}^{\top}\right)^{-1}\right\|_{\infty} \\
&\leq \sqrt{m}\left\|\left(R_{\underline{k}_{\mathrm{U}}+1} + H_{\underline{k}_{\mathrm{U}}+1}\Gamma_{\underline{k}_{\mathrm{U}}+1|\underline{k}_{\mathrm{U}}}H_{\underline{k}_{\mathrm{U}}+1}^{\top}\right)^{-1}\right\| \\
&= \sqrt{m}\left(\sigma_{\min}\left(R_{\underline{k}_{\mathrm{U}}+1} + H_{\underline{k}_{\mathrm{U}}+1}\Gamma_{\underline{k}_{\mathrm{U}}+1|\underline{k}_{\mathrm{U}}}H_{\underline{k}_{\mathrm{U}}+1}^{\top}\right)\right)^{-1} \\
&\leq \sqrt{m}\left(\sigma_{\min}\left(R_{\underline{k}_{\mathrm{U}}+1}\right)\right)^{-1} \\
&< \sqrt{m}r_1^{-1},
\end{aligned}$$

it follows that

$$\begin{aligned}
\left\|K_{\underline{k}_{\mathrm{U}}+1}\right\|_{\infty} &\leq \left\|\Gamma_{\underline{k}_{\mathrm{U}}+1|\underline{k}_{\mathrm{U}}}\right\|_{\infty}\left\|H_{\underline{k}_{\mathrm{U}}+1}^{\top}\right\|_{\infty}\left\|\left(R_{\underline{k}_{\mathrm{U}}+1} + H_{\underline{k}_{\mathrm{U}}+1}\Gamma_{\underline{k}_{\mathrm{U}}+1|\underline{k}_{\mathrm{U}}}H_{\underline{k}_{\mathrm{U}}+1}^{\top}\right)^{-1}\right\|_{\infty} \\
&< \sqrt{mn}r_1^{-1}\left(\left\|\Gamma_{\underline{k}_{\mathrm{U}}|\underline{k}_{\mathrm{U}}}\right\|a_1a_2 + q_2\right).
\end{aligned}$$

**Step 2**: As stated in (C.13), Kalman gain associated with the observable subsystem is given by

$$\check{K}_k^{(1)} = \check{\Gamma}_{k|k-1}^{(1)}\left(\check{H}_k^{(1)}\right)^{\top}\left(R_k + \check{H}_k^{(1)}\check{\Gamma}_{k|k-1}^{(1)}\left(\check{H}_k^{(1)}\right)^{\top}\right)^{-1}.$$

According to Lemma 2, there exist constants $\check{c}_1$ and $\check{c}_2$ such that the error covariance of the observable subsystem satisfies

$$\check{c}_1 I < \check{\Gamma}_{k|k}^{(1)} < \check{c}_2 I, \quad \text{for all } k \in (\underline{k}_{\mathrm{U}}, \bar{k}_{\mathrm{U}}]. \tag{C.15}$$

Given that $\check{\Gamma}_{k|k-1}^{(1)} = \check{A}_k^{(1)} \check{\Gamma}_{k-1|k-1}^{(1)} \left(\check{A}_k^{(1)}\right)^\top + \check{Q}_{k-1}^{(1)}$, we have

$$\left\|\check{\Gamma}_{k|k-1}^{(1)}\right\|_\infty \leq \check{a}_1 \check{a}_2 \left\|\check{\Gamma}_{k-1|k-1}^{(1)}\right\|_\infty + \left\|\check{Q}_{k-1}^{(1)}\right\|_\infty < \sqrt{d_1}\left(\check{a}_1 \check{a}_2 \check{c}_2 + q_2\right),$$

with $\check{a}_1$ and $\check{a}_2$ defined as

$$\check{a}_1 = \max_{k \in (\underline{k}_\mathrm{U}, \bar{k}_\mathrm{U}]} \left\|A_k^{(1)}\right\|_\infty, \quad \check{a}_2 = \max_{k \in (\underline{k}_\mathrm{U}, \bar{k}_\mathrm{U}]} \left\|\left(A_k^{(1)}\right)^\top\right\|_\infty.$$

Following the similar argument as in Step 1, we obtain

$$\left\|\check{K}_k^{(1)}\right\|_\infty < \sqrt{3d_1} r_1^{-1}\left(\check{a}_1 \check{a}_2 \check{c}_2 + q_2\right), \quad \text{for all } k \in (\underline{k}_\mathrm{U}+1, \bar{k}_\mathrm{U}].$$

**Step 3**: Define the Lyapunov function of the observable subsystem as

$$\check{V}_k = \left(\check{\boldsymbol{\eta}}_{k|k}^{(1)}\right)^\top \left(\check{\Gamma}_{k|k}^{(1)}\right)^{-1} \check{\boldsymbol{\eta}}_{k|k}^{(1)}.$$

According to Lemma 3 in [53], the one-step change of $\check{V}_k$ is given by:

$$\begin{aligned}
\Delta\check{V}_{k+1} &= \check{V}_{k+1} - \check{V}_k \\
&= -\left(\check{\boldsymbol{\eta}}_{k|k}^{(1)}\right)^\top \left(\check{\Gamma}_{k|k}^{(1)} + \check{\Gamma}_{k|k}^{(1)}\left(\check{A}_k^{(1)}\right)^\top \times \right. \\
&\qquad \left. \left(\check{Q}_k^{(1)} + \check{\Gamma}_{k+1|k}^{(1)}\left(\check{H}_k^{(1)}\right)^\top R_{k+1}^{-1} \check{H}_k^{(1)} \check{\Gamma}_{k+1|k}^{(1)}\right)^{-1} \check{A}_k^{(1)} \check{\Gamma}_{k|k}^{(1)}\right)^{-1} \check{\boldsymbol{\eta}}_{k|k}^{(1)} \\
&\leq -\left\|\check{\Gamma}_{k|k}^{(1)} + \check{\Gamma}_{k|k}^{(1)}\left(\check{A}_k^{(1)}\right)^\top \times \right. \\
&\qquad \left. \left(\check{Q}_k^{(1)} + \check{\Gamma}_{k+1|k}^{(1)}\left(\check{H}_k^{(1)}\right)^\top R_{k+1}^{-1} \check{H}_k^{(1)} \check{\Gamma}_{k+1|k}^{(1)}\right)^{-1} \check{A}_k^{(1)} \check{\Gamma}_{k|k}^{(1)}\right\|^{-1} \left\|\check{\boldsymbol{\eta}}_{k|k}^{(1)}\right\|^2,
\end{aligned}$$

where

$$\begin{aligned}
&\left\|\check{\Gamma}_{k|k}^{(1)} + \check{\Gamma}_{k|k}^{(1)}\left(\check{A}_k^{(1)}\right)^\top \left(\check{Q}_k^{(1)} + \check{\Gamma}_{k+1|k}^{(1)}\left(\check{H}_k^{(1)}\right)^\top R_{k+1}^{-1} \check{H}_k^{(1)} \check{\Gamma}_{k+1|k}^{(1)}\right)^{-1} \check{A}_k^{(1)} \check{\Gamma}_{k|k}^{(1)}\right\| \\
&< \check{c}_2 + q_1^{-1}\left\|\check{\Gamma}_{k|k}^{(1)}\left(\check{A}_k^{(1)}\right)^\top \check{A}_k^{(1)} \check{\Gamma}_{k|k}^{(1)}\right\| \leq \check{c}_2 + q_1^{-1}\left\|\check{\Gamma}_{k|k}^{(1)}\right\| \left\|\left(\check{A}_k^{(1)}\right)^\top \check{A}_k^{(1)}\right\| \left\|\check{\Gamma}_{k|k}^{(1)}\right\| < \check{c}_2 + q_1^{-1}\check{c}_2^2 \check{a}_3,
\end{aligned}$$

with $\check{a}_3$ defined as

$$\check{a}_3 = \max_{k\in(\underline{k}_{\mathrm{U}},\bar{k}_{\mathrm{U}}]} \sigma_{\max}\left(\check{A}_k^{(1)}\right).$$

It follows that the Lyapunov function $\check{V}_k$ satisfies

$$\check{c}_2^{-1}\left\|\check{\boldsymbol{\eta}}_{k|k}^{(1)}\right\|^2 < \check{V}_k < \check{c}_1^{-1}\left\|\check{\boldsymbol{\eta}}_{k|k}^{(1)}\right\|^2, \quad \text{and } \check{V}_{k+1} - \check{V}_k < -\check{c}_3\left\|\check{\boldsymbol{\eta}}_{k|k}^{(1)}\right\|^2, \quad \text{for all } k \in (\underline{k}_{\mathrm{U}}, \bar{k}_{\mathrm{U}}],$$

where

$$\check{c}_3 = \check{c}_2 + q_1^{-1}\check{c}_2^2\check{a}_3.$$

Hence, for all $k \in (\underline{k}_{\mathrm{U}}+1, \bar{k}_{\mathrm{U}}]$, the 2-norm of the mean estimation error of the observable subsystem satisfies

$$\begin{aligned}
\left\|\check{\boldsymbol{\eta}}_{k|k}^{(1)}\right\| &< \left(\check{c}_2\check{V}_k\right)^{\frac{1}{2}} \\
&< \left(\check{c}_2\check{V}_{\underline{k}_{\mathrm{U}}+1}\left(1-\check{c}_3\check{c}_1\right)^{k-\underline{k}_{\mathrm{U}}-1}\right)^{\frac{1}{2}} \\
&< \left(\check{c}_2\check{c}_1^{-1}\left\|\check{\boldsymbol{\eta}}_{\underline{k}_{\mathrm{U}}+1|\underline{k}_{\mathrm{U}}+1}^{(1)}\right\|^2\left(1-\check{c}_3\check{c}_1\right)^{k-\underline{k}_{\mathrm{U}}-1}\right)^{\frac{1}{2}} \\
&= \left(\check{c}_2\check{c}_1^{-1}\right)^{\frac{1}{2}}\left\|\check{\boldsymbol{\eta}}_{\underline{k}_{\mathrm{U}}+1|\underline{k}_{\mathrm{U}}+1}^{(1)}\right\|\left(\left(1-\check{c}_3\check{c}_1\right)^{\frac{1}{2}}\right)^{k-\underline{k}_{\mathrm{U}}-1}.
\end{aligned} \tag{C.16}$$

Moreover, the mean estimation error of the observable subsystem is given as follows:

$$\check{\boldsymbol{\eta}}_{k|k}^{(1)} = \prod_{\kappa=k}^{\underline{k}_{\mathrm{U}}+2}\check{\Upsilon}_{\kappa}^{(1)}\check{\boldsymbol{\eta}}_{\underline{k}_{\mathrm{U}}+1|\underline{k}_{\mathrm{U}}+1}^{(1)}, \quad \text{for all } k \in (\underline{k}_{\mathrm{U}}+1, \bar{k}_{\mathrm{U}}], \tag{C.17}$$

where $\check{\Upsilon}_{\kappa}^{(1)} = \check{\Gamma}_{\kappa|\kappa}^{(1)}\left(\check{\Gamma}_{\kappa|\kappa-1}^{(1)}\right)^{-1}\check{A}_{\kappa-1}^{(1)}$. Combining (C.16) and (C.17), it is concluded based on the definition of matrix induced norm that

$$\left\|\prod_{\kappa=k}^{\underline{k}_{\mathrm{U}}+2}\check{\Upsilon}_{\kappa}^{(1)}\right\| \leq \left(\check{c}_2\check{c}_1^{-1}\right)^{\frac{1}{2}}\left(\left(1-\check{c}_3\check{c}_1\right)^{\frac{1}{2}}\right)^{k-\underline{k}_{\mathrm{U}}-1}, \quad \text{for } k \in (\underline{k}_{\mathrm{U}}+1, \bar{k}_{\mathrm{U}}]. \tag{C.18}$$

**Step 4**: Vectorizing both sides of (B.4) yields that for $k \in (\underline{k}_{\mathrm{U}}, \bar{k}_{\mathrm{U}}]$,

$$\mathrm{vec}\left\{\check{\Gamma}^{(12)}_{k+1|k}\right\} = \left(\check{A}^{(2)}_k \otimes \check{\Upsilon}^{(1)}_k\right) \mathrm{vec}\left\{\check{\Gamma}^{(12)}_{k|k-1}\right\} + \mathrm{vec}\left\{\check{\Upsilon}^{(1)}_k \check{\Gamma}^{(1)}_{k|k-1}\left(\check{A}^{(21)}_k\right)^\top\right\} + \mathrm{vec}\left\{\check{Q}^{(12)}_k\right\},$$

which implies that for $k \in (\underline{k}_{\mathrm{U}}+1, \bar{k}_{\mathrm{U}}]$,

$$\mathrm{vec}\left\{\check{\Gamma}^{(12)}_{k+1|k}\right\} = \left(\prod_{\kappa=k}^{\underline{k}_{\mathrm{U}}+2}\left(\check{A}^{(2)}_\kappa \otimes \check{\Upsilon}^{(1)}_\kappa\right)\right) \mathrm{vec}\left\{\check{\Gamma}^{(12)}_{\underline{k}_{\mathrm{U}}+2|\underline{k}_{\mathrm{U}}+1}\right\} + \Phi_k, \tag{C.19}$$

where

$$\begin{aligned}
\Phi_k =& \mathrm{vec}\left\{\check{\Upsilon}^{(1)}_k \check{\Gamma}^{(1)}_{k|k-1}\left(\check{A}^{(21)}_k\right)^\top + \check{Q}^{(12)}_k\right\} \\
&+ \left(\check{A}^{(2)}_k \otimes \check{\Upsilon}^{(1)}_k\right) \mathrm{vec}\left\{\check{\Upsilon}^{(1)}_{k-1} \check{\Gamma}^{(1)}_{k-1|k-2}\left(\check{A}^{(21)}_{k-1}\right)^\top + \check{Q}^{(12)}_{k-1}\right\} \\
&+ \left(\check{A}^{(2)}_k \otimes \check{\Upsilon}^{(1)}_k\right)\left(\check{A}^{(2)}_{k-1} \otimes \check{\Upsilon}^{(1)}_{k-1}\right) \mathrm{vec}\left\{\check{\Upsilon}^{(1)}_{k-2} \check{\Gamma}^{(1)}_{k-2|k-3}\left(\check{A}^{(21)}_{k-2}\right)^\top + \check{Q}^{(12)}_{k-2}\right\} \\
&+ \cdots + \prod_{\kappa=k}^{\underline{k}_{\mathrm{U}}+3}\left(\check{A}^{(2)}_\kappa \otimes \check{\Upsilon}^{(1)}_\kappa\right) \mathrm{vec}\left\{\check{\Upsilon}^{(1)}_{\underline{k}_{\mathrm{U}}+2} \check{\Gamma}^{(1)}_{\underline{k}_{\mathrm{U}}+2|\underline{k}_{\mathrm{U}}+1}\left(\check{A}^{(21)}_{\underline{k}_{\mathrm{U}}+2}\right)^\top + \check{Q}^{(12)}_{\underline{k}_{\mathrm{U}}+2}\right\}.
\end{aligned}$$

The explicit form of $\check{A}^{(2)}_k \otimes \check{\Upsilon}^{(1)}_k$ reads

$$\check{A}^{(2)}_k \otimes \check{\Upsilon}^{(1)}_k = \begin{pmatrix} \check{A}^{(2)}_k(1,1)\check{\Upsilon}^{(1)}_k & \cdots & \check{A}^{(2)}_k(1,d_2)\check{\Upsilon}^{(1)}_k \\ \vdots & \ddots & \vdots \\ \check{A}^{(2)}_k(d_2,1)\check{\Upsilon}^{(1)}_k & \cdots & \check{A}^{(2)}_k(d_2,d_2)\check{\Upsilon}^{(1)}_k \end{pmatrix},$$

hence

$$\prod_{\kappa=k}^{\underline{k}_{\mathrm{U}}+2}\left(\check{A}^{(2)}_\kappa \otimes \check{\Upsilon}^{(1)}_\kappa\right) = \begin{pmatrix} \vartheta_k(1,1)\prod_{\kappa=k}^{\underline{k}_{\mathrm{U}}+2}\check{\Upsilon}^{(1)}_\kappa & \cdots & \vartheta_k(1,d_2)\prod_{\kappa=k}^{\underline{k}_{\mathrm{U}}+2}\check{\Upsilon}^{(1)}_\kappa \\ \vdots & \ddots & \vdots \\ \vartheta_k(d_2,1)\prod_{\kappa=k}^{\underline{k}_{\mathrm{U}}+2}\check{\Upsilon}^{(1)}_\kappa & \cdots & \vartheta_k(d_2,d_2)\prod_{\kappa=k}^{\underline{k}_{\mathrm{U}}+2}\check{\Upsilon}^{(1)}_\kappa \end{pmatrix},$$

where $\vartheta_k(i,j)$ is the $(i,j)^{\mathrm{th}}$ element of $\prod_{\kappa=k}^{\underline{k}_{\mathrm{U}}+2}\check{A}^{(2)}_\kappa$. Define

$$P = \begin{pmatrix} \mathbf{0}_{d_2,n-d_2} & I_{d_2} \end{pmatrix},$$

and given that the top right block of $\check{A}_k$ is a zero matrix $\mathbf{0}_{d_1,d_2}$ (as shown in (B.1)), it can be concluded that

$$\prod_{\kappa=k}^{\underline{k}_{\mathrm{U}}+2} \check{A}_{\kappa}^{(2)} = P\left(\prod_{\kappa=k}^{\underline{k}_{\mathrm{U}}+2} \check{A}_{\kappa}\right)P^{\top} = P\left(\prod_{\kappa=k}^{\underline{k}_{\mathrm{U}}+2} UA_{\kappa}U^{\top}\right)P^{\top} = PU\left(\prod_{\kappa=k}^{\underline{k}_{\mathrm{U}}+2} A_{\kappa}\right)U^{\top}P^{\top}. \quad \text{(C.20)}$$

Also note that the $(i,j)^{th}$ element of $\prod_{\kappa=k}^{\underline{k}_{\mathrm{U}}+2} A_{\kappa}$ satisfies

$$0 \leq \left(\prod_{\kappa=k}^{\underline{k}_{\mathrm{U}}+2} A_{\kappa}\right)(i,j) \leq 1, \quad \text{for all } i,j \in \{1,2,\cdots,n\} \text{ and } k \in (\underline{k}_{\mathrm{U}}, \bar{k}_{\mathrm{U}}],$$

which is true for the SMM due to properties (P.1)-(P.2), and holds for the SMM-J due to Lemma 8. Hence, it can be derived from (C.20) that

$$\left\|\prod_{\kappa=k}^{\underline{k}_{\mathrm{U}}+2} \check{A}_{\kappa}^{(2)}\right\|_{\infty} \leq \left\|\prod_{\kappa=k}^{\underline{k}_{\mathrm{U}}+2} \check{A}_{\kappa}\right\|_{\infty} \leq \left\|U\left(\prod_{\kappa=k}^{\underline{k}_{\mathrm{U}}+2} A_{\kappa}\right)U^{\top}\right\|_{\infty} \leq \sqrt{n}\left\|\prod_{\kappa=k}^{\underline{k}_{\mathrm{U}}+2} A_{\kappa}\right\| \leq n^2.$$

Consequently,

$$\begin{aligned}\left\|\prod_{\kappa=k}^{\underline{k}_{\mathrm{U}}+2}\left(\check{A}_{\kappa}^{(2)} \otimes \check{\Upsilon}_{\kappa}^{(1)}\right)\right\|_{\infty} &\leq n^2\left\|\prod_{\kappa=k}^{\underline{k}_{\mathrm{U}}+2} \check{\Upsilon}_{\kappa}^{(1)}\right\|_{\infty} \\ &\leq n^2\sqrt{d_1}\left(\frac{\check{c}_2}{\check{c}_1}\right)^{\frac{1}{2}}\left((1-\check{c}_3\check{c}_1)^{\frac{1}{2}}\right)^{k-\underline{k}_{\mathrm{U}}-1} = \bar{t}\bar{q}^{k-\underline{k}_{\mathrm{U}}-1}, \quad \text{(C.21)}\end{aligned}$$

where the last inequality is due to (C.18). Recall from (C.15) that $\check{c}_1 I < \check{\Gamma}_{k|k}^{(1)} < \check{c}_2 I$ for $k \in (\underline{k}_{\mathrm{U}}, \bar{k}_{\mathrm{U}}]$. Since $\check{\Gamma}_{k|k-1}^{(1)} = \check{A}_k^{(1)}\check{\Gamma}_{k-1|k-1}^{(1)}\left(\check{A}_k^{(1)}\right)^{\top} + \check{Q}_{k-1}^{(1)}$, it follows that $\left\|\check{\Gamma}_{k|k-1}^{(1)}\right\|_{\infty} \leq \sqrt{d_1}\left(\check{a}_1\check{a}_2\check{c}_2 + q_2\right)$ for all $k \in (\underline{k}_{\mathrm{U}}+1, \bar{k}_{\mathrm{U}}]$, and the prior error covariance of the observable subsystem satisfies $q_1 I < \check{\Gamma}_{k|k-1}^{(1)}$for $k \in (\underline{k}_{\mathrm{U}}, \bar{k}_{\mathrm{U}}]$. As a consequence,

$$\left\|\check{\Upsilon}_k^{(1)}\right\|_{\infty} \leq \sqrt{d_1}\left\|\check{\Gamma}_{k|k}^{(1)}\left(\check{\Gamma}_{k|k-1}^{(1)}\right)^{-1}\right\| < \sqrt{d_1}\check{c}_2 q_1^{-1}, \quad \text{for } k \in (\underline{k}_{\mathrm{U}}, \bar{k}_{\mathrm{U}}]. \quad \text{(C.22)}$$

Define $\check{a}_4$ as

$$\check{a}_4 = \max_{k\in(\underline{k}_{\mathrm{U}},\bar{k}_{\mathrm{U}}]}\left\|\check{A}_k^{(21)}\right\|_{\infty},$$

it follows that[1]

$$\begin{aligned}
&\left\|\mathrm{vec}\left\{\check{\Upsilon}_k^{(1)}\check{\Gamma}_{k|k-1}^{(1)}\left(\check{A}_k^{(21)}\right)^\top\right\}+\mathrm{vec}\left\{\check{Q}_k^{(12)}\right\}\right\|_\infty \\
&\le \left\|\check{\Upsilon}_k^{(1)}\check{\Gamma}_{k|k-1}^{(1)}\left(\check{A}_k^{(21)}\right)^\top\right\|_\infty+\left\|\check{Q}_k^{(12)}\right\|_{\max} \\
&< \sqrt{d_1}\check{c}_2 q_1^{-1}\check{a}_4\left\|\check{\Gamma}_{k|k-1}^{(1)}\right\|_\infty+q_2 \\
&< d_1\check{c}_2\check{a}_4\left(\check{a}_1\check{a}_2\check{c}_2+q_2\right)q_1^{-1}+q_2 \\
&= \bar{p}, \quad \text{for } k\in(\underline{k}_{\mathrm{U}}+1,\bar{k}_{\mathrm{U}}].
\end{aligned} \tag{C.23}$$

Substituting (C.21) and (C.23) into (C.19), we obtain that for $k\in(\underline{k}_{\mathrm{U}}+1,\bar{k}_{\mathrm{U}}]$,

$$\left\|\mathrm{vec}\left\{\check{\Gamma}_{k+1|k}^{(12)}\right\}\right\|_\infty \le \mathrm{b}\left(k\right)\triangleq \bar{t}\bar{q}^{k-\underline{k}_{\mathrm{U}}-1}\left\|\mathrm{vec}\left\{\check{\Gamma}_{\underline{k}_{\mathrm{U}}+2|\underline{k}_{\mathrm{U}}+1}^{(12)}\right\}\right\|_\infty+\bar{p}+\bar{t}\bar{p}\sum_{\iota=1}^{k-\underline{k}_{\mathrm{U}}-2}\bar{q}^\iota,$$

where $\mathrm{b}(k)$ is either a non-increasing or a non-decreasing function of $k$. Hence, we obtain that for $k\in(\underline{k}_{\mathrm{U}},\bar{k}_{\mathrm{U}}]$,

$$\begin{aligned}
&\left\|\mathrm{vec}\left\{\check{\Gamma}_{k+1|k}^{(12)}\right\}\right\|_\infty \\
&\le \max\left\{\left\|\mathrm{vec}\left\{\check{\Gamma}_{\underline{k}_{\mathrm{U}}+2|\underline{k}_{\mathrm{U}}+1}^{(12)}\right\}\right\|_\infty,\quad \mathrm{b}(\underline{k}_{\mathrm{U}}+2),\quad \lim_{k\to\infty}\mathrm{b}(k)\right\} \\
&\le \max\left\{\left\|\mathrm{vec}\left\{\check{\Gamma}_{\underline{k}_{\mathrm{U}}+2|\underline{k}_{\mathrm{U}}+1}^{(12)}\right\}\right\|_\infty,\quad \bar{t}\bar{q}\left\|\mathrm{vec}\left\{\check{\Gamma}_{\underline{k}_{\mathrm{U}}+2|\underline{k}_{\mathrm{U}}+1}^{(12)}\right\}\right\|_\infty+\bar{p},\quad \frac{\bar{t}\bar{p}\bar{q}}{1-\bar{q}}+\bar{p}\right\},
\end{aligned}$$

where

$$\begin{aligned}
\left\|\mathrm{vec}\left\{\check{\Gamma}_{\underline{k}_{\mathrm{U}}+2|\underline{k}_{\mathrm{U}}+1}^{(12)}\right\}\right\|_\infty \le \left\|\check{\Gamma}_{\underline{k}_{\mathrm{U}}+2|\underline{k}_{\mathrm{U}}+1}^{(12)}\right\|_\infty &< \sqrt{n}a_1a_2\left\|\Gamma_{\underline{k}_{\mathrm{U}}+1|\underline{k}_{\mathrm{U}}+1}\right\|+\sqrt{n}q_2 \\
&\le \sqrt{n}a_1a_2\left\|\Gamma_{\underline{k}_{\mathrm{U}}+1|\underline{k}_{\mathrm{U}}}\right\|+\sqrt{n}q_2 \\
&< n\sqrt{n}\left\|\Gamma_{\underline{k}_{\mathrm{U}}|\underline{k}_{\mathrm{U}}}\right\|\left(a_1a_2\right)^2+n\sqrt{n}a_1a_2q_2+\sqrt{n}q_2 \\
&= \bar{\gamma}.
\end{aligned}$$

Also since

$$\check{K}_k^{(21)}=\left(\check{\Gamma}_{k|k-1}^{(12)}\right)^\top\left(\check{H}_k^{(1)}\right)^\top\left(R_k+\check{H}_k^{(1)}\check{\Gamma}_{k|k-1}^{(1)}\left(\check{H}_k^{(1)}\right)^\top\right)^{-1},$$

[1]Recall that for matrix $M\in\mathbb{R}^{p\times q}$, $\|M\|_{\max}\le\|M\|_2=\max_{1\le r\le p,1\le c\le q}|M(r,c)|$.

it follows that for $k \in (\underline{k}_{\mathrm{U}}+1, \bar{k}_{\mathrm{U}}]$,

$$\left\|\check{K}_k^{(21)}\right\|_\infty \leq \sqrt{m} r_1^{-1} \left\|\left(\check{\Gamma}_{k|k-1}^{(12)}\right)^\top\right\|_\infty \leq \sqrt{m} d_1 r_1^{-1} \max\left\{\bar{\gamma}, \quad \bar{t}\bar{q}\bar{\gamma}+\bar{p}, \quad \frac{\bar{t}\bar{p}\bar{q}}{1-\bar{q}}+\bar{p}\right\}.$$

**Step 5**: Combining Steps 1, 2 and 4, it can be concluded that for $k \in (\underline{k}_{\mathrm{U}}, \bar{k}_{\mathrm{U}}]$

$$\begin{aligned}
&\|K_k\|_\infty = \left\|U^\top \check{K}_k\right\|_\infty \leq n \left\|\check{K}_k\right\|_\infty \\
\leq & \frac{d_1\sqrt{m}}{r_1} \max\left\{\frac{\sqrt{n}}{d_1}\left(\left\|\Gamma_{\underline{k}_{\mathrm{U}}|\underline{k}_{\mathrm{U}}}\right\| a_1 a_2 + q_2\right), \frac{1}{\sqrt{d_1}}\left(\check{a}_1\check{a}_2\check{c}_2+q_2\right), \bar{\gamma}, \bar{t}\bar{q}\bar{\gamma}+\bar{p}, \frac{\bar{t}\bar{p}\bar{q}}{1-\bar{q}}+\bar{p}\right\} \\
\triangleq & \mathrm{k}\left(\left\|\Gamma_{\underline{k}_{\mathrm{U}}|\underline{k}_{\mathrm{U}}}\right\|\right),
\end{aligned}$$

which completes the proof.

## C.6 Proof of Lemma 8

The proof is divided into two steps. In Step 1, we apply properties (P.3) and (P.4) to show that (4.13) holds for the modes where the junction solver follows diverge case I or diverge case II. In Step 2, properties (P.3) and (P.5) are applied to show that (4.13) holds for the modes where the junction solver follows diverge case III.

For all $\underline{k}+1 \leq \ell < k \leq \bar{k}$ and $i, j \in \{1, 2, \cdots, n\}$, the $(i,j)^{\text{th}}$ entry of $\prod_{\kappa=k}^{\ell} A_\kappa$ reads

$$\left(\prod_{\kappa=k}^{\ell} A_\kappa\right)(i,j) = \sum_{r=1}^{n}\left(\left(\prod_{\kappa=k}^{\ell+1} A_\kappa\right)(i,r)\right)\left(A_\ell(r,j)\right). \tag{C.24}$$

**Step 1**: Suppose $A_k$ is under a mode where the junction solver follows diverge case I or diverge case II. Recall from (P.4) that

$$\sum_{r=1}^{n} A_k(r,j) \leq 1, \quad \text{for all } k \in (\underline{k}, \bar{k}] \text{ and } j \in \{1, 2, \cdots, n\}.$$

Hence, the $(i,j)^{\text{th}}$ entry of $\prod_{\kappa=k}^{\ell} A_\kappa$ is no greater than the convex combination of all the entries on the $i^{\text{th}}$ row of $\prod_{\kappa=k}^{\ell+1} A_\kappa$. Moreover, recall from (P.3) that

$$0 \leq A_k(r,c) \leq 1, \quad \text{for all } k \in (\underline{k}, \bar{k}] \text{ and } r, c \in \{1, 2, \cdots, n\},$$

it follows that

$$0 \leq \left(\prod_{\kappa=k}^{\ell} A_\kappa\right)(i,j) \leq 1, \quad \text{for all } k \in (\underline{k}, \bar{k}],\ \ell \in [\underline{k}+1, k) \text{ and } i,j \in \{1,2,\cdots,n\},$$

thus (4.13) follows directly by setting $\ell = \underline{k}+1$ in the above equation.

**Step 2**: Suppose $A_k$ is under a mode where the junction solver follows diverge case III. We prove for the case where $\mathrm{f}(\rho_k^{n_1}, \rho_k^{n_1+1}) = \mathrm{r}(\rho_k^{n_1+1})$, and the proof for the case where $\mathrm{f}(\rho_k^{n_1}, \rho_k^{n_1+1}) = \mathrm{s}(\rho_k^{n_1}) - \mathrm{r}(\rho_k^{n_1+n_2+1})$ follows by symmetry.

Recall from (P.5) that

$$\sum_{r=1}^{n} A_k(r,j) \leq 1, \quad \text{for all } k \in (\underline{k}, \bar{k}] \text{ and } j \in \{j | j \in \{1,2,\cdots,n\}, j \neq n_1+1\}. \tag{C.25}$$

For $j = n_1+1$, the sum of all entries of $A_k$ on column $j$ is given by

$$\begin{aligned}\sum_{r=1}^{n} A_k(r, n_1+1) &= A_k(n_1, n_1+1) + A_k(n_1+1, n_1+1) + A_k(n_1+n_2+1, n_1+1) \\ &= \frac{w\Delta t}{\Delta x} + \left(1 - \frac{w\Delta t}{\Delta x}\right) + \frac{w\Delta t}{\Delta x} = 1 + \frac{w\Delta t}{\Delta x}, \quad \text{for all } k \in (\underline{k}, \bar{k}].\end{aligned}$$

Additionally, one may note that for all $k \in (\underline{k}, \bar{k}]$,

$$A_k(r, n_1+n_2+1) = \begin{cases} 1 & \text{if } r = n_1+n_2+1 \\ 0 & \text{otherwise.} \end{cases}$$

It follows that for all $\underline{k}+1 \leq \ell < k \leq \bar{k}$,

$$\left(\prod_{\kappa=k}^{\ell} A_\kappa\right)(r, n_1+n_2+1) = \begin{cases} 1 & \text{if } r = n_1+n_2+1 \\ 0 & \text{otherwise.} \end{cases} \tag{C.26}$$

Combining (C.25) and (C.26) with (C.24), we obtain that for all $(i,j) \neq (n_1+n_2+1, n_1+1)$, the $(i,j)^{\text{th}}$ entry of $\prod_{\kappa=k}^{\ell} A_\kappa$ is no greater than the convex combination of all the (non-zero) entries on the $i^{\text{th}}$ row of $\prod_{\kappa=k}^{\ell+1} A_\kappa$. Also recall from (P.5) that for all $k \in (\underline{k}, \bar{k}]$,

$$A_k(r,c) = 0, \quad \text{for all } r \in \{n_1+1, \cdots, n\} \text{ and } c \in \{1, \cdots n_1\},$$

which yields that for all $\underline{k}+1 \leq \ell < k \leq \bar{k}$,

$$\left(\prod_{\kappa=k}^{\ell+1} A_\kappa\right)(r,c) = 0, \quad \text{for all } r \in \{n_1+1, \cdots, n\} \text{ and } c \in \{1, \cdots n_1\},$$

thus

$$\left(\prod_{\kappa=k}^{\ell+1} A_\kappa\right)(n_1+n_2+1, n_1) = 0, \quad \text{for all } \underline{k}+1 \leq \ell < k \leq \bar{k}.$$

Hence for $(i,j) = (n_1+n_2+1, n_1+1)$, the $(i,j)^{\text{th}}$ entry of $\prod_{\kappa=k}^{\ell} A_\kappa$ is also no greater than the convex combination of all the (non-zero) entries on the $i^{\text{th}}$ row of $\prod_{\kappa=k}^{\ell+1} A_\kappa$. Moreover, according to (P.3) it holds that $0 \leq A_k(r,c) \leq 1$ for all $k \in (\underline{k}, \bar{k}]$ and $r, c \in \{1, 2, \cdots, n\}$. It can be concluded that

$$0 \leq \left(\prod_{\kappa=k}^{\ell} A_\kappa\right)(i,j) \leq 1, \quad \text{for all } k \in (\underline{k}, \bar{k}],\ \ell \in [\underline{k}+1, k) \text{ and } i, j \in \{1, 2, \cdots, n\},$$

thus (4.13) follows directly by setting $\ell = \underline{k}+1$ in the above equation.

# APPENDIX D

# PROOF OF PROPOSITIONS

## D.1 Proof of Proposition 8

According to Lemma 5, when $\underline{k}_{\mathrm{O}} < k \leq \bar{k}_{\mathrm{O}}$ the error covariance satisfies $\mathrm{c}_1(\Gamma_{\underline{k}_{\mathrm{O}}|\underline{k}_{\mathrm{O}}})I \leq \Gamma_{k|k}^{-1} \leq \mathrm{c}_2(\Gamma_{\underline{k}_{\mathrm{O}}|\underline{k}_{\mathrm{O}}})I$. Given Lemma 6, it follows that for $\underline{k}_{\mathrm{O}} < k \leq \bar{k}_{\mathrm{O}}$,

$$\left\|\prod_{\kappa=k-1}^{\underline{k}_{\mathrm{O}}} F_{\kappa+1}A_{\kappa}\right\| \leq \mathrm{a}\left(\Gamma_{\underline{k}_{\mathrm{O}}|\underline{k}_{\mathrm{O}}}\right)\mathrm{q}\left(\Gamma_{\underline{k}_{\mathrm{O}}|\underline{k}_{\mathrm{O}}}\right)^{k-\underline{k}_{\mathrm{O}}},$$

where $\mathrm{a}\left(\Gamma_{\underline{k}_{\mathrm{O}}|\underline{k}_{\mathrm{O}}}\right) \geq 1$ provides an upper bound for the increase of the mean estimation error when the section first switches to an observable mode at time $\underline{k}_{\mathrm{O}}+1$, and $0 < \mathrm{q}\left(\Gamma_{\underline{k}_{\mathrm{O}}|\underline{k}_{\mathrm{O}}}\right) < 1$ describes the convergence rate of the mean estimation error in observable modes. Hence when $\underline{k}_{\mathrm{O}} < k \leq \bar{k}_{\mathrm{O}}$, the 2-norm of $\boldsymbol{\eta}_{k|k}$ satisfies

$$\begin{aligned}
\left\|\boldsymbol{\eta}_{k|k}\right\| &\leq \left\|\prod_{\kappa=k-1}^{\underline{k}_{\mathrm{O}}} F_{\kappa+1}A_{\kappa}\right\| \left\|\boldsymbol{\eta}_{\underline{k}_{\mathrm{O}}|\underline{k}_{\mathrm{O}}}\right\| \\
&\quad + \hat{c}\left(1 + \sum_{\iota=1}^{k-\underline{k}_{\mathrm{O}}-1}\left\|\prod_{\kappa=k-1}^{\underline{k}_{\mathrm{O}}+\iota} F_{\kappa+1}A_{\kappa}\right\|\right) \\
&\leq \hat{c} + \left\|\boldsymbol{\eta}_{\underline{k}_{\mathrm{O}}|\underline{k}_{\mathrm{O}}}\right\| \mathrm{a}\left(\Gamma_{\underline{k}_{\mathrm{O}}|\underline{k}_{\mathrm{O}}}\right)\mathrm{q}\left(\Gamma_{\underline{k}_{\mathrm{O}}|\underline{k}_{\mathrm{O}}}\right)^{k-\underline{k}_{\mathrm{O}}} \\
&\quad + \sum_{\iota=1}^{k-\underline{k}_{\mathrm{O}}-1} \hat{c}\mathrm{a}\left(\Gamma_{\underline{k}_{\mathrm{O}}|\underline{k}_{\mathrm{O}}}\right)\mathrm{q}\left(\Gamma_{\underline{k}_{\mathrm{O}}|\underline{k}_{\mathrm{O}}}\right)^{k-\underline{k}_{\mathrm{O}}-\iota} \\
&= \hat{c} + \left\|\boldsymbol{\eta}_{\underline{k}_{\mathrm{O}}|\underline{k}_{\mathrm{O}}}\right\| \mathrm{a}\left(\Gamma_{\underline{k}_{\mathrm{O}}|\underline{k}_{\mathrm{O}}}\right)\mathrm{q}\left(\Gamma_{\underline{k}_{\mathrm{O}}|\underline{k}_{\mathrm{O}}}\right)^{k-\underline{k}_{\mathrm{O}}} \\
&\quad + \frac{\hat{c}\mathrm{a}\left(\Gamma_{\underline{k}_{\mathrm{O}}|\underline{k}_{\mathrm{O}}}\right)\mathrm{q}\left(\Gamma_{\underline{k}_{\mathrm{O}}|\underline{k}_{\mathrm{O}}}\right)}{1-\mathrm{q}\left(\Gamma_{\underline{k}_{\mathrm{O}}|\underline{k}_{\mathrm{O}}}\right)}\left(1 - \mathrm{q}\left(\Gamma_{\underline{k}_{\mathrm{O}}|\underline{k}_{\mathrm{O}}}\right)^{k-\underline{k}_{\mathrm{O}}-1}\right) \\
&\triangleq \mathrm{u}\left(\Gamma_{\underline{k}_{\mathrm{O}}|\underline{k}_{\mathrm{O}}}, k\right),
\end{aligned}$$

where for a fixed $\Gamma_{\underline{k}_{\mathrm{O}}|\underline{k}_{\mathrm{O}}}$, the function $\mathrm{u}\left(\Gamma_{\underline{k}_{\mathrm{O}}|\underline{k}_{\mathrm{O}}}, k\right)$ is either non-increasing or non-decreasing with respect to $k$.

As a consequence, for all $\epsilon > 0$, there exists function $\hat{\mathrm{t}}\left(\epsilon, \left\|\boldsymbol{\eta}_{\underline{k}_{\mathrm{O}}|\underline{k}_{\mathrm{O}}}\right\|, \Gamma_{\underline{k}_{\mathrm{O}}|\underline{k}_{\mathrm{O}}}\right) \geq 0$ such that for all $k - \underline{k}_{\mathrm{O}} > \hat{\mathrm{t}}\left(\epsilon, \left\|\boldsymbol{\eta}_{\underline{k}_{\mathrm{O}}|\underline{k}_{\mathrm{O}}}\right\|, \Gamma_{\underline{k}_{\mathrm{O}}|\underline{k}_{\mathrm{O}}}\right)$,

$$\left\|\boldsymbol{\eta}_{k|k}\right\| < \epsilon + \hat{c} + \frac{\hat{c}\mathrm{a}\left(\Gamma_{\underline{k}_{\mathrm{O}}|\underline{k}_{\mathrm{O}}}\right)\mathrm{q}\left(\Gamma_{\underline{k}_{\mathrm{O}}|\underline{k}_{\mathrm{O}}}\right)}{1 - \mathrm{q}\left(\Gamma_{\underline{k}_{\mathrm{O}}|\underline{k}_{\mathrm{O}}}\right)}.$$

When $\mathrm{a}\left(\Gamma_{\underline{k}_{\mathrm{O}}|\underline{k}_{\mathrm{O}}}\right)\mathrm{q}\left(\Gamma_{\underline{k}_{\mathrm{O}}|\underline{k}_{\mathrm{O}}}\right)\left\|\boldsymbol{\eta}_{\underline{k}_{\mathrm{O}}|\underline{k}_{\mathrm{O}}}\right\| \leq \frac{\hat{c}\mathrm{a}\left(\Gamma_{\underline{k}_{\mathrm{O}}|\underline{k}_{\mathrm{O}}}\right)\mathrm{q}\left(\Gamma_{\underline{k}_{\mathrm{O}}|\underline{k}_{\mathrm{O}}}\right)}{1-\mathrm{q}\left(\Gamma_{\underline{k}_{\mathrm{O}}|\underline{k}_{\mathrm{O}}}\right)}$, we have

$$\mathrm{u}(\Gamma_{\underline{k}_{\mathrm{O}}|\underline{k}_{\mathrm{O}}}, \underline{k}_{\mathrm{O}} + 1) \leq \lim_{k\to\infty} \mathrm{u}(\Gamma_{\underline{k}_{\mathrm{O}}|\underline{k}_{\mathrm{O}}}, k),$$

and $\mathrm{u}\left(\Gamma_{\underline{k}_{\mathrm{O}}|\underline{k}_{\mathrm{O}}}, k\right) \leq \lim_{k\to\infty} \mathrm{u}(\Gamma_{\underline{k}_{\mathrm{O}}|\underline{k}_{\mathrm{O}}}, k)$ non-decreasing with respect to $k \in (\underline{k}_{\mathrm{O}}, \bar{k}_{\mathrm{O}}]$, thus

$$\hat{\mathrm{t}}\left(\epsilon, \|\boldsymbol{\eta}_{\underline{k}_{\mathrm{O}}|\underline{k}_{\mathrm{O}}}\|, \Gamma_{\underline{k}_{\mathrm{O}}|\underline{k}_{\mathrm{O}}}\right) = 0.$$

On the other hand, $\mathrm{u}\left(\Gamma_{\underline{k}_{\mathrm{O}}|\underline{k}_{\mathrm{O}}}, k\right)$ is a decreasing function with respect to $k$ when $\mathrm{u}(\Gamma_{\underline{k}_{\mathrm{O}}|\underline{k}_{\mathrm{O}}}, \underline{k}_{\mathrm{O}}+1) > \lim_{k\to\infty} \mathrm{u}(\Gamma_{\underline{k}_{\mathrm{O}}|\underline{k}_{\mathrm{O}}}, k)$. In this case,

$$\hat{\mathrm{t}}\left(\epsilon, \left\|\boldsymbol{\eta}_{\underline{k}_{\mathrm{O}}|\underline{k}_{\mathrm{O}}}\right\|, \Gamma_{\underline{k}_{\mathrm{O}}|\underline{k}_{\mathrm{O}}}\right) = \log_{\mathrm{q}\left(\Gamma_{\underline{k}_{\mathrm{O}}|\underline{k}_{\mathrm{O}}}\right)}\left(\epsilon\left(\mathrm{a}\left(\Gamma_{\underline{k}_{\mathrm{O}}|\underline{k}_{\mathrm{O}}}\right)\left\|\boldsymbol{\eta}_{\underline{k}_{\mathrm{O}}|\underline{k}_{\mathrm{O}}}\right\| - \frac{\hat{c}\mathrm{a}\left(\Gamma_{\underline{k}_{\mathrm{O}}|\underline{k}_{\mathrm{O}}}\right)}{1-\mathrm{q}\left(\Gamma_{\underline{k}_{\mathrm{O}}|\underline{k}_{\mathrm{O}}}\right)}\right)^{-1}\right).$$

Furthermore, the upper bound of $\left\|\boldsymbol{\eta}_{k|k}\right\|$ is given as follows:

$$\begin{aligned}\left\|\boldsymbol{\eta}_{k|k}\right\| &\leq \max\left\{\mathrm{u}\left(\Gamma_{\underline{k}_{\mathrm{O}}|\underline{k}_{\mathrm{O}}}, \underline{k}_{\mathrm{O}} + 1\right), \lim_{k\to\infty} \mathrm{u}\left(\Gamma_{\underline{k}_{\mathrm{O}}|\underline{k}_{\mathrm{O}}}, k\right)\right\} \\ &= \max\left\{\hat{c} + \mathrm{a}\left(\Gamma_{\underline{k}_{\mathrm{O}}|\underline{k}_{\mathrm{O}}}\right)\mathrm{q}\left(\Gamma_{\underline{k}_{\mathrm{O}}|\underline{k}_{\mathrm{O}}}\right)\left\|\boldsymbol{\eta}_{\underline{k}_{\mathrm{O}}|\underline{k}_{\mathrm{O}}}\right\|,\right. \\ &\qquad \left.\hat{c} + \hat{c}\mathrm{a}\left(\Gamma_{\underline{k}_{\mathrm{O}}|\underline{k}_{\mathrm{O}}}\right)\mathrm{q}\left(\Gamma_{\underline{k}_{\mathrm{O}}|\underline{k}_{\mathrm{O}}}\right)\left(1 - \mathrm{q}\left(\Gamma_{\underline{k}_{\mathrm{O}}|\underline{k}_{\mathrm{O}}}\right)\right)^{-1}\right\}.\end{aligned}$$

for all $k \in (\underline{k}_{\mathrm{O}}, \bar{k}_{\mathrm{O}}]$, which concludes the proof.

## D.2 Proof of Proposition 9

The proof can be done by a straightforward application of the results in Propositions 2 and 8. Note that when the section is unobservable at time 0 (i.e., $\underline{k}_{\mathrm{U}}^{1}=0$), we have $\underline{k}_{\mathrm{U}}^{r+1}=\bar{k}_{\mathrm{O}}^{r}$ and $\bar{k}_{\mathrm{U}}^{r}=\underline{k}_{\mathrm{O}}^{r}$ for all $r\in\mathbb{Z}^{+}$. When the section is observable at time 0 (i.e., $\underline{k}_{\mathrm{O}}^{1}=0$), we have $\underline{k}_{\mathrm{O}}^{r+1}=\bar{k}_{\mathrm{U}}^{r}$ and $\bar{k}_{\mathrm{O}}^{r}=\underline{k}_{\mathrm{U}}^{r}$ for all $r\in\mathbb{Z}^{+}$.

**Step 1**: When $r\geq 2$.

*(a) For the $r^{th}$ unobservable time interval $k\in(\underline{k}_{\mathrm{U}}^{r},\bar{k}_{\mathrm{U}}^{r}]$*: When the observable time interval right before $(\underline{k}_{\mathrm{U}}^{r},\bar{k}_{\mathrm{U}}^{r}]$ is sufficiently long such that condition (5.16) is satisfied, the estimation error at time $\underline{k}_{\mathrm{U}}^{r}$ satisfies (note that the observable time interval right before $(\underline{k}_{\mathrm{U}}^{r},\bar{k}_{\mathrm{U}}^{r}]$ can also be written as $(\bar{k}_{\mathrm{U}}^{r-1},\underline{k}_{\mathrm{U}}^{r}]$)

$$\left\|\boldsymbol{\eta}_{\underline{k}_{\mathrm{U}}^{r}|\underline{k}_{\mathrm{U}}^{r}}\right\|\leq\epsilon+\hat{c}+\frac{\hat{c}\mathrm{a}\left(\Gamma_{\bar{k}_{\mathrm{U}}^{r-1}|\bar{k}_{\mathrm{U}}^{r-1}}\right)\mathrm{q}\left(\Gamma_{\bar{k}_{\mathrm{U}}^{r-1}|\bar{k}_{\mathrm{U}}^{r-1}}\right)}{1-\mathrm{q}\left(\Gamma_{\bar{k}_{\mathrm{U}}^{r-1}|\bar{k}_{\mathrm{U}}^{r-1}}\right)}$$

based on Proposition 8. As a consequence, Proposition 2 gives

$$\boldsymbol{\rho}_{k|k}^{l}>-\left(\epsilon+\hat{c}+\frac{\hat{c}\mathrm{a}\left(\Gamma_{\bar{k}_{\mathrm{U}}^{r-1}|\bar{k}_{\mathrm{U}}^{r-1}}\right)\mathrm{q}\left(\Gamma_{\bar{k}_{\mathrm{U}}^{r-1}|\bar{k}_{\mathrm{U}}^{r-1}}\right)}{1-\mathrm{q}\left(\Gamma_{\bar{k}_{\mathrm{U}}^{r-1}|\bar{k}_{\mathrm{U}}^{r-1}}\right)}\right)\left(c_{0}+(n-2)\,\mathrm{c}\left(\Gamma_{\underline{k}_{\mathrm{U}}^{r}|\underline{k}_{\mathrm{U}}^{r}}\right)\right),$$

$$\boldsymbol{\rho}_{k|k}^{l}<\varrho_{\mathrm{m}}+\left(\epsilon+\hat{c}+\frac{\hat{c}\mathrm{a}\left(\Gamma_{\bar{k}_{\mathrm{U}}^{r-1}|\bar{k}_{\mathrm{U}}^{r-1}}\right)\mathrm{q}\left(\Gamma_{\bar{k}_{\mathrm{U}}^{r-1}|\bar{k}_{\mathrm{U}}^{r-1}}\right)}{1-\mathrm{q}\left(\Gamma_{\bar{k}_{\mathrm{U}}^{r-1}|\bar{k}_{\mathrm{U}}^{r-1}}\right)}\right)\left(c_{0}+(n-2)\,\mathrm{c}\left(\Gamma_{\underline{k}_{\mathrm{U}}^{r}|\underline{k}_{\mathrm{U}}^{r}}\right)\right),$$

for all $l\in\{1,\cdots,n\}$ and $k\in(\underline{k}_{\mathrm{U}}^{r},\bar{k}_{\mathrm{U}}^{r}]$. Consequently, the estimation error satisfies $\left\|\boldsymbol{\eta}_{k|k}\right\|\leq\hat{\mathrm{e}}\left(\epsilon,\Gamma_{\bar{k}_{\mathrm{U}}^{r-1}|\bar{k}_{\mathrm{U}}^{r-1}},\Gamma_{\underline{k}_{\mathrm{U}}^{r}|\underline{k}_{\mathrm{U}}^{r}}\right)$ for all $k\in(\underline{k}_{\mathrm{U}}^{r},\bar{k}_{\mathrm{U}}^{r}]$.

*(b) For the $r^{th}$ observable time interval $k\in(\underline{k}_{\mathrm{O}}^{r},\bar{k}_{\mathrm{O}}^{r}]$*: Note that the unobservable time interval right before $(\underline{k}_{\mathrm{O}}^{r},\bar{k}_{\mathrm{O}}^{r}]$ is written as $(\underline{k}_{\mathrm{U}}^{r},\bar{k}_{\mathrm{U}}^{r}]=(\bar{k}_{\mathrm{O}}^{r-1},\underline{k}_{\mathrm{O}}^{r}]$ when the section is unobservable at time 0, and is written as $(\underline{k}_{\mathrm{U}}^{r-1},\bar{k}_{\mathrm{U}}^{r-1}]=(\bar{k}_{\mathrm{O}}^{r-1},\underline{k}_{\mathrm{O}}^{r}]$ when the section is observable at time 0. Similar to Case $(a)$ in Step 1, when $\bar{k}_{\mathrm{O}}^{r-1}-\underline{k}_{\mathrm{O}}^{r-1}$ satisfies condition (5.16), the estimation error at time $\underline{k}_{\mathrm{O}}^{r}$ satisfies

$$\left\|\boldsymbol{\eta}_{\underline{k}_{\mathrm{O}}^{r}|\underline{k}_{\mathrm{O}}^{r}}\right\|\leq\hat{\mathrm{e}}\left(\epsilon,\Gamma_{\underline{k}_{\mathrm{O}}^{r-1}|\underline{k}_{\mathrm{O}}^{r-1}},\Gamma_{\bar{k}_{\mathrm{O}}^{r-1}|\bar{k}_{\mathrm{O}}^{r-1}}\right).$$

Applying Proposition 8, it is concluded that for $k \in (\underline{k}^r_{\rm O}, \bar{k}^r_{\rm O}]$,

$$\left\|\boldsymbol{\eta}_{k|k}\right\| \leq \max\left\{\hat{c} + \mathrm{a}\left(\Gamma_{\underline{k}^r_{\rm O}|\underline{k}^r_{\rm O}}\right) \mathrm{q}\left(\Gamma_{\underline{k}^r_{\rm O}|\underline{k}^r_{\rm O}}\right) \hat{\mathrm{e}}\left(\epsilon, \Gamma_{\underline{k}^{r-1}_{\rm O}|\underline{k}^{r-1}_{\rm O}}, \Gamma_{\bar{k}^{r-1}_{\rm O}|\bar{k}^{r-1}_{\rm O}}\right), \right.$$
$$\left. \hat{c} + \hat{c}\mathrm{a}\left(\Gamma_{\underline{k}^r_{\rm O}|\underline{k}^r_{\rm O}}\right) \mathrm{q}\left(\Gamma_{\underline{k}^r_{\rm O}|\underline{k}^r_{\rm O}}\right) \left(1 - \mathrm{q}\left(\Gamma_{\underline{k}^r_{\rm O}|\underline{k}^r_{\rm O}}\right)\right)^{-1}\right\}.$$

**Step 2**: When $r = 1$ and $\underline{k}^1_{\rm U} = 0$.

*(a) For the $1^{st}$ unobservable time interval $k \in (\underline{k}^1_{\rm U}, \bar{k}^1_{\rm U}]$*: In this case, the section is unobservable at time 0. Since $\boldsymbol{\rho}^l_{0|0} \in [0, \varrho_{\rm m}]$, the initial estimation error satisfies $\left\|\boldsymbol{\eta}_{0|0}\right\| \leq \sqrt{n}\varrho_{\rm m}$. According to Proposition 2, we have

$$\boldsymbol{\rho}^l_{k|k} > -\sqrt{n}\varrho_{\rm m}\left(c_0 + (n-2)\,\mathrm{c}\left(\Gamma_{0|0}\right)\right)$$
$$\boldsymbol{\rho}^l_{k|k} < \varrho_{\rm m} + \sqrt{n}\varrho_{\rm m}\left(c_0 + (n-2)\,\mathrm{c}\left(\Gamma_{0|0}\right)\right),$$

for all $l \in \{1, \cdots, n\}$ and $k \in (\underline{k}^1_{\rm U}, \bar{k}^1_{\rm U}]$. It follows that

$$\left\|\boldsymbol{\eta}_{k|k}\right\| \leq \sqrt{n}\left(\sqrt{n}\varrho_{\rm m}\left(c_0 + (n-2)\,\mathrm{c}\left(\Gamma_{0|0}\right)\right) + \varrho_{\rm m}\right) = \hat{\mathrm{e}}_0\left(\Gamma_{0|0}\right), \quad \text{for } k \in (\underline{k}^1_{\rm U}, \bar{k}^1_{\rm U}].$$

*(b) For the $1^{st}$ observable time interval $k \in (\underline{k}^1_{\rm O}, \bar{k}^1_{\rm O}]$*: When the section switches from an unobservable mode at time $\underline{k}^1_{\rm O}$ to an observable mode at time $\underline{k}^1_{\rm O} + 1$, it is shown in Case $(a)$ of Step 2 that the mean error is upper bounded by $\left\|\eta_{\underline{k}^1_{\rm O}|\underline{k}^1_{\rm O}}\right\| \leq \hat{\mathrm{e}}_0\left(\Gamma_{0|0}\right)$. Applying Proposition 8, it follows that for $k \in (\underline{k}^1_{\rm O}, \bar{k}^1_{\rm O}]$,

$$\left\|\boldsymbol{\eta}_{k|k}\right\| \leq \max\left\{\hat{c} + \mathrm{a}\left(\Gamma_{\underline{k}^1_{\rm O}|\underline{k}^1_{\rm O}}\right) \mathrm{q}\left(\Gamma_{\underline{k}^1_{\rm O}|\underline{k}^1_{\rm O}}\right) \hat{\mathrm{e}}_0\left(\Gamma_{0|0}\right), \right.$$
$$\left. \hat{c} + \hat{c}\mathrm{a}\left(\Gamma_{\underline{k}^1_{\rm O}|\underline{k}^1_{\rm O}}\right) \mathrm{q}\left(\Gamma_{\underline{k}^1_{\rm O}|\underline{k}^1_{\rm O}}\right) \left(1 - \mathrm{q}\left(\Gamma_{\underline{k}^1_{\rm O}|\underline{k}^1_{\rm O}}\right)\right)^{-1}\right\}.$$

**Step 3**: When $r = 1$ and $\underline{k}^1_{\rm O} = 0$.

*(a) For the $1^{st}$ unobservable time interval $k \in (\underline{k}^1_{\rm U}, \bar{k}^1_{\rm U}]$*: In this case, the section is observable at time 0. When $\bar{k}^1_{\rm O} - \underline{k}^1_{\rm O}$ is larger than the third residence time listed in (5.16), the estimation error at time $\bar{k}^1_{\rm O}$ satisfies

$$\left\|\boldsymbol{\eta}_{\bar{k}^1_{\rm O}|\bar{k}^1_{\rm O}}\right\| \leq \epsilon + \hat{c} + \frac{\hat{c}\mathrm{a}\left(\Gamma_{0|0}\right) \mathrm{q}\left(\Gamma_{0|0}\right)}{1 - \mathrm{q}\left(\Gamma_{0|0}\right)}$$

based on Proposition 8. As a consequence, Proposition 2 gives

$$\boldsymbol{\rho}^l_{k|k} > -\left(\epsilon + \hat{c} + \frac{\hat{c}\mathrm{a}\left(\Gamma_{0|0}\right)\mathrm{q}\left(\Gamma_{0|0}\right)}{1-\mathrm{q}\left(\Gamma_{0|0}\right)}\right)\left(c_0 + (n-2)\,\mathrm{c}\left(\Gamma_{\underline{k}^1_{\mathrm{U}}|\underline{k}^1_{\mathrm{U}}}\right)\right),$$
$$\boldsymbol{\rho}^l_{k|k} < \varrho_{\mathrm{m}} + \left(\epsilon + \hat{c} + \frac{\hat{c}\mathrm{a}\left(\Gamma_{0|0}\right)\mathrm{q}\left(\Gamma_{0|0}\right)}{1-\mathrm{q}\left(\Gamma_{0|0}\right)}\right)\left(c_0 + (n-2)\,\mathrm{c}\left(\Gamma_{\underline{k}^1_{\mathrm{U}}|\underline{k}^1_{\mathrm{U}}}\right)\right),$$

for all $l \in \{1, \cdots, n\}$ and $k \in (\underline{k}^1_{\mathrm{U}}, \bar{k}^1_{\mathrm{U}}]$. Consequently, the estimation error satisfies $\left\|\boldsymbol{\eta}_{k|k}\right\| \leq \hat{\mathrm{e}}\left(\epsilon, \Gamma_{0|0}, \Gamma_{\underline{k}^1_{\mathrm{U}}|\underline{k}^1_{\mathrm{U}}}\right)$ for all $k \in (\underline{k}^1_{\mathrm{U}}, \bar{k}^1_{\mathrm{U}}]$.

*(b) For the $1^{st}$ observable time interval $k \in (\underline{k}^1_{\mathrm{O}}, \bar{k}^1_{\mathrm{O}}]$*: Since the section is observable at time 0, it holds that $\underline{k}^1_{\mathrm{O}} = 0$. In this case, we have $\Gamma_{\underline{k}^1_{\mathrm{O}}|\underline{k}^1_{\mathrm{O}}} = \Gamma_{0|0}$ and $\left\|\boldsymbol{\eta}_{\underline{k}^1_{\mathrm{O}}|\underline{k}^1_{\mathrm{O}}}\right\| = \left\|\boldsymbol{\eta}_{0|0}\right\| \leq \sqrt{n}\varrho_{\mathrm{m}}$. Then we can directly apply Proposition 8 and conclude that

$$\left\|\boldsymbol{\eta}_{k|k}\right\| \leq \max\left\{\hat{c} + \mathrm{a}\left(\Gamma_{0|0}\right)\mathrm{q}\left(\Gamma_{0|0}\right)\sqrt{n}\varrho_{\mathrm{m}}, \hat{c} + \frac{\hat{c}\mathrm{a}\left(\Gamma_{0|0}\right)\mathrm{q}\left(\Gamma_{0|0}\right)}{1-\mathrm{q}\left(\Gamma_{0|0}\right)}\right\}, \quad \text{for } k \in (\underline{k}^1_{\mathrm{O}}, \bar{k}^1_{\mathrm{O}}].$$

We conclude the proof by combining the above three steps.